



Functional analysis and characterization of the type I secretion
system and its substrate, the giant adhesin SiiE,
of Salmonella enterica

Dissertation

Zur Erlangung des Grades
„**Doctor rerum naturalium**“

(Dr. rer. nat.)

des Fachbereichs Biologie/Chemie

an der Universität Osnabrück

vorgelegt von

Nathalie X. Sander

aus Stade

Osnabrück, März 2022

Hauptberichterstatter:

Prof. Dr. Michael Hensel

2. Berichterstatter:

Prof. Dr. Guntram Grassl

Weitere Mitglieder der

Prüfungskommission:

Prof. Dr. Karlheinz Altendorf

Dr. Michael Holtmannspötter

Table of contents

I.	Summary/Zusammenfassung	1
I.1.	Summary	1
I.2.	Zusammenfassung	2
II.	Introduction	4
II.1.	<i>Salmonella</i> pathogenicity	4
II.2.	The SPI4-T1SS is a key player during invasion of polarized cells	5
II.2.1.	Interplay of the SPI4-T1SS and the SPI1-T3SS for an efficient adhesion to and invasion of polarized cells	5
II.2.2.	The SPI4-T1SS is essential for adhesion to polarized cells	6
II.2.3.	The giant substrate SiiE mediates first close contact to the host cell during invasion process	7
II.2.4.	The non-canonical subunits SiiAB forming a proton channel essential for invasion process	8
II.3.	Secretion mechanisms of T1SS are diverse	9
II.4.	The flagellum is co-expressed with invasion genes	12
II.4.1.	Structure and rotation of the flagellum	12
II.4.2.	Role of the flagellum during pathogenesis	13
II.5.	Organoids – a complex system for analysis of host-pathogens interactions	14
II.5.1.	Organoids – diversity and multidimensional nature	14
II.5.2.	Organoids for analysis of host-pathogen interactions	16
II.5.3.	Organoids as infection model for <i>S. enterica</i>	16
II.6.	Dual-color 3D dSTORM for localization analysis of the SPI4-T1SS	17
II.6.1.	Dual-color 3D dSTORM for localization analyses	17
II.6.2.	Novel nanobody tags – ALFA-Tag and Spot-tag	19
II.7.	Aims of this work	20
III.	Results	23

III.1. Conserved secretion mechanisms of the giant adhesin SiiE of <i>Salmonella enterica</i> and other two-step secreted adhesins	23
III.1.1. Abstract.....	23
III.1.2. Introduction	24
III.1.3. Results.....	27
III.1.4. Discussion.....	49
III.1.5. Materials and Methods	53
III.1.6. Acknowledgements	62
III.1.7. Supplements	63
III.1.8. References.....	66
III.2. The extended cytosolic domain of SiiB is critical for SiiAB proton channel function of <i>Salmonella enterica</i>	70
III.2.1. Abstract.....	70
III.2.2. Introduction	71
III.2.3. Results.....	72
III.2.4. Discussion and Outlook	81
III.2.5. Materials and Methods	82
III.2.6. Acknowledgements	86
III.2.7. Supplements	87
III.2.8. References.....	90
III.3. Functional interaction between SPI4-T1SS encoded proton channel SiiAB and the flagellum in <i>Salmonella enterica</i>	92
III.3.1. Abstract.....	92
III.3.2. Introduction	93
III.3.3. Results.....	95
III.3.4. Discussion.....	113
III.3.5. Materials and Methods	116
III.3.6. Acknowledgements	126
III.3.7. Supplements	127
III.3.8. References.....	136

III.4. Establishment of a novel infection model for <i>Salmonella</i> adhesion and invasion – human intestinal organoids.....	140
III.4.1. Abstract	141
III.4.2. Introduction	142
III.4.3. Results.....	148
III.4.4. Discussion	175
III.4.5. Outlook	180
III.4.6. Materials and Methods.....	181
III.4.7. Acknowledgements	188
III.4.8. References	189
III.5. Contributions of Co-Authors	196
IV. Discussion	198
IV.1. SiiE belongs to a new family of T1SS substrates	199
IV.1.1. Adhesive T1SS substrates are retained on the cell surface	199
IV.1.2. SiiE is retained in the OM	200
IV.1.3. SiiE is post-translationally modified for release	202
IV.2. SiiAB – a promiscuous all-rounder?	203
IV.2.1. Proton channel SiiAB play an important role for the initial steps of SiiE secretion and not for release.....	204
IV.2.2. The cytosolic domain of SiiB has effects on SiiE and the flagellum.....	205
IV.2.3. Possible SiiAB integration in and interaction with the flagellar rotor	206
IV.2.4. 3D dSTORM is capable for localization of proton channels in the IM of STM...	208
IV.3. The future is now – tissues and organs in a dish.....	209
IV.4. Conclusions and Outlook	212
V. References	217
VI. List of abbreviations	228
VII. <i>Curriculum vitae</i>	230
VIII. List of publications.....	232
IX. Danksagung.....	233
X. Erklärung über die Eigenständigkeit der erbrachten wissenschaftlichen Leistungen	236

XI. Supplements on DVD..... 237

I. Summary/Zusammenfassung

I.1. Summary

Salmonella enterica is a facultative intracellular pathogen, able to invade various hosts and successfully replicate within them. Invasion of polarized cells by *S. enterica* serovar Typhimurium (STM) occurs in dependence of the type 1 secretion system (T1SS), encoded on *Salmonella* Pathogenicity Island 4 (SPI4). The 595 kDa non-fimbrial adhesin SiiE is the substrate of the SPI4-T1SS and mediates the first close contact to the host cells apical side. This allows for the type 3 secretion system (T3SS) of the SPI1 to translocate its effector proteins into the host cells cytosol, leading to actin remodeling, membrane ruffle formation and finally uptake of the pathogen. The SPI4-T1SS belongs to the family of ATP-binding cassette (ABC) transporters and is characteristically composed of the ATPase SiiF in the inner membrane (IM), the periplasmic adaptor protein (PAP) SiiD and the secretin SiiC. Further there are two non-canonical proteins encoded, namely SiiA and SiiB, which are known to form a proton channel in the IM. Every single subunit was found to be essential for invasion of polarized cells. The substrate SiiE is transiently retained on the cell surface during secretion process and protrudes the lipopolysaccharide (LPS) layer, a step essential for adhesion. Following translocation of the SPI1-T3SS effector proteins, SiiE is released into the extracellular space.

Utilizing a variety of techniques, I was able to show that the transient retention of SiiE only occurs in the outer membrane (OM) protein SiiC and not in the whole two membrane-spanning T1SS. My analyses showed that the proton channel SiiAB is involved in initial steps of secretion and not necessary for release of SiiE, further narrowing down possible modes of action. I found a potential proteolytic cleavage site in the N-terminal part of SiiE, essential for release of the adhesin and discovered a potential retention domain in its N-terminus, too bulky to pass through the secretin. Additionally, I gained first hints that the large cytosolic domain of SiiB is not only involved in SiiE retention mechanism, but also in flagellar-dependent movement under swarming conditions. Using dual-color 3D direct stochastic optical reconstruction microscopy (dSTORM), I was able to localize SiiAB in the IM and SiiB not only at the SPI4-T1SS, but during SiiE retention maximum primarily at the flagellum. Intriguingly, the synthetic expression of *siiAB* as well as synthetic expression of the flagellar stator unit *motAB* both showed an increase of velocity. Furthermore, I successfully established murine and human intestinal organoid cell culture for microscopic and quantitative analyses of STM and *S. Paratyphi A* (SPA) invasion processes. Thus, with this work I was able to reveal new insights of the SPI4-T1SS, its substrate SiiE and the non-canonical subunits SiiAB that pave the way for further SPI4-T1SS investigations and also other secretion systems and their associated subunits.

I.2. Zusammenfassung

Salmonella enterica ist ein fakultativ intrazelluläres Pathogen, das in verschiedene Wirte eindringen und erfolgreich in ihnen replizieren kann. Die Invasion durch *S. enterica* serovar Typhimurium (STM) in polarisierte Zellen ist abhängig vom Typ-1-Sekretionssystem (T1SS), das auf der *Salmonella* Pathogenitätsinsel 4 (SPI4) kodiert ist. Das 595 kDa große, nicht-fimbrilliäre Adhäsins SiiE ist das Substrat des SPI4-T1SS und vermittelt den ersten engen Kontakt zur apikalen Seite der Wirtszelle. Dies ermöglicht es dem Typ-3-Sekretionssystem (T3SS) der SPI1, seine Effektorproteine in das Zytosol der Wirtszelle zu translozieren, was zu einem Aktinumbau, zur Bildung von Membranausstülpungen und schließlich zur Aufnahme des Pathogens führt. Das SPI4-T1SS gehört zur Familie der *ATP-binding cassette* (ABC)-Transporter und besteht charakteristischerweise aus der ATPase SiiF in der inneren Membran (IM), dem periplasmatischen Adaptorprotein (PAP) SiiD und dem Sekretin SiiC. Darüber hinaus werden zwei akzessorische Proteine, SiiA und SiiB, kodiert, von denen bekannt ist, dass sie einen Protonenkanal in der IM bilden. Jede einzelne Untereinheit ist hierbei essentiell für die Invasion in polarisierte Zellen. Das Substrat SiiE wird während des Sekretionsprozesses vorübergehend auf der Zelloberfläche zurückgehalten und übertagt die Lipopolysaccharidschicht (LPS), ein für die Adhäsion wesentlicher Schritt. Nach der Translokation der SPI1-T3SS-Effektorproteine wird SiiE in den extrazellulären Raum freigesetzt.

Mithilfe verschiedener Techniken konnte ich zeigen, dass die transiente Retention von SiiE nur in SiiC in der äußeren Membran und nicht im gesamten, die Zellhülle durchspannenden, T1SS stattfindet. Meine Analysen zeigten, dass der Protonenkanal SiiAB an den ersten Schritten der Sekretion beteiligt ist, für die Freisetzung von SiiE allerdings nicht benötigt wird, was die möglichen Wirkmechanismen weiter einschränkt. Ich fand eine potenzielle Schnittstelle im N-terminus von SiiE, die für die Freisetzung des Adhäsins wesentlich ist. Darüber hinaus fand ich eine potenzielle Retentionsdomäne im N-Terminus, die zu groß sein könnte, um das Sekretin zu passieren. Außerdem habe ich erste Hinweise gefunden, dass die verlängerte zytosolische Domäne von SiiB nicht nur am SiiE-Retentionsmechanismus beteiligt ist, sondern auch am Flagellen-abhängigen Schwärmen. Mittels zweifarbiger 3D direkter stochastischer optischer Rekonstruktionsmikroskopie (dSTORM) konnte ich SiiAB in der IM und SiiB nicht nur am SPI4-T1SS lokalisieren, sondern während des SiiE-Retentionsmaximums vor allem an der Flagelle nachweisen. Interessanterweise zeigten sowohl die synthetische Expression von *siAB* als auch die synthetische Expression des flagellaren Stators *motAB* eine Erhöhung der Schwimmgeschwindigkeit. Des Weiteren habe ich erfolgreich die murine und humane intestinale Organoid-Zellkultur für mikroskopische und quantitative Analysen der Invasion von STM und *S. Paratyphi A* (SPA) etabliert. Mit dieser Arbeit konnte ich neue Erkenntnisse über das

SPI4-T1SS, sein Substrat SiiE und die akzessorischen Untereinheiten SiiAB gewinnen, die den Weg für weitere SPI4-T1SS-Untersuchungen und auch andere Sekretionssysteme und deren assoziierte Untereinheiten ebnen.

II. Introduction

II.1. *Salmonella* pathogenicity

The interplay between a host and a pathogen is described by virulence factors and adaptation of the pathogen as well as host cell factors (Casadevall and Pirofski, 1999). The virulence factors are characterized by their toxicity, activity (Kolmer and Liu, 2000), antigen variation, transmission, adherence, invasion and replication (Casadevall and Pirofski, 2001). To investigate such host-pathogen interactions, *Salmonella enterica* is used as a model system. It causes a range of infections in various hosts depending on the serovar, ranging from a self-limiting gastroenteritis to life-threatening typhoid fever (Haraga *et al.*, 2008).

S. enterica serovar Typhimurium (STM) is a food-borne intracellular replicating pathogen, able to overcome the gut commensals, adhere to and invade host cells and successfully replicate within them and evade the host cell immune response (Gunn, 2011). Genes, important for virulence are organized in so-called Pathogenicity Islands. For *S. enterica*, up to 19 *Salmonella* Pathogenicity Islands (SPI) are described (Gerlach *et al.*, 2008; Hensel, 2004; Marcus *et al.*, 2000). For *Salmonella*, the type 3 secretion systems (T3SSs) of the SPI1 and SPI2 are of great importance. Whereas the SPI1-T3SS translocates effector proteins essential for invasion process, the SPI2-T3SS is required for intracellular survival of the pathogen (Haraga *et al.*, 2008). Following translocation of SPI1-T3SS effector proteins, actin is remodeled and membrane ruffles are formed, leading to uptake of the pathogen. Inside the host cell, *Salmonella* resides in a modified phagosome, the *Salmonella*-containing vacuole (SCV), allowing survival and replication of the pathogen (Chakravorty *et al.*, 2002). Upon phagosome maturation, the SPI2-T3SS translocates its effector proteins into the host cell cytosol. This is essential for SCV integrity and induction of an extensive tubular network, the *Salmonella*-induced filaments (SIF), which are necessary for nutrition and survival of the pathogen (Liss *et al.*, 2017).

Besides the SPI1-T3SS, another secretion system is essential for invasion of polarized cells. The SPI4-T1SS and its substrate SiiE are essential for the first close intimate contact to the host cell (Gerlach *et al.*, 2007a). Following adhesion to the apical side of the host cell, the SPI1-T3SS is in position to translocate its effector proteins. The non-fimbrial adhesin SiiE is retained on the cell surface during secretion process, protruding the lipopolysaccharide (LPS) layer with its immense length of 175 ± 5 nm, thus allowing attachment of the C-terminal moiety to glycosylated structures on the host cell membrane and subsequent proper positioning of the SPI1-T3SS (Griessl *et al.*, 2013; Wagner *et al.*, 2014; Wagner *et al.*, 2011).

II.2. The SPI4-T1SS is a key player during invasion of polarized cells

For successful host colonization, STM possesses various adhesive structures. *Salmonella* is not only equipped with fimbrial adhesins like type I fimbriae or Curli, but additionally with auto-transported adhesins like MisL and ShdA and T1SS adhesins BapA and SiiE (Wagner *et al.*, 2011). BapA, a non-fimbrial adhesin comparable to SiiE, involved in biofilm-formation, is encoded on the SPI9 (Latasa *et al.*, 2005). SPI4 gene expression is regulated by the transcriptional activator HilA, which in turn is regulated by the master regulator SirA (Ahmer *et al.*, 1999; Gerlach *et al.*, 2007a; Main-Hester *et al.*, 2008). As genes of the SPI1-T3SS are also regulated by SirA and HilA, a tight co-regulation of both loci is likely (Gerlach *et al.*, 2007a).

II.2.1. Interplay of the SPI4-T1SS and the SPI1-T3SS for an efficient adhesion to and invasion of polarized cells

Polarized epithelial cells of the intestinal layer form a protective barrier against the entry of microbes from the intestinal flora, as well as pathogens. To overcome this intestinal barrier, food-borne pathogens are equipped with various virulence-associated proteins, systems and

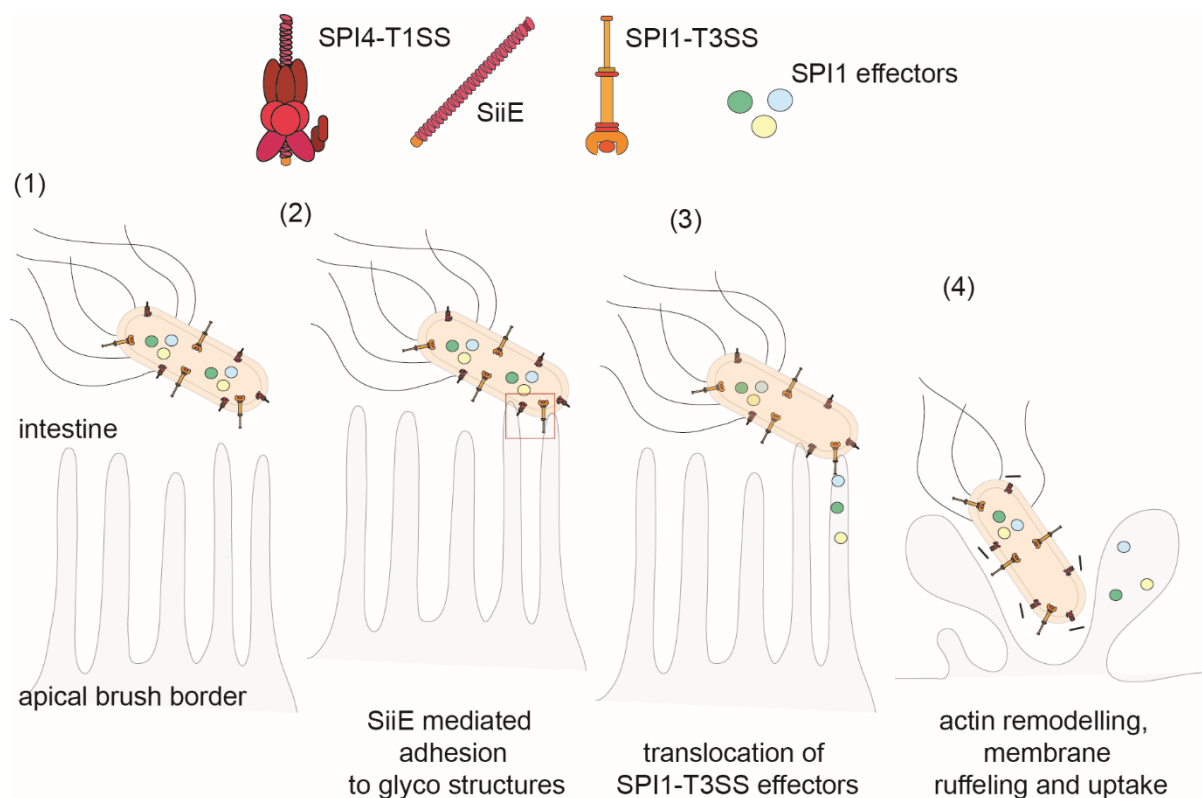


Figure II.1. SPI4-T1SS dependent adhesion and SPI1-T3SS-dependent invasion of STM. The apical brush border of polarized epithelial cells possesses a dense array of microvilli (1). The SPI4-T1SS substrate SiiE mediates the first close contact to the host cell membrane (2). Subsequently, the SPI1-T3SS can be properly located (2) and translocates its effector proteins inside the host cell (3). Effector protein translocation leads to actin remodeling, membrane ruffling and uptake of the pathogen (4). Without the SPI4-T1SS and SiiE, effector protein translocation is inefficient and STM is not internalized. Model based on (Gerlach *et al.*, 2008).

mechanisms (Sansonetti, 2004). The SPI1-T3SS and the SPI4-T1SS were both shown to be essential for invasion of polarized cells (Gerlach *et al.*, 2008) (Figure II.1). However, for invasion of non-polarized cells, only the SPI1-T3SS is required (Gerlach *et al.*, 2007a). The SPI4-T1SS secreted substrate SiiE is needed to mediate the first close contact to the host cell apical brush border (Gerlach *et al.*, 2008) (Figure II.1, 2). Thus, allowing the SPI1-T3SS to properly locate at the host cell membrane and efficiently translocate its effector proteins inside the host cell cytosol (Figure II.1, 3). Following effector protein translocation, actin rearrangements and membrane ruffling take place, which finally lead to the uptake of the pathogen (Figure II.1, 4). Without adhesion mediated by the SPI4-T1SS and its substrate SiiE, invasion of epithelial cells in their physiological state, i.e. polarized, is not possible (Gerlach *et al.*, 2008). Thus, the SPI4-T1SS is required for the invasion process of STM.

II.2.2. The SPI4-T1SS is essential for adhesion to polarized cells

The SPI4 is a 27 kb pathogenicity island, containing six open reading frames (ORFs), *siiA* to *siiF* (Main-Hester *et al.*, 2008). The SPI4-T1SS consists of the characteristic subunits of an (ATP-binding cassette) ABC transporter: the ATPase SiiF in the inner membrane (IM), the peri-

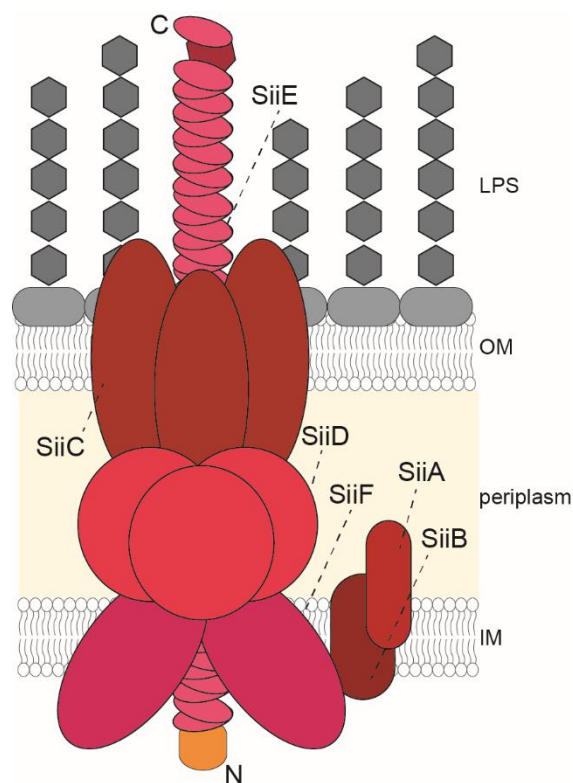


Figure II.2. The SPI4-T1SS and non-canonical subunits SiiAB. The SPI4-T1SS displays the characteristic composition of an (ATP-binding cassette) ABC transporter with the ATPase SiiF in the IM, the periplasmic adaptor protein (PAP) SiiD in the periplasm and the secretin SiiC in the OM. The 595 kDa adhesin SiiE is the substrate of the canonical SPI4-T1SS (Gerlach *et al.*, 2007b). The two non-canonical subunits SiiA and SiiB form a proton channel in the IM (Wille *et al.*, 2014).

plasmic adaptor protein (PAP) SiiD, spanning the periplasm and the secretin SiiC (Figure II.2) (Gerlach *et al.*, 2007b). The 595 kDa adhesin SiiE is also encoded by a SPI4 gene and is the substrate of the canonical subunits of the SPI4-T1SS (Gerlach *et al.*, 2007b). Additionally, there are two non-canonical subunits, namely SiiA and SiiB, known to form a proton channel in the IM, (Wille *et al.*, 2014). During secretion, SiiE is retained on the cell surface, enabling the adhesin to mediate adhesion to the host cell (Wagner *et al.*, 2011).

II.2.3. The giant substrate SiiE mediates first close contact to the host cell during invasion process

The SPI4-T1SS substrate SiiE is a non-fimbrial adhesin, composed of 53 bacterial immunoglobulin (Blg) domains (Barlag and Hensel, 2015; Gerlach *et al.*, 2007b; Wagner *et al.*, 2011) (Figure II.3 A). The N-terminal part of SiiE consists of a coiled-coil domain of 8 heptads, flanked by two β -sheet domains (Wagner *et al.*, 2011). In the C-terminus Blg52 and Blg53 are separated by a putatively unfolded domain termed *insertion*. Additionally, the secretion signal is located in the last C-terminal moiety (Wagner *et al.*, 2011). By EM analysis, it was shown that SiiE has a linear molecular structure of approximately 175 ± 5 nm length, protruding the LPS layer (Wagner *et al.*, 2011). Initially, SiiE associates with the IM and is recognized by its T1SS and subsequently secreted into the extracellular space, depending on binding of extracellular Ca^{2+} (Barlag and Hensel, 2015; Griessl *et al.*, 2013; Wagner *et al.*, 2011). SiiE possesses conserved aspartate and glutamate residues, forming two Ca^{2+} -binding sites per Blg domain, shown to stabilize SiiE structure (Griessl *et al.*, 2013) (Figure II.3). Type I Ca^{2+} -binding sites are located at the interface of two Blg domains and contain three aspartate residues that are characteristic for Blg domain proteins (Peters *et al.*, 2017). In contrast to this, type II Ca^{2+} -binding sites are specific for SiiE and consist of two aspartate residues within a Blg domain (Peters *et al.*, 2017). SiiE binds to glycosylated structures on the host cell membrane, containing N-acetylglucosamine and/or α -2,3 sialic acid (Figure II.3 B) and following adhesion, it is secreted into the extracellular space (Gerlach *et al.*, 2007b).

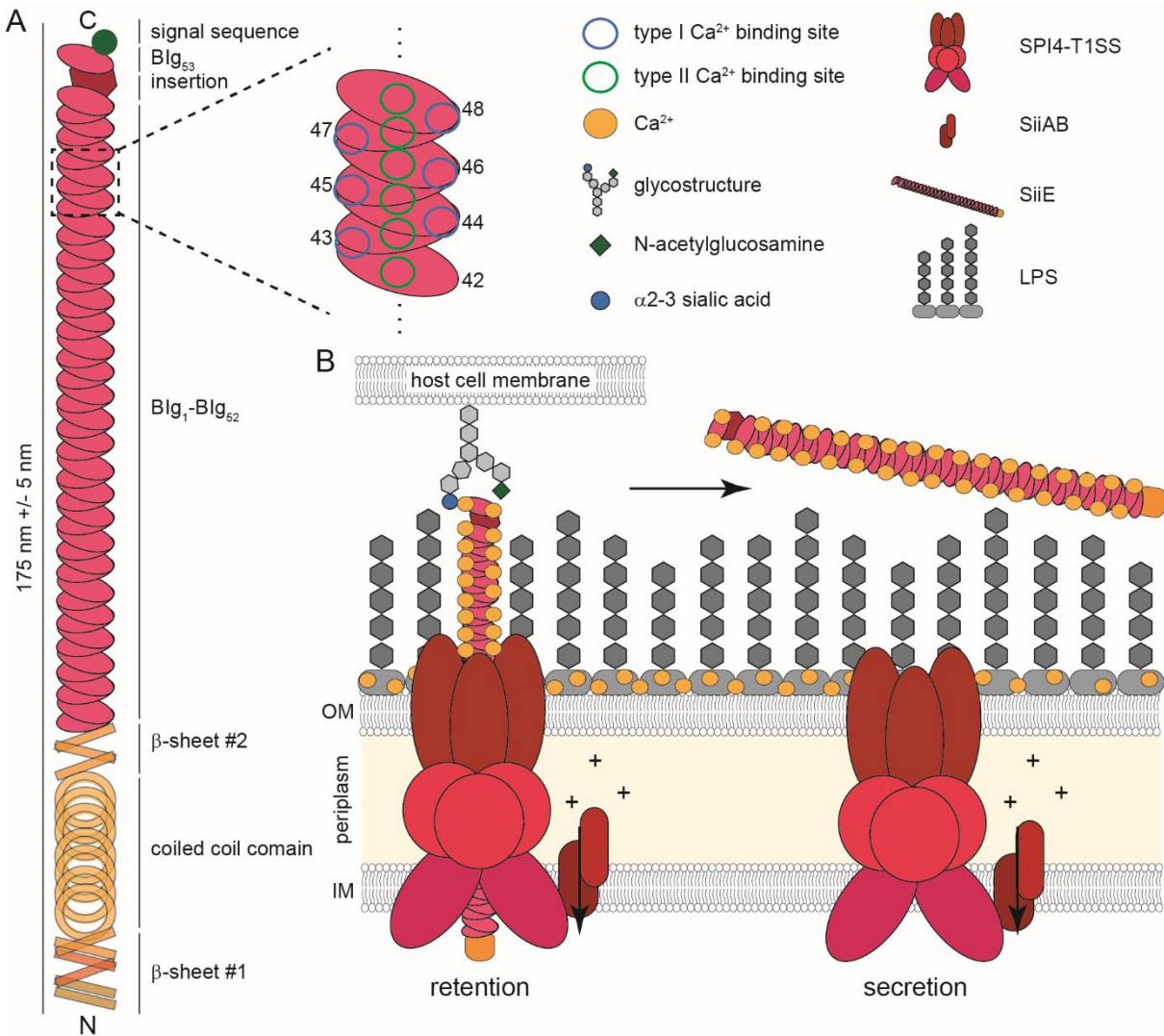


Figure II.3. Overview of SiiE structure and secretion mechanism. Shown is an overview of the SiiE structure (A) and the retention and secretion of SiiE (B). A) SiiE consists of 53 Blg domains with an insertion between Blg52 and Blg53 and a C-terminal secretion signal. The N-terminal portion is composed of a coiled-coil domain, flanked by two regions, consisting of β-sheets. The Blg domains possess type I Ca²⁺-binding sites (blue) and type II Ca²⁺-binding sites (green). Ca²⁺-binding was shown to be important for SiiE secretion (B) and stabilization. B) During secretion process, SiiE is retained on the cell surface, mediating first close contact to glycosylated structures on the host cell membrane via its C-terminal moiety. It was shown that SiiE binds in a lectin-like manner to N-acetylglucosamine and/or α-2,3 sialic acid. Following binding and SPI1-T3SS effector protein translocation, SiiE is fully secreted into the extracellular space. Proton channel SiiAB uses proton-motive force (PMF) to support invasion mechanism.

II.2.4. The non-canonical subunits SiiAB forming a proton channel essential for invasion process

The SPI4 locus additionally encodes an accessory non-canonical proton channel, SiiAB, located in the IM (Wille *et al.*, 2014). SiiAB play an essential role for invasion by transporting ions across the IM (Wille *et al.*, 2014). SiiA and SiiB share similarities regarding composition and structure with the stator complexes MotAB, PomAB, ExbBD and TolQR (Kirchweger *et al.*,

2019; Wille *et al.*, 2014) (Figure II.4). ExbBD together with TonB transfer the energy from the proton-motive force (PMF) of the IM to OM ion transporters (Ollis *et al.*, 2009). Contrary, MotAB, PomAB and TolQR couple the IM PMF to protein actions in the IM (Minamino *et al.*, 2018; Zhu *et al.*, 2014). SiiA was found to harbor a conserved critical aspartate residue (D13), comparable to MotB (D33) and ExbD (D25), a mutation of which inhibits proton channel function (Braun *et al.*, 1996; Wille *et al.*, 2014). MotB and PomB contain a peptidoglycan (PG)-binding (PGB) domain, important for binding to the PG after interaction with the C-ring (Minamino and Imada, 2015). A similar PGB was also described for SiiA (Kirchweiger *et al.*, 2019). Comparable to MotA, SiiB harbors a large cytoplasmic region, which however interacts in a different way with SiiF as postulated for MotA and the rotor (Blair and Berg, 1991; Dean *et al.*, 1984; Deme *et al.*, 2020b; Wille *et al.*, 2014; Zhou *et al.*, 1995). Recent studies clearly show a 5:2 stoichiometry for ExbBD stator units (Celia *et al.*, 2019). Such a 5:2 stoichiometry was also confirmed for MotAB, and appears to be a conserved structure across the MotAB/PomAB family (Deme *et al.*, 2020a, b; Santiveri *et al.*, 2020).

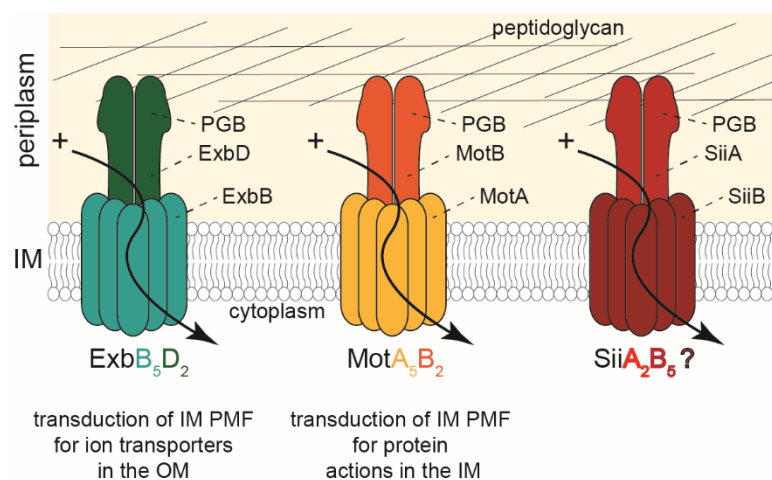


Figure II.4. Proton channels generating torque by using ion flux and PMF. Shown are the proton channels ExbBD (left), MotAB (center) and SiiAB (right). These proton channels use the PMF of the IM to transduce energy. ExbBD transduces energy for ion transporters in the OM, whereas MotAB transduces energy for flagellar rotation. ExbD, MotB and SiiA possess a PGB domain, important for channel function. For ExbBD and MotAB now a stoichiometry of 5:2 was shown. Thus, we postulate a comparable stoichiometry for SiiAB.

II.3. Secretion mechanisms of T1SS are diverse

Secretion by T1SS is a highly conserved mechanism used by many Gram-negative bacteria to secrete small substrates as bacteriocins like CvaC, as well as large proteins like the 900 kDa protein LapA of *Pseudomonas fluorescens* (Smith *et al.*, 2018b) (Figure II.5 A, C). Many of the T1SS substrates belong to the repeats-in-toxin (RTX) family, for example HlyA (Figure II.5 B) and CyaA (Smith *et al.*, 2018b). From these studies, a model of single-step secretion emerged,

where the substrate is directly secreted from the cytosol into the extracellular space without a periplasmic intermediate step (Andersen *et al.*, 2000; Kanonenberg *et al.*, 2013; Koronakis *et al.*, 1989; Mackman *et al.*, 1985) (Figure II.5 A, B).

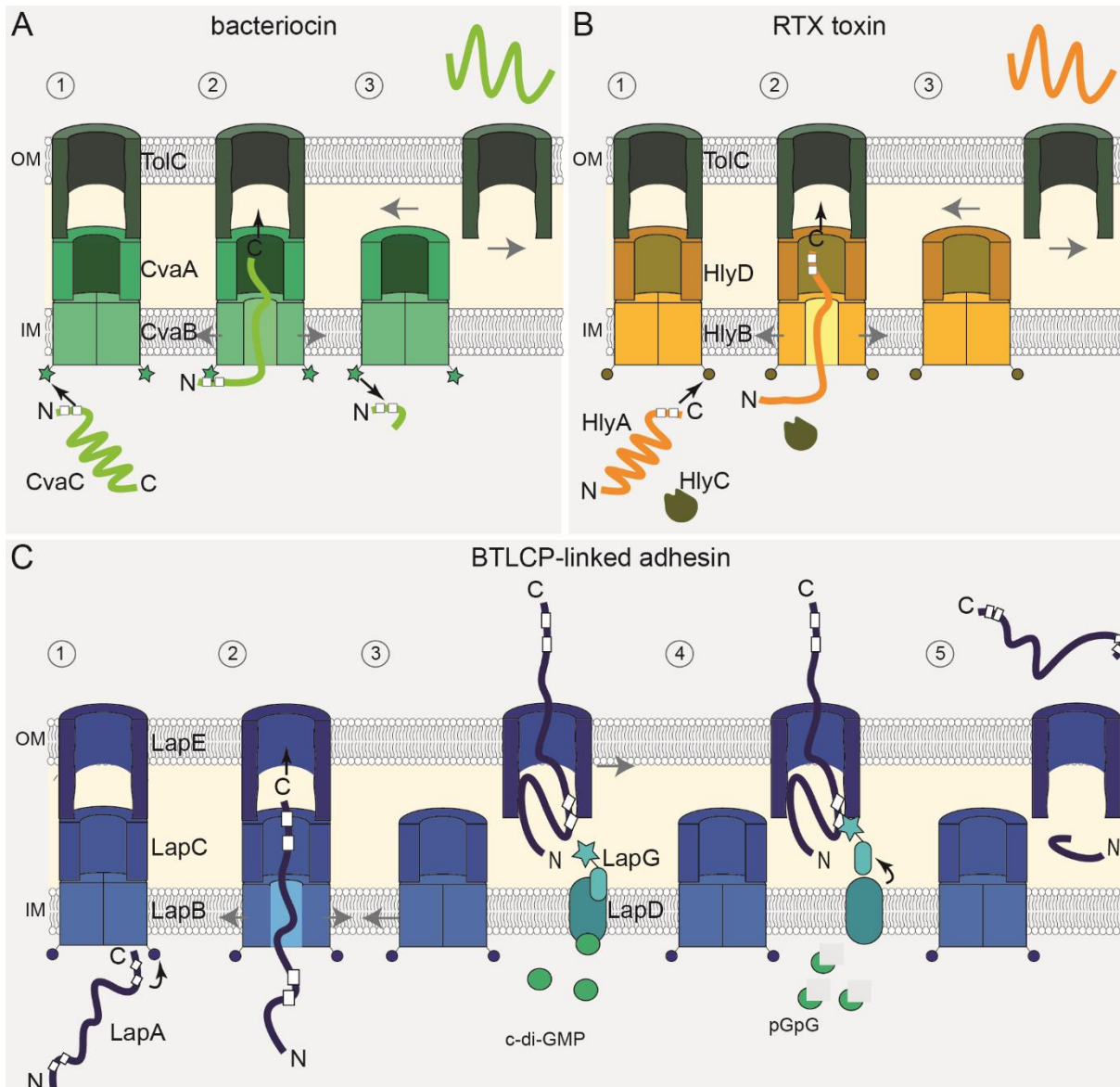


Figure II.5 Schematic overview of the three T1SS secretion mechanisms and the SPI4-T1SS. Shown are known mechanisms for bacteriocins (A), RTX toxins (B), BTLCP-linked/RTX adhesins (C). T1SS consisting of the ATP-binding cassette (ABC) transporter in the IM, the periplasmic adaptor protein (PAP) and the secretin in the outer membrane (OM). The T1SS substrates are transported unfolded to the T1SS and recognized by the ABC transporter. In response to substrate recognition, the secretion of the different substrates can be performed as shown above. A) and B) representing the one-step secretion of a substrate, whereas C) displays secretion in two steps with an intermediate step. White squares illustrate the glycine-rich regions of the T1SS substrates. A) First, during secretion of the bacteriocin CvaC (colicin V) of *E. coli*, the N-terminal glycine-rich secretion motif is recognized by the ABC transporter CvaB (1). The Ca^{2+} -dependent N-terminal C39 peptidase (green stars) of CvaB cleaves CvaC near the double-glycine site and by this activating the bacteriocin (2). Following secretion, TolC dissociates from CvaAB, undergoing conformational changes to a closed state (3). B) The T1SS for secretion of RTX toxin HlyA of *E. coli* consists of the ABC transporter HlyB, the PAP HlyD and the OM pore TolC. The N-terminus of HlyB contains a catalytically inactive C39-like domain (CLD, brown circles). The CLD of HlyB recognizes the C-terminal glycine-rich RTX motifs of HlyA (1), which are essential for recruitment

of TolC (2). For activation, HlyC post-translationally modifies HlyA and HlyA is secreted into the extracellular space (3). C) Secretion mechanism of BTLCP-linked/RTX adhesin LapA of *Pseudomonas fluorescens*. The T1SS consists of LapB (ABC transporter), LapC (PAP), LapE (secretin), LapA (substrate) and the two accessory proteins LapG and LapD, essential for N-terminal cleavage and release of LapA into the environment. Unfolded LapA is C-terminally recognized by LapB (1) and is secreted from C- to N-terminal direction (2). During secretion process, LapA is retained on the cell surface to mediate adhesion to surfaces if biofilm conditions are promoted and c-di-GMP levels are high, thus protecting LapA from proteolysis by LapG (3). In response to lower c-di-GMP levels, LapG is released from LapD and cleaves the canonical di-alanine motif within the N-terminal LapA retention domain (4). LapA is released into the extracellular space, its N-terminal domain remains in the periplasm and LapBC again can interact with LapE (5).

The calcium-binding RTX motifs result in an intrinsically disordered state, until the substrate is secreted into the calcium-rich environment, where it adopts its final folded structure essential for its biological function. For CyaA, extracellular Ca²⁺ binding is also important for secretion of the substrate (Bumba *et al.*, 2016).

T1SS characteristically are composed of the ATP-binding cassette (ABC) transporter in the IM, a periplasmic adaptor protein (PAP) and a secretin (Smith *et al.*, 2018b) (Figure II.5). For one-step secretion, the substrates are recognized by its T1SS via an N-terminal (bacteriocins) or C-terminal (all other known substrates) secretion signal and directly secreted into the extracellular space, following recruitment of the secretin (Figure II.5 A, B) (Thanabalu *et al.*, 1998). Whereas bacteriocins are N-terminally cleaved by an intrinsic C39 peptidase of the ABC transporter for release and activation, ABC transporters of RTX toxins only possess a catalytically inactive C39-like domain (CLD) (Lecher *et al.*, 2012; Smith *et al.*, 2018b). Such a CLD was also found to be present in the SPI4-T1SS ABC transporter SiiF (Wille *et al.*, 2014). For activation of the toxin, HlyA is post-translationally modified by the acyltransferase HlyC, which does not affect the secretion process in general (Ludwig *et al.*, 1996). In contrast to this, during two-step secretion, substrates like LapA, MplBP and SiiE are retained on the cell surface during secretion, a step important for adhesion (Guo *et al.*, 2017; Smith *et al.*, 2018a; Wagner *et al.*, 2011) (Figure II.5 C). LapA is retained and released in a c-di-GMP-dependent manner. While this biofilm-associated substrate is N-terminally cleaved for secretion like bacteriocins, this happens via interaction of two accessory proteins, LapD and LapG (Smith *et al.*, 2018a). Such accessory proteins were designated as bacterial transglutaminase-like cysteine proteinases (BTLCP), characterized by their invariant Cys-His-Asp triads often linked to T1SS machinery and large RTX-containing proteins (Ginalski *et al.*, 2004). The SPI4-T1SS also encodes the two non-canonical subunits SiiA and SiiB, described to be involved in invasion (Wille *et al.*, 2014).

II.4. The flagellum is co-expressed with invasion genes

II.4.1. Structure and rotation of the flagellum

The first bacterial swimming was observed in the seventeenth century (van Leeuwenhoek, 1677), thus it has long been known that the ability to move is essential for many bacteria for survival and pathogenicity and that various bacteria use the flagellum for a directed movement (Berg and Anderson, 1973; Duan *et al.*, 2013; Haiko and Westerlund-Wikstrom, 2013; Silverman and Simon, 1974). The flagellum consists of a long external filament, built up from the rod, the hook, the hook filament junction, the filament and the filament cap and a large motor region consisting of basal body rings located in the cell envelope (Berg, 2003; Nakamura and Minamino, 2019) (Figure II.6). The rod is connected to the basal body MS ring acting as a drive shaft (Minamino, 2018). The hook is located between the rod and the filament for torque transition from the motor to the filament (Minamino, 2018). An ion-powered rotor and a ring of a varying number of stator complexes, surrounding the rotor, represent the motor region of the flagellum in different bacteria (Coulton and Murray, 1978; Khan *et al.*, 1988; Khan *et al.*, 1992; Khan *et al.*, 1991). Stator units of the bacterial flagellum form ion channels and are located in the IM, directly connected to the motor (Coulton and Murray, 1978; Khan *et al.*, 1988; Khan *et al.*, 1992; Khan *et al.*, 1991; Stader *et al.*, 1986; Wilson and Macnab, 1988). The number of active stator units is regulated in response to environmental changes (Berg, 2003; Macnab, 2004; Minamino *et al.*, 2008; Morimoto and Minamino, 2014). The rotational direction of the motor can be changed by chemotactic signaling, leading to a higher adaptation to the environment (Minamino *et al.*, 2019). MotAB displays the best-studied example for the prokaryotic rotary motor stator unit family that uses energy from the transmembrane (TM) ion gradient instead of ATP in order to generate mechanical work (Kuhlbrandt and Davies, 2016; Lai *et al.*, 2020; Mandadapu *et al.*, 2015). Stator complexes use H⁺ or Na⁺ ion flow across the IM, in turn generating torque in the cytoplasmic region (C-ring) of the rotor complex (Blair and Berg, 1988, 1990; Kojima, 2015; Larsen *et al.*, 1974). These complexes are present in an inactive, plugged form and are activated by motor incorporation and peptidoglycan binding (Hosking *et al.*, 2006).

Following incorporation of the stator unit into the motor region, the stator unit is unplugged and the PGB domain dimerizes (Santiveri *et al.*, 2020). Docking of the MotA cytoplasmic loop to the rotor C-ring induces the ion flux through the channel and release of the MotB-PGB domain to bind to the PG surrounding the flagellar basal body (Kojima *et al.*, 2018; Zhu *et al.*, 2014). The ion flux is suggested to lead to conformational changes in the cytoplasmic region of MotA, which in turn generates torque in the rotor (Kim *et al.*, 2008a; Kojima and Blair, 2001; Mandadapu *et al.*, 2015).

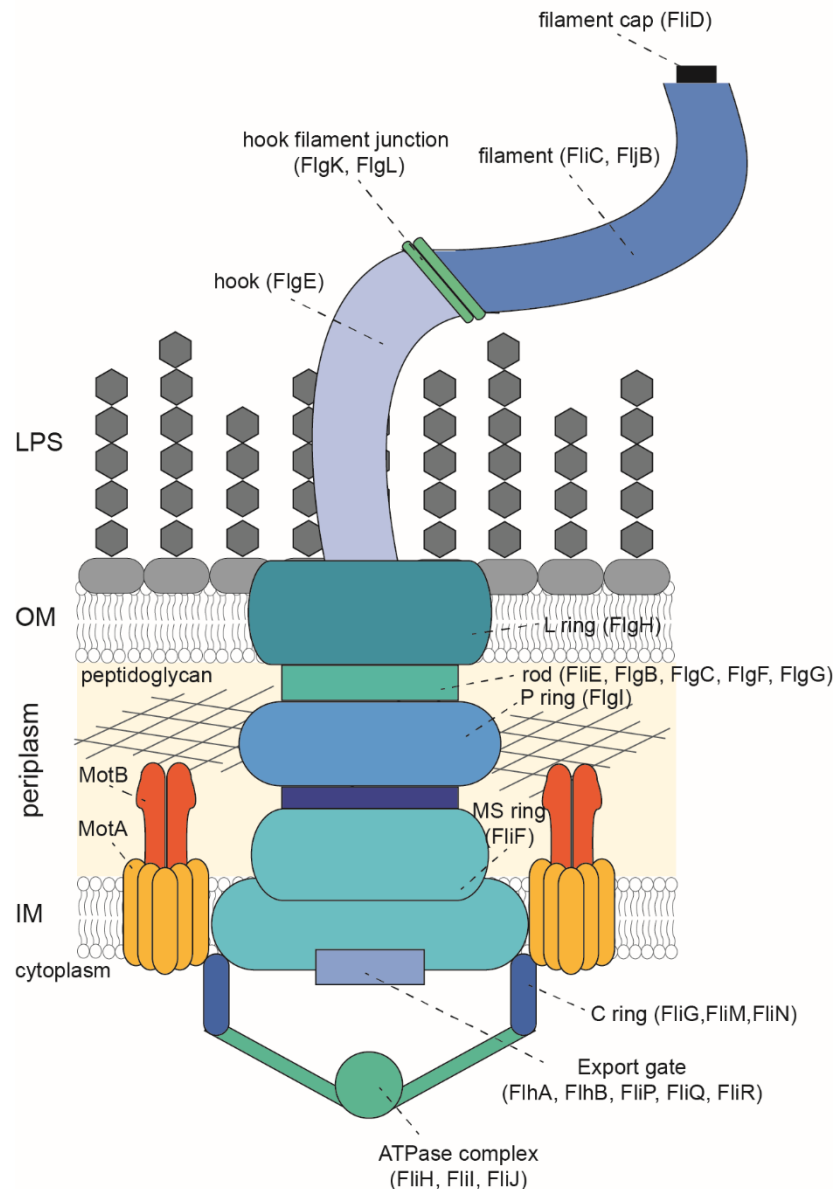


Figure II.6. Schematic overview of the flagellum. Shown is the schematic overview of the flagellum. The flagellum consists of the rotor, spanning the cell envelope, the rod, the hook, the hook filament junctions, the filament and the filament cap. The rotor is surrounded by numerous stator complexes (MotAB). Other proteins as indicated. Model modified from (Minamino, 2018).

II.4.2. Role of the flagellum during pathogenesis

Bacterial motility is not only important for the directed motility in gradients towards nutrients, but also during host infection and thus is considered as virulence factor. Motility was found to be essential for biofilm development and maturation by *P. aeruginosa*, *Yersinia enterocolitica*, *Listeria monocytogenes* and *E. coli*, but also during infection as described for pathogens like *Campylobacter jejuni* and *S. enterica* (Haiko and Westerlund-Wikstrom, 2013; Kim *et al.*, 2008b; Koirala *et al.*, 2014; Lemon *et al.*, 2007; Mertins *et al.*, 2013; Partridge and Harshey,

2013; Sauer *et al.*, 2002; Wood *et al.*, 2006). It was shown that methylation of STM flagella supports adhesion to host cells and hence their invasion (Horstmann *et al.*, 2020). T3SS are critical for the pathogenicity and host-pathogen interactions of many Gram-negative bacteria (Duan *et al.*, 2013). T3SS translocate (tT3SS) effector proteins into the host cell leading to reprogramming of the host cell in a way that is beneficial for the pathogen (Gerlach *et al.*, 2008). However, the flagellar assembly (fT3SS) displays the basis for tT3SS for translocation, adapted for a pathogenic lifestyle (Cornelis, 2006; Duan *et al.*, 2013). It was shown that the flagellar T3SS can be associated with bacterial pathogenicity and is co-regulated with virulence genes during infection (Duan *et al.*, 2013).

Many *S. enterica* serovars possess two flagellin proteins, FliC or FliB, due to flagellar phase variation (Lederberg, 1956). Bacteria expressing *fliC* show distinct advantages during colonization of the epithelium and in motility in comparison to *fliB*-expressing bacteria (Horstmann *et al.*, 2017). As the thousands surface-exposed flagellin molecules are a prime target for host immune response, many intracellular bacteria evolved mechanisms to prevent recognition, e.g. post-translational modifications like glycosylation of the flagellin (De Maayer and Cowan, 2016; Horstmann *et al.*, 2020). However, STM does not glycosylate its flagellin (Horstmann *et al.*, 2020). STM was shown to methylate flagellar lysine residues like many other Enterobacteriaceae, which was also suggested to be involved in virulence (De Maayer and Cowan, 2016; Horstmann *et al.*, 2020). Methylation of the flagellum increases adhesion of STM, thus supports invasion and colonization (Horstmann *et al.*, 2020).

II.5. Organoids – a complex system for analysis of host-pathogens interactions

II.5.1. Organoids – diversity and multidimensional nature

Organoids are 3D *in vitro* cell culture systems, originating from self-organizing stem cells, able to mimic *in vivo* structures and functions of the originating organ (Dutta *et al.*, 2017). Organoids can be derived from organ-specific adult stem cells (ASC) or pluripotent stem cells (PSC) (Lancaster and Knoblich, 2014) (Figure II.7). For the generation of organoids from PSC, cells are grown in medium mimicking an embryonic development. Therefore, single organoids possess a variety of different cell types, but have a limited expansion potential (Aguilar *et al.*, 2021). PSC can differentiate to tissues recapitulating what happens in organogenesis, where tissues are derived from embryonic stem cells (ESC) (Li *et al.*, 2014b). In comparison to this, growth factors for ASC differentiation mimic tissue regeneration. The resulting organoids consist of the pure epithelial cells, shown to have an immense expansion potential with a high

genetic stability (Blokzijl *et al.*, 2016; Huch *et al.*, 2015). To date, many different organs and tissues were successfully cultivated (Figure II.7).

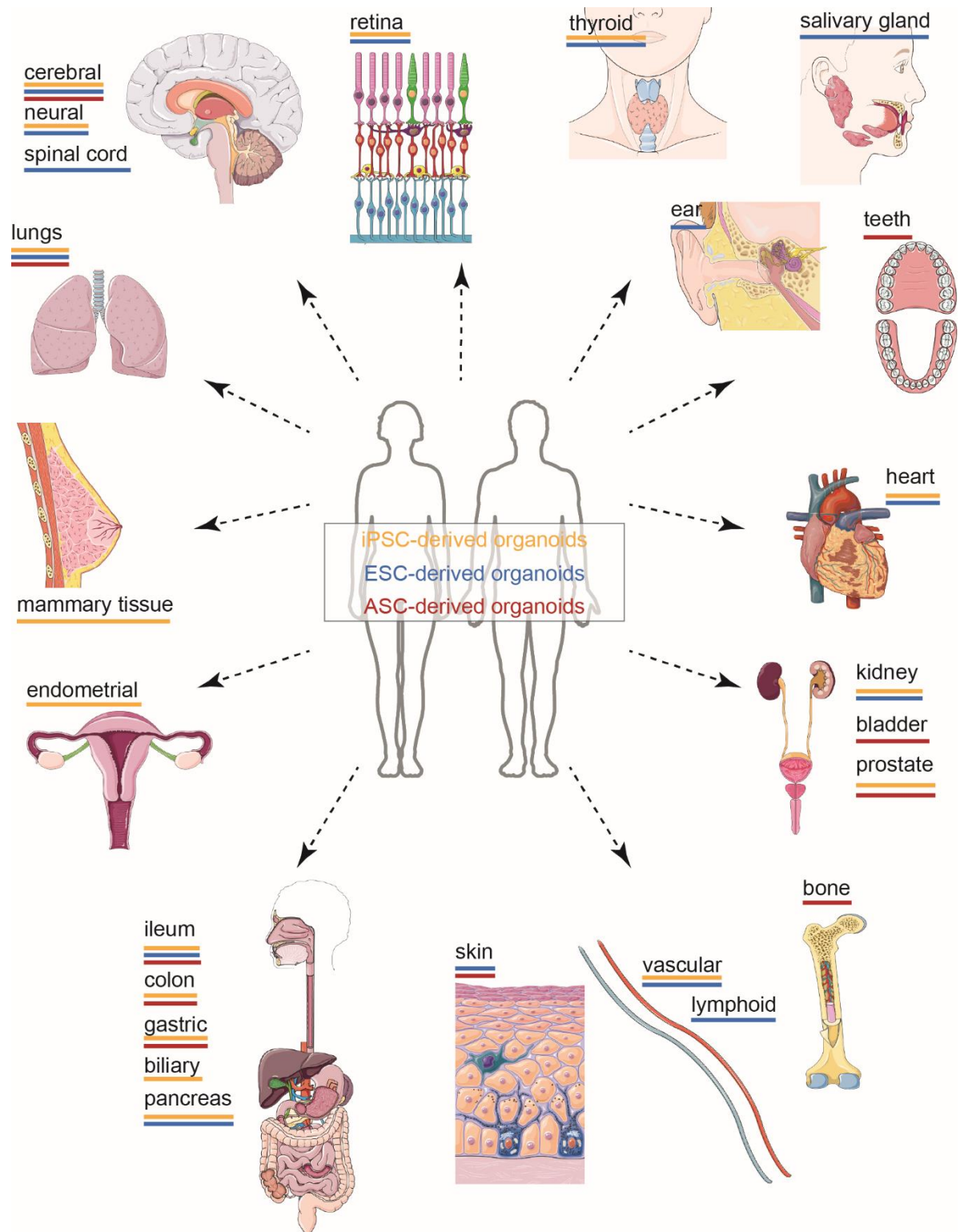


Figure II.7. Successful cultivated organoids from tissues and organs. Organoid systems and tissue of origin. Different types of stem cells – pluripotent (PSC, orange), embryonal (ESC, blue) or adult (ASC, red) stem cells – of many organs and tissues have been successfully cultivated using the organoid technology. Organ and human model images are imported from Servier Medical Art by Servier, accessed on 22nd February 2022. Scheme based on (Azar *et al.*, 2021).

Simpler cell culture models mostly only contain one cell type and are cancerous, transformed or genetically immortalized, and are often not able to mimic important epithelial functions like polarization, barrier formation, and cell differentiation (Aguilar *et al.*, 2021). Thus, making investigations of host-pathogen interactions or diseases more difficult to interpret caused by error-filled genomes (Beskow, 2016; Gaush *et al.*, 1966; Ponce de Leon-Rodriguez *et al.*, 2019). Organoids can be widely used in disease investigations like genetic diseases or cancer, but also in regenerative medicine (Azar *et al.*, 2021). The most inter-individual variations, caused by genetic factors, gender and age differences, are displayed in the ASC, hence allowing very specialized investigations of diseases, but are difficult to be generalized (Azar *et al.*, 2021). In the future, organoid systems will help us to gain a better understanding of organism biology and development of diseases.

II.5.2. Organoids for analysis of host-pathogen interactions

Organoids were not only shown to be applicable for disease investigations, but also for analysis of host-pathogen interactions (Azar *et al.*, 2021). Model systems for host-pathogen interactions face the challenge to model a single organism but also to be capable of interplay with microorganisms (Aguilar *et al.*, 2021). For example, iPSC-derived lung bud infected organoids displayed shedding and swelling as seen in human lungs, depicting the capability to recapitulate lung development and potential use for investigations of fibrotic lung diseases (Chen *et al.*, 2017). Furthermore, human intestinal organoids derived from PSC were used for analysis of viral infectious diseases like the coronavirus (Zhou *et al.*, 2017), norovirus and other gastrointestinal viruses (Ettayebi *et al.*, 2016; Finkbeiner *et al.*, 2012), as well as Dengue virus, Zika virus (Lang *et al.*, 2018) and HIV infections (Ye *et al.*, 2014). In addition, ESC were already used to study host-pathogen interactions with infectious organisms as *Helicobacter pylori*, *Clostridium difficile* or *S. enterica* (Bartfeld, 2016; Leslie *et al.*, 2015). In order to investigate host-pathogen interactions, different methods can be used for 3D and 2D infections as well as tissue engineering (Aguilar *et al.*, 2021). 3D organoids can be infected by microinjection either from the apical or basal side. An alternative to microinjection is the apical-out infection, where pathogens can directly be introduced into the medium. Additionally, single cells can be simply infected during passaging of the organoids and re-embedded in the matrix until the end of infection. For 2D infections, it is possible to infect extracellular matrix-coated monolayers, the apical side of cell layers grown in transwell inserts, as well as the basolateral side or air-liquid-interfaces (Aguilar *et al.*, 2021).

II.5.3. Organoids as infection model for *S. enterica*

For analyses of host-pathogen interactions between organoids and STM, the pathogen was for example microinjected into 3D cultivated organoids already (Forbester *et al.*, 2018; Lees *et*

et al., 2019). The intestine is surrounded by a monolayer of epithelial cells, typically forming villi and crypts to enlarge the surface of the intestine, whereas the intestinal epithelium displays an effective barrier against the invasion of microorganisms (Turner, 2009). The epithelium consists of the four major differentiated cell types: enterocytes, enteroendocrine cells (EEC), goblet cells and Paneth cells. Additionally, multipotent stem cells, namely Lgr5⁺ crypt based columnar (CBC) cells and +4 cells, as well as a small population of epithelial cells that include tuft and microfold (M) cells (Beumer and Clevers, 2016; Gerbe and Jay, 2016; Iismaa *et al.*, 2018; Takashima *et al.*, 2013) are part of distinct areas of the villus and crypt, respectively. With exception of Paneth cells, which are located at the bottom of the crypt and involved in stem cell maintenance, the other differentiated cells migrate to the tip of the villus (Gassler, 2017; Gomez and Boudreau, 2021). Enterocytes are the most abundant cell type (Egi Kardia, 2020). Whereas goblet cells function in production and secretion of mucus, EECs synthesize hormones and neuropeptides. Absorptive cells are not only involved in metabolic and digestive functions, but also express specific reporters on their surface, important for the innate immune response as well as M cells (Peterson and Artis, 2014; Pott and Hornef, 2012; van der Flier and Clevers, 2009). Thus, intestinal organoids display an important investigation tool to analyze *Salmonella* infection in more detail. Especially, more insights can be gained regarding human-restricted life-threatening *S. enterica* serovars Paratyphi A (SPA) and Typhi (STY) by use of human-derived organoids.

II.6. Dual-color 3D dSTORM for localization analysis of the SPI4-T1SS

For analyses of adhesive structures, infection assays, biofilm assays, proteomic analyses and many others can be performed, but for a detailed localization-function correlation, microscopy has to be performed. However, the diffraction limit of 200 nm for conventional light microscopy, described by Ernst Abbe, is too low to resolve the exact localization of complexes in the cell. To circumvent the resolution limit of conventional wide-field microscopy of 200-300 nm in lateral and 500-800 nm in axial dimensions, super-resolution microscopy (SRM) like stochastic reconstruction microscopy (STORM) can be used (Figure II.8) (Hensel *et al.*, 2013; Schermelleh *et al.*, 2010).

II.6.1. Dual-color 3D dSTORM for localization analyses

By total internal reflection microscopy (TIRFM) the axial resolution can be increased to 100-200 nm (Schermelleh *et al.*, 2010). To further overcome the diffraction limit, specific characteristics of fluorescence dyes and techniques can be utilized (Huang *et al.*, 2010). Photoswitch-

ing between a fluorescent and a non-fluorescent state of fluorophores can increase the resolution to below 100 nm (Hell, 2009). These photoswitching signals can have either a targeting or a stochastic readout. For STORM analyses photoswitchable synthetic dyes can be used (Figure II.8) (Rust *et al.*, 2006). These dyes are able to reversibly switch between the ON- and OFF-state, resulting in a blinking state. If a second fluorophore, responsible for activation of the first fluorophore by energy transfer, is absent, the technique is called direct STORM (dSTORM) (Bates *et al.*, 2007; Hensel *et al.*, 2013; van de Linde *et al.*, 2008) (Figure II.8). In each frame, only a subset of fluorophores is in an active state at the same time. Thousands of frames are recorded and each point spread function (PSF) is calculated to its center by using a Gaussian fit (Hensel *et al.*, 2013; Sahl and Moerner, 2013). In the end, the PSFs are superimposed. The dSTORM technique was shown to also be functional in multicolor SRM (Huang *et al.*, 2008; Mass *et al.*, 2020; van de Linde *et al.*, 2008; Wilmes *et al.*, 2012). By dual-color

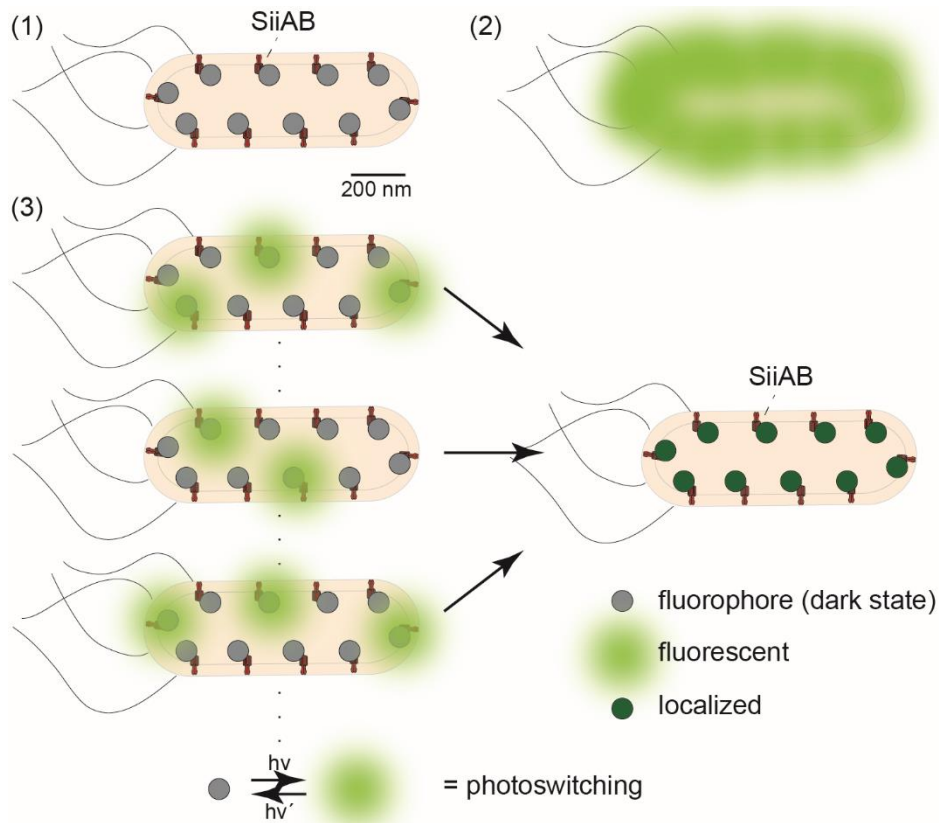


Figure II.8. Principle of photoswitching and STORM microscopy. Shown is the schematically overview of photoswitching fluorescent dyes. (1) Possible arrangement of SiiAB located in the IM, tagged with fluorophores in dark state. (2) Conventional fluorescence microscopy, where all fluorophores are activated at the time during acquisition. Due to overlapping signals of the point spread function (PSF), the information and structure cannot be clearly read out. (3) During dSTORM imaging, only a subset of fluorophores is in an active state in each frame recorded due to photoswitching. A different number of fluorophores will be in an active state in single frames. By Gaussian fit, the center of each PSF can be calculated. Thus, a super-resolution image can be reconstituted in the end.

3D dSTORM imaging, a 5-fold increase in resolution compared to 3D spatial structured illumination microscopy (SIM) can be achieved (Malkusch *et al.*, 2012). If a cylindrical lens is added in the imaging path of a TIRF microscope a localization in 3D can be obtained by changing the ellipticity and orientation of the detected signals in accordance to its relative z-position (Huang *et al.*, 2008). The exact z-position can be determined by comparing these signals with signals of a calibration curve, hence generating a reconstituted localized 3D image.

II.6.2. Novel nanobody tags – ALFA-Tag and Spot-tag

Epitope tags are widely used for many analyses like expression and purification of recombinant proteins, immune precipitations, mass spectrometry and also for immunostaining (Kocaoglu and Carlson, 2016; Nooh and Bahouth, 2017; Shi *et al.*, 2015; Smits and Vermeulen, 2016; Waugh, 2005). Different tags were generated – often as byproducts during development of antibodies against specific proteins – ideal for specific applications, but possibly not compatible with others (Braun *et al.*, 2016; Braun *et al.*, 1996; Evan *et al.*, 1985; Field *et al.*, 1988; Hochuli *et al.*, 1987; Virant *et al.*, 2018). However, due to the large size of the antibodies used as binders between the protein of interest and the fluorophore in immunostaining, these tags and antibodies are far from ideal for SRM on a subcellular level. Recently a novel class of tags, recognized by camelid single-domain antibodies, also known as nanobodies, have been introduced (Braun *et al.*, 2016; Muyldermans, 2013; Virant *et al.*, 2018). These new tags are aimed to not affect the structure, topology, localization, oligomerization, solubility or interactions of the protein (Hoffmann *et al.*, 2005; Stadler *et al.*, 2013). Therefore the tag has to be small, monomeric, highly soluble and electroneutral (Esposito and Chatterjee, 2006).

The ALFA-tag is a 15 amino acid (aa) epitope tag, forming a small and stable α -helix, independent of its position within the fusion protein (Gotzke *et al.*, 2019) (Figure II.9 A). The ALFA-tag is hydrophilic, uncharged at physiological pH and does not contain residues targeted by amine-reactive fixatives or cross-linkers (Gotzke *et al.*, 2019). This tag can be inserted at the N- or C-terminus of a protein or even between two folded domains (Gotzke *et al.*, 2019). Additionally, the ALFA-tag has the broadest application spectrum in life sciences and the developed nanobody (NbALFA) with ~ 26 pM affinity allows not only SRM, immunoprecipitations and Western blot detections, but also detection of proteins within living cells (Gotzke *et al.*, 2019). As a result of the arrangement of the complementary determining regions (CDR), forming a hydrophobic cavity, the ALFA peptide is oriented parallel to the central axis of NbALFA (Gotzke *et al.*, 2019; Muyldermans, 2013).

Another innovative small tag is the 12 aa Spot-Tag, also capable of many applications in combination with a nanobody with ~ 7 nM affinity for C-terminal insertion (Metterlein, 2018; Virant *et al.*, 2018) (Figure II.9 B). In general, the tag can be inserted N- or C-terminally. The Spot-

Tag originates from a linear epitope of the unstructured N-terminus (aa16-27) of β -catenin (BC2) (Metterlein, 2018). The wild-type sequence has been optimized by off-rate screenings to increase specific binding to the Spot-nanobody (Metterlein, 2018). These novel tags offer a number of new possibilities and have the potential to ease the use of techniques for super resolution microscopy.

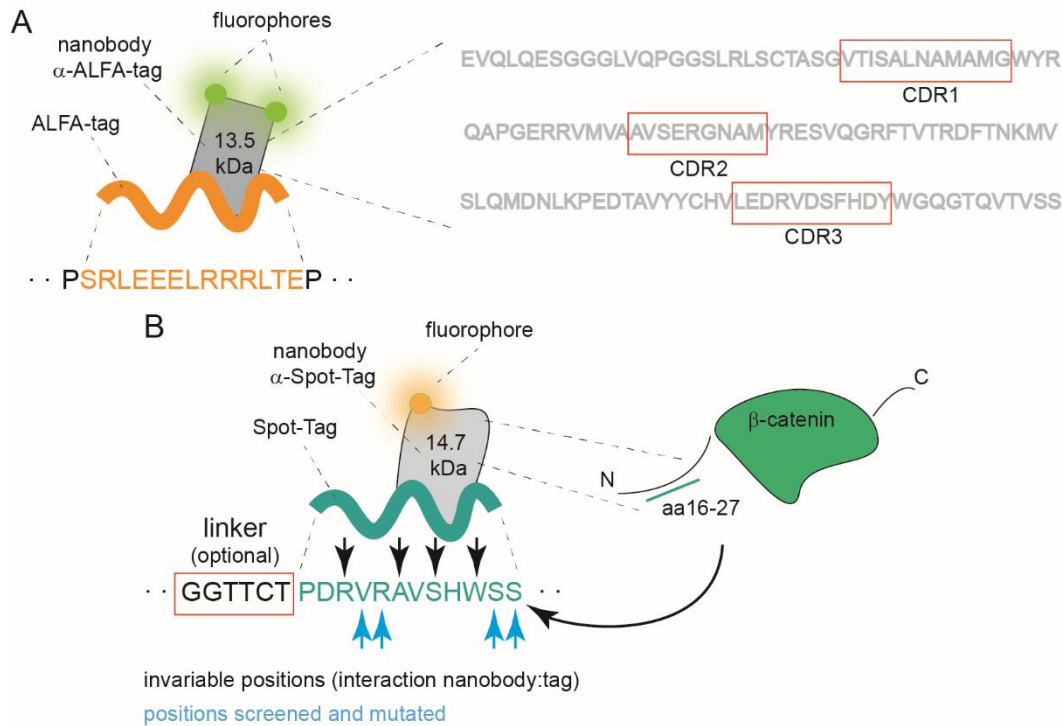


Figure II.9. Novel ALFA-tag and Spot-Tag and related nanobodies. Schematic overview of the novel ALFA-tag and Spot-Tag. Shown are the sequences of the ALFA-tag (A) and the Spot-Tag (B), forming α -helical structures, which are specifically bound by their nanobodies, coupled to two fluorophores (nanobody α -ALFA-tag) or one fluorophore (nanobody α -Spot-Tag). A) Left: The ALFA-tag is flanked by prolines. Right: The complementary determining regions (CDR) form a hydrophobic cavity, in which the ALFA peptide can introduce parallel to the central axis of NbALFA. B) Left: A linker, here optimized for *E. coli*, can be introduced to enhance performance. Right: The Spot-Tag originates from the aa16-27 of β -catenin and besides invariable positions (left, black), additional positions were screened and mutated (left, blue) to increase binding specificity of the nanobody α -Spot-Tag (Metterlein, 2018). Models based on (Gotzke *et al.*, 2019; Metterlein, 2018).

II.7. Aims of this work

In this work, the SPI4-T1SS, its substrate SiiE and the non-canonical subunits SiiAB were taken into focus. The following open questions and topics were addressed in this thesis:

- i) How is SiiE retained on the bacterial surface? Since SiiE is secreted in two steps like the giant T1SS substrates LapA and MplBP (Guo *et al.*, 2017; Smith *et al.*, 2018a), I

- investigate whether SiiE is retained in a comparable way in the OM, or in a novel assembly, e.g. in the whole channel and if there is a potential retention domain in the N-terminus (Figure II.10 i).
- ii) What is the mechanism of SiiE release? Post-translational modifications resulting in substrate release into the environment were described for various T1SS substrates (Smith *et al.*, 2018b). The release of Bacteriocins and BTLCP-linked adhesins for example is mediated by proteolytic cleavage (Smith *et al.*, 2018b). Consequently, I am interested in whether SiiE is released by post-translational modification, e.g. proteolytic cleavage, as it has been shown for other T1SS (Figure II.10 ii).
 - iii) Do SiiAB contribute to SiiE secretion? If so, at which step during secretion are they involved? SiiAB function as a proton channel and are involved in invasion and SiiE retention (Wille *et al.*, 2014). In the context of this thesis, I want to shed more light on the detailed mechanism of SiiAB function during SiiE secretion (Figure II.10 iii).
 - iv) What does SiiB possess an extended cytosolic domain for? SiiB was shown to possess a large cytosolic domain, comparable to MotA (Blair and Berg, 1991; Dean *et al.*, 1984; Deme *et al.*, 2020b; Wille *et al.*, 2014; Zhou *et al.*, 1995). Additionally, such an extended cytosolic domain was described for mechanosensitive channels. Thus, I also focus on potential functions of the cytosolic domain of SiiB solely for adhesion, invasion and SiiE secretion (Figure II.10 iv).
 - v) What is the subcellular localization of SiiAB? Intriguingly, there are similarities to the stator of the flagellum, MotAB (Kirchweger *et al.*, 2019; Wille *et al.*, 2014) and the flagellum is co-regulated with virulence genes during invasion of STM. Since different conserved stator complexes were shown to act at the flagellum in dependence of environmental changes, I conclude a possible function of SiiAB at the flagellum. I want to implement dual-color 3D dSTORM SRM to visualize the subcellular localization of SiiAB and possible cross-talks between the SPI4-T1SS and the flagellum (Figure II.10 v).
 - vi) In addition to the analysis of the SPI4-T1SS, another focus of this work is the establishment of intestinal organoid cell culture for microscopic and quantitative analyses of *S. enterica* infection processes, with focus on adhesion and invasion. As organoid cell culture with its diverse cell types and possibilities was shown to be a method with immense potential for host-pathogen interaction analyses in the future, it is critical to develop assays capable to gain new insights in these processes (Figure II.10 vi).

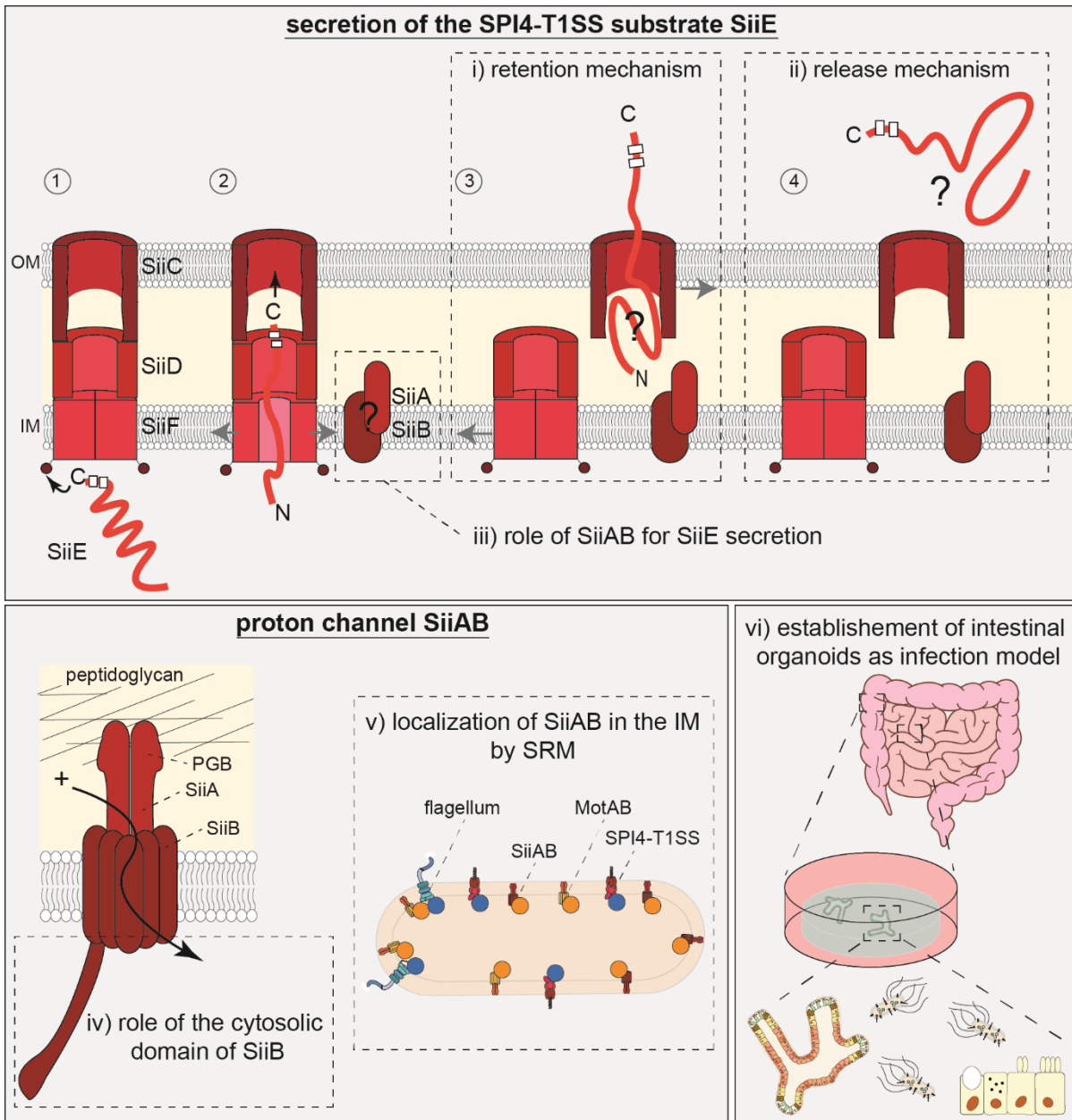


Figure II.10. Aims of the thesis. The SPI4-T1SS is essential for adhesion to polarized epithelial cells. The SPI4-T1SS consist of the ABC transporter SiiF in the IM, the PAP SiiD in the periplasm and the secretin SiiC in the OM. Two non-canonical proteins encoded on SPI4, SiiA and SiiB, form a proton channel in the IM. During secretion of the SPI4-T1SS substrate SiiE, it is retained on the cell surface, mediating first close contact to the host cell apical side. Since it is not known if SiiE is retained in whole T1SS channel or in a single subunit like SiiC as described for LapA and LapE, the detailed secretion mechanism is addressed (i). Additionally, because *siiAB* mutants also show an altered retention, they may play a role in SiiE secretion (iii). In a last step, SiiE is secreted into the medium, but the release mechanism is also not known. Thus, I want to analyze the release of SiiE (ii). SiiB possesses an extended cytosolic domain comparable to MotA and I am interested in its function for invasion related proteins (iv). Since the localization and function of SiiAB is not clear, I want to analyze the subcellular localization of the proton channel by 3D dSTORM SRM and role for invasion related complexes (v). Organoid cell culturing opens new opportunities. Thus, another focus of this work is the establishment of intestinal organoid cell culture for microscopic and quantitative analyses of *S. enterica* infection, with focus on adhesion and invasion (vi).

III. Results

III.1. Conserved secretion mechanisms of the giant adhesin SiiE of *Salmonella enterica* and other two-step secreted adhesins

Nathalie Sander¹ and Michael Hensel^{1,2}

¹Division of Microbiology, University Osnabrueck, Osnabrueck, Germany

²CellNanOs – Center for Cellular Nanoanalytics, University Osnabrueck, Osnabrueck, Germany

III.1.1. Abstract

Type 1 secretion systems (T1SS) are characterized by their structure, consisting of an ATP-binding cassette (ABC) transporter, a periplasmic adaptor protein (PAP) and an outer membrane (OM) secretin. Some functions and mechanisms are homologous to each other and conserved. Most T1SS secrete their substrates in one step, but also two-step secretion is described for substrates like the biofilm-associated adhesin LapA of *Pseudomonas* spp. or the ice-binding protein of *Marinomonas primoryensi* (MplBP). The virulence-associated adhesin SiiE of *Salmonella enterica*, encoded by genes on *Salmonella* Pathogenicity Island 4 (SPI4), is known to be retained on the cell surface during secretion. SiiE mediates the first close contact to the host cell membrane, essential for the efficient invasion by the pathogen. However, the detailed mechanisms for retention and release of SiiE are still not known: Are there conserved steps in secretion comparable to other known T1SS? Here we show by various over-expression experiments, structure modelling, cryo-TEM analyses, and OM isolation that SiiE is retained in the OM and that the SPI4-T1SS dissociates during the secretion process. Furthermore, we found a potential retention domain in the N-terminal part of SiiE that appears absent in released SiiE. Additionally, the accessory proteins SiiAB are involved in steps prior to retention in the OM. With these results, we gained new insights in secretion process of SiiE and can limit possible modes of action of SiiE during adhesion and invasion.

III.1.2. Introduction

Type 1 secretion systems (T1SS) are highly conserved regarding their structure and also mechanisms. Besides bacteriocins as CvaC from *Escherichia coli*, so-called repeats-in-toxins (RTX) like CyaA and HlyA from *Bordetella pertussis* and *E. coli* represent well described T1SS substrates. The model resulting from various studies suggests a one-step secretion without an intermediate step during secretion where the unfolded substrates are directly translocated into the environment (Andersen *et al.*, 2000; Kanonenberg *et al.*, 2013; Koronakis *et al.*, 1989; Mackman *et al.*, 1985). Due to low Ca^{2+} concentrations in the cytoplasm, the glycine- and aspartate-rich Ca^{2+} -binding RTX motifs are intrinsically disordered (Chenal *et al.*, 2009; Gangola and Rosen, 1987). Upon secretion, the Ca^{2+} -rich environment leads to folding of these regions as a consequence of direct Ca^{2+} -binding, resulting in the final folded structure, essential for the biological functions (Chenal *et al.*, 2009).

T1SS can secrete diverse proteins, many playing a role for the pathogenicity of the bacteria, ranging from small substrates like bacteriocins (<10 kDa) up to giant adhesins like LapA from *Pseudomonas* spp. (900 kDa) (Smith *et al.*, 2018a) or the ice-binding protein (IBP) of *Marinomonas primoryensi* (MplBP, 1.5 MDa) (Guo *et al.*, 2017). The 600 kDa virulence-associated adhesin SiiE of *Salmonella enterica* serovar Typhimurium (STM) also belongs to the giant T1SS secreted substrates (Gerlach *et al.*, 2007b). Large adhesins are often involved in host colonization, invasion, or beneficial interactions with the host as described for SiiE (Gerlach *et al.*, 2007b).

Nevertheless, despite this diversity, there are homologies in structure and mechanisms of secretion. Most T1SSs consist of the characteristic canonical subunits: an ATP-binding cassette (ABC) transporter in the inner membrane (IM), a periplasmic adaptor protein (PAP) located in the periplasm and an outer membrane (OM) secretin (Wagner *et al.*, 1983; Wandersman and Delepelaire, 1990). Additionally, the dissociation of the OM secretin from the ABC transporter-PAP complex during secretion process is described (Smith *et al.*, 2018b). However, there are also exceptions, combining sec-translocation across the IM with the secretion via a PAP and secretin as it is described for CexE and Aap (T1SSp) (Icke *et al.*, 2021). Despite the differences in secretion mechanisms, T1SS have three main steps in common: (1) the recognition of the unfolded substrate in the cytoplasm by the ABC transporter, (2) the secretion through the canonical subunits of the T1SS, and (3) the release into the extracellular space (Smith *et al.*, 2018b). Conserved strategies have been described for these steps: The substrate recognition (1) can take place C-terminal like for HlyA and LapA, or N-terminal like for CvaC (Boyer and Tai, 1998; Gray *et al.*, 1986; Jarchau *et al.*, 1994; Mackman *et al.*, 1987). The secretion (2) can be divided into one-step secretion like for bacteriocins as CvaC and RTX toxins like HlyA

(Boyer and Tai, 1998; Kanonenberg *et al.*, 2013; Thanabalu *et al.*, 1998) and two-step secretions as described for RTX adhesins like LapA (Boyd *et al.*, 2012; Navarro *et al.*, 2011; Newell *et al.*, 2011). For the two-step secretion an intermediate is described, where the substrate is retained in the OM during secretion and released into the environment under defined conditions (Smith *et al.*, 2018a). For release into the environment (3) or activation, T1SS substrates can be proteolytically cleaved like CvaC and LapA, or post-translationally modified like HlyA.

In general, T1SS ABC transporters contain at least two transmembrane domains (TMD) and two nucleotide binding domains (NBD) (ter Beek *et al.*, 2014). If a single ABC transporter harboring a TMD and a NBD dimerizes in the IM, the requirements for a T1SS are satisfied (Smith *et al.*, 2018b). By cross-linking experiments, it was shown that the ABC transporter HlyB and the PAP HlyD can form a stable complex, even without binding of the substrate HlyA (Thanabalu *et al.*, 1998). Upon binding of HlyBD to the unfolded C-terminal secretion signal of HlyA, the HlyBD-TolC secretion system is initiated. Following secretion of HlyA, beginning with the C-terminus, the complex disassembles into HlyBD and TolC again (Lenders *et al.*, 2015; Thanabalu *et al.*, 1998). TolC is a well-characterized OM protein, forming the homotrimeric secretin complex, essential for various secretion systems. Each monomer consists of a 40 Å long β -sheet domain located in the OM, a 100 Å long periplasmic α -helical domain and a periplasmic α/β domain (Koronakis *et al.*, 2000). The α -helical domain controls opening and closing of the membrane pore. In the closed conformation, the pore diameter is only 3.9 Å, thus preventing secretion. In the open state, its diameter is increased to approximately 20 Å (Pei *et al.*, 2011). The secretin TolC can also form a complex with the bacteriocin T1SS subunits CvaAB (Gilson *et al.*, 1990). Although in contrast to HlyA, CvaC is recognized at its N-terminal double glycine (GG) motif by the C39 peptidase domain of CvaB, it is as well secreted from the C- to the N-terminus (Gilson *et al.*, 1990). The C39 peptidase cleaves CvaC near the GG motif, leading not only to secretion of the substrate, but also to activation of the bacteriocin. It was shown that HlyB and many other T1SS ABC transporters contain additional N-terminal regions, very similar to the C39 peptidase domain of CvaB (Lecher *et al.*, 2012). In contrast to CvaB, the C39 domain of HlyB lacks the critical cysteine residue (C39), thus rendering the domain catalytically inactive. This domain was called the C39-like domain (CLD) (Lecher *et al.*, 2012). The CLD of HlyB binds to the glycine-rich RTX motifs, located at the C-terminus of HlyA. However, it could be shown that ligand binding sites are located at opposite sites in C39 and CLD domains of CvaB and HlyB (Lecher *et al.*, 2012).

In addition to the canonical subunits, several T1SS substrates require accessory proteins for their secretion and/or proper function. Some proteins like HlyA are synthesized in a premature form. HlyA is activated by post-translational modification by the acyltransferase HlyC, which

catalytically transfers acyl chains to Lys⁵⁶⁴ and Lys⁶⁹⁰ of pro-HlyA, leading to mature α -hemo-lysin of *E. coli* (Ludwig *et al.*, 1996). A new family of bacterial transglutaminase-like cysteine proteinases (BTLCP) with invariant Cys-His-Asp catalytic triads, often linked to T1SS apparatus and large RTX proteins was described (Ginalski *et al.*, 2004). It was suggested that these BTLCP proteins post-translationally modify the substrates by either transamidase, acetylase or hydrolase activity (Ginalski *et al.*, 2004). As an example for the BTLCP, LapG, a periplasmic Ca²⁺-dependent cysteine protease, cleaves an N-terminal di-alanine motif, resulting in the release of LapA into the environment, and thus a decrease in biofilm formation (Boyd *et al.*, 2012; Boyd *et al.*, 2014; Navarro *et al.*, 2011; Newell *et al.*, 2011). Additionally, LapG activity is controlled by the IM c-di-GMP receptor LapD (Boyd and O'Toole, 2012). It was shown that the phosphodiesterase domain of LapD binds cytoplasmic c-di-GMP, leading to conformational changes in LapD that promote LapG binding (Navarro *et al.*, 2011; Newell *et al.*, 2011; Newell *et al.*, 2009). Due to this interaction, LapA is able to remain in the OM to promote biofilm formation. Contrarily, low cytoplasmic c-di-GMP levels result in dissociation of LapG from LapD and cleavage of LapA (Cooley *et al.*, 2016a; Monds *et al.*, 2007; Navarro *et al.*, 2011; Newell *et al.*, 2009). Hence, these two accessory proteins regulate cell surface retention of the biofilm-associated RTX adhesin LapA in response to levels of a cytoplasmic second messenger and by proteolytic cleavage. Homologous proteins to LapG and LapD were found in genomes of over 1,300 bacterial species from 120 classes of the Proteobacteria (Smith *et al.*, 2018a), underlining that this strategy for adhesin localization is quite common (Ambrosius *et al.*, 2016; Cooley *et al.*, 2016b; Gjermansen *et al.*, 2010; Perez-Mendoza *et al.*, 2011; Zhou *et al.*, 2015).

The T1SS of STM, encoded by genes in SPI4, displays the characteristic subunit composition of T1SS, comprising the ABC transporter SiiF in the IM, SiiD as PAP, and SiiC as secretin. As the other T1SS substrates described above, the 600 kDa substrate SiiE associates with the IM, is recognized by its T1SS and subsequently secreted into the extracellular space (Wagner *et al.*, 2011). The secretion of SiiE is dependent on extracellular Ca²⁺, binding to the type I and type II Ca²⁺ binding sites located at the 53 repetitive bacterial immunoglobulin (BIg) domains of SiiE (Barlag and Hensel, 2015; Griessl *et al.*, 2013). Comparable to LapA and *MplBP*, SiiE is retained on the cell-surface during secretion process, mediating the first close contact to the host cell membrane during invasion process (Gerlach *et al.*, 2007b). Nevertheless, it was not known if retention occurs in the assembled channel or only in the secretin SiiC, as when homologous structures such as LapA and *MplBP* were considered, the latter might even be more likely. After retention on cell surface, SiiE is released into the extracellular space; the detailed mechanism however was not described. Additionally, the SPI4 also encodes two accessory non-canonical subunits, namely SiiA and SiiB, known to form a proton channel in the IM (Wille *et al.*, 2014). It was shown that SiiAB play an essential role in adhesion and invasion, but their

role for the SiiE secretion process is still not fully understood. Thus, we set out to gain new insights into the secretion mechanism of SiiE and the cognate T1SS, and to compare these with previously described secretion mechanisms.

III.1.3. Results

III.1.3.1. Retention of SiiE by SiiC and dissociation of the complex during secretion of SiiE

During the secretion process, not only ABC transporters in the IM and PAP, but also the secretins play important roles. Since TolC is the best-characterized secretin, we chose TolC for comparison to SPI4-T1SS secretin SiiC. Additionally, we used LapE, which retains LapA in the OM, for our structural analyses. These three OM proteins have similar molecular weights of 54, 50, and 50.5 kDa for TolC, LapE, and SiiC, respectively, and thus are good candidates for comparative analysis.

Bioinformatic analyses reveal comparable structures of secretins TolC, LapE and SiiC

Prediction algorithms can provide information about structure and function of unknown proteins by considering homologue structures. Hence, protein models can be estimated based only on an analysis of the amino acid (aa) sequence. By the analysis of the primary and secondary structures of TolC, LapE and SiiC via ali2D (Gabler *et al.*, 2020), we did not only see comparable arrangements of the aa sequence regarding charge, hydrophobicity and size, but also in the secondary structure pattern (Figure S III.1.1, Figure III.1.1 D). For an improved spatial simulation, we used the tertiary structure model prediction tool trRosetta (Du, 2021; Yang *et al.*, 2020). The determined TM-scores are indicative of the validity of prediction (Figure III.1.1 D). All calculated TM-scores showed very high (TolC, 0.782 and LapE, 0.752), or high confidence (SiiC, 0.645) in predicted tertiary structure models. We could show that TolC, LapE and SiiC are predicted to possess comparable structural arrangements with a β -sheet domain (blue) located in the OM and an α -helical domain (orange) ranging into the periplasm (Figure III.1.1). As the length of these domains is described for the crystal structure of TolC (Koronakis *et al.*, 2000), we used these known parameters to validate the measurements for the indicated length. The published length of the β -barrel domain (40 Å), as well as the periplasmic α -helical domain (100 Å) were conclusive with the measurements we performed (in brackets), thus validating the approach (Figure III.1.1 A). The β -sheet domain of LapE showed a comparable length of 38.3 Å (Figure III.1.1 B). The predicted β -sheet domain of SiiC (30 Å) was smaller than those of other secretins (Figure III.1.1 C). Nevertheless, monomers of TolC, LapE and SiiC all comprise four β -sheets, indicative of a certain homology. In comparison to TolC, LapE and SiiC seem to have a longer periplasmic α -helical domain with 107 Å.

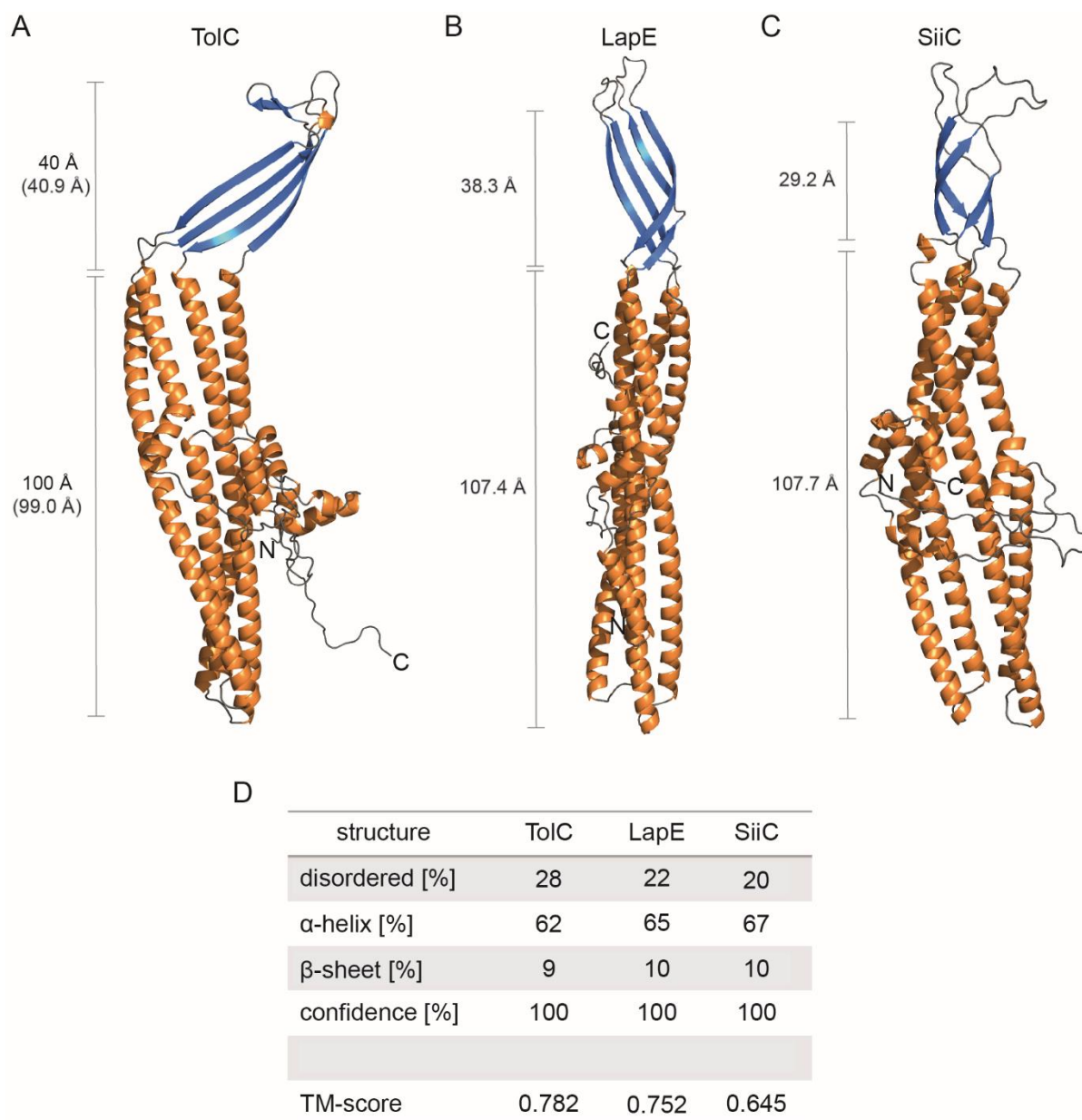


Figure III.1.1. Structural prediction of the OM proteins TolC, LapE and SiiC. A) Tertiary structure model prediction for the OM secretin TolC by trRosetta (Du, 2021; Yang *et al.*, 2020). A 40 Å long β-sheet domain is inserted in the OM, whereas the 100 Å periplasmic α-helical domain is located in the periplasm (Koronakis *et al.*, 2000). Gray numbers in brackets show length measured in Pymol. B-C) Tertiary structure model prediction for the OM secretins LapE (B) and SiiC (C) by trRosetta analyses. Figures indicate the predicted length. Loop=gray, β-sheet=blue, α-helix=orange. D) Percentages of predicted secondary structure and confidence, calculated by Phyre2 algorithms. TM-score for modelling by trRosetta (D). TM-score > 0.5 = high confidence, TM-score > 0.7 = very high confidence.

SiiC oligomers show a higher instability than TolC trimers

It is known that TolC forms trimers in the OM to build the secretion channel (Koronakis *et al.*, 1997). In order to investigate the oligomeric state of SiiC, we used TolC as a positive control for oligomerization (Figure III.1.2). For the analysis, we used STM WT and *siiC* overexpression

strain (introduced in more detail later). Cells were grown for 2.5 h, pelleted and treated with SDS cracking buffer, containing 2% or 4% SDS. Cracking buffer with 2% SDS was used for a less harsh treatment of the samples. In addition, the samples were boiled only as a control for monomeric TolC and SiiC (*). We were able to show an expected size of 54 kDa for TolC in samples denatured by boiling, concurrent with monomeric TolC (Figure III.1.2, left, *). If we treated the samples with SDS buffer without boiling, only slight bands appeared at 54 kDa and we detected an increased signal at ~160 kDa, especially in conditions with 2% SDS. In contrast to TolC, SiiC only showed monomeric sizes (50.5 kDa) in all conditions (Figure III.1.2, right). To exclude effects of the *siiC* overexpression on a possible trimeric state of SiiC, we additionally tested plasmid-encoded *siiC* without overexpression, but also could not confirm a stable trimeric state for SiiC (data not shown). However, considering TolC, LapE and other described secretins and the predicted tertiary structure of SiiC, a trimeric state of SiiC is the most probable situation, which led us to the assumption that SiiC oligomers might be less stable than TolC trimers.

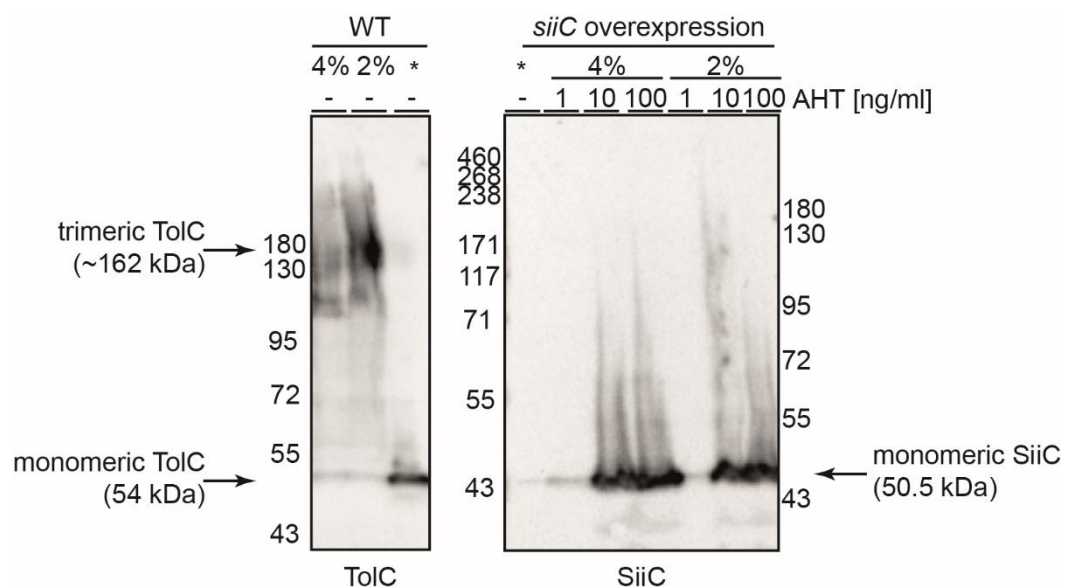


Figure III.1.2. Western blot analysis of oligomeric states of TolC and SiiC. Western blot analysis of SiiC (right) in comparison to TolC (left). Strains were inoculated for 2.5 h, 1 ml was harvested and pellet was resuspended in SDS cracking buffer according to the OD_{600} . SDS concentrations of 2% and 4% were tested for less harsh treatment of the samples. Additionally, samples were boiled (*) as a control. Western blot was performed with antibodies α -TolC (1:2,000) and α -HA (1:10,000), α -rabbit HRP-conjugated (1:10,000) and α -rat HRP-conjugated (1:10,000). Marker and molecular weight of the proteins as indicated.

The siiC overexpression leads to higher SiiE retention, adhesion and invasion

Since the retention in the secretin is described for RTX adhesins like *MplBP* and *LapA* (Guo *et al.*, 2018; Smith *et al.*, 2018a), we decided to analyze if SiiE is retained in the whole channel

or only in the secretin SiiC (Figure III.1.3 A) by overexpression of the OM protein SiiC (Figure III.1.3 B). Assuming that SiiE is retained in the assembled T1SS, overexpression of *siiC* alone would not have an effect on SiiE retention and, consequently, would not increase STM adhesion and invasion (Figure III.1.3 B, left). In contrast, in the case of retention of SiiE only in the OM, an overexpression of *siiC* could lead to an increase in SiiE retention, adhesion, and invasion (Figure III.1.3 B, right). This experimental set-up gave us first hints towards the detailed mechanism behind SiiE retention. *siiC* overexpression occurred plasmid-encoded under *tetA* promoter control, thus making *siiC* expression inducible with anhydrotetracycline hydrochloride (AHT). First, induction was verified by Western blot analysis of protein biosynthesis with different AHT concentrations ranging from 0-100 ng/ml AHT (Figure III.1.3, C). The subcultures were induced with AHT 1 h after inoculation and grown for an additional 1.5 h. Due to the lack of an antibody against SiiC, a HA-Tag was fused C-terminally to SiiC. When AHT was omitted, we did not detect any signal for the HA-Tag. Following induction with 10 ng/ml AHT, we received the best expression result. Since we obtained a double band and no increased SiiC biosynthesis with 50 and 100 ng/ml AHT, we decided against such high concentrations. The overexpression of *siiC* did not result in any growth defects (Figure S III.1.2). We tested the effects of overexpression of *siiC* in the OM on SiiE retention by confocal microscopy (Figure III.1.3, D) and dot blot analysis (Figure III.1.4, A and B). Due to the fact that $\Delta siiC$ behaves like $\Delta siiE$ (Figure III.1.3, D) (Gerlach *et al.*, 2008), only $\Delta siiC$ is shown as a negative control from this point on. As a positive control, we used STM WT. Not only could we visually demonstrate that an increased amount of SiiC in the OM leads to higher SiiE retention on the cell surface (Figure III.1.3, D), but showed also by quantitative Dot blot analysis that SiiE retention was significantly increased (164%) compared to WT (Figure III.1.4, A). Furthermore, we noticed that the *siiC* overexpression led to the characteristic secretion kinetic with a retention maximum after 2.5 h and a minimum after 6 h and a secretion maximum after 6 h and minimum after 2.5 h (Figure III.1.4, B). As a result of increased SiiE amounts retained on the cell surface, also adhesion (175%) and invasion (142%) increased (Figure III.1.4, C and D). Interestingly, adhesion showed a higher increase than invasion, underlining the essential role of SiiE for adhesion to polarized cells. Although the kinetics of secretion were not altered, we have been able to show a phenotypic difference to the WT regarding SiiE retention, adhesion and invasion in dependence of the OM secretin SiiC, suggesting a role of SiiC in regulating the amount of SiiE present on the cell surface.

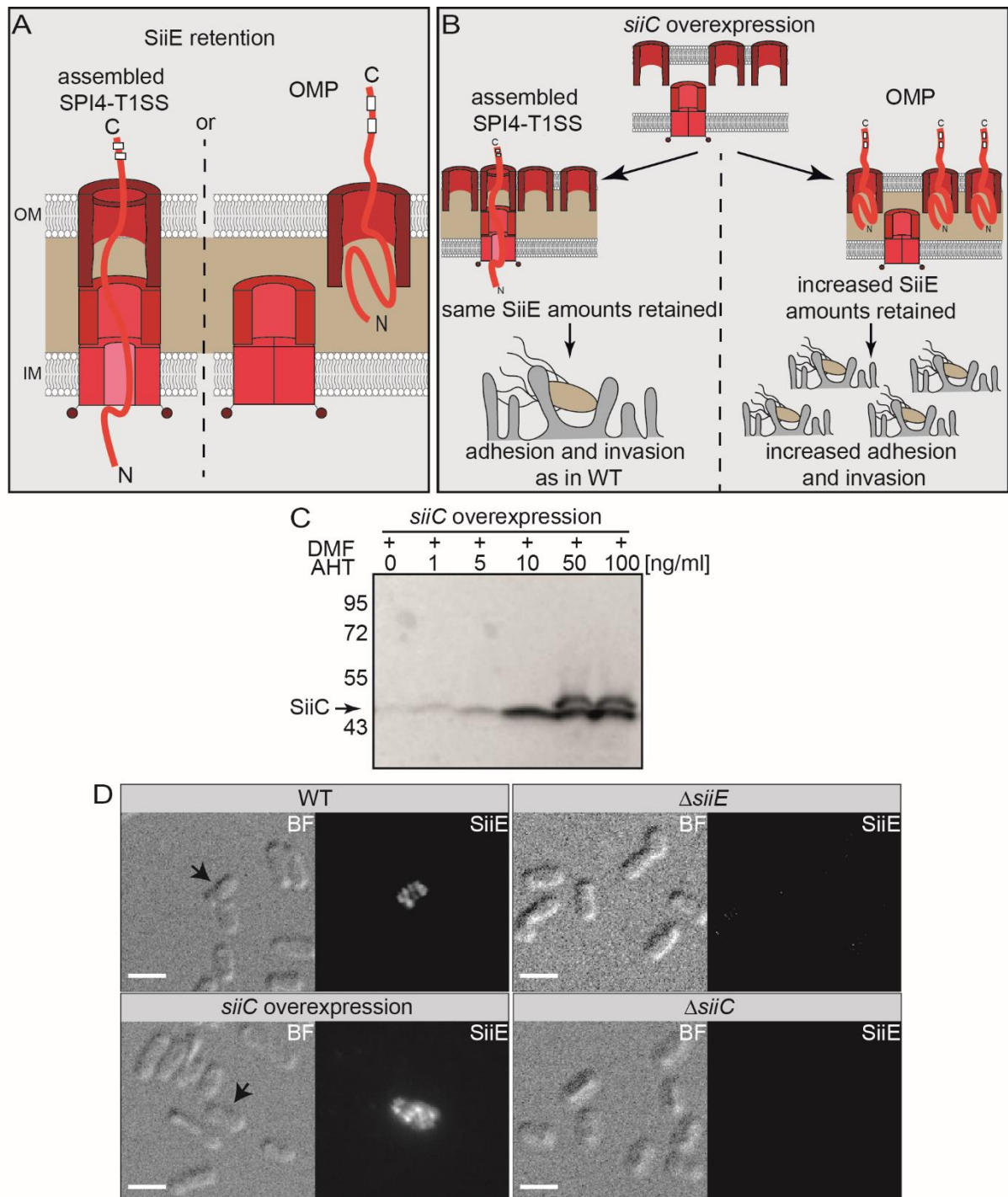


Figure III.1.3. *siiC* overexpression – experimental procedure and effect on SiiE surface signal. A) Illustration of the secretion step in focus. Until now, SiiE retention has been assumed to occur in the fully assembled channel, with the N-terminus localized in the cytoplasm (left). However, it is also conceivable that retention, as described for LapA and *MplBP*, occurs only in the secretin, here SiiC (right). B) Schematic overview of the experimental approach. *siiC* overexpression and analysis of retention, secretion, adhesion and invasion. If SiiE is not retained only in SiiC, overexpression will not lead to an increased SiiE retention, adhesion and invasion (left). If SiiE is retained only by SiiC, overexpression will lead to an increased SiiE retention, adhesion and invasion (right). C) Western blot against HA-Tag (SiiC) following induction with indicated AHT concentrations. Subcultures were grown for 2.5 h with AHT induction after 1 h, pelleted and boiled in SDS cracking buffer. SDS-PAGE and Western blot with antibodies α -HA (1:10,000) and α -rat HRP-conjugated (1:10,000) were performed. Marker as indicated. D) Microscopic analysis of SiiE surface signal. Subcultures were grown for 2.5 h with AHT induction after 1 h, pelleted by centrifugation and fixed with 3% PFA in PBS. Bacteria were stained for surface-bound

SiiE with Alexa488-coupled antibody against primary α -SiiE antibody. For microscopy, a widefield microscope, 100x with oil was used. Scale bar, 2 μ m.

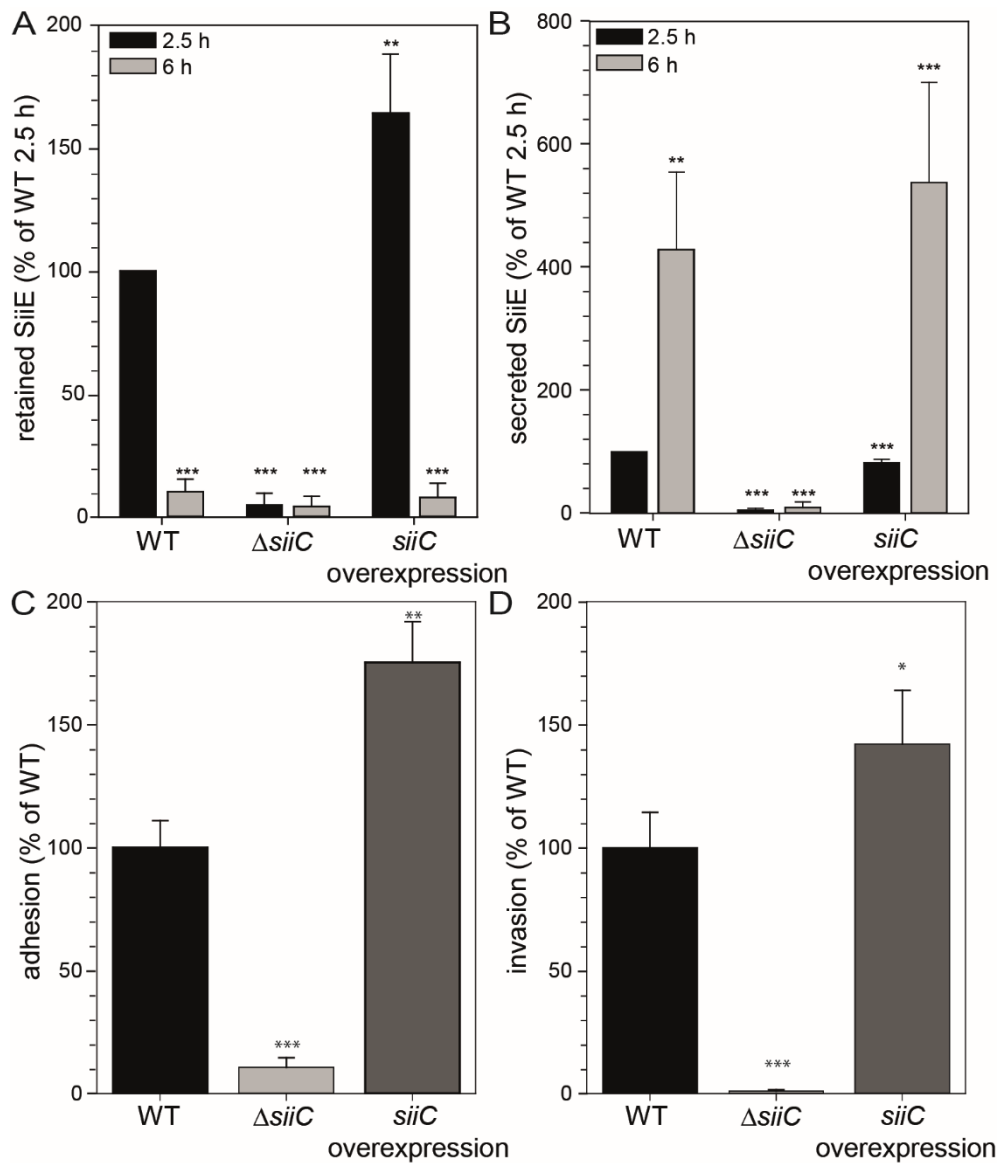


Figure III.1.4. SiiE retention, secretion, adhesion and invasion in response to *siiC* overexpression. A-B) Dot blot analysis of the retention (A) and secretion (B) of SiiE in response to *siiC* overexpression. Subcultures were grown for 2.5 h and 6 h with AHT induction after 1 h. For retention samples, cells were fixed with 3% PFA in PBS and for secretion samples, the supernatant was precipitated with TCA and boiled according to the OD_{600} . 5 μ l of the samples were spotted on equilibrated membranes in triplicates and membranes were decorated against SiiE and LPS. The LPS signal was used for normalization of sample loading. C) Adhesion to and D) invasion of polarized MDCK cells following *siiC* overexpression. Subcultures were grown for 2.5 h with AHT induction after 1 h and MDCK were infected with MOI 5. Statistical analyses compared to WT with at least biological triplicates by two-tailed t-test: ***, $p < 0.001$; **, $p < 0.01$; *, $p < 0.05$; n.s., not significant.

SiiE is retained by SiiC only

To find more evidence for a direct interaction of SiiE with SiiC in the OM, we isolated the OM and then performed a pulldown assay (Figure III.1.5). Another plasmid under *tetA* promoter control was used with *siiABCDEF* encoded. For practical reasons, a truncated SiiE form with a deletion of Blg 2 to 48 was used (mini SiiE). Protein biosynthesis and functionality were confirmed before by Western blot and Dot blot analyses (data not shown). The OM isolation was performed with 2.5 h subcultures, induced as described above. Since we used 2.5 h cultures, there was not yet much mini SiiE in the supernatant (S) detectable (Figure III.1.5, A). As a control for cell integrity of the starting cultures, we also checked for SiiC contaminations in the supernatant (S). Following the OM isolation with EDTA, we detected mini SiiE and SiiC in the OM fraction (OM). This fraction was used for incubation with Protein A sepharose beads coupled to SiiE antibodies. As a control for the self-labeled beads, purified mini SiiE was used (Figure III.1.5, B). Proteins were eluted with glycine, pH 2.6 (E1) and beads were boiled in SDS cracking buffer following glycine elution as a control (E2). Since we were able to elute not only mini SiiE but also SiiC from an OM fraction, we assume direct interaction of SiiC and SiiE.

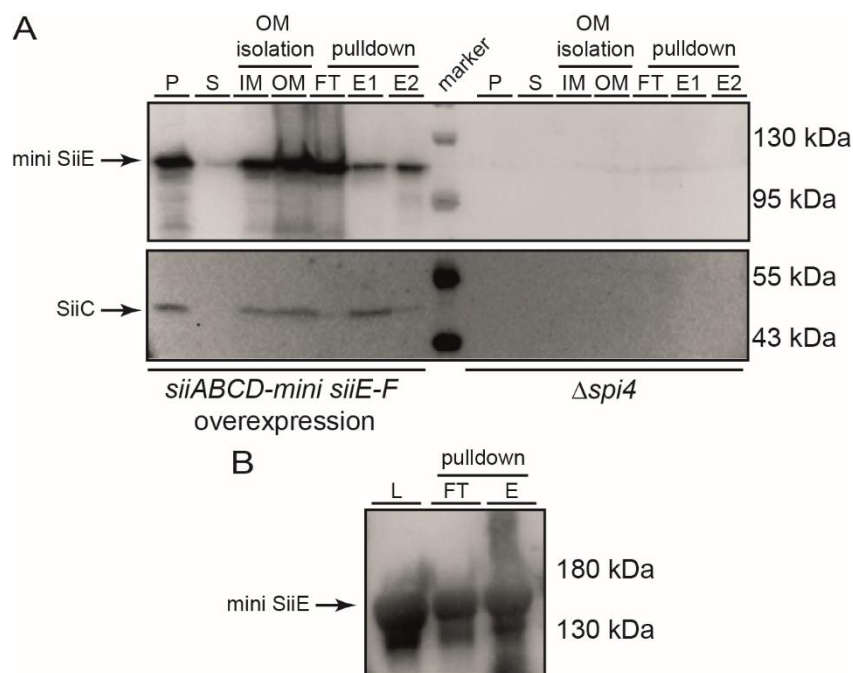


Figure III.1.5. Evidence for a direct interaction of SiiE and SiiC. A) Cells were grown for 1 h, induced by addition of AHT, and further cultured for 1.5 h and harvested by centrifugation. Pellet was resuspended in sucrose-containing buffer and treated with lysozyme and EDTA. After incubation, OM containing supernatant was collected by centrifugation. OM supernatant was incubated with Protein A Sepharose beads decorated with α -SiiE antibody. Whole cell lysate pellet (P), supernatant (S), IM/intact cell fraction (IM) and OM fraction (OM) after OM isolation, flow through (FT) and eluted samples (E1, E2) are shown. Eluate 1 = treatment with glycine, pH 2.6, for a less harsh elution of mini SiiE together with SiiC. Neutralization of the sample occurred with 1 M Tris. Eluate 2 = boiling at 100 °C for 5 min after glycine step. B) As a control for bead binding, beads were also treated with purified mini SiiE as indicated. Load (L, 10 μ g), flow through (FT) and eluate (E) after boiling the beads are shown. Marker as indicated on the right side of the blots.

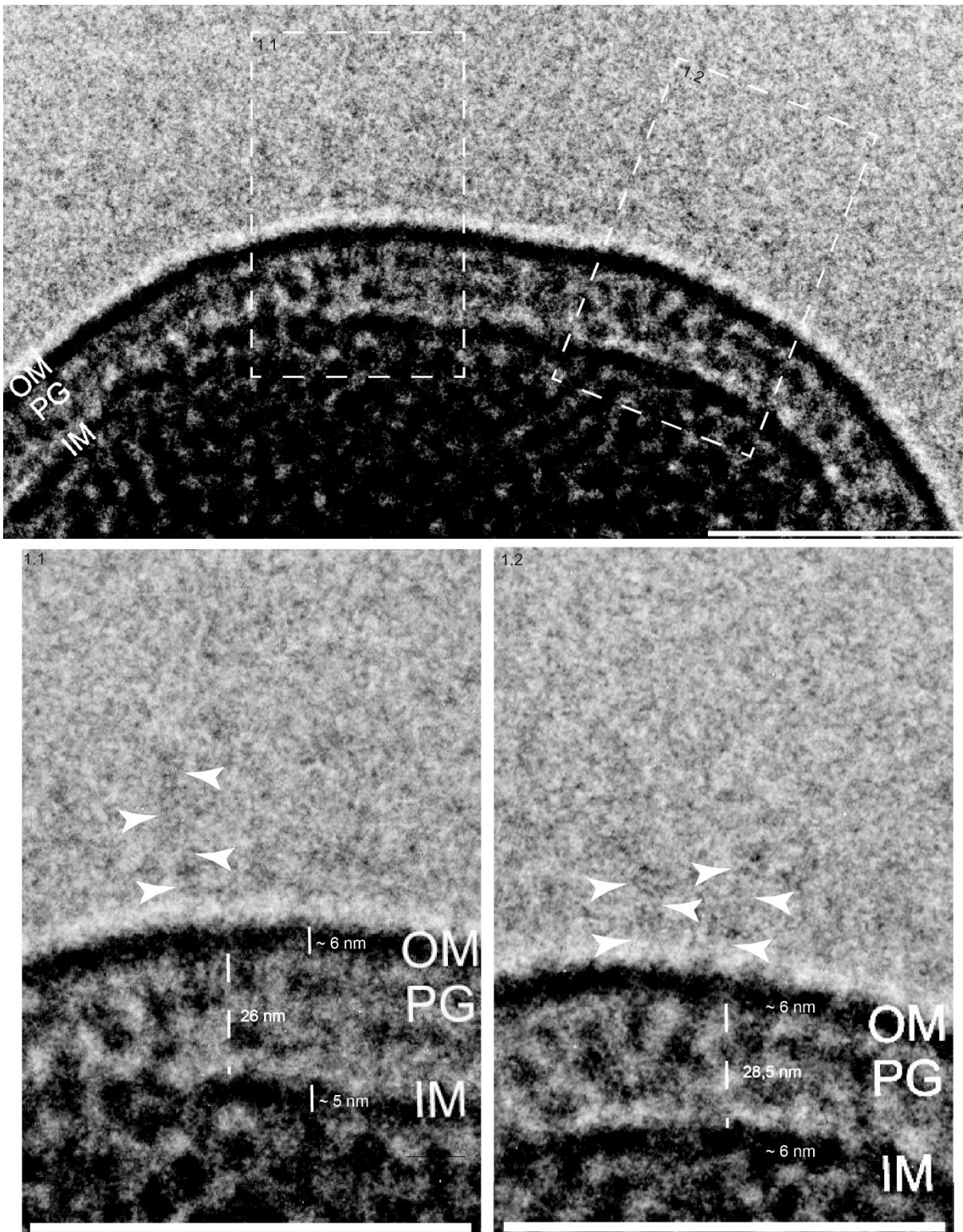


Figure III.1.6. Cryo-TEM visualization of mini SiiE retained on minicell surface. O/N cultures of bacteria were diluted 1:31 in 3 ml fresh LB with 50 $\mu\text{g/ml}$ carbenicillin. Subcultures were incubated at 37 $^{\circ}\text{C}$ for 2 h, with aeration and thereafter, Tet-On gene expression induced by adding 10 ng/ml AHT. After an incubation for 1.5 h at 37 $^{\circ}\text{C}$, with aeration, minicells were enriched and isolated by several centrifugation steps. Then, 4 μl of the minicell enriched suspension was transferred to freshly glow discharged EM grids (Quantifoil grid, Cu 300 mesh, R2/1) and vitrified by plunge-freezing with a Leica EM GP2 system at 10 $^{\circ}\text{C}$ and 80% humidity. Visualisation of minicells was performed with a 200 keV JEOL JEM 2100 Plus system. Scale bars were generated and also, contrast and brightness of images was changed by using Adobe Photoshop CS6 software. Scale bar 100 nm.

Additionally, we performed cryo-TEM analysis of mini SiiE complexes in membranes (Figure III.1.6 shows an exemplary cell). On the one hand, we found complexes, located in the IM and periplasm (Figure III.1.6, 1.1), but also areas with mini SiiE retained on the cell surface without an associated complex in the IM with protein-like structures only visible in the OM (Figure III.1.6, 1.1, 1.2). For this analysis, mini cells lacking other frequently surface structures were imaged. A length of approximately 175 nm is published for secreted SiiE structures from supernatant fractions (Griessl *et al.*, 2013). By tertiary structure model prediction, we found a length of ~20 nm for the N-terminal part of SiiE without any Blg domain (Figure III.1.7 B). We used this information to obtain an approximate length of a single Blg domain, resulting in approximately 3.3 nm per Blg domain. With a number of 6 Blg domains for the mini SiiE we used for this analysis, we expected a range of approximately 20 nm for this area and a total length of ~40 nm. We found mini SiiE structures indicated on the cell surface, covering at least the area of the Blg domains of mini SiiE. If we additionally take IM, OM and periplasm into account, mini SiiE had to span an area of approximately 40 nm for retention in the assembled channel.

T1SS modelling reveals retention of SiiE N-terminus in the secretin SiiC

Further, by tertiary structure model prediction via trRosetta (Du, 2021; Yang *et al.*, 2020) and crystal structure analyses of known T1SS and other membrane components (Bunikis *et al.*, 2008; Linhartova I., 2015; Wang *et al.*, 2017), we were able to build a schematic SPI4-T1SS (only the canonical subunits) to obtain a better spatial model (Figure III.1.7 A). The confidence scores for SiiC (TM-score 0.645) and SiiD (TM-score 0.658) were high and for SiiF very high (TM-score 0.707) (Figure III.1.7 A). With these findings, we demonstrated that SiiC and SiiD are predicted to span the periplasm and are comparable to other known secretion system subunits (Bunikis *et al.*, 2008; Linhartova I., 2015; Smith *et al.*, 2018b; Wang *et al.*, 2017). As published before, the N-terminus of SiiF is also predicted to be located in the cytoplasm, enabling the interaction of SiiF and SiiB (Wille *et al.*, 2014). Besides the canonical subunits of the SPI4-T1SS, we modelled the N-terminus of SiiE ranging from β -sheet #1 to β -sheet #2 without any Blg domains (TM-score 0.371) (Figure III.1.7 B) (Wagner *et al.*, 2011). Together with the results of cryo-TEM analyses described above, where we found potential mini SiiE structures retained on the cell surface, we conclude that not only Blg domains, but also β -sheet #2 potentially protrudes the OM and that SiiE is retained in the OM and not within the completely assembled SPI4-T1SS. In order to reach the periplasm, SiiE has to span approximately 15 nm (~10.8 nm α -helical domain SiiC, ~6 nm OM, Figure III.1.1 and Figure III.1.6), nearly covering the whole domain sequence displayed for β -sheet #1 to β -sheet #2 in the SiiE N-terminus (Figure III.1.7 B).

Results

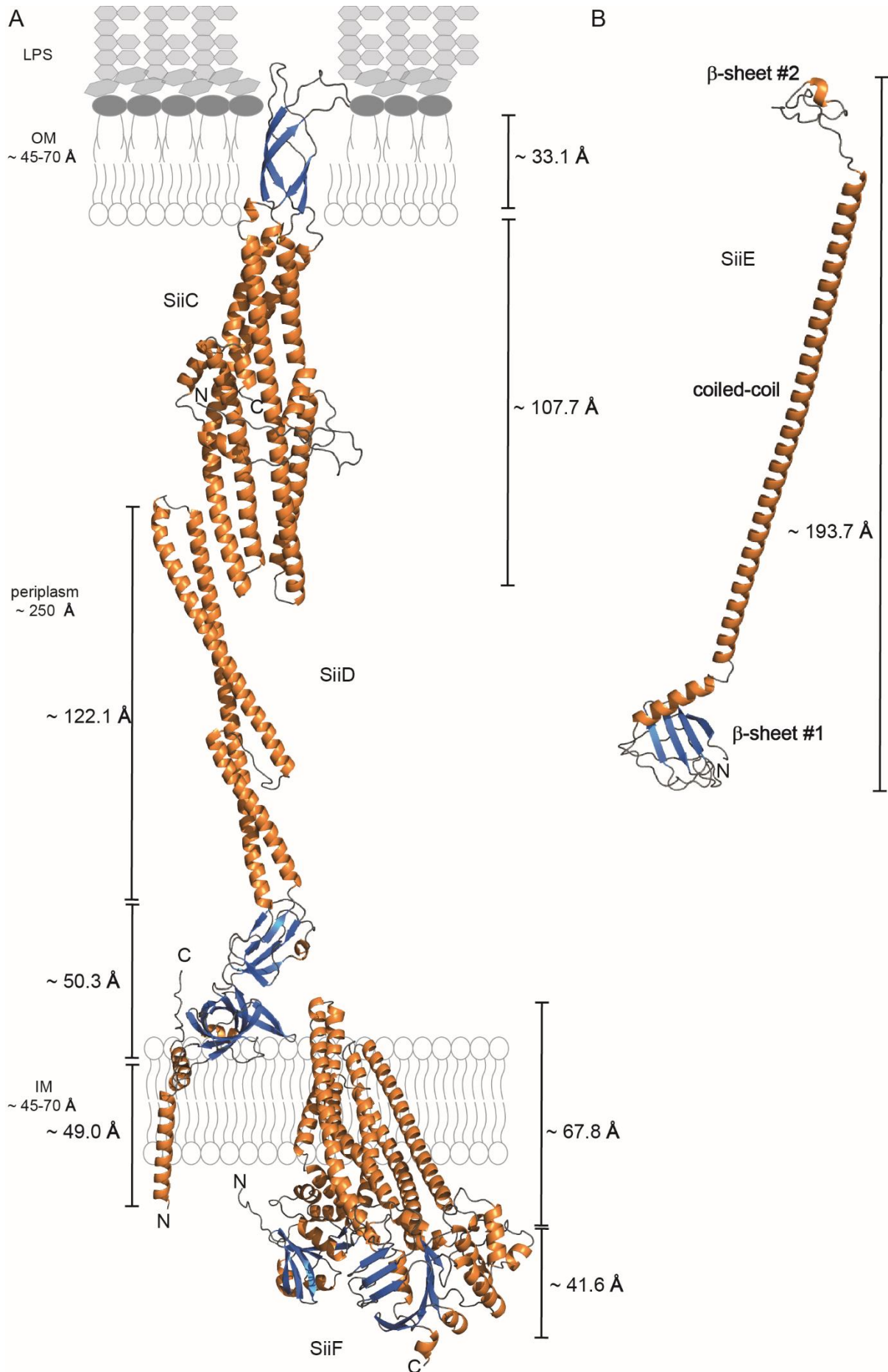


Figure III.1.7. Schematic overview of the modelled canonical SPI4-T1SS subunits SiiCDF and N-terminal part of SiiE. Shown is the schematic overview of the tertiary structure predictions of the ABC transporter SiiF (TM-score 0.707), the PAP SiiD (TM-score 0.658) and the secretin SiiC (TM-score 0.645) (from Figure III.1.1) (A) and the N-terminal part of SiiE from the N-terminus up to β -sheet #2 (Wagner *et al.*, 2011) (TM-score 0.371). Lipopolysaccharides (LPS) as indicated. (B). Proteins were modelled by trRosetta. Loop=gray, β -sheet=blue, α -helix=orange. TM-scores for modelling by trRosetta. TM-score > 0.4 = middle confidence, TM-score > 0.5 = high confidence, TM-score > 0.7 = very high confidence. Length as indicated.

Thus, in combination with the results of the *siiC* overexpression, we assumed that a retention of (mini) SiiE in the whole secretion channel is not possible and that a model with a SiiE retention in the secretin SiiC is more likely, especially when considering other RTX adhesins (Guo *et al.*, 2018; Smith *et al.*, 2018a).

III.1.3.2. SiiAB take part in secretion before SiiC retains SiiE on cell surface

As many other T1SS, the SPI4-T1SS also harbors two non-canonical subunits, namely SiiA and SiiB (Wille *et al.*, 2014). We could show that SiiAB form a proton channel in the IM and that there is a direct interaction between SiiB and SiiF (Wille *et al.*, 2014). Since mutations led to an altered SiiE retention, adhesion and invasion, we concluded a specific role of this proton channel for SiiE secretion and function (Wille *et al.*, 2014). However, the detailed mechanism of SiiAB function for the T1SS and the SiiE secretion process remained unclear (Figure III.1.8 A). We did not know if SiiAB are important in the initial steps of secretion, the retention or the release of SiiE.

*The *siiC* overexpression cannot rescue proton channel deficient phenotypes*

To gain more insights in the function of SiiAB for the SPI4-T1SS and SiiE, we used the introduced *siiC* overexpression and the resulting phenotype for further investigations (Figure III.1.8 B). We transformed *siiAB* mutant strains with the *siiC* overexpression plasmid (Figure S III.1.3). The mutants either lacked the proton channel (Δ *siiAB*) or by exchange of a critical aspartate residue in SiiA (*siiA*_{D13E}), lost the proton channel function (Wille *et al.*, 2014). In case of SiiAB playing a role prior to retention of SiiE in the OM, even with a *siiC* overexpression, the *siiAB* mutant phenotype would be prominent. The lack of the proton channel function could then prevent subsequent steps such as retention in the OM or release into the environment. Thus, retention and secretion of SiiE, as well as adhesion and invasion would consequently be similar to the mutant phenotype (Figure III.1.8 B, left). In case of proton channel function not being essential prior to retention, following retention or rather non-essential at all, we predicted the same phenotype with *siiC* overexpression alone as shown before with a higher retention, adhesion and invasion (Figure III.1.8 B, right).

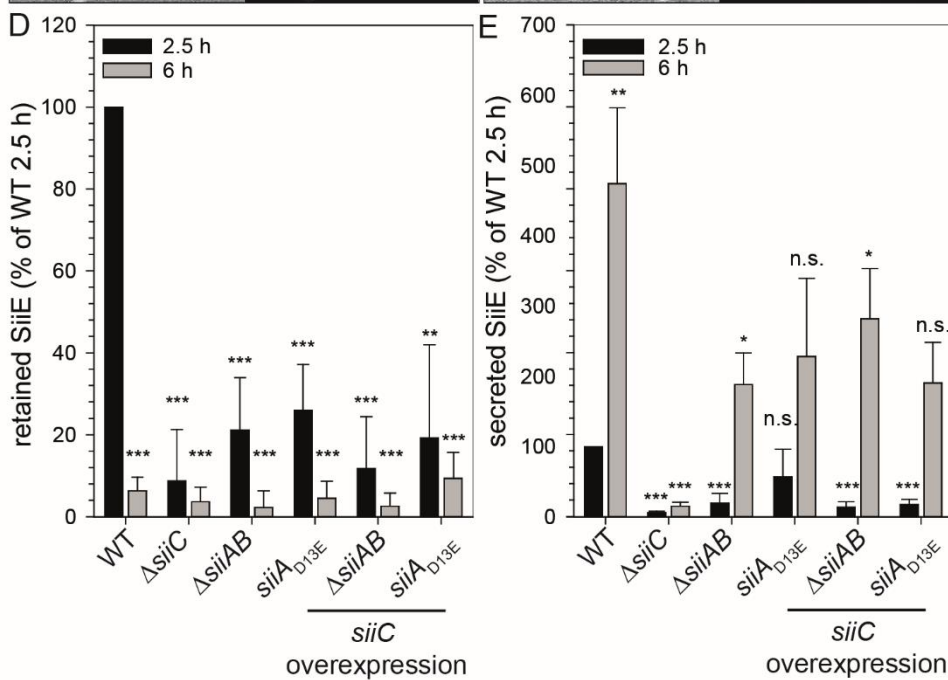
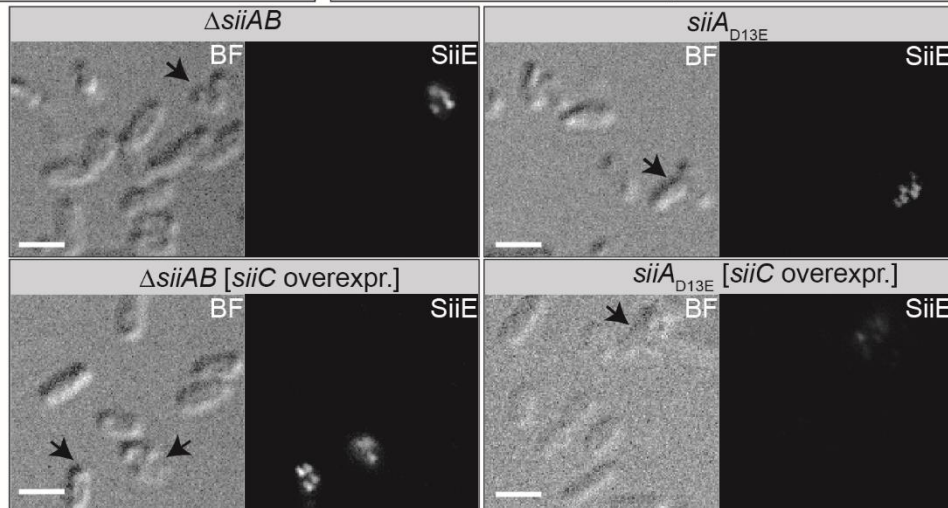
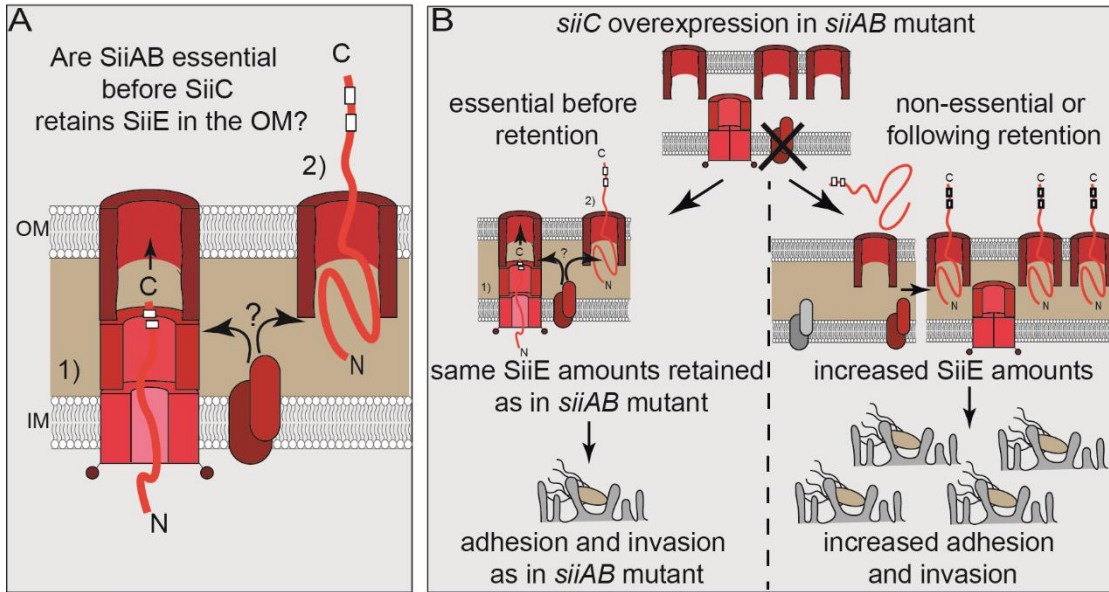


Figure III.1.8. *siiC* overexpression in *siiAB* deficient strains – experimental procedure and effect on SiiE. A) Model for potential functions of SiiAB before SiiE is retained by SiiC or released into the extracellular space. It is possible that SiiAB are essential in initial steps of secretion (1) or during retention of SiiE in the OM (2). B) Schematic overview of the experimental approach of the *siiC* overexpression in *siiAB* deficient strains and analysis of retention, secretion, adhesion and invasion. In case the proton channel function is important before SiiE is retained in the OM, the *siiAB* mutant phenotype would be prominent (left). Contrary, if the proton channel function is not essential in the indicated steps, we predicted the same phenotype as with *siiC* overexpression alone. C) Microscopic analysis of SiiE surface signal. Subcultures were grown for 1 h, induced by addition of AHT, and further cultured for 1.5 h, pelleted by centrifugation and fixed with 3% PFA in PBS. Bacteria were stained for surface-bound SiiE with Alexa488-coupled antibody against primary α -SiiE antibody. For microscopy, a widefield microscope, 100x with oil was used. Scale bar, 2 μ m. D-E) Dot blot analysis of the retention (D) and secretion (E) of SiiE in response to *siiC* overexpression. Subcultures were grown for 1 h, induced by addition of AHT, and further cultured for 1.5 h and 5 h and pelleted by centrifugation. For retention samples, cells were fixed with 3% PFA in PBS and for secretion samples, supernatant was precipitated with TCA and boiled in SDS cracking buffer. 5 μ l of the samples were spotted on equilibrated membranes in triplicates and membranes were incubated with antisera against SiiE or LPS. The LPS signal was used for normalization of sample loading. Statistical analyses compared to WT with at least biological triplicates by two-tailed t-test: ***, $p < 0.001$; **, $p < 0.01$; *, $p < 0.05$; n.s., not significant.

As described above, in addition to a microscopic analysis, a quantitative Dot blot analysis was performed for *siiC* overexpression (Figure III.1.8 C-E). Here, we demonstrated that with the overexpression of the OM protein SiiC, the *siiAB* mutant phenotype remained. The retention of SiiE was significantly decreased in comparison to the WT with 12% (Δ *siiAB*) and 19% (*siiA*_{D13E}) after 2.5 h, comparable to the background strains (Figure III.1.8 D). The secretion of SiiE was less influenced as described before (Wille *et al.*, 2014) (Figure III.1.8 E). However, mutations and *siiC* overexpression did not alter the retention and secretion kinetics. As a consequence of the decreased amounts of SiiE retained on the cell surface, adhesion and invasion were also significantly reduced in comparison to the WT, equal to the background strains. The adhesion with *siiC* overexpression was decreased to 25% and 21% in Δ *siiAB* and *siiA*_{D13E} and thus comparable to Δ *siiAB* (26%) and *siiA*_{D13E} (28%) (Figure III.1.9 A). The invasion of Δ *siiAB* and *siiA*_{D13E} with and without *siiC* overexpression was even more decreased to 1% of WT (Figure III.1.9 B).

From these results, we not only conclude that SiiAB are important for the retention and function of SiiE, but also further limit possible steps in which they might act as a proton channel. Since these mutants did not show the previously described *siiC* overexpression phenotype, we assume that SiiAB are involved either in initial steps of secretion of SiiE or in SiiE retention.

To further analyze this SiiAB specific phenotype, we then constructed a plasmid under *tetA* promoter control on which *siiA*, *siiB*, and *siiC* are overexpressed (Figure S III.1.3).

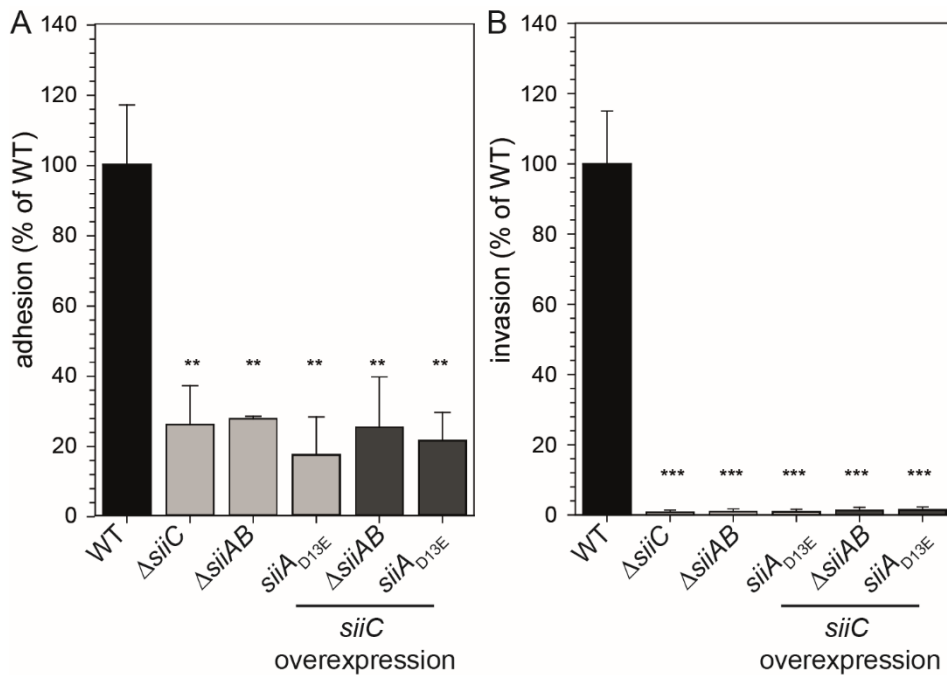


Figure III.1.9. Adhesion and invasion are decreased in response to *siiC* overexpression in *siiAB*-deficient STM. Adhesion to (A) and invasion of (B) polarized MDCK cells as function of *siiC* overexpression. Subcultures were grown for 2.5 h with AHT induction after 1 h and MDCK were infected with MOI 5. Statistical analyses compared to WT with at least biological triplicates by two-tailed t-test: ***, $p < 0.001$; **, $p < 0.01$.

Overexpression of siiABC leads to a higher increase of retention of SiiE, adhesion and invasion

To gain further insight into the secretion mechanism of SiiE in dependence on SiiA, SiiB, and SiiC, we simultaneously overexpressed these three genes and examined the resulting phenotype as described above (Figure III.1.10). While retention after 2.5 h showed exactly the same result as *siiC* overexpression alone (164% of the WT), secretion was also comparable to the WT as before with *siiC* overexpression alone (Figure III.1.10 B and C). Again, the secretion kinetics of SiiE did not change with the introduced overexpression of some subunits of SPI4-T1SS. Interestingly, adhesion and invasion showed a higher increase compared to *siiC* overexpression alone (Figure III.1.10 D and E). Adhesion and invasion were increased to 216% and 232% of the WT, respectively.

Thus, all results taken together, we propose that the OM secretin SiiC determines the amount of SiiE that can be retained on the cell surface. The non-canonical subunits SiiA and SiiB are not only important in steps prior to the retention of SiiE in the OM, but also to play an additional role for either SiiE function during adhesion or other invasion factors, based on the increased adhesion and invasion in comparison to overexpression of only *siiC*.

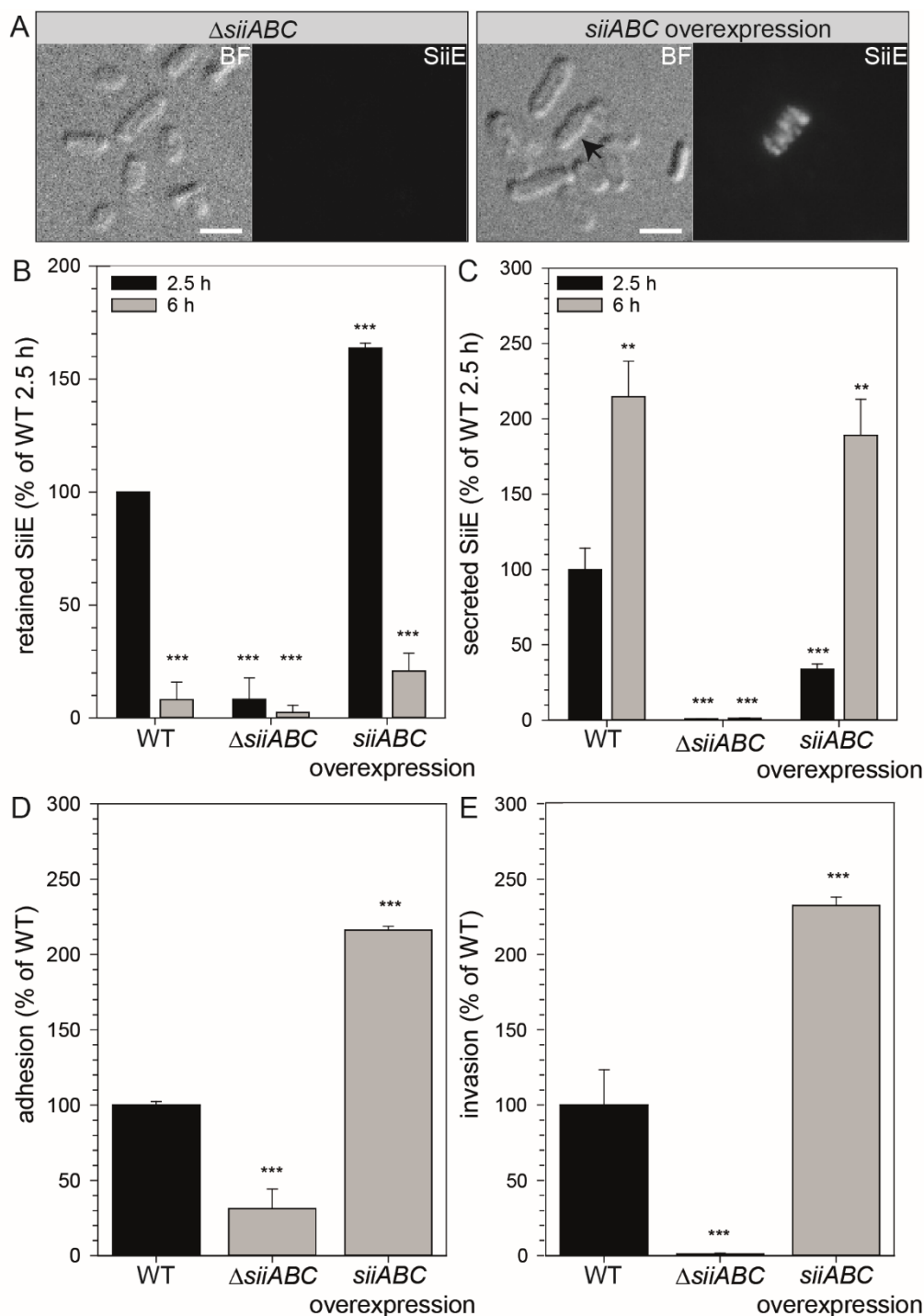


Figure III.10. SiiE retention, secretion, adhesion and invasion in response to *siiABC* overexpression. A) Microscopic analysis of SiiE surface signal. Subcultures were grown for 2.5 h with AHT induction after 1 h, pelleted by centrifugation and fixed with 3% PFA in PBS. Bacteria were stained for surface-bound SiiE with Alexa488-coupled antibody against primary α -SiiE antibody. For microscopy, a widefield microscope, 100x with oil was used. Scale bar 2 μ m. B-C) Dot blot analysis of the retention (B) and secretion (C, exemplary) of SiiE in response to *siiABC* overexpression. Subcultures were grown for 2.5 h and 6 h and induced with AHT after 1 h and pelleted by centrifugation. For retention samples, cells were fixed with 3% PFA in PBS and for secretion samples, supernatant was precipitated with TCA and boiled in SDS cracking buffer. 5 μ l of the samples were spotted on equilibrated membranes in triplicates and membranes were decorated against SiiE and LPS. The LPS signal was used for normalization of sample loading. D) Adhesion to and invasion (E) of polarized MDCK cells following *siiABC* overexpression. Subcultures were grown for 2.5 h with AHT induction after 1 h and MDCK were infected

with MOI 5. Statistical analyses compared to WT with at least biological triplicates by two-tailed t-test: ***, $p < 0.001$; **, $p < 0.01$.

III.1.3.3. SiiE is released by post-translational processing comparable to LapA and MplBP

In comparison to one-step secreted T1SS substrates, two-step secreted substrates are not immediately released into the extracellular space. These substrates, for example LapA, MplBP and also SiiE are retained on the cell surface during the secretion process to mediate adhesion, and are released under defined conditions (Boyd *et al.*, 2014; Guo *et al.*, 2018; Smith *et al.*, 2018a; Wagner *et al.*, 2011). In order to anchor these giant adhesins in the OM, the substrates possess distinct features, as a retention domain with a hydrophobic surface in the N-terminus (Guo *et al.*, 2017; Smith *et al.*, 2018a). We decided to analyze the retention and release of SiiE in consideration of the RTX adhesins LapA and MplBP with focus on the N-terminal domain.

The N-terminal domain of SiiE is a potential retention domain

The analyses of the N-terminal retention modules of MplBP and LapA showed a hydrophobic surface, which potentially supports anchoring of the adhesins by interaction with the IM (Guo *et al.*, 2018; Smith *et al.*, 2018a). Thus, maybe resulting in an increased efficiency of protease targeting (Smith *et al.*, 2018b). Also for bacteriocins like CvaC a particular hydrophobic N-terminus was described to lead to a better accessibility for proteolytic cleavage (Gilson *et al.*, 1990). Protein folding and the stability of protein structures are mainly driven by the hydrophobic effect. Thus, making the knowledge of hydrophobic regions and its prediction important for understanding the structure and function of proteins (Kyte and Doolittle, 1982).

We used hydrophobicity plots to compare the aa sequences of CvaC, MplBP, LapA and SiiE (Figure S III.1.4). The plots were generated by Kyte and Doolittle scale, describing the hydrophobicity of an aa sequence (Kyte and Doolittle, 1982). The bacteriocin CvaC is secreted in one-step and shows distinct regions regarding the hydrophobicity (Figure S III.1.4 A). CvaC is cleaved N-terminally after the first 15 aa from 103 aa to 88 aa (Zhang *et al.*, 1995), displayed here as a neutral area in the first aa, followed by a hydrophobic region and a highly hydrophilic part after 55 aa. In comparison to CvaC, MplBP shows two hydrophobic regions with a higher score and one with a lower score in the first 120 aa (Figure S III.1.4 B). These hydrophobic regions are interrupted by a few very hydrophilic aa (areas around aa 30 and 90). The sequence of LapA directly starts with a very high score, which steadily decreases until aa 65 (Figure S III.1.4 C). After this maximum of hydrophilic aa, the curve remains around zero. The first 10 aa of SiiE also indicate a hydrophilic area as for CvaC and MplBP, followed by three hydrophobic areas, interrupted by small hydrophilic regions (Figure S III.1.4 D). After 110 aa, we found a highly hydrophilic peak, not described for one of the other proteins. With some

differences in the detailed plot curve, *MplBP*, LapA and SiiE showed three hydrophobic areas, ending with a highly hydrophilic peak after 90 aa, 70 aa and 110 aa, respectively. As described above, hydrophobic areas can indicate interactions of the N-terminus with the inner membrane like LapA and *MplBP*. CvaC only showed one hydrophobic peak here, before highly hydrophilic region after aa 55.

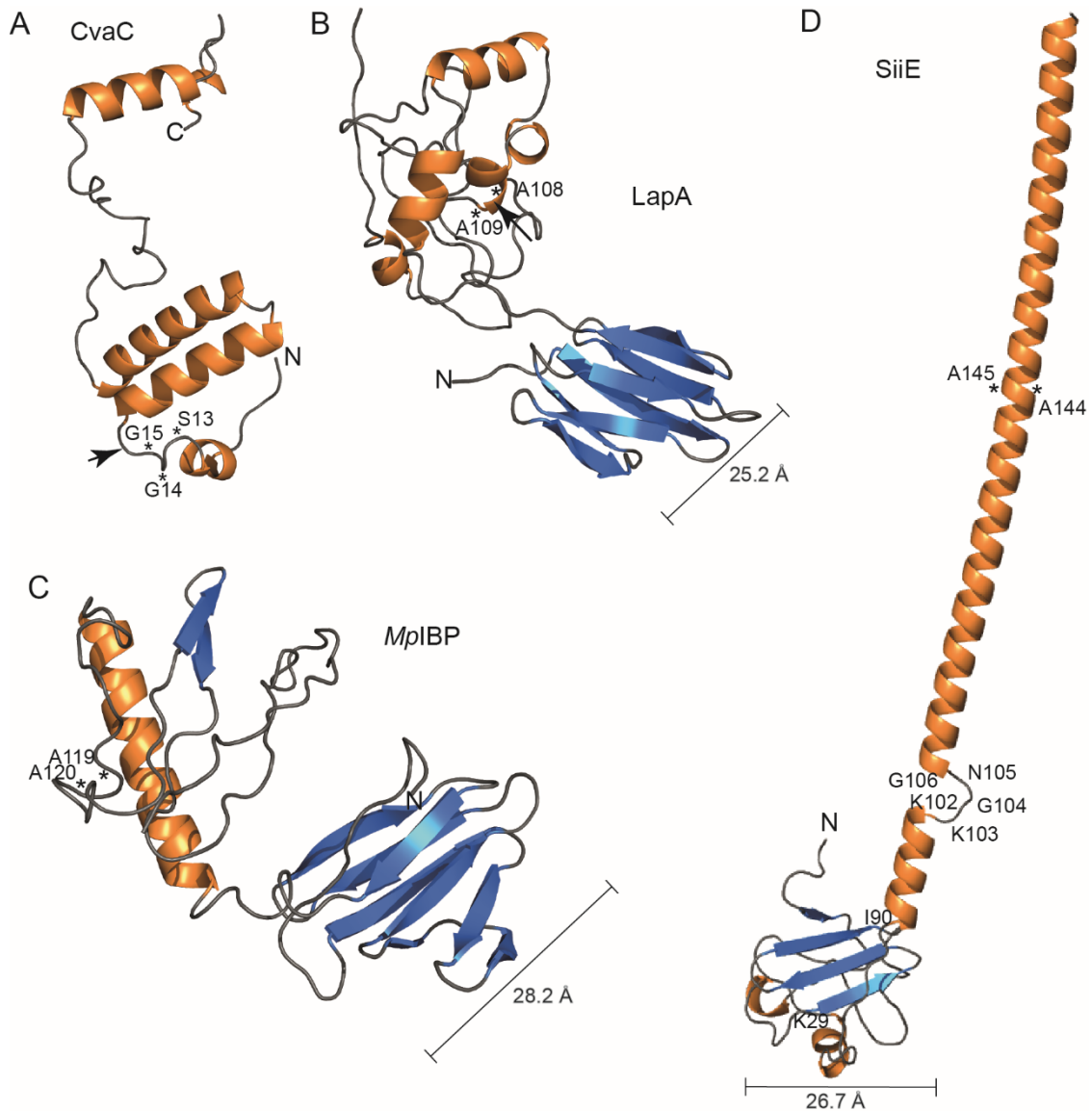


Figure III.1.11. Structure prediction of CvaC and the N-terminal retention domains of *MplBP*, LapA and SiiE. Shown are the predicted N-terminal regions of *MplBP*, LapA and SiiE, modelled with trRosetta. Tertiary structure model prediction for CvaC (A) and the first 180 aa of the substrates LapA (B), *MplBP* (C), and SiiE (D). Arrows indicate the cleavage sites for CvaC (A) and LapA (B). A) A Ser-Gly-Gly motif in CvaC is recognized by the intrinsic C39 protease of CvaB. For release and activation, the C39 protease cleaves CvaC near this motif (Fath *et al.*, 1994) (indicated by arrow). B) LapA is cleaved in the N-terminal retention domain between Ala108-Ala109 (indicated by arrow), located in the periplasm, by the periplasmic accessory protein LapG (Smith *et al.*, 2018a). C) A putative LapG cleavage site for *MplBP* was also found at positions Ala119-Ala120 (Guo *et al.*, 2018). Numbers indicate determined lengths. Loops = gray, β -sheet = blue, α -helix = orange. TM-score for modelling by trRosetta: 0.541 (CvaC), 0.562 (LapA), 0.521 (*MplBP*), and 0.383 (SiiE). TM-score > 0.4 = middle confidence, TM-score > 0.5 = high confidence.

Aside from hydrophobicity, tertiary structure model predictions can give hints about protein structures. Just as for the hydrophobicity plots, the first 180 aa of *MplBP*, *LapA* and *SiiE* and the whole sequence of *CvaC* were used here for analysis by trRosetta. We modelled the N-terminal domain of *SiiE* in comparison to *MplBP* and *LapA* as two-step secreted substrates and additionally *CvaC* as one-step secreted substrate (Figure III.1.11). The models predicted by trRosetta showed high confidences for *CvaC* (TM-score 0.541) (Figure III.1.11 A), *LapA* (TM-score 0.562) (Figure III.1.11 B) and *MplBP* (TM-score 0.521) (Figure III.1.11 C) and match the published data (Guo *et al.*, 2018; Smith *et al.*, 2018a). Additionally, we analyzed the first 180 aa of *SiiE* with trRosetta (TM-score 0.383) (Figure III.1.11 D). The N-terminal Region I (RI) of *MplBP* is described as OM anchor, retaining *MplBP* on cell surface to mediate adhesion (Guo *et al.*, 2017). This RI is divided into an N-terminal part (RIN), located in the periplasm, a C-terminal region (RIC) in the extracellular environment and an OM spanning domain in the center of RI (RIM) (Guo *et al.*, 2018; Guo *et al.*, 2017). It was shown that the RI of *MplBP* possesses a β -sandwich fold in the dimensions of 24 Å by 28 Å by 26 Å, which was suggested to be too large to pass through the secretin TolC, consequently inhibiting the release of the adhesin. This domain is followed by a proteolysis-sensitive region (Guo *et al.*, 2018). Since RIM is not suggested to contain transmembrane sequences, it is thought to interact with the OM secretin (Guo *et al.*, 2017; Krogh *et al.*, 2001). Analyses of the N-terminus of *LapA* showed comparable results of a folded N-terminal domain that inhibits secretion of the adhesin into the extracellular space (Figure III.1.11 B) (Smith *et al.*, 2018a). We noticed comparable structures in the very N-terminal region between *LapA*, *MplBP* and *SiiE*, consisting of β -sheets. We measured the diameter of the N-terminal retention domains and found diameters of 28.2 Å for *MplBP*, 25.2 Å for *LapA* and 26.7 Å for a potential retention domain of *SiiE*. Due to similarities between TolC, *LapE* and *SiiC* (Figure III.1.1) and the N-terminal domains of the substrates (Figure III.1.11 B-D), in combination with the results of the analyses described above (Figure III.1.3-10), we conclude a potential retention domain in *SiiE* β -sheet #1.

Analyses of protein levels of cytosolic and secreted SiiE suggest a proteolytic cleavage for substrate release

Release by proteolytic cleavage is not only described for RTX adhesins like *LapA*. Bacteriocins like *CvaC* undergo proteolytic cleavage as well, not only for release, but also for activation (Fath *et al.*, 1994; Zhang *et al.*, 1995). This bacteriocin is cleaved by the intrinsic C39 protease of *CvaB* recognizing a Ser-Gly-Gly motif following the first 15 aa of *CvaC* (Figure III.1.11 A) (Fath *et al.*, 1994; Zhang *et al.*, 1995). The RTX adhesin *LapA* possesses a double alanine motif at positions 108 and 109, which is recognized and cleaved by the periplasmic adaptor protein *LapG* (Figure III.1.11 B) (Newell *et al.*, 2011; Smith *et al.*, 2018a). The first 195 aa of *MplBP* were defined as RI N-terminal and middle regions (RINM), of which aa12-187 could be

resolved by NMR (Guo *et al.*, 2018). Additionally, they found a potential LapG cleavage site at Ala119-Ala120 (Figure III.1.11 C). Instead of a TAAG motif like in other RTX adhesins, *MplBP* possesses a PAAG motif, less common for RTX adhesins (Guo *et al.*, 2018). Similar to LapA and *MplBP*, SiiE possess a double alanine motif at positions 144/145 (Figure III.1.11 D). Nevertheless, a LAEE motif as in SiiE is quite uncommon for RTX adhesins (Guo *et al.*, 2018). However, SiiE has a double lysine at positions 102/103 and two glycine in direct proximity (position 104 and 106).

As a result of alignments, structural predictions and the results from above experiments, a proteolytic cleavage was considered for release of SiiE. We investigated this possibility by analyses of cytosolic and secreted SiiE. For this purpose, we used truncated forms of SiiE to improve resolution.

We inserted a 3xFLAG-tag between aa116 and aa117 after β -sheet #1 (Wagner *et al.*, 2011) and performed a Western blot analysis of cytosolic and secreted mini SiiE (Figure III.1.12 A). If a proteolytic cleavage against our assumptions would occur after this position, no FLAG-tag signal would be detected on the Western blot. We detected mini SiiE in the supernatant fraction, but also the FLAG-tag at position 116. Thus, we knew that a possible cleavage site has to be located within the first 115 aa of SiiE. Additionally, we got a first hint for a slight size shift between cytosolic and secreted mini SiiE. The cleavage of the first 115 aa would result in a size shift of 12 kDa.

Based on experiments for CvaC and for mini LapA (Gilson *et al.*, 1990; Newell *et al.*, 2011) (Newell *et al.*, 2011), a more truncated form of mini SiiE was used to further improved distinction of processed forms. Studies of the 1.5 MDa adhesin *MplBP* revealed a proteolytic cleavage between Ala119 and Ala120 (~12 kDa) (Guo *et al.*, 2018). The truncated form of LapA showed a size shift of 15 kDa (from 145 kDa to 130 kDa) (Newell *et al.*, 2011). Interestingly, the protease domain of CvaB, a C39 protease, is a cysteine protease, too (Zhang *et al.*, 1995). The truncated mini SiiE was comparable to mini LapA and showed a sizeshift of ~6 kDa between the cytosolic and the secreted substrate (Figure III.1.12 B, C). This size shift of 6 kDa directed us to a further limitation for a possible cleavage. In purely arithmetical terms, the first 58 aa were calculated for such a size shift.

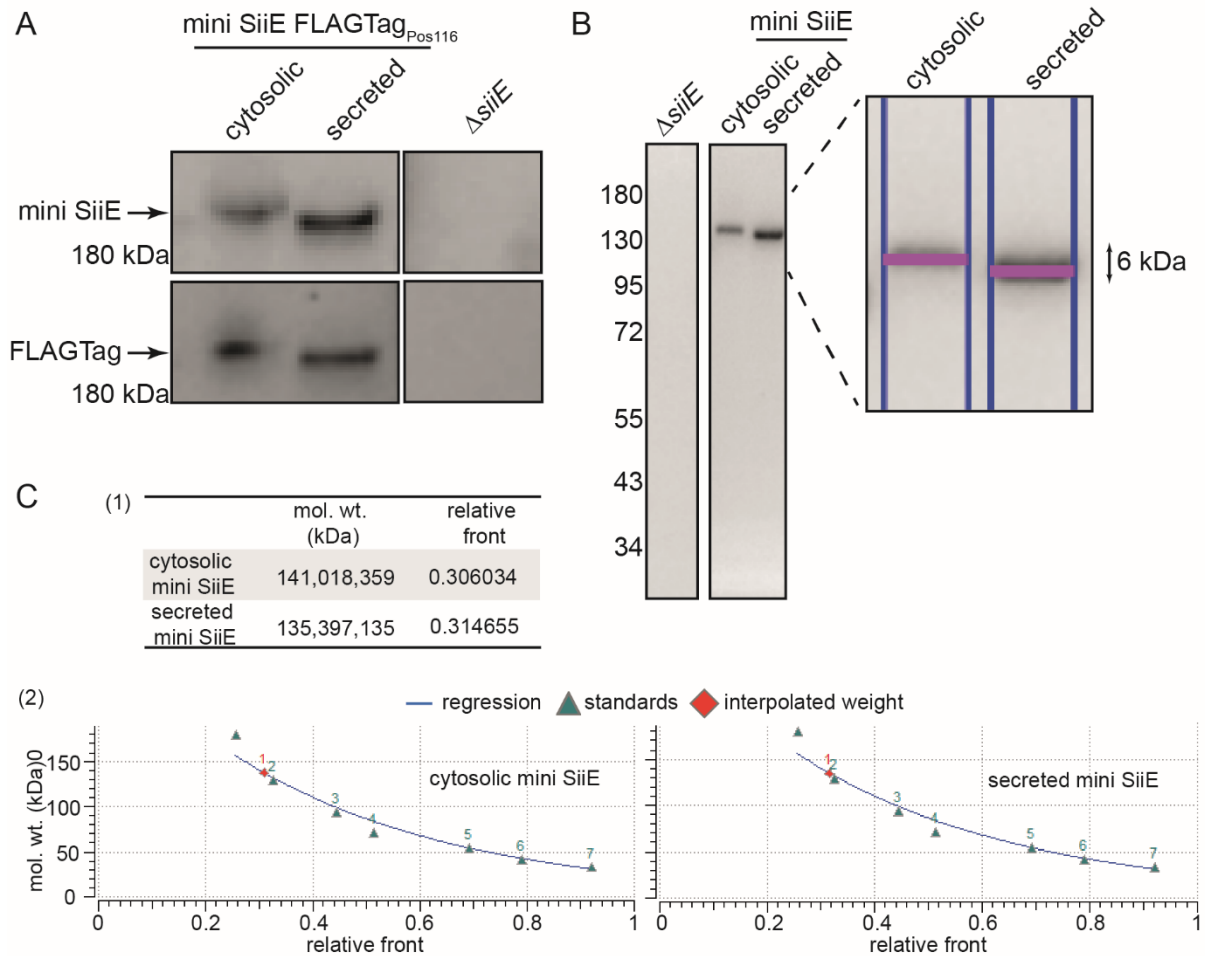


Figure III.1.12. Analyses of proteolytic cleavage of secreted mini SiiE. A) Western blot analysis of cytosolic and secreted mini SiiE tagged with 3xFLAG tag at position 116 in the N-terminus. Subcultures were grown for 2.5 h (cytosolic SiiE) and 6 h (secreted mini SiiE) and were boiled in SDS cracking buffer and SDS-PAGE was performed. Following semi-dry transfer, membranes were decorated with α -SiiE (1:10,000) and FLAG tag (1:2,000) antibodies. Marker as indicated on the left site of the blot. B) Western blot analysis of cytosolic and secreted mini SiiE. Subcultures were grown for 2.5 h (cytosolic SiiE) and 6 h (secreted mini SiiE) and were boiled in SDS cracking buffer. SDS-PAGE and Western blot were performed. α -SiiE antibody (1:10,000) was used for blot decoration. Marker as indicated. Validation of the size shift with ImageLab software. C) Data of the size shift calculated by ImageLab. 1) Molecular weight and relative front of cytosolic and secreted mini SiiE. 2) Standard curves for cytosolic (left) and secreted (right) mini SiiE. Regression method was linear (semi-log). Formula: $y = -1.05 \cdot x + 2.46$, R-squared value: 0.976587.

To further corroborated these results and reveal further details of processing of SiiE, we performed mass spectrometry (MS) analyses of cytosolic and secreted mini SiiE (Figure III.1.13). In a first attempt we tested the peptide coverage of the N-terminus after digestion with trypsin, pepsin and ArgC (data not shown). For further analyses, we used trypsin for digestion (Figure III.1.13 A). Due to trypsin digestion, the first 8 aa were not found in cytosolic and secreted samples. Defined peptides were analyzed by quantification (Figure III.1.13 B, C). A standard peptide with a comparable area in the cytosolic and secreted sample from the central area of mini SiiE was chosen and a C-terminal peptide was used for comparison (Figure III.1.13

B). Only peptides found in both samples were selected for quantification (without post-translational modifications). In the N-terminal part, we identified one peptide that showed a 2-fold enrichment in the cytosolic sample compared to the secreted sample (aa9-26) (Figure III.1.13 C). Peptides covering SiiE starting at aa44 were found in both samples in comparable amounts. The peptide ranging from aa44-58 was less abundant in both samples (data not shown). The peptide from 76-83 was found in higher and comparable amounts (data not shown).

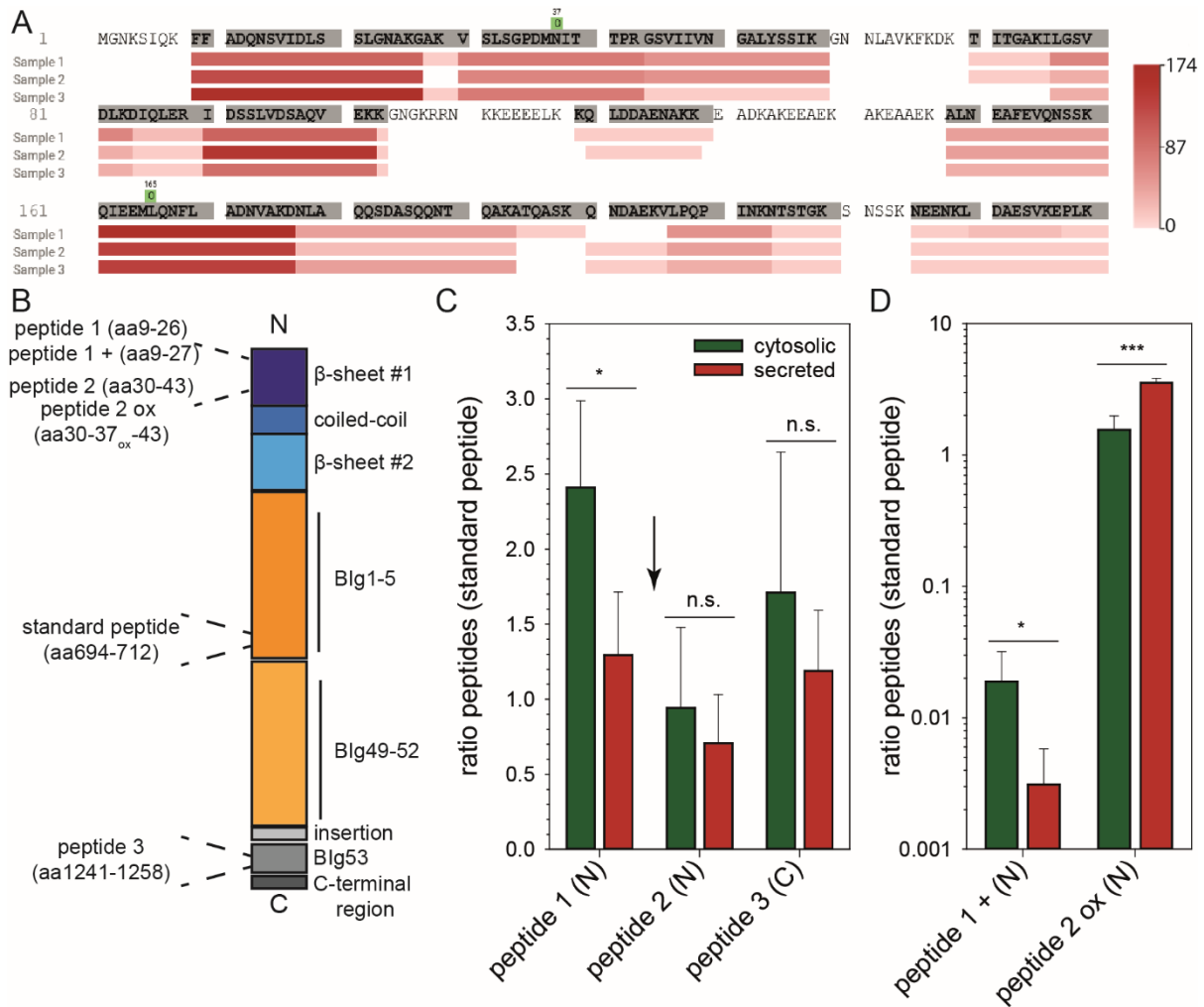


Figure III.1.13. Qualitative and quantitative MS analysis of the N-terminus of cytosolic and secreted mini SiiE. Shown are the qualitative (A) and quantitative (C) analyses of cytosolic and secreted mini SiiE. Subcultures were grown for 2.5 h (cytosolic SiiE) and 6 h (secreted mini SiiE) and were boiled in SDS cracking buffer, and SDS-PAGE was performed. Following Coomassie stain, selected bands were excised and proteins were digested with trypsin. A) Qualitative MS analysis of the N-terminus of secreted mini SiiE. (aa1-240). B) Localizations of the peptides in mini SiiE are shown schematically. C) Quantitative MS analysis of the N-terminus of mini SiiE. Cytosolic peptides are depicted in green and secreted peptides in red. Peptide 1 and 2 are defined as N-terminal peptides (aa9-43), as standard peptide a central peptide was chosen (aa562-582) and for comparison, a C-terminal peptide (aa1241-1258) was used. D) Semi-specific digestion of mini SiiE. Shown are the peptide 1 with an additional aa (G) at position 27 (peptide 1 +) and peptide 2 with oxidation (peptide 2 ox). Potential cleavage site as indicated between position aa27 and aa30. Statistical analyses with at least biological triplicates by one-tailed t-test: ***, $p < 0.001$; *, $p < 0.05$; n.s., not significant.

shown). To further analyze a potential cleavage site between peptide 1 and peptide 2, we performed an additional Peaks analysis with a semi-specific digestion, instead of a specific trypsin digestion. With this method, we gained more insights in possible differences in the peptide pattern of cytosolic and secreted SiiE (Figure III.1.13 D). In the semi-specific digestion we found peptide 1 + and peptide 2 ox. Peptide 1 + was similar to peptide 1, with exception of an additional glycine, which was found in significantly lower abundance in the secreted sample. Interestingly, we found significantly increased amounts of peptide 2 ox, the same as peptide 2, but with an additional oxidation at position 37, in the secreted sample. We concluded that this oxidation can take place because of the oxidative environment the secreted mini SiiE is extracted from. This would explain why we did not find these quantities in the cytosolic sample. Thus, we concluded that the potential cleavage site between aa27 and aa30, bringing aa28 (alanine) and aa29 (lysine) into focus. The first 29 aa have a calculated molecular weight of approximately 3 kDa and are located in the β -sheet #1 (Figure III.1.13 B), supporting the previous results described above.

It was already shown that deletions of aa76-116 and aa97-116 in β -sheet #1 result in a decreased retention and increased secretion (Wagner *et al.*, 2011), underlining our recent results regarding a proteolytic cleavage in the N-terminal domain of SiiE.

In this manuscript, we demonstrated that SiiE potentially displays another member of the new subfamily of RTX adhesins. Interestingly, although other family members like LapA and MplBP are important for adhesion to surfaces, for example during biofilm formation, SiiE in contrast mediates adhesion to polarized epithelial cells, underlining the differences between the functions of the substrates. Additionally, due to the infection process, SiiE shows a more dynamic switch between retention and secretion, making it even more interesting that SiiE secretion mechanism follows mechanisms already described for other large adhesins like LapA associated with biofilm formation and not cell adhesion. Thus, further analyses can be performed to reveal more details for the SPI4-T1SS mechanistic. Especially the role of the non-canonical subunits SiiA and SiiB is of interest, since they are not comparable to LapG and LapD.

III.1.4. Discussion

With our new findings, we gained more insight in the secretion steps of SiiE. We not only postulate that SiiC retains SiiE in the OM (Figure III.1.14, 1) during secretion process like LapE does with LapA, but additionally could show that the accessory proton channel SiiAB play an important role for the initial steps of SiiE secretion and not for release (Figure III.1.14, 2, 4). Further, we identified a potential retention domain in the N-terminal region of SiiE, localized in the β -sheet #1 (Figure III.1.14). This potential anchor, comparable to LapA and *MplBP*, consists of β -sheets and is possibly too large to fit through SiiC. Thus, this domain probably has to be cleaved by a yet unknown protease, so that SiiE can be released into the environment after mediating adhesion to the host cell. We gained hints that SiiE is potentially cleaved in the first 43-58 aa (Figure III.1.14, 3). Taken this together and other RTX adhesin family members into account, SiiE can be proposed as an additional member of this family of adhesins. Other T1SS mechanisms described for bacteriocins and RTX toxins seem to be less likely. Since the function of the accessory proteins SiiAB is not fully uncovered, it remains unclear whether SiiE is also a member of the BTLCP-linked adhesins, maybe modifying SiiE in a not yet described manner. However, a proteolytic cleavage of SiiE by SiiAB can be excluded here regarding the results of this study. Thus, the proton channel potentially post-translationally modifies SiiE in another way or supports SiiE in initial steps of secretion. It is described that many T1SS

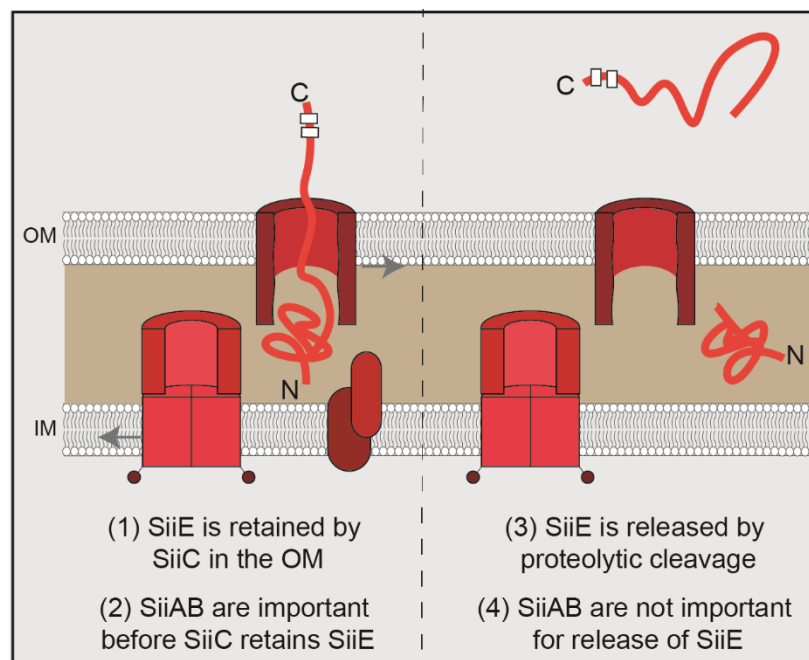


Figure III.1.14. New insights in SiiE secretion mechanism. Left: During secretion, SiiE is retained on cell surface comparable to LapA. We could show that SiiE comparable to LapA is only retained in the secretin SiiC (1). Additionally, we can limit mode of action of SiiAB as proton channel to initial secretion steps or retention (2, 4). Right: Following retention, SiiE is secreted by proteolytic cleavage comparable to LapA (3).

substrates require the function of accessory proteins for post-translational modification, activation or a convenient localization (Smith *et al.*, 2018b). As it is described that SiiAB mutant strains are not able to adhere nor to invade (Wille *et al.*, 2014) and taken together with our new findings, it is possible that the proton channel supports proper localization or activation of SiiE, so that SiiE can efficiently mediate adhesion. This would enable the SPI1-T3SS to optimally translocating the effector proteins into the host cell, leading to membrane ruffling and uptake of the pathogen (Gerlach *et al.*, 2007a). This idea can be supported by our findings that the *siiABC* overexpression does not lead to higher amounts of SiiE retained on cell surface, which seems to be determined by SiiC in the OM, but to higher adhesion and invasion rates than *siiC* overexpression alone. Probably this SPI4-encoded proton channel not only functions at the SPI4-T1SS, but additionally play a role for other key players upregulated during invasion process like the flagellum. The similarities between SiiAB and the stator complex of the flagellum, MotAB, are already described (Kirchweger *et al.*, 2019; Wille *et al.*, 2014). Contrary to the activation of LapG (Boyd *et al.*, 2014), the trigger for SiiAB action is still not known. It is also possible that opening of the SiiF channel for SiiE secretion leads to activation of SiiAB for the process. Due to the fact that it was shown that SiiF interacts with SiiB in the IM (Wille *et al.*, 2014), activation by mechanical changes in the IM could be possible. This could also lead to an optimized secretion process of SiiE or retention in the OM by SiiC. We could not show a comparable trimeric state of SiiC to TolC, leading us to the assumption that SiiC is less stable than TolC. Considering the time span a functional SPI4-T1SS is required for, it has to assemble and disassemble, hence a less stable conformation of SiiC might be advantageous. After mediating adhesion, SiiE is suggested to be released into the environment before the bacterium is engulfed, comparable to LapA and MplBP (Barlag and Hensel, 2015; Guo *et al.*, 2018; Smith *et al.*, 2018a). Although RIC belongs to the N-terminal region (RI) of MplBP, it possesses immunoglobulin-like (Ig) folds, comparable to the first bacterial Ig (Blg) domains of SiiE following β -sheet #2 (Guo *et al.*, 2018; Wagner *et al.*, 2011). To span the IM, periplasm and OM to reach the cytoplasm for SiiE retention, the first Blg domains with their calcium bindings sites, essential for stabilization and function of SiiE (Peters *et al.*, 2017), have to be located in the OM secretin SiiC or PAP SiiD, respectively. Additionally, with our results based on the *siiC* overexpression, modelling and cryo-TEM analyses, we would exclude this as a retention mechanism at this point. To retain large RTX adhesins on the cell surface, a putative retention module was described for the adhesin MplBP from *M. primoryensis* with an N-terminal domain comparable to LapA (Guo *et al.*, 2017). Based on nuclear magnetic resonance (NMR) structural studies, it was suggested that the N-terminal domain of MplBP is arranged as a β -sandwich fold in the dimensions of 24 Å by 28 Å by 26 Å. This retention domain is too large to pass through the secretin TolC oligomer with pore diameter of only 20 Å in an open state and consequently

inhibits release of the adhesin. It was shown that this folded domain is followed by a proteolysis-sensitive region (Guo *et al.*, 2018). Analyses of the N-terminus of LapA support the comparable model of a folded N-terminal domain inhibiting release of the adhesin into extracellular space (Smith *et al.*, 2018a). Furthermore, the analysis of the N-terminal retention modules of MplBP and LapA showed a hydrophobic surface, which potentially supports anchoring of the adhesins by interaction with the IM. This could lead to an increased efficiency of protease targeting. It was also shown that ABC transporters of RTX toxins and adhesins differ in their CLD domains, thus it was concluded that BTLCP-linked/RTX adhesins build a new subclass of T1SS and can be differentiated from RTX toxin transporters. If β -sheet #1 displays a potential knot domain that is cleaved for release of SiiE, it is more likely that parts of the coiled-coil domain and β -sheet #2 are comparable to RIM of MplBP (Guo *et al.*, 2018) and interacting with SiiC in the OM. It was shown that a deletion of β -sheet #2 leads to an increased retention after 3.5 h, but to a depletion in invasion at the same time (Wagner *et al.*, 2011). The deletion of β -sheet #2 could lead to higher amounts of SiiE retained on cell surface, as the coiled-coil and β -sheet #1 are delocalized in SiiC and not present in the periplasm anymore, inhibiting proteolytic cleavage or other interactions, also with SiiC. In contrast to this, deletion of the aa97-116 in β -sheet #1 did not result in a loss of invasion, but also to increased amounts of SiiE retained on the cell surface after 3.5 h, while secretion was not affected at all after 6 h (Wagner *et al.*, 2011). As described in our findings, a potential protease site is located in or near β -sheet #1, which by the deletion of the aa97-116 maybe is covered due to conformational changes and thus increasing retention. Taken together with this study, probably more SiiE is retained by SiiC on the cell surface compared to WT after 3.5 h, but as a total, same amounts as of WT were secreted after 6 h. In the described study, it was not investigated whether SiiE is still retained on the cell surface after 6 h (Wagner *et al.*, 2011). Interestingly, deletion of aa76-116 in β -sheet #1 showed the opposite phenotype with decreased amounts of SiiE retained on the cell surface and no invasion at all (Wagner *et al.*, 2011). Considering our new results, this phenotype could be a consequence of improper folding of the potential retention plug or a decreased diameter that cannot be held back by the secretin SiiC. An immediate secretion into the environment could explain the reduced retention, invasion and unaffected secretion. These findings underline the role of β -sheet #1 and β -sheet #2 for controlled retention and release of SiiE. As proteolytic cleavage is a common mechanism among the RTX adhesin family, together with the results of this study, we would suggest that SiiE is also released by a proteolytic cleavage. A post-translational modification as described for RTX toxins like HlyA is rather unlikely in this case (Nicaud *et al.*, 1985). Contrary to LapA, we exclude a double alanine motif as cleavage site for SiiE. The first double alanine motif can be found at position 144/145 in the coiled-coil domain of SiiE, which does not fit the other results of this study. In our MS analysis we found a potential cleavage site between aa27 to aa30 (Figure

III.1.13 D), which makes this area interesting for further mutations and investigations. The aa28 is an alanine and aa29 a lysine. As there are less proteases described to cleave alanine, we conclude that lysine is the preferable target. Nevertheless, proline-endopeptidases were described to also accept alanine in position P1 and in most cases lysine, histidine or arginine was found in position P2 (Fulop *et al.*, 1998). Serine proteases like Clp are encoded by many pathogens such as *Mycobacterium tuberculosis*, *Bacillus licheniformis* and *Pseudomonas aeruginosa* (Patel, 2017). Due to the energy limitation in the periplasm, only a handful of proteases can be considered. DegP and its paralogues DegS and DegQ could be one of the proteins of interest here (Mo *et al.*, 2006). They degrade accumulated proteins in the periplasm under heat shock and other stress conditions (Bass *et al.*, 1996; Waller and Sauer, 1996). Non-specific proteolysis of folded proteins is inhibited as only unfolded proteins devoid of disulfide bonds are prone to cleavage (Strauch and Beckwith, 1988; Strauch *et al.*, 1989). SiiE lacks cysteine residues and consequently disulfide bonds. DegP is known to act on at least partially unfolded substrates and the cleavage site is normally between a pair of hydrophobic residues like Val and Ile (Jones *et al.*, 2002). However, as we found an approximately 6 kDa shift in our Western Blot analysis of secreted mini SiiE, the potential cleavage site could be present within the first 58 aa (Figure III.1.12 B, C). The hydrophobic area in the N-terminus of SiiE we demonstrated by hydrophobicity plots, not only possesses Val or Ile in the first aa, but additionally three Val-Ile motifs, from which two are directly in a row (Val46-Ile47-Ile48-Val49). These motifs can be found in the first 49 aa, matching the area of our results from this study. Due to trypsin digestion, only distinct peptides were found here, thus also the following peptide ranging from aa44-58 should be taken into account and more investigated. It is already described that the pilin subunit PapA for example is a natural substrate for DegP proteolysis (Jones *et al.*, 2002). Also other non-pilus adhesins like HMW1 and HMW2 of *Haemophilus influenzae* were found as *in vivo* substrates for DegP (St Geme and Grass, 1998). Consequently, distinct aa exchanges in the β -sheet #1 domain potentially lead to a loss of secretion. Taken together, further investigations of the first aa of the β -sheet #1 domain and potential proteases in the near future will lead us to a more detailed characterization of the retention and secretion mechanism of SiiE and a potentially novel way of proteolytic cleavage of RTX adhesin family members in the periplasm.

III.1.5. Materials and Methods

III.1.5.1. Bacterial strains and growth conditions

Bacterial strains used in this study are listed in Table III.1.1. Bacteria were grown aerobically in LB or on LB agar plates, if necessary supplemented with carbenicillin (cb, 50 µg/ml). For induction of the Tet-on system encoded on the plasmids used (Table III.1.2), anhydrotetracycline (AHT) was added (1-100 ng/ml final concentration) 1 h after inoculation of the subculture for additional 1.5 h (1:31).

Table III.1.1. Bacterial strains used in this study.

Designation	Relevant characteristics	Reference
S. Typhimurium NCTC 12023	wild type	NCTC 12023
WRG205	<i>siiA</i> _{D13E} ::FRT	(Wille <i>et al.</i> , 2014)
MvP589	Δ <i>spi4</i> ::FRT	(Gerlach and Hensel, 2007)
MvP1311	<i>siiF</i> _{G500E} ::FRT	(Wille <i>et al.</i> , 2014)
MvP1387	Δ <i>siiAB</i> ::FRT	this study
MvP2303	Δ <i>flil</i> ::FRT Δ <i>fimD</i> ::FRT <i>ΔminD::aph</i>	lab collection
MvP2780	Δ <i>siiF</i> ::FRT	this study
MvP2779	Δ <i>siiE</i> ::FRT	this study
MvP2808	Δ <i>siiC</i> ::FRT	this study
MvP3052	Δ <i>siiABC</i> ::FRT	this study

III.1.5.2. Construction of plasmids

The gene encoding SiiC was amplified from genomic DNA of STM WT (NCTC 12023). The HA-tag was inserted via site-directed mutagenesis. For generation of *siiABC* overexpression plasmid, SiiC-HA encoding genes were amplified from p5569 and inserted into p5216, containing genes encoding SiiA and SiiB under *tetA* promoter control. Mini SiiE was generated by amplification of distinct parts of SiiE-encoding genes of STM WT. Plasmids for Tet-on expression were generated by Gibson assembly (GA) according to manufacturer's instructions (NEB) using p4645 as vector, with exception of p5144 as vector for generation of p5514. Oligonucleotides used are listed in Table III.1.3.

Table III.1.2. Plasmids used in this study.

Plasmid	Relevant characteristics, resistance	Reference
pWRG462	<i>P</i> _{<i>siiA</i>} :: <i>siiAB</i> ::3xFLAG tag, cb ^R	lab collection
p4251	<i>tetR P</i> _{<i>tetA</i>} , cb ^R	lab collection

p4645	<i>tetR P_{tetA}::siiABCDF</i>	lab collection
p4676	<i>tetR P_{tetA}::siiABCD-miniSiiE</i> <i>Blg1.5::49.5-F</i>	lab collection
p5144	<i>mini SiiE Blg5::49, cb^R</i>	lab collection
p5514	<i>mini SiiE Blg5::49 β-sheet</i> <i>#1::3xFLAG tag_{Pos116}, cb^R</i>	this study
p5216	<i>tetR P_{tetA}::siiAB</i>	this study
p5568	<i>tetR P_{tetA}::siiC, cb^R</i>	this study
p5569	<i>tetR P_{tetA}::siiC::HA, cb^R</i>	this study
p5598	<i>tetR P_{tetA}::siiABC::HA, cb^R</i>	this study
p5640	<i>tetR P_{tetA}::siiABCD-miniSiiE</i> <i>Blg1::49-53-F, cb^R</i>	this study
p5643	<i>tetR P_{tetA}::siiABCD-miniSiiE</i> <i>Blg4::49-53-F, cb^R</i>	this study
p5644	<i>tetR P_{tetA}::siiABCD-miniSiiE Blg1-5::49-53-F, cb^R</i>	this study
p5726	<i>tetR P_{tetA}::siiABC::HA-D-miniSiiE</i> <i>Blg1::49-53-F, cb^R</i>	this study
p5777	<i>tetR P_{tetA}::siiABCD-miniSiiE Blg1-5::49-53-siiF_{G500E}, cb^R</i>	this study

Table III.1.3. Oligonucleotides used in this study.

Designation	Sequence (3' -> 5')	Purpose
Vf-pWSK29-siiABCDF	TAATAACGGAGGCCCTCAC	p4645 Vector for p5640 and p5644
Vr-pWSK29-siiABCDF	CATAATATTATATTCCTCAAGGTGTATC	p4645 Vector for p5640 and p5644
1f siiE N-term	GAGAGTGAATATAATATTATGGGAAATAAAA-GCATACAA	STM gen. DNA insert for p5640 and p5644
2r siiE C-term	GAGGGGCCTCCGTTATTATGCGTGTTCTTCTT-GATT	STM gen. DNA insert for p5640, p5643 and p5644
1r siiE Big1-49	GGTAAATACCTTGATATGGGAATCGA-TAGTAATGAC	STM gen. DNA insert for p5640
2f siiE Big1-49	GTCATTACTATCGAT-TCCCATATCAAGGTATTTACCAG	STM gen. DNA insert for p5640
1r siiE Blg4-49	GGTAAATACCTTGATATGAGTATCAATAAC-GTAACTAAA	STM gen. DNA insert for p5643

2f siiE Blg4-49	AGTTACGTTATTGATACTCAT- ATCAAGGTATTTACCAG	STM gen. DNA insert for p5643
1r siiE Blg5-49	GGTAAATACCTTGATATGAGTTTGAA- TAGTAAAAGAATATTTAAC	STM gen. DNA insert for p5644
2f siiE Blg5-49	TCTTTTACTATTCAAACATCAT- ATCAAGGTATTTACCAG	STM gen. DNA insert for p5644
Vf-p5144-bsheet1	TTAAAAAAGCAGCTTGACG	p5144 Vector for p5514
Vr-p5144-bsheet1	TTCCTCTTCTTCCTTC	p5144 Vector for p5514
bsheet1-3xFLAG-p5144-for	GAAGGAAGAAGAGGAAGACTACAAAGACCATG	pWRG462 insert for p5514
bsheet1-3xFLAG-p5144-rev	CAAGCTGCTTTTTTAACTTGTCATCGTCATC	pWRG462 insert for p5514
Vf-p5216-siiC-HA	CAGCTTTTGTTCCTTTAGTGAG	p5216 Vector for p5598
Vr-p5216-siiC-HA	TTTTTTTCCTCCTTGTTAAACAAACG	p5216 Vector for p5598
1f-p5216-siiC-HA	CGTTTGTTAAACAAGGAGGAAAAAAATGAA- GATTAAGATGTTTTTTCTGA	p5569 Insert for p5598
1r-p5216-siiC-HA	CTCACTAAAGGGAACAAAAGCTGCTCAAGCG- TAGTCTGGGA	p5569 Insert for p5598
1f-SDM-siiC HA-p4251	CCCAGACTACGCTTGAGAATTCCTGCAGCCCG	p5568 SDM for p5569
1r-SDM-siiC HA-p4251	ACGTCGTATGGGTATTTTATTACATTTAAC	p5568 SDM for p5569
Vf-p5640-SiiC-HA	AATAGAAGACAAAGCGATCATCTC	p5640 vector for p5726
Vr-p5640-SiiC-HA	TTTTTTTCCTCCTTGTTAAACAAACG	p5640 vector for p5726
1f-p5640-SiiC-HA	CGTTTGTTAAACAAGGAGGAAAAAAATGAA- GATTAAGATGTTTTTTCTGA	p5669 insert for p5726
1r-p5640-SiiC-HA	GAGATGATCGCTTTGTCTTCTATTTCAAGCG- TAGTCTGGGAC	p5669 insert for p5726
Vf-SiiF point mutation_p5644	AAATAAGCAGCGCTTGTCG	p5644 vector for p5777

Results

Vr-SiiF point mutation_p5644	AAGTAAACCCCCTCACCC	p5644 vector for p5777
1r-siiF point mut_p5644	CGACAAGCGCTGCTTATTTTACATTAA- TAATTTATCCGGAGAA	MvP1311 gen. DNA 128/37insert for p5777
1f-siiF point mut_p5644	GGGTGAGGGGGTTTACTTAT	MvP1311 gen. DNA insert for p5777

III.1.5.3. Label-free mass spectrometry of cytosolic and secreted mini SiiE

Sample preparation and protein extraction from Tris-Acetate gels for in-gel digestion

For sample preparation, bacteria were inoculated 1:31 in LB, supplemented with 50 µg/ml carbenicillin if necessary, induced with AHT after 1 h after inoculation and grown for 2.5 h (cytosolic sample) (unpublished data, PhD thesis Nathalie Sander) and 6 h (secreted sample) due to retention and secretion maxima of SiiE (Gerlach *et al.*, 2007b). For cytosolic sample, secretion-deficient strain was used and 1 ml was pelleted by centrifugation at 10,000 x *g*. Pellet was boiled in 1x SDS cracking buffer according to the OD₆₀₀. For secretion samples, 1.8 ml supernatant was sterile filtered, precipitated with TCA and boiled in 1 x SDS cracking buffer according to the OD₆₀₀. Tris-acetate gels (3-8% polyacrylamide, NUPAGE Tris-acetate gel, Mini: 8 cm x 8 cm (1 or 1.5 mm thick)) were used and Coomassie stain was performed as described previously. Lanes of interest were cut out of the gel and destained with 30% acetonitrile in 100 mM NH₄HCO₃ after a washing step with ultrapure water. Destaining steps were repeated until destain solution and gel pieces remained colorless. Gel pieces were washed three times with ultrapure water and were incubated with 100% acetonitrile for 15 min at 20 °C. Samples were dried at 10 mbar at 37 °C in a vacuum concentrator.

Protein digestion

Samples were reduced with 10 mM DTT (in 100 mM NH₄HCO₃) for 5 min at 20 °C and 30 min at 50 °C. Following reduction, the supernatant was removed and gel pieces were incubated with 100% acetonitrile for 15 min at 20 °C. For alkylation, 54 mM iodoacetamide (in 100 mM NH₄HCO₃) was added and samples were incubated for 15 min at RT in the dark. As described above, samples were destained and treated with acetonitrile. A volume of 50-100 µl trypsin solution (Promega, 0.01 mg/ml in 50 mM NH₄HCO₃ with 5% acetonitrile) was added to dried gel pieces. Samples were incubated o/N at 37 °C. The next day, the reaction was stopped by adding 100% formic acid to a final concentration of 1% and supernatant was removed and stored. To the gel pieces, 30 µl 100% acetonitrile were added and incubated with shaking for 20-30 min, followed by 3 min in a sonification bad. Supernatant was transferred into a new cup

and acetonitrile was evaporated in a vacuum concentrator. Dried peptides were resuspended in first collected digested supernatant. For digestion with pepsin (Promega, pH 1.3), 0.04 M pepsin solution was added at a ratio 1:100 for 9 h at 37 °C and reaction was stopped by heating at 95 °C for 10 min. For ArgC digestion, the samples were resuspended in 50 mM Tris-HCl (pH 7.6 – 7.9), 5 mM CaCl₂ and 2 mM EDTA, activated with activation buffer (50 mM Tris-HCl, 50 mM DTT, 2 mM EDTA) and digested with 0.1 µg ArgC. The peptide containing supernatant was transferred to HPLC vials with 1 µg digested protein was measured by mass spectrometry. Protein concentration was determined using an IMPLEN NanoPhotometer®.

Label-free protein quantification by mass spectrometry

HPLC/MS-MS analysis performed using an Ultimate 3000 Nano HPLC (ThermoFisher). For analyses, a volume of 5-10 µl was desalted and concentrated using a precolumn (ThermoFisher, C18 PepMap 5 µm, 100 A with dimension of 300 µm (id) x 5 mm (length)). The corresponding solvent was water supplemented with 0.1% TFA/H₂O (flow rate of 25 µl/min). The loaded and washed precolumn was switched into the `nano flow line` (250 nl/min) with an Easy Spray column (ThermoFisher, PepMap RSLC C18, 2 µm, 100 A with dimension of 75 µm (id) x 500 mm) at the end. Peptides were continuously eluted by 80% ACN and 0.1% in H₂O in 160 min. The electro spray ionization (ESI) was done at 1,500 V (ESI Spray Source, ThermoFisher). A Q-Exactive Plus orbitrap mass spectrometer (ThermoFisher) was used to determine the MS/MS (HCD fragmentation) data under the following conditions (Table III.1.4):

Table III.1.4. Settings for label-free protein quantification by mass spectrometry.

	MS	MS precursor selection	MSMS
resolution	70,000		17,500
AGC target	3e6	5e2	1e5
rax IT	50 ms		80 ms
MS Range	375-1800 m/z		
loop Count			10
NCE			27
isolation Width			1.4 m/z
charge		2-5	

Data analysis

The resulting data were loaded to and analyzed by Peaks Studio X and PeaksOnline (Bioinformatics Solution Inc, Canada). *De novo* search was performed for peptide identification by a DB search using a protein database for STM 14028 (*Salmonella* Typhimurium strain 14028s_11_1; 5,372 proteins). Peaks Q (*de novo* assisted Quantification) and Peaks DB (In-

depth *de novo* assisted search) were performed. The MS tolerance was adjusted to 20.0 ppm, the MS/MS tolerance to 0.2 Da and two missed cleavages were allowed. The digest mode was set “specific”. Further, carbamido-methylation of cysteines and oxidation of methionine for fixed post translationally modifications and for variable modifications were chosen, respectively. Peptides were analyzed regarding their area. A standard peptide from the central area of mini SiiE was chosen (with a comparable area in cytosolic and secreted sample) and a C-terminal peptide was used as control. In the N-terminal part, two peptides were found that were significantly increased in their amount in cytosolic sample than in secreted sample (aa2-19 and aa2-43). Peptides from aa44 on were found in both samples in comparable amounts.

III.1.5.4. Western blot

Western blot detection for protein biosynthesis

For sample preparation, bacteria were inoculated 1:31 in LB, supplemented with 50 µg/ml carbenicillin if necessary, induced with AHT after 1 h after inoculation and grown for 2.5 h. 1 ml was pelleted by centrifugation at 10,000 x *g*. Pellet was boiled in 1x SDS cracking buffer according to the OD₆₀₀. SDS Laemmli gels were run for 20 min at 80 V and 75 min with 150 V. Semi-dry Western blot (WB) was performed with 0.45 µm nitrocellulose membrane with 0.8 mA/cm². Following Ponceau S stain, membranes were blocked with 5% skimmed dry milk powder in TBS-T (0.1% Tween20 in TBS) for at least 30 min at RT. Primary antibodies were incubated o/N in blocking solution at 4 °C. The next day, membranes were washed three times with TBS-T and incubated with HRP-conjugated secondary antibody in blocking solution for 1 h at RT. Antibodies, used in this study are mentioned in Table III.1.5 and Table III.1.6. Membranes were washed an additional three times with TBS-T, treated with Pierce™ ECL Western blotting Substrate (ThermoFisher) after manufacturer’s instructions and imaged with Chemi-Doc™ Imager (Bio-Rad) and ImageLab software.

Western blot analysis of trimeric TolC and SiiC

Samples were prepared as described above. Different SDS concentrations were tested (2% and 4%) to determine, if lower SDS concentration in the loading buffer can support oligomers of SiiC and TolC. TolC was used as control for a trimeric complex here. PAGE and Western blots were performed as described above. Membranes were incubated with primary antibodies α-TolC (kindly provided by Lutz Schmitt, Institute of Biochemistry, Heinrich Heine University Düsseldorf, Germany), α-HA HRP-conjugated secondary antibodies as described above (Table III.1.5 and Table III.1.6).

Analyses of proteolytic cleavage of secreted mini SiiE by Western blot

For Western blot analysis of cytosolic and secreted mini SiiE tagged with 3xFLAG tag, subcultures were grown for 2.5 h (cytosolic SiiE) and 6 h (secreted mini SiiE) and were boiled in SDS cracking buffer according to OD₆₀₀ and SDS-PAGE was performed (8% Laemmli gel). Gels were run for 20 min at 80 V and for 75 min at 150 V. Next, semi-dry transfer was performed for 75 min at 0.8 mA/cm² membrane onto nitrocellulose membranes. Protein transfer was verified by Ponceau S red staining. Membranes were blocked with 5% skimmed dry milk powder in TBS-T. In both analyses α -SiiE and for analysis of mini SiiE with FLAG-tag α -FLAG tag antibody in blocking solution were used for blot development o/N at 4 °C (Table III.1.5 and Table III.1.6). Membranes were treated as described above. The size of mini SiiE was calculated using ImageLab software. The regression method was linear (semi-log), formula: $y = -1.05 \cdot x + 2.46$, R-squared value: 0.976587.

Table III.1.5. Primary antibodies used in this study.

Antigen	Host	Dilution	Purpose
GST-SiiE-C	rabbit	1:10,000	WB (SiiE and mini SiiE)
GST-SiiE-C	rabbit	1:1,000	IF (SiiE and mini SiiE)
ToIC	rabbit	1:2,000	WB
HA tag	rat	1:10,000	WB
FLAG tag	mouse	1:2,000	WB
<i>Salmonella</i> O Antiserum Group B Factors	rabbit	1:10,000	DB

Table III.1.6. Secondary antibodies used in this study.

Species reactivity	Host	Conjugated with	Dilution	Purpose
rabbit	goat	HRP	1:10,000	WB
rat	goat	HRP	1:10,000	WB
mouse	goat	HRP	1:10,000	WB
rabbit	goat	Alexa488	1:1,000	IF
rabbit	goat	IRDye800CW	1:20,000	DB

III.1.5.5. OM isolation and pulldown assay for SiiE and SiiC

Bacteria were grown for 2.5 h, induced with AHT after 1 h and 15 ml were harvested by centrifugation at 9,000 x *g* for 10 min at 4 °C. Pellet was resuspended in sucrose containing buffer (0.5 M sucrose, 10 mM Tris pH 7.5) and treated with lysozyme (final concentration 144 µg/ml) for 2 min on ice and subsequently EDTA (0.75 mM final) for 7 min on ice. After incubation, OM containing supernatant was collected by centrifugation at 9,000 x *g* for 10 min. OM supernatant was incubated with Protein A Sepharose beads decorated with α-SiiE IgG antibody for 2 h at 4 °C on an orbital shaker. For bead decoration, Protein A Sepharose beads were equilibrated and washed with 0.1% Triton X-100 in PBS. Following equilibration, beads were incubated with 1 ml α-SiiE serum for 3 h at 4 °C on an orbital shaker. Afterwards, beads were washed three times with 0.1% Triton X-100 in PBS and used for pulldown assays. During the experimental procedure, samples of whole cell lysate, supernatant, intact cells, IM fraction and OM fraction, load, flow through and eluate were taken and boiled in SDS cracking buffer according to the OD₆₀₀. After incubation, beads were washed with 0.1% Triton X-100 in PBS. To elute SiiC and mini SiiE, beads were treated with 0.1 M glycine (pH 2.6) to carefully extract mini SiiE together with SiiC (eluate 1). After neutralization of the sample with 1 M Tris, beads were boiled in SDS cracking buffer at 95 °C for 5 min (eluate 2). As controls *Δspi4* background strain and purified mini SiiE for bead decoration were used. SDS-PAGE and semi-dry Western blot were performed as described above. The antibodies used are listed in Table III.1.5 and Table III.1.6.

III.1.5.6. Dot blot analysis of retained and secreted SiiE and mini SiiE

For Dot blot analysis, bacteria were inoculated in appropriate medium and grown for 2.5 h (SiiE retention maximum, unpublished data, PhD thesis Nathalie Sander) and 6 h (SiiE secretion maximum) (Gerlach *et al.*, 2007b). Dot blot was performed as published before (Peters *et al.*, 2017). The antibodies used for the Dot blots are described in Table III.1.5 and Table III.1.6.

III.1.5.7. Transmission electron microscopy

O/N cultures of bacteria were diluted 1:31 in 3 ml fresh LB with 50 µg/ml carbenicillin. Subcultures were incubated at 37 °C for 1 h, with aeration and thereafter, Tet-On gene expression induced by adding 10 ng/ml AHT. After further incubation for 1.5 h at 37 °C with aeration, minicells were enriched and isolated by several centrifugation steps. At first, 3 ml of the 2.5 h subculture was centrifuged at 4000 x *g* for 5 min. and thereafter, supernatant was transferred to a new vessel, whereas the cell pellet was discarded. This procedure was repeated once. The supernatant was centrifuged for 10 min at 15,000 x *g* and minicell pellet was resuspended in

30 µl of PBS. Then, 4 µl of the minicell enriched suspension was transferred to freshly glow discharged EM grids (Quantifoil grid, Cu 300 mesh, R2/1) and vitrified by plunge-freezing with a Leica EM GP2 system at 10 °C and 80% humidity. Visualisation of minicells was performed with a 200 keV JEOL JEM 2100 Plus system. Scale bars were generated and also, contrast and brightness of images was changed by using Adobe Photoshop CS6 software.

III.1.5.8. Fluorescence microscopy of retained SiiE

For the microscopic analysis of SiiE surface signal, subcultures were grown for 2.5 h with AHT induction after 1 h, pelleted by centrifugation at 7,000 x *g* and fixed with 3% PFA in PBS for 15 min at RT. Following fixation, bacteria were washed three times with PBS and treated with blocking solution (supplemented with 2% goat serum) for at least 30 min at RT. Bacteria were stained against surface bound SiiE with primary antibody against SiiE and Alexa488-conjugated secondary antibody (Table III.1.5 and Table III.1.6). For microscopy, Zeiss Axio Observer.Z1 coupled with a TIRF module was used. The used objective was the alpha Plan-Apochromat 100x/1.46 Oil DIC (UV) M27. Imaging with AxioCam MR R3 with a camera adapter 1.0 x, total magnification 100x, Zoom 1.0x.

III.1.5.9. Cell culture

MDCK cells (subline pf, obtained from Prof. Dr. M. Goppelt-Struebe, Med. Klinik 4, Universitätsklinikum Erlangen) were cultured as described before (Gerlach *et al.*, 2008). For adhesion and invasion assays, cells were seeded in 24-well plates at a density of 1×10^5 cells per well 5 days before infection to ensure differentiation of cells. At the day of infection, cell density was 5×10^5 cells per well. Due to the long incubation time, the medium was supplemented with penicillin and streptomycin. The medium was changed to antibiotic-free medium one day before infection (at least 4 h before infection).

III.1.5.10. Adhesion and invasion assay

To determine adhesion, cells were treated with 3 µg/ml Cytochalasin D 1 h before infection, to inhibit actin remodeling and uptake of the pathogen. For infection, 2.5 h subcultures of infecting STM were grown, MDCK cells were infected in technical triplicates at multiplicity of infection (MOI) 5, and incubated for 25 min at 37 °C in an atmosphere of 5% CO₂. The cells were washed three times with prewarmed PBS. To determine adhesion, cells were lysed directly with 0.5% deoxycholate in PBS (freshly prepared). To determine invasion, cells were treated

with 500 µl medium containing 100 µg/ml gentamicin per well for 1 h, washed three times with prewarmed PBS and lysed with 0.5% deoxycholate in PBS (freshly prepared). Lysis was performed for 10 min at 37 °C on a shaking platform. Lysates were collected in single tubes and serial dilutions of inoculum and lysates were plated logarithmic on MH plates to determine CFU. Plates were incubated o/N at 37 °C and CFU were counted the next day with Acolyte software. The percentages of adhered and invaded bacteria were calculated.

III.1.5.11. Bioinformatic analyses

Primary and secondary structure analysis of TolC, LapE and SiiC was performed with Ali2D (Gabler *et al.*, 2020) and visualization with 2dSS (Laboratory of Computational and Quantitative Biology (LCQB) (freeware). Gaps were allowed for primary sequence comparison. Percentages of modelled structures and confidence, calculated by Phyre2 (Kelley *et al.*, 2015) algorithms. Tertiary structure model predictions were performed by trRosetta algorithms (Du, 2021; Yang *et al.*, 2020) and visualized with Pymol. TM-score for modelling by trRosetta. TM-score > 0.4 = medium, TM-score > 0.5 = high, TM-score > 0.7 = very high confidence. The hydrophobicity plots were performed with Expasy ProtScale and the amino acid scale for hydrophobicity after Kyte and Doolittle was used (Kyte and Doolittle, 1982).

III.1.6. Acknowledgements

This study was supported by the SFB944. We like to thank Dr. Stefan Walter (University Osnabrueck, CellNanOs, service unit for mass spectrometry) for the proteomic analyses and support with data analyses and Pascal Felgner for the Cryo-TEM image of mini SiiE.

III.1.7. Supplements

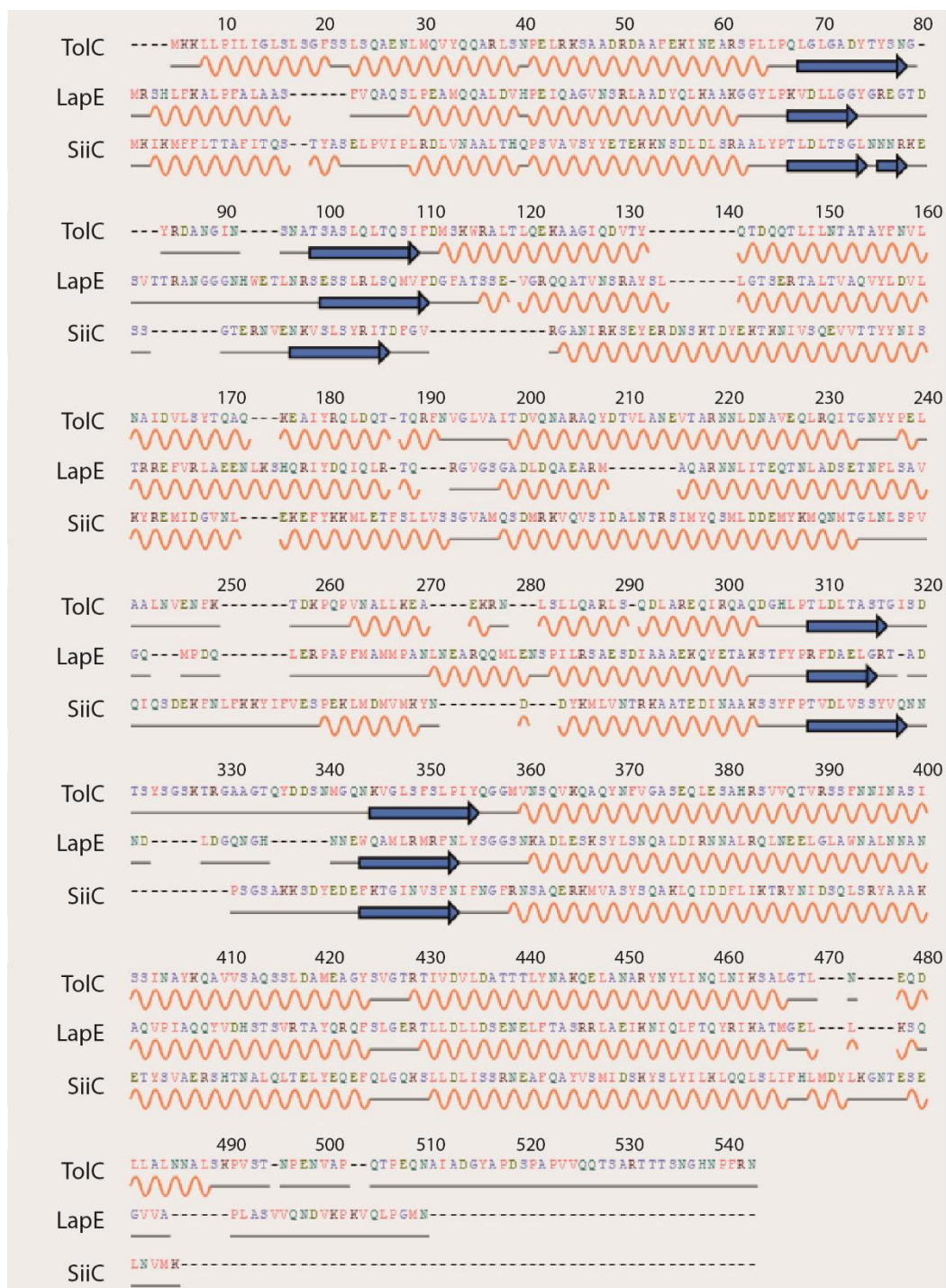


Figure S III.1.1. Primary and secondary structure analysis of TolC, LapE and SiiC. TolC (top), LapE (center) and SiiC (below) by Ali2D (Gabler *et al.*, 2020) and visualization by 2dSS (Laboratory of Computational and Quantitative Biology (LCQB)). Gaps allowed for primary sequence comparison. Color codes/symbols: α -helix = orange, β -sheet = blue, loops = gray; hydrophobic amino acids (CVILPFIYMW) = light pink, small amino acids (GAST) = light purple, polar amino acids (NQH) = turquoise green, negatively charged amino acids (DE) = light green and positively charged amino acids (KR) = brown.

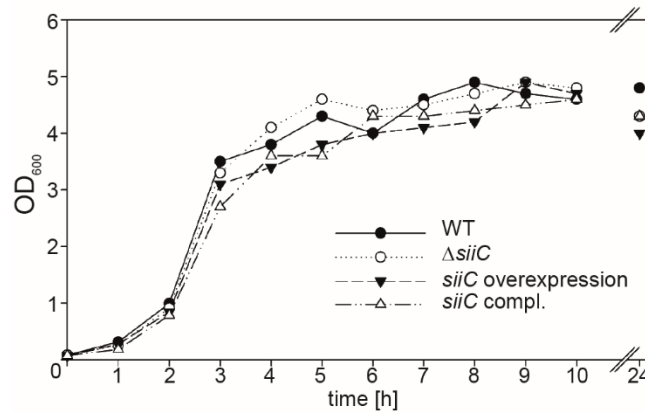


Figure S III.1.2. Growth curve *siiC* overexpression. For the analyses of growth kinetics, bacteria were grown overnight (o/N) in LB, supplemented with 50 μ g/ml carbenicillin if necessary, at 37 °C. First, OD₆₀₀ was determined and subcultures were inoculated to OD₆₀₀=0.01 in 100 ml fresh LB medium in 500 ml flasks and incubated with 160 rpm 37 °C. OD₆₀₀ was measured as indicated.

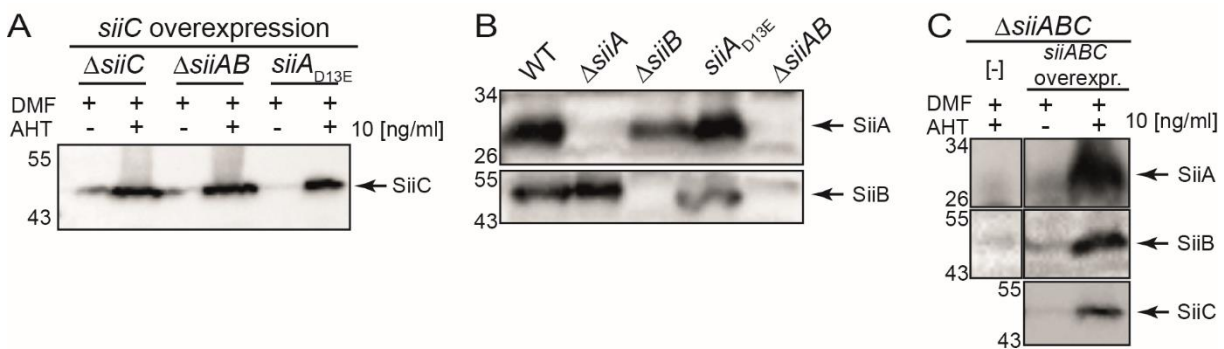


Figure S III.1.3. Analyses of protein levels after *siiC* overexpression in *siiAB* mutant backgrounds and *siiABC* overexpression. Western blot against SiiA, SiiB and HA-Tag (SiiC). Subcultures were grown for 2.5 h with AHT induction after 1 h, pelleted by centrifugation at 7,000 x *g* and boiled in SDS cracking buffer according to the OD₆₀₀. SDS-PAGE and Western blot with antibodies α -SiiA (1:10,000), α -SiiB (1:10,000) and α -HA (1:10,000), α -rabbit HRP-conjugated (1:10,000) and α -rat HRP-conjugated (1:10,000) were performed. Marker and weights of the proteins as indicated.

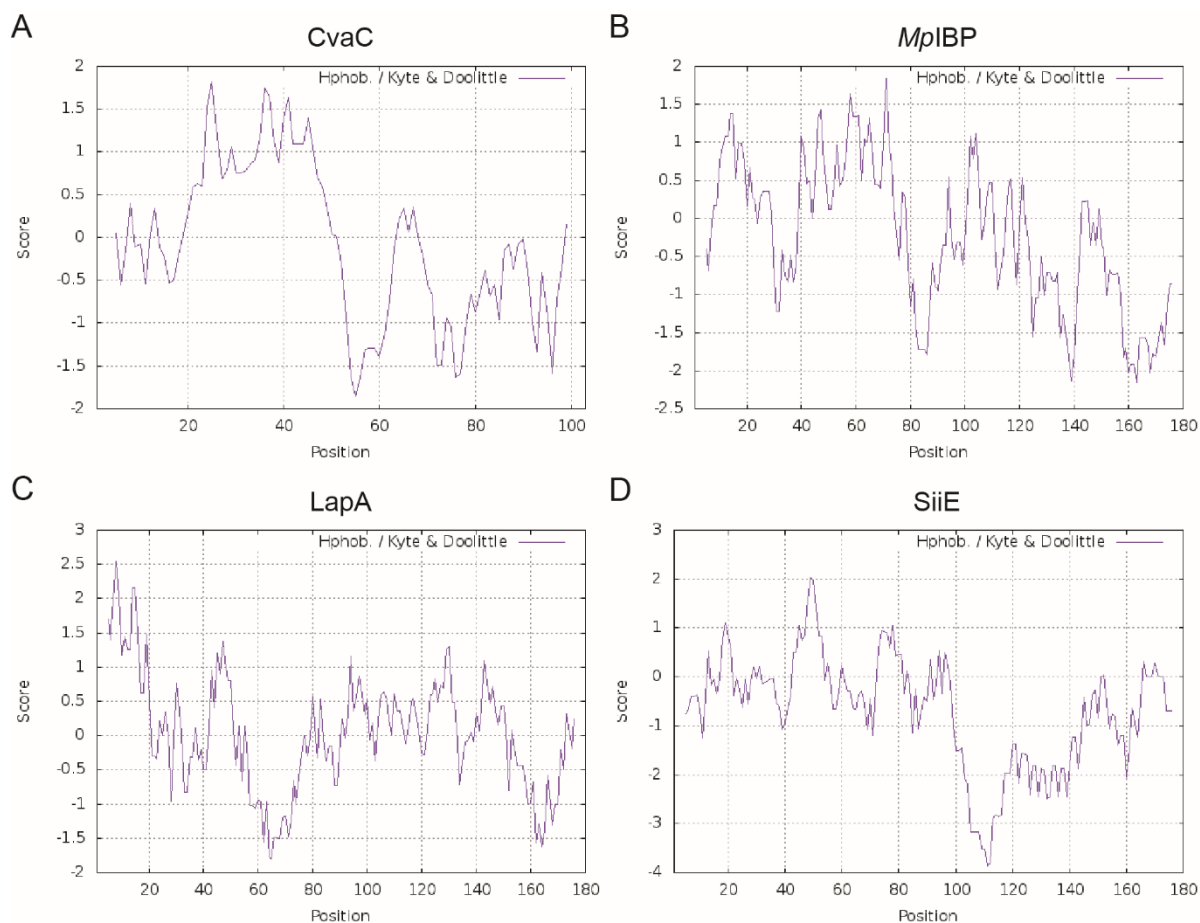


Figure S III.1.4. Hydrophobicity plots of CvaC, N-terminal parts of MplBP, LapA and SiiE after Kyte and Doolittle. Shown is the hydrophobicity (Y-axis) of the amino acid (aa) sequences (X-axis) of the proteins according to Kyte-Doolittle (Kyte and Doolittle, 1982). The Kyte-Doolittle scale indicates hydrophobic aa. Positive values indicate hydrophobic amino acids, whereas negative values indicate hydrophilic amino acids. For CvaC (A) the whole sequence is shown (103 aa), for MplBP (B), LapA (C) and SiiE (D) only the first 180 aa of the N-terminus are depicted due to their sizes. By analyzing the shape of the plot, we gained information about parts of the protein.

III.1.8. References

- Ambrosio, N., Boyd, C.D., GA, O.T., Fernandez, J., and Sisti, F. (2016). Homologs of the LapD-LapG c-di-GMP Effector System Control Biofilm Formation by *Bordetella bronchiseptica*. *PLoS One* 11, e0158752.
- Andersen, C., Hughes, C., and Koronakis, V. (2000). Chunnel vision. Export and efflux through bacterial channel-tunnels. *EMBO Rep* 1, 313-318.
- Barlag, B., and Hensel, M. (2015). The giant adhesin SiiE of *Salmonella enterica*. *Molecules* 20, 1134-1150.
- Bass, S., Gu, Q., and Christen, A. (1996). Multicopy suppressors of *prc* mutant *Escherichia coli* include two HtrA (DegP) protease homologs (HhoAB), DksA, and a truncated R1pA. *J Bacteriol* 178, 1154-1161.
- Boyd, C.D., Chatterjee, D., Sondermann, H., and O'Toole, G.A. (2012). LapG, required for modulating biofilm formation by *Pseudomonas fluorescens* Pf0-1, is a calcium-dependent protease. *J Bacteriol* 194, 4406-4414.
- Boyd, C.D., and O'Toole, G.A. (2012). Second messenger regulation of biofilm formation: breakthroughs in understanding c-di-GMP effector systems. *Annu Rev Cell Dev Biol* 28, 439-462.
- Boyd, C.D., Smith, T.J., El-Kirat-Chatel, S., Newell, P.D., Dufrene, Y.F., and O'Toole, G.A. (2014). Structural features of the *Pseudomonas fluorescens* biofilm adhesin LapA required for LapG-dependent cleavage, biofilm formation, and cell surface localization. *J Bacteriol* 196, 2775-2788.
- Boyer, A.E., and Tai, P.C. (1998). Characterization of the *cvaA* and *cvi* promoters of the colicin V export system: iron-dependent transcription of *cvaA* is modulated by downstream sequences. *J Bacteriol* 180, 1662-1672.
- Bunikis, I., Denker, K., Ostberg, Y., Andersen, C., Benz, R., and Bergstrom, S. (2008). An RND-type efflux system in *Borrelia burgdorferi* is involved in virulence and resistance to antimicrobial compounds. *PLoS Pathog* 4, e1000009.
- Chenal, A., Guijarro, J.I., Raynal, B., Delepierre, M., and Ladant, D. (2009). RTX calcium binding motifs are intrinsically disordered in the absence of calcium: implication for protein secretion. *J Biol Chem* 284, 1781-1789.
- Cooley, R.B., O'Donnell, J.P., and Sondermann, H. (2016a). Coincidence detection and bi-directional transmembrane signaling control a bacterial second messenger receptor. *Elife* 5.
- Cooley, R.B., Smith, T.J., Leung, W., Tierney, V., Borlee, B.R., O'Toole, G.A., and Sondermann, H. (2016b). Cyclic Di-GMP-Regulated Periplasmic Proteolysis of a *Pseudomonas aeruginosa* Type Vb Secretion System Substrate. *J Bacteriol* 198, 66-76.
- Du, S., Wang, Ye, Wei, Peng, Anishchenko, Baker, Yang (2021). The trRosetta server for fast and accurate protein structure prediction. *Nature Protocols*.
- Fath, M.J., Zhang, L.H., Rush, J., and Kolter, R. (1994). Purification and characterization of colicin V from *Escherichia coli* culture supernatants. *Biochemistry* 33, 6911-6917.
- Fulop, V., Bocskei, Z., and Polgar, L. (1998). Prolyl oligopeptidase: an unusual beta-propeller domain regulates proteolysis. *Cell* 94, 161-170.
- Gabler, F., Nam, S.Z., Till, S., Mirdita, M., Steinegger, M., Soding, J., Lupas, A.N., and Alva, V. (2020). Protein Sequence Analysis Using the MPI Bioinformatics Toolkit. *Curr Protoc Bioinformatics* 72, e108.
- Gangola, P., and Rosen, B.P. (1987). Maintenance of intracellular calcium in *Escherichia coli*. *J Biol Chem* 262, 12570-12574.
- Gerlach, R.G., Claudio, N., Rohde, M., Jackel, D., Wagner, C., and Hensel, M. (2008). Cooperation of *Salmonella* pathogenicity islands 1 and 4 is required to breach epithelial barriers. *Cell Microbiol* 10, 2364-2376.
- Gerlach, R.G., and Hensel, M. (2007). *Salmonella* pathogenicity islands in host specificity, host pathogen-interactions and antibiotics resistance of *Salmonella enterica*. *Berl Munch Tierarztl Wochenschr* 120, 317-327.

- Gerlach, R.G., Jackel, D., Geymeier, N., and Hensel, M. (2007a). *Salmonella* pathogenicity island 4-mediated adhesion is coregulated with invasion genes in *Salmonella enterica*. *Infect Immun* 75, 4697-4709.
- Gerlach, R.G., Jackel, D., Stecher, B., Wagner, C., Lupas, A., Hardt, W.D., and Hensel, M. (2007b). *Salmonella* Pathogenicity Island 4 encodes a giant non-fimbrial adhesin and the cognate type 1 secretion system. *Cell Microbiol* 9, 1834-1850.
- Gilson, L., Mahanty, H.K., and Kolter, R. (1990). Genetic analysis of an MDR-like export system: the secretion of colicin V. *EMBO J* 9, 3875-3884.
- Ginalski, K., Kinch, L., Rychlewski, L., and Grishin, N.V. (2004). BTLCIP proteins: a novel family of bacterial transglutaminase-like cysteine proteinases. *Trends Biochem Sci* 29, 392-395.
- Gjermansen, M., Nilsson, M., Yang, L., and Tolker-Nielsen, T. (2010). Characterization of starvation-induced dispersion in *Pseudomonas putida* biofilms: genetic elements and molecular mechanisms. *Mol Microbiol* 75, 815-826.
- Gray, L., Mackman, N., Nicaud, J.M., and Holland, I.B. (1986). The carboxy-terminal region of haemolysin 2001 is required for secretion of the toxin from *Escherichia coli*. *Mol Gen Genet* 205, 127-133.
- Griessl, M.H., Schmid, B., Kassler, K., Braunsmann, C., Ritter, R., Barlag, B., Stierhof, Y.D., Sturm, K.U., Danzer, C., Wagner, C., *et al.* (2013). Structural insight into the giant Ca(2)(+)-binding adhesin SiiE: implications for the adhesion of *Salmonella enterica* to polarized epithelial cells. *Structure* 21, 741-752.
- Guo, S., Langelaan, D.N., Phippen, S.W., Smith, S.P., Voets, I.K., and Davies, P.L. (2018). Conserved structural features anchor biofilm-associated RTX-adhesins to the outer membrane of bacteria. *FEBS J* 285, 1812-1826.
- Guo, S., Stevens, C.A., Vance, T.D.R., Olijve, L.L.C., Graham, L.A., Campbell, R.L., Yazdi, S.R., Escobedo, C., Bar-Dolev, M., Yashunsky, V., *et al.* (2017). Structure of a 1.5-MDa adhesin that binds its Antarctic bacterium to diatoms and ice. *Sci Adv* 3, e1701440.
- Icke, C., Hodges, F.J., Pullela, K., McKeand, S.A., Bryant, J.A., Cunningham, A.F., Cole, J.A., and Henderson, I.R. (2021). Glycine acylation and trafficking of a new class of bacterial lipoprotein by a composite secretion system. *Elife* 10.
- Jarchau, T., Chakraborty, T., Garcia, F., and Goebel, W. (1994). Selection for transport competence of C-terminal polypeptides derived from *Escherichia coli* hemolysin: the shortest peptide capable of autonomous HlyB/HlyD-dependent secretion comprises the C-terminal 62 amino acids of HlyA. *Mol Gen Genet* 245, 53-60.
- Jones, C.H., Dexter, P., Evans, A.K., Liu, C., Hultgren, S.J., and Hruby, D.E. (2002). *Escherichia coli* DegP protease cleaves between paired hydrophobic residues in a natural substrate: the PapA pilin. *J Bacteriol* 184, 5762-5771.
- Kanonenberg, K., Schwarz, C.K., and Schmitt, L. (2013). Type I secretion systems - a story of appendices. *Res Microbiol* 164, 596-604.
- Kelley, L.A., Mezulis, S., Yates, C.M., Wass, M.N., and Sternberg, M.J. (2015). The Phyre2 web portal for protein modeling, prediction and analysis. *Nat Protoc* 10, 845-858.
- Kirchweger, P., Weiler, S., Egerer-Sieber, C., Blasl, A.T., Hoffmann, S., Schmidt, C., Sander, N., Merker, D., Gerlach, R.G., Hensel, M., *et al.* (2019). Structural and functional characterization of SiiA, an auxiliary protein from the SPI4-encoded type 1 secretion system from *Salmonella enterica*. *Mol Microbiol* 112, 1403-1422.
- Koronakis, V., Koronakis, E., and Hughes, C. (1989). Isolation and analysis of the C-terminal signal directing export of *Escherichia coli* hemolysin protein across both bacterial membranes. *EMBO J* 8, 595-605.
- Koronakis, V., Li, J., Koronakis, E., and Stauffer, K. (1997). Structure of TolC, the outer membrane component of the bacterial type I efflux system, derived from two-dimensional crystals. *Mol Microbiol* 23, 617-626.
- Koronakis, V., Sharff, A., Koronakis, E., Luisi, B., and Hughes, C. (2000). Crystal structure of the bacterial membrane protein TolC central to multidrug efflux and protein export. *Nature* 405, 914-919.

- Krogh, A., Larsson, B., von Heijne, G., and Sonnhammer, E.L. (2001). Predicting transmembrane protein topology with a hidden Markov model: application to complete genomes. *J Mol Biol* 305, 567-580.
- Kyte, J., and Doolittle, R.F. (1982). A simple method for displaying the hydropathic character of a protein. *J Mol Biol* 157, 105-132.
- Lecher, J., Schwarz, C.K., Stoldt, M., Smits, S.H., Willbold, D., and Schmitt, L. (2012). An RTX transporter tethers its unfolded substrate during secretion via a unique N-terminal domain. *Structure* 20, 1778-1787.
- Lenders, M.H., Weidtkamp-Peters, S., Kleinschrodt, D., Jaeger, K.E., Smits, S.H., and Schmitt, L. (2015). Directionality of substrate translocation of the hemolysin A Type I secretion system. *Sci Rep* 5, 12470.
- Linhartova I., O.R., Bumba L., Masin J., Sebo P. (2015). RTX Toxins: A Review. *Toxinology Microbial Toxins*, 1-29.
- Ludwig, A., Garcia, F., Bauer, S., Jarchau, T., Benz, R., Hoppe, J., and Goebel, W. (1996). Analysis of the in vivo activation of hemolysin (HlyA) from *Escherichia coli*. *J Bacteriol* 178, 5422-5430.
- Mackman, N., Baker, K., Gray, L., Haigh, R., Nicaud, J.M., and Holland, I.B. (1987). Release of a chimeric protein into the medium from *Escherichia coli* using the C-terminal secretion signal of haemolysin. *EMBO J* 6, 2835-2841.
- Mackman, N., Nicaud, J.M., Gray, L., and Holland, I.B. (1985). Identification of polypeptides required for the export of haemolysin 2001 from *E. coli*. *Mol Gen Genet* 201, 529-536.
- Mo, E., Peters, S.E., Willers, C., Maskell, D.J., and Charles, I.G. (2006). Single, double and triple mutants of *Salmonella enterica* serovar Typhimurium *degP* (*htrA*), *degQ* (*hhoA*) and *degS* (*hhoB*) have diverse phenotypes on exposure to elevated temperature and their growth in vivo is attenuated to different extents. *Microb Pathog* 41, 174-182.
- Monds, R.D., Newell, P.D., Gross, R.H., and O'Toole, G.A. (2007). Phosphate-dependent modulation of c-di-GMP levels regulates *Pseudomonas fluorescens* Pf0-1 biofilm formation by controlling secretion of the adhesin LapA. *Mol Microbiol* 63, 656-679.
- Navarro, M.V., Newell, P.D., Krasteva, P.V., Chatterjee, D., Madden, D.R., O'Toole, G.A., and Sondermann, H. (2011). Structural basis for c-di-GMP-mediated inside-out signaling controlling periplasmic proteolysis. *PLoS Biol* 9, e1000588.
- Newell, P.D., Boyd, C.D., Sondermann, H., and O'Toole, G.A. (2011). A c-di-GMP effector system controls cell adhesion by inside-out signaling and surface protein cleavage. *PLoS Biol* 9, e1000587.
- Newell, P.D., Monds, R.D., and O'Toole, G.A. (2009). LapD is a bis-(3',5')-cyclic dimeric GMP-binding protein that regulates surface attachment by *Pseudomonas fluorescens* Pf0-1. *Proc Natl Acad Sci U S A* 106, 3461-3466.
- Nicaud, J.M., Mackman, N., Gray, L., and Holland, I.B. (1985). Characterisation of HlyC and mechanism of activation and secretion of haemolysin from *E. coli* 2001. *FEBS Lett* 187, 339-344.
- Patel, S. (2017). A critical review on serine protease: Key immune manipulator and pathology mediator. *Allergol Immunopathol (Madr)* 45, 579-591.
- Pei, X.Y., Hinchliffe, P., Symmons, M.F., Koronakis, E., Benz, R., Hughes, C., and Koronakis, V. (2011). Structures of sequential open states in a symmetrical opening transition of the TolC exit duct. *Proc Natl Acad Sci U S A* 108, 2112-2117.
- Perez-Mendoza, D., Coulthurst, S.J., Humphris, S., Campbell, E., Welch, M., Toth, I.K., and Salmond, G.P. (2011). A multi-repeat adhesin of the phytopathogen, *Pectobacterium atrosepticum*, is secreted by a Type I pathway and is subject to complex regulation involving a non-canonical diguanylate cyclase. *Mol Microbiol* 82, 719-733.
- Sander, N. (2022). Functional analysis and characterization of the type 1 secretion system and its cognate substrate, the giant adhesin SiiE, of *Salmonella enterica*. University of Osnabrueck
- Peters, B., Stein, J., Klingl, S., Sander, N., Sandmann, A., Taccardi, N., Sticht, H., Gerlach, R.G., Muller, Y.A., and Hensel, M. (2017). Structural and functional dissection reveals distinct roles of Ca²⁺-binding sites in the giant adhesin SiiE of *Salmonella enterica*. *PLoS Pathog* 13, e1006418.

- Smith, T.J., Font, M.E., Kelly, C.M., Sondermann, H., and O'Toole, G.A. (2018a). An N-Terminal Retention Module Anchors the Giant Adhesin LapA of *Pseudomonas fluorescens* at the Cell Surface: a Novel Subfamily of Type I Secretion Systems. *J Bacteriol* 200.
- Smith, T.J., Sondermann, H., and O'Toole, G.A. (2018b). Type 1 Does the Two-Step: Type 1 Secretion Substrates with a Functional Periplasmic Intermediate. *J Bacteriol* 200.
- St Geme, J.W., 3rd, and Grass, S. (1998). Secretion of the *Haemophilus influenzae* HMW1 and HMW2 adhesins involves a periplasmic intermediate and requires the HMWB and HMWC proteins. *Mol Microbiol* 27, 617-630.
- Strauch, K.L., and Beckwith, J. (1988). An *Escherichia coli* mutation preventing degradation of abnormal periplasmic proteins. *Proc Natl Acad Sci U S A* 85, 1576-1580.
- Strauch, K.L., Johnson, K., and Beckwith, J. (1989). Characterization of degP, a gene required for proteolysis in the cell envelope and essential for growth of *Escherichia coli* at high temperature. *J Bacteriol* 171, 2689-2696.
- ter Beek, J., Guskov, A., and Slotboom, D.J. (2014). Structural diversity of ABC transporters. *J Gen Physiol* 143, 419-435.
- Thanabalu, T., Koronakis, E., Hughes, C., and Koronakis, V. (1998). Substrate-induced assembly of a contiguous channel for protein export from *E.coli*: reversible bridging of an inner-membrane translocase to an outer membrane exit pore. *EMBO J* 17, 6487-6496.
- Wagner, C., Polke, M., Gerlach, R.G., Linke, D., Stierhof, Y.D., Schwarz, H., and Hensel, M. (2011). Functional dissection of SiiE, a giant non-fimbrial adhesin of *Salmonella enterica*. *Cellular microbiology* 13, 1286-1301.
- Wagner, W., Vogel, M., and Goebel, W. (1983). Transport of hemolysin across the outer membrane of *Escherichia coli* requires two functions. *J Bacteriol* 154, 200-210.
- Waller, P.R., and Sauer, R.T. (1996). Characterization of degQ and degS, *Escherichia coli* genes encoding homologs of the DegP protease. *J Bacteriol* 178, 1146-1153.
- Wandersman, C., and Delepelaire, P. (1990). TolC, an *Escherichia coli* outer membrane protein required for hemolysin secretion. *Proc Natl Acad Sci U S A* 87, 4776-4780.
- Wang, Z., Fan, G., Hryc, C.F., Blaza, J.N., Serysheva, I., Schmid, M.F., Chiu, W., Luisi, B.F., and Du, D. (2017). An allosteric transport mechanism for the AcrAB-TolC multidrug efflux pump. *Elife* 6.
- Wille, T., Wagner, C., Mittelstadt, W., Blank, K., Sommer, E., Malengo, G., Dohler, D., Lange, A., Sourjik, V., Hensel, M., *et al.* (2014). SiiA and SiiB are novel type I secretion system subunits controlling SPI4-mediated adhesion of *Salmonella enterica*. *Cell Microbiol* 16, 161-178.
- Yang, J., Anishchenko, I., Park, H., Peng, Z., Ovchinnikov, S., and Baker, D. (2020). Improved protein structure prediction using predicted interresidue orientations. *Proc Natl Acad Sci U S A* 117, 1496-1503.
- Zhang, L.H., Fath, M.J., Mahanty, H.K., Tai, P.C., and Kolter, R. (1995). Genetic analysis of the colicin V secretion pathway. *Genetics* 141, 25-32.
- Zhou, G., Yuan, J., and Gao, H. (2015). Regulation of biofilm formation by BpfA, BpfD, and BpfG in *Shewanella oneidensis*. *Front Microbiol* 6, 790.

III.2. The extended cytosolic domain of SiiB is critical for SiiAB proton channel function of *Salmonella enterica*

Nathalie Sander¹ and Michael Hensel^{1,2}

¹Division of Microbiology, University Osnabrueck, Osnabrueck, Germany

²CellNanOs – Center for Cellular Nanoanalytics, University Osnabrueck, Osnabrueck, Germany

III.2.1. Abstract

The type 1 secretion system (T1SS) encoded on the *Salmonella* Pathogenicity Island 4 (SPI4) secretes its substrate, the giant adhesin SiiE. The SPI4-T1SS and SiiE were shown to be important for *Salmonella* virulence as SiiE mediates the first close contact to membranes of polarized host cells, enabling the SPI1-encoded type 3 secretion system (T3SS) to secrete an effector protein cocktail into the host cells cytosol, leading to membrane ruffling and uptake of the pathogen. The SPI4-T1SS shows homologies to already known ATP-binding cassette (ABC) transporters. Interestingly, there are two additional accessory proteins encoded by genes in SPI4, namely SiiA and SiiB. SiiA and SiiB together form a proton channel in the inner membrane (IM) and were shown to be involved in SiiE retention and secretion, and consequently adhesion and invasion. SiiAB possess similarities to other known proton channels of the MotA/ExbB family. Although SiiB was predicted to harbor an extended cytoplasmic part, its detailed structure, function and mechanism are still poorly understood. Here, we demonstrated that mutant strains deficient in *siiAB* still retain SiiE on the cell surface, but are unable to adhere to, nor to invade polarized cells. Additionally, by bioinformatics analysis of the large C-terminal cytosolic domain of SiiB, we found similarities to mechanosensitive channels, as well as to methyl-accepting proteins (MCP), indicating a direct connection to membrane-associated effects like membrane tension changes. By analyses of SiiE retention, motility and host cell infection, we were able to link a role of the cytosolic domain of SiiB directly to motility in swarm agar, functions as proton channel and control of SiiE function.

III.2.2. Introduction

By deploying protein secretion systems encoded by virulence clusters called *Salmonella* Pathogenicity Islands (SPI) (Gerlach *et al.*, 2008; Gerlach and Hensel, 2007; Gerlach *et al.*, 2007a), the pathogen *Salmonella enterica* serovar Typhimurium (STM) is able to invade and to proliferate within host cells. It was already shown that the SPI4-encoded type 1 secretion system (T1SS) and its substrate, the giant adhesin SiiE, are essential for adhesion and invasion of polarized cells by supporting translocation of effector proteins by the SPI1-encoded type 3 secretion system (T3SS) (Gerlach *et al.*, 2008; Wagner *et al.*, 2011).

T1SS were shown to be highly conserved regarding their structure and mechanisms. Two secretion mechanisms are described: a one-step secretion of the unfolded substrate directly into the environment without an intermediate step during translocation (Andersen *et al.*, 2000; Kanonenberg *et al.*, 2013; Koronakis *et al.*, 1989; Mackman *et al.*, 1985); and a two-step secretion, where the substrate is temporary retained on the cell surface during translocation, before its release into the environment (Guo *et al.*, 2017; Smith *et al.*, 2018). The Ca²⁺-rich environment leads to folding of the substrates, a consequence of direct Ca²⁺-binding, resulting in the final folded structure (Chenal *et al.*, 2009). The SPI4-T1SS of STM is composed of the ATP-binding cassette (ABC) transporter SiiF in the inner membrane (IM), of the periplasmic adaptor protein (PAP) SiiD, and SiiC, the outer membrane (OM) secretin. The 600 kDa substrate SiiE associates with the IM, is recognized by the SPI4-T1SS, and subsequently secreted into the extracellular space (Wagner *et al.*, 2011). The extracellular Ca²⁺ binds to the type I and type II Ca²⁺ binding sites, located at the 53 repetitive bacterial immunoglobulin (BIg) domains of SiiE, supporting secretion (Barlag and Hensel, 2015; Griessl *et al.*, 2013; Peters *et al.*, 2017). During secretion, SiiE is retained on the cell-surface. Thus, the first close contact to the host cell membrane during invasion process is mediated by the SPI4-T1SS and SiiE, so subsequently effector proteins of the SPI1-T3SS can be translocated into the host cell (Gerlach *et al.*, 2007b). Following its temporary retention, SiiE is released into the extracellular space. Furthermore, the SPI4 encodes two accessory non-canonical subunits, SiiA and SiiB, forming a proton channel in the IM (Wille *et al.*, 2014). It was shown that SiiAB play an essential role for effective invasion of polarized host cells by transport of ions across the membrane (Wille *et al.*, 2014), adhesion and the initial steps of SiiE secretion (unpublished data, PhD thesis Nathalie Sander, 2022a). However, the detailed mechanism of SiiAB function for SiiE, adhesion and invasion is still not known. SiiAB were shown to share similarities with the well-characterized stator complex MotAB (Kirchwegger *et al.*, 2019). Comparable to MotB (D33), SiiA was found to express a critical aspartate residue (D13), essential for proton channel function (Wille *et al.*, 2014). Comparable to MotA, SiiB harbors a large cytoplasmic region, which was shown to interact with SiiF as it is postulated for MotA and the flagellar rotor (Blair and Berg,

1991; Dean *et al.*, 1984; Deme *et al.*, 2020; Wille *et al.*, 2014; Zhou *et al.*, 1995). Such an extended structure is also known for mechanosensitive channels like MscS and MscL (Rasmussen and Rasmussen, 2018). This cytoplasmic domain was further shown to sense macromolecular crowding in the cytoplasm (Rowe *et al.*, 2014). Furthermore, the mechano-sensitive channel YnaI was recently described to be important during invasion of *Salmonella* (Edwards *et al.*, 2012; Miller, unpublished).

Thus, we focused on SiiAB and especially SiiB and its large cytoplasmic domain to gain more insights in SiiAB function for the SPI4-T1SS. So far we were able to show that SiiAB are important for initial steps of SiiE secretion (unpublished data, PhD thesis Nathalie Sander, 2022a) and furthermore demonstrated a localization of SiiB at the flagellum (unpublished data, PhD thesis Nathalie Sander, 2022c). We primarily concentrated on this domain and potential downstream effects on SiiE, adhesion, invasion and motility. Additionally, we also investigated further potential homologies to other channels by bioinformatic analyses.

III.2.3. Results

III.2.3.1. Δ siiAB retains SiiE on the cell surface, but adhesion and invasion are inhibited

In a first attempt, we investigated the role of SiiAB directly before and during infection. Thus, we checked for SiiE retention at other time points than the described maxima of retention (2.5 h) by Dot blot to analyze SiiE retention kinetic in Δ siiAB (Figure III.2.1 A). STM WT was used as positive control and Δ siiE as negative control (not shown). We found similar kinetics with a maximum after 2.5 h in a *siiAB* mutant, comparable to STM WT, although Δ siiAB only showed 56.5% amounts of SiiE retained on cell surface in comparison to WT. In STM WT, at 1.5 h we found 7.4% amounts of SiiE retained on the surface and after the retention maximum, the SiiE surface signal was continuously decreasing (3.5 h: 16.3%; 4.5 h: 7.1%; 5.5 h: 3.4%; 6.5 h: 1.8%). Δ siiAB showed no retention after 1.5 h and following the maximum after 2.5 h, retention was decreasing (3.5 h: 11.6%; 4.5 h: 9.2%; 5.5 h: 6.2%; 6.5 h: 5.9%). Interestingly, after 4.5 h retention in Δ siiAB was slightly increased in comparison to WT.

As we found retention of SiiE was 56.5% of WT retained in Δ siiAB after 2.5 h, we were interested in the adhesion and invasion phenotype. Therefore, we infected polarized MDCK cells with WT and Δ siiAB (Figure III.2.1 D-E), and simultaneously checked for SiiE retention prior to infection. For this we diluted the bacteria first in PBS (for comparison also in LB) and then in MEM infection medium, just as for an infection assay. During these preparations, samples were fixed with PFA, stained against SiiE and surface-bound SiiE was measured for 50,000 single bacteria by flow cytometry (Figure III.2.1 B-C).

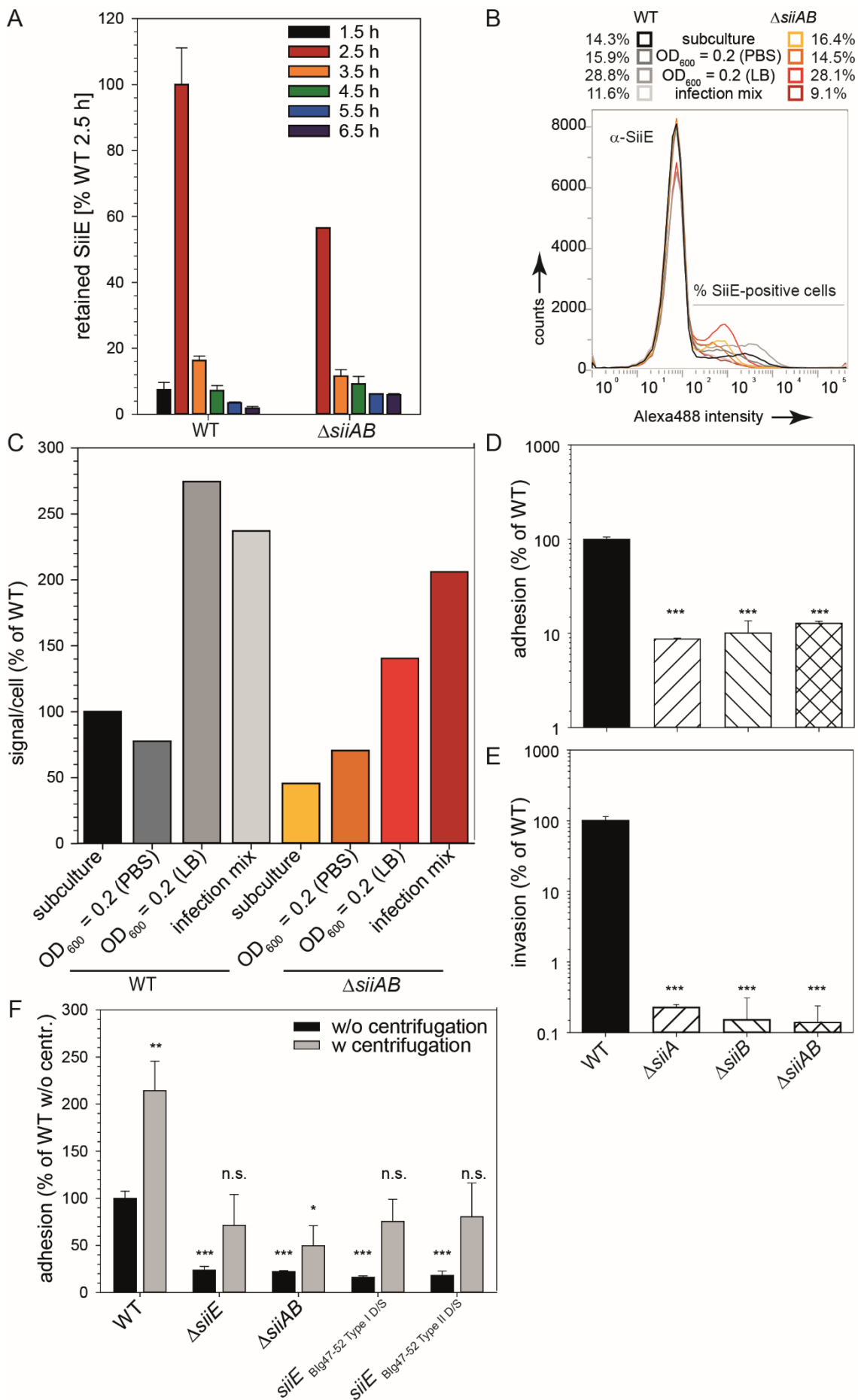


Figure III.2.1. Although $\Delta siiAB$ retains SiiE on cell surface, significantly decreased adhesion and invasion can be observed. Shown are the SiiE retention at different time points (A), directly before infection (B, C) and effects on adhesion and invasion (D-F) in dependence of SiiAB. A) Dot blot analysis of the retention of SiiE of $\Delta siiAB$ in comparison to STM WT after defined time points. To investigate SiiE retention over time, subcultures were grown for 1.5 h, 2.5 h, 3.5 h, 4.5 h, 5.5 h and 6.5 h. For retention samples, cells were fixed with 3% PFA in PBS. 5 μ l of the samples were spotted on equilibrated membranes in triplicates and membranes were decorated against SiiE and LPS. The LPS signal was used for normalization of sample loading. B) Histogram of the Alexa488-positive cells and the counts by flow cytometry. WT was used as positive control and $\Delta siiE$ as negative control for gating (not shown). SiiE-positive cells as indicated. C) SiiE signal intensities of Alexa488-positive cells. D)-E) Adhesion to (D) and invasion of (E) polarized MDCK cells of $\Delta siiA$, $\Delta siiB$ and $\Delta siiAB$ in comparison to WT. Subcultures were grown for 2.5 h and MDCK were infected with MOI 5. F) Adhesion to polarized MDCK cells of $\Delta siiAB$ in comparison to *siiE* mutants without (w/o) and with (w) centrifugation. Subcultures were grown for 2.5 h and MDCK were infected with MOI 5. Adhesion and invasion: statistical analyses compared to WT with biological triplicates by two-tailed t-test: ***, $p < 0.001$; **, $p < 0.01$; *, $p < 0.05$; n.s., not significant.

We used STM WT and $\Delta siiE$ strains as positive and negative control, respectively (not shown). First, we gated the bacteria with an unstained STM WT sample (not shown). Stained strains behaved like the unstained control and showed no aggregates. In a second step, we gated the SiiE-positive cells with help of the positive and negative control (not shown). We found 14.3% SiiE-positive cells in WT and 16.4% in $\Delta siiAB$ (Figure III.2.1 B). After dilution in PBS, a comparable numbers of positive cells were found in both cases (WT: 15.9%; $\Delta siiAB$: 14.5%). Interestingly, a dilution in LB led to an approximately 2-fold increase in positive cells in both strains (WT: 28.8%; $\Delta siiAB$: 28.1%). The dilution from PBS to infection medium resulted in slightly decreased amounts of positive cells. Whereas, in WT we found 11.6% positive cells, the number of positive cells was slightly more decreased from 16.4% in subculture to 9.1% in $\Delta siiAB$. However, for infection a comparable amount of cells showed SiiE signal on their surface. To further analyze the signal per cell, we calculated the mean fluorescence, taking the positive cells and the fluorescence signal into account (Figure III.2.1 C). Whereas dilution in PBS only showed a slight decrease in the signal/cell (77.6%) in WT, dilution in LB and infection medium showed an increase to 274.4% in LB and 237% in infection medium. In $\Delta siiAB$ only 45.6% of WT SiiE signal/cell was found. During dilution steps in PBS and MEM, the signal/cell continuously increased up to 206.2% SiiE/cell in $\Delta siiAB$. Thus, we not only concluded comparable SiiE amounts during infection process, but additionally that retained SiiE on $\Delta siiAB$ can neither mediate adhesion nor invasion (Figure III.2.1 D-E). Adhesion and invasion were significantly reduced in $\Delta siiA$, $\Delta siiB$ and $\Delta siiAB$, as already published (Wille *et al.*, 2014).

Next, contact between bacteria and MDCK cells was increased by centrifugation (Figure III.2.1 F). Recently we showed that SiiB localizes at the flagellum during SiiE retention maximum (unpublished data, PhD thesis Nathalie Sander, 2022c). However, a deletion of *siiAB* had no impact on velocity, but significantly on stop behavior in medium without host cells and synthetic expression of *siiAB* can increase velocity comparable to synthetic expression of *motAB*. As it

was shown that SiiE is important for the first intimate contact to the host cell, we focused on adhesion. As in all other analyses, we used STM WT and as a negative control a *siiE* deletion strain. Additionally, we used mutant strains with deficient Ca²⁺-binding sites in SiiE (Griessler *et al.*, 2013). Interestingly, we found that a Δ *siiAB* mutant behaves like Δ *siiE* and also with centrifugation adhesion cannot be increased to WT level.

All in all, we showed on single cell level that the decreased signal of the population analysis by Dot blot was due to decreased amounts of SiiE per cell in the subculture. We additionally found that SiiE amounts per cell in Δ *siiAB* were comparable to WT in infection mix, yet adhesion and invasion were highly reduced. While we already demonstrated a role of SiiAB as a proton channel in the initial steps of SiiE secretion, we here show a direct effect of SiiAB on SiiE functionality (unpublished data, PhD thesis Nathalie Sander, 2022a).

III.2.3.2. Modelling of proton channels and mechanosensitive channels in comparison to SiiB

Similarities of SiiAB to MotAB were already described (Kirchweger *et al.*, 2019) and similar to MotA, SiiB harbors a large cytoplasmic region, which was shown to interact with SiiF. An interaction is also postulated for MotA and the rotor (Blair and Berg, 1991; Dean *et al.*, 1984; Deme *et al.*, 2020; Wille *et al.*, 2014; Zhou *et al.*, 1995). We modelled SiiAB in comparison to MotAB and found less identity of the C-terminal domain of SiiB with other proton channels (unpublished data, PhD thesis Nathalie Sander, 2022c). Thus, we decided to focus on the C-terminal domain of SiiB (aa206-462) for additional analysis (Figure III.2.2 D). The resulting model included the aa242-462 due to restricted homologies to other channels. Based on BLAST results for SiiB (data not shown), we decided to model additional IM channels. We exemplarily modelled ExbB for the family of proton channels like MotA (Deme *et al.*, 2020), MscS as one of the best-characterized mechanosensitive channels (Rasmussen and Rasmussen, 2018) and Ynal that was shown to be a mechanosensitive channel and important during invasion of STM (Flegler *et al.*, 2020; Miller, unpublished) (Figure III.2.2, Figure S III.2.2).

For ExbB, MscS and SiiB 3 transmembrane helices (TMH) were predicted, whereas for Ynal 5 TMH were predicted (Figure S III.2.1). Additionally, we found an N-terminal signal sequence predicted for SiiB (aa1-26) (Figure S III.2.1 D), but not for the other proteins. With a lower probability a cleavage site (cs) is predicted for A23 (cs score: 0.042) and S25 (0.072) of SiiB by SignalP 5.0 (data not shown) (Almagro Armenteros *et al.*, 2019).

Surveying, we could see a mix of α -helices and β -sheets for MscS, Ynal and the cytosolic domain of SiiB. For MscS critical asparagine residues were described, important for channel

conductance (Wang *et al.*, 2018). In this case, N117 (polar, uncharged) located in TMH3 helix was shown to interact with the critical N167 (polar, uncharged). Homologies of this residues cannot be found in ExbB. In Ynal we found this pattern to be conserved with N166. In MscS and Ynal a polar serine is present right before the first critical aspartate (S116, MscS; S165, Ynal) and a non-polar proline prior to the second asparagine (P166, MscS; P216 Ynal), indicating similarities between these two channels. Both sequences showed the first critical asparagine after 10 aa (MscS) and 11 aa (Ynal) in the cytosol (Figure S III.2.1 B, C). In the multiple sequence alignment (Figure S III.2.2) we also found a homologue asparagine in SiiB, but at position 165 (with S164), predicted to be located in the periplasm and not in the cytosol (Figure S III.2.1 C, Figure S III.2.2). Nevertheless, we found other potential asparagine residues at positions 227, 330, 401 and 420 (Figure III.2.2 D). For position 226 a serine was found as in MscS and Ynal and instead of a proline, the non-polar glycine (G329), methionine (M400) or alanine (A419) were found. As the residues N117 and N167 were described to interact, we concluded depending on the models that N227 and N420 potentially function the same way, but the model prediction was restricted here for aa242-462.

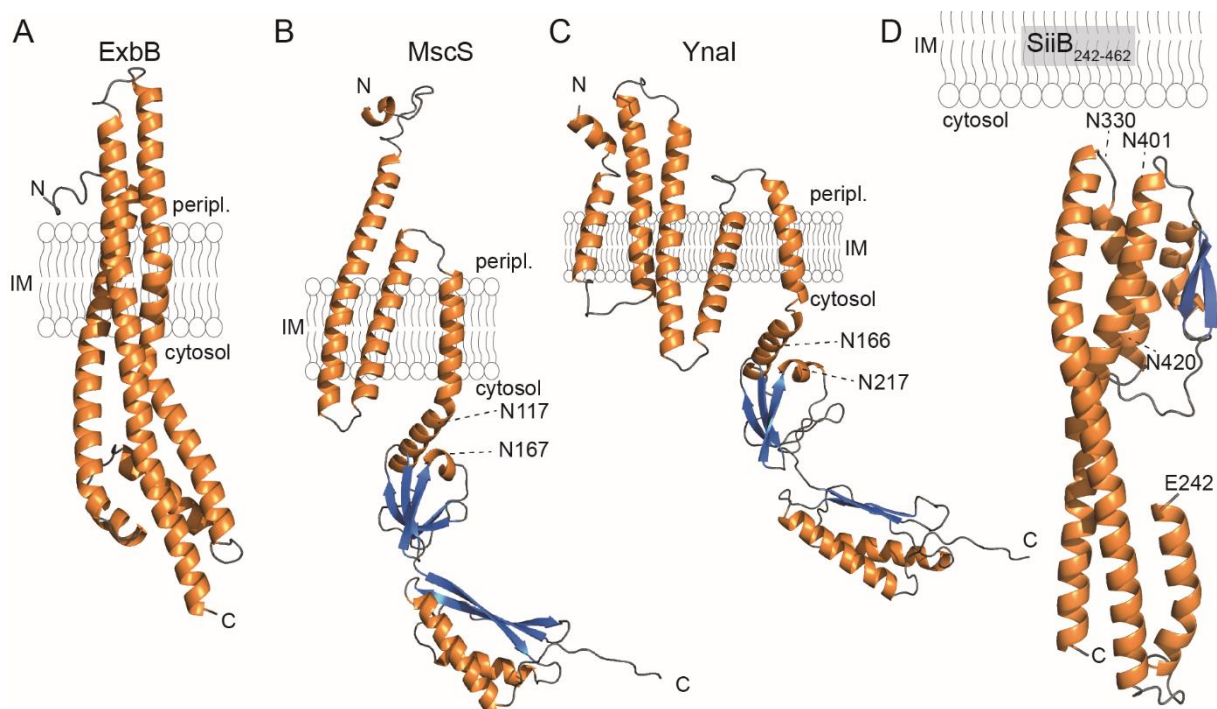


Figure III.2.2. Modeling of SiiB reveal similarities to ExbB, MscS and Ynal. Tertiary structure model prediction for STM ExbB (A), STM MscS (B), STM Ynal (C) and STM SiiB₂₄₂₋₄₆₂ (D) by Phyre2 (Kelley *et al.*, 2015). Loop, gray; β -sheet, blue; α -helix, orange. A) Proton channel STM ExbB from ExbBD MotAB family. B) Best characterized mechanosensitive channel STM MscS. C) Newly described mechanosensitive channel STM Ynal, described to be involved in STM invasion. D) C-terminal cytosolic domain (aa208-462). Confidences: ExbB 100%; MscS 100%; Ynal 100%; SiiB₂₄₂₋₄₆₂ 68.6%. Scale of the IM: 5 nm.

III.2.3.3. SiiB cytosolic domain influences proton channel and SiiE function

Since we found potential similarities in the cytosolic domain of SiiB to mechanosensitive channels, we wanted to investigate the role of this domain of SiiB in further analyses and under different osmotic pressures during infection (2.5 h subculture) (Figure III.2.3). We used PBS with different osmotic pressure, adjusted with NaCl. The cytoplasmic solutes of bacteria lead to an osmotic pressure of approximately 400 mOsm (Booth, 2014). To check if the cytosolic domain is important for proton channel function, we used *siiA*_{D13E} mutant for comparison here.

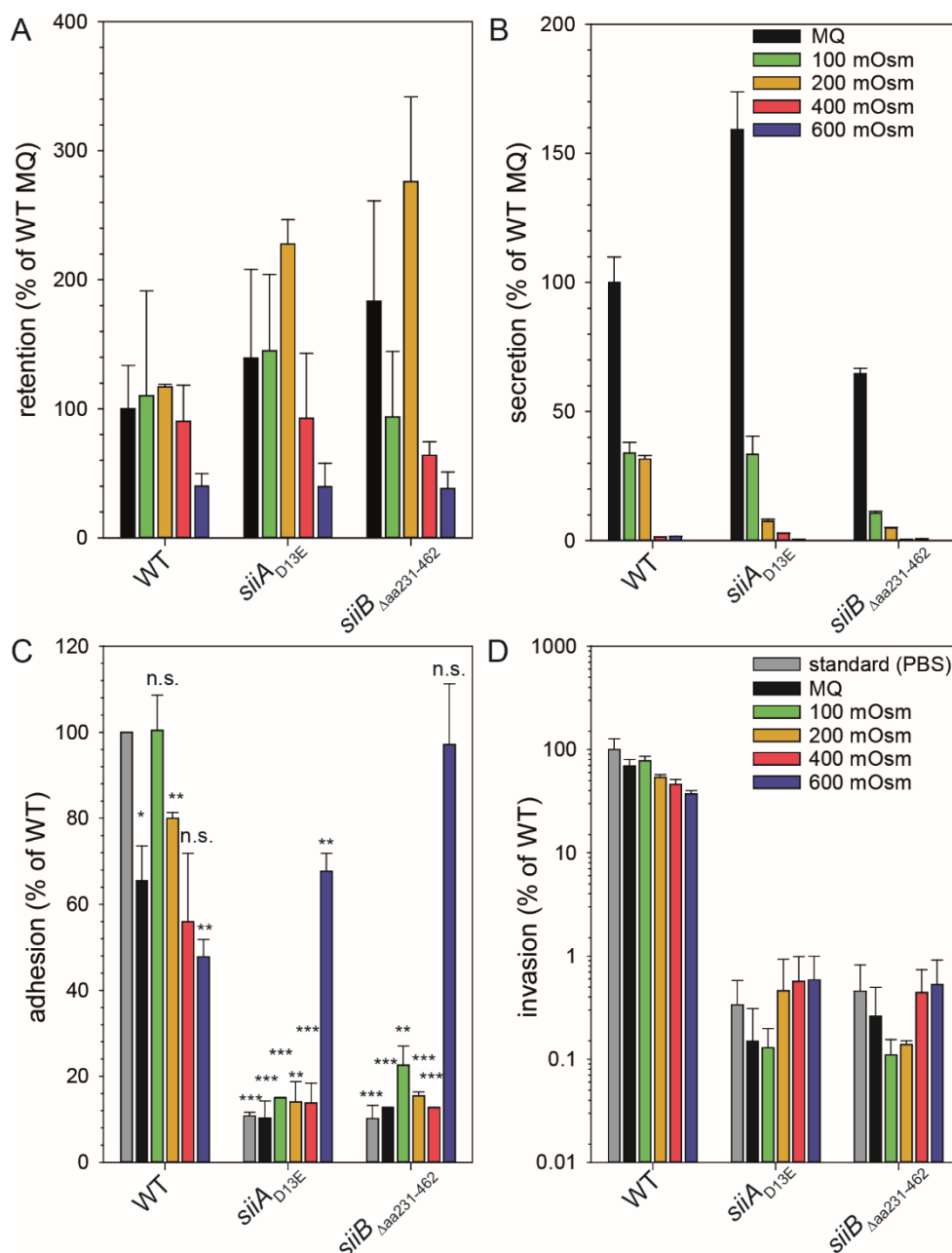


Figure III.2.3. Effect of osmotic pressure on SiiE in dependence of the cytosolic domain of SiiB and proton channel function. A-B) Dot blot analysis of the retention (A) and secretion (B) of SiiE in response to *siiB*_{Δaa210-462} expression. Subcultures were grown for 2.5 h and 6 h with AHT induction after

1 h. For retention samples, cells were fixed with 3% PFA in PBS and for secretion samples, the supernatant was precipitated with TCA and protein was dissolved in SDS-PAGE sample buffer with volumes adjusted to the cell density as determined by OD₆₀₀. 5 µl of the samples were spotted on equilibrated membranes in triplicates and membranes were immunolabeled with antiserum against SiiE or LPS. The LPS signal was used for normalization of sample loading. C) Adhesion to, and D) invasion of polarized MDCK cells following *siiB*_{Δaa231-462} expression. Subcultures were grown for 2.5 h with AHT induction after 1 h and MDCK were infected with MOI 5. MQ: Milli-Q water. Adhesion: statistical analyses compared to WT with at least biological duplicates by two-tailed t-test: ***, p < 0.001; **, p < 0.01; *, p < 0.05; n.s., not significant.

WT was not affected regarding retention, with exception of incubation in 600 mOsm PBS (40.1%) (Figure III.2.3 A). The same was shown for *siiA*_{D13E} (39.6%) and *siiB*_{Δaa231-462} (38.1%). Noticeably, we found increased amounts of SiiE retained in PBS with 200 mOsm in *siiA*_{D13E} (227.6%) and *siiB*_{Δaa231-462} (276.2%). Secretion was comparable for the strains with the highest secretion in Milli-Q water (MQ) (Figure III.2.3 B), with exception of 200 mOsm. In *siiA*_{D13E} (7.4%) and *siiB*_{Δaa231-462} (4.9%) secretion was more decreased than in WT (31.6%) during incubation with 200 mOsm PBS, matching the increased retention at 200 mOsm. Invasion was not affected (Figure III.2.3 D) and mutant strains showed the significantly reduced invasion as published before (Wille *et al.*, 2014). Adhesion was not influenced in the mutant strains, with exception of 600 mOsm (Figure III.2.3 C). Strain expressing *siiA*_{D13E} or *siiB*_{Δaa231-462} showed increased adhesion with 67.7% or 97.1% in comparison to the other osmolarities, but decreased in comparison to WT, respectively. Interestingly, WT showed more varying influences in the different media. In MQ, 400 mOsm and 600 mOsm PBS, the WT was decreased to 65.5% (MQ), 56% (400 mOsm) and 47.8% (600 mOsm), whereas the mutant strains were increased in 600 mOsm PBS, with simultaneously less SiiE on cell surface. Thus, we concluded a potential role of the cytosolic domain for SiiE retention and function under different osmotic pressure, although further assays with a SiiE mutant strain have to be performed.

In a next step, we wanted to analyze the cytosolic domain of SiiB by overexpression of only this part (Figure III.2.4, Figure III.2.5). If the cytosolic domain of SiiB triggers downstream effects, overexpression potentially leads to an altered retention, secretion, adhesion or invasion. We introduced a plasmid under anhydrotetracycline (AHT)-inducible *tetA* promoter control in WT and Δ *siiB* and tested expression of the construct (Figure S III.2.3 A). Following induction with 10 ng/ml AHT a clear band at 28 kDa can be observed. Additionally, WT was also expressing chromosomal SiiB (51.5 kDa). Furthermore, we checked for a potential toxicity of the overexpression of the cytosolic domain (Figure S III.2.3 B). We measured OD₆₀₀, adjusted to an OD 0.2, diluted the bacteria and plated them. We found no significant influence of the cytosolic domain on vitality.

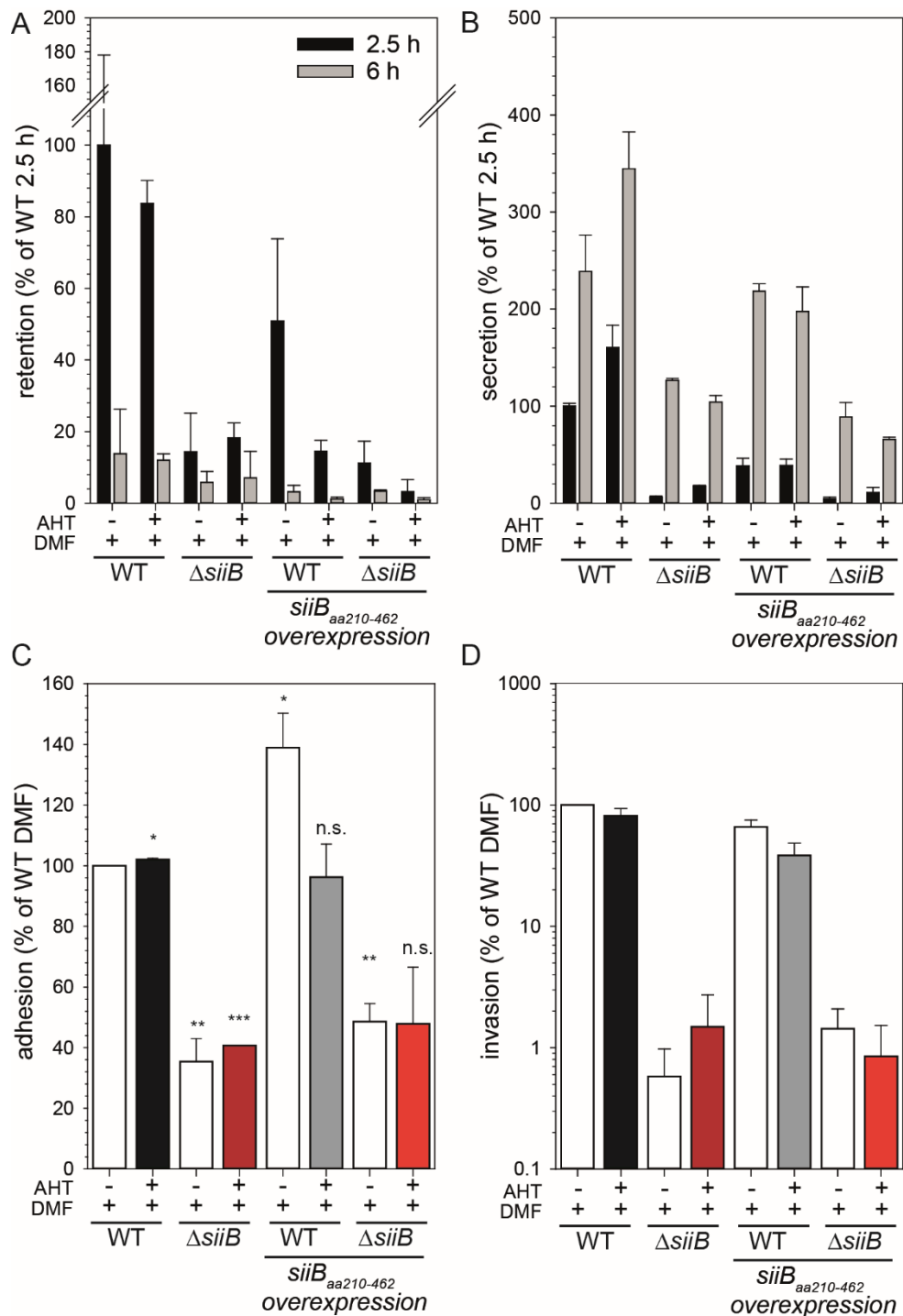


Figure III.2.4. SiiE function in dependence of the cytosolic domain of SiiB. A-B) Dot blot analysis of the retention (A) and secretion (B) of SiiE in response to *siiB*_{aa210-462} overexpression. Subcultures were grown for 2.5 h and 6 h with AHT induction after 1 h. For retention samples, cells were fixed with 3% PFA in PBS and for secretion samples, the supernatant was precipitated with TCA. 5 μ l of the samples were spotted on equilibrated membranes in triplicates and membranes were immunolabeled with anti-serum against SiiE and LPS. The LPS signal was used for normalization of sample loading. C) Adhesion to and D) invasion of polarized MDCK cells following *siiB*_{aa210-462} overexpression. Subcultures were grown for 2.5 h with AHT induction after 1 h and MDCK were infected with MOI 5. Adhesion: statistical analyses compared to WT with at least biological duplicates by two-tailed t-test: ***, $p < 0.001$; **, $p < 0.01$; *, $p < 0.05$; n.s., not significant.

Following expression and toxicity check, we analyzed the effect of the overexpression of the cytosolic domain (*siiB_{aa210-462}*) on SiiE and adhesion and invasion (Figure III.2.4). Retention (Figure III.2.4 A) and secretion (Figure III.2.4 B) kinetics were not influenced. We found a decreased amount of SiiE retained on cell surface in Δ *siiB* (14.4% after 2.5 h and 5.8% after 6 h) and a decreased secretion with 6% after 2.5 h and 126.6% after 6 h. Secretion was not affected by *siiB_{aa210-462}* overexpression in WT and Δ *siiB*. Retention was decreased after *siiB_{aa210-462}* overexpression in WT and Δ *siiB*. Thus, we concluded a role of the cytosolic domain of SiiB for SiiE retention only. Nevertheless, neither adhesion (Figure III.2.4 C), nor invasion (Figure III.2.4 D) were influenced by the overexpression.

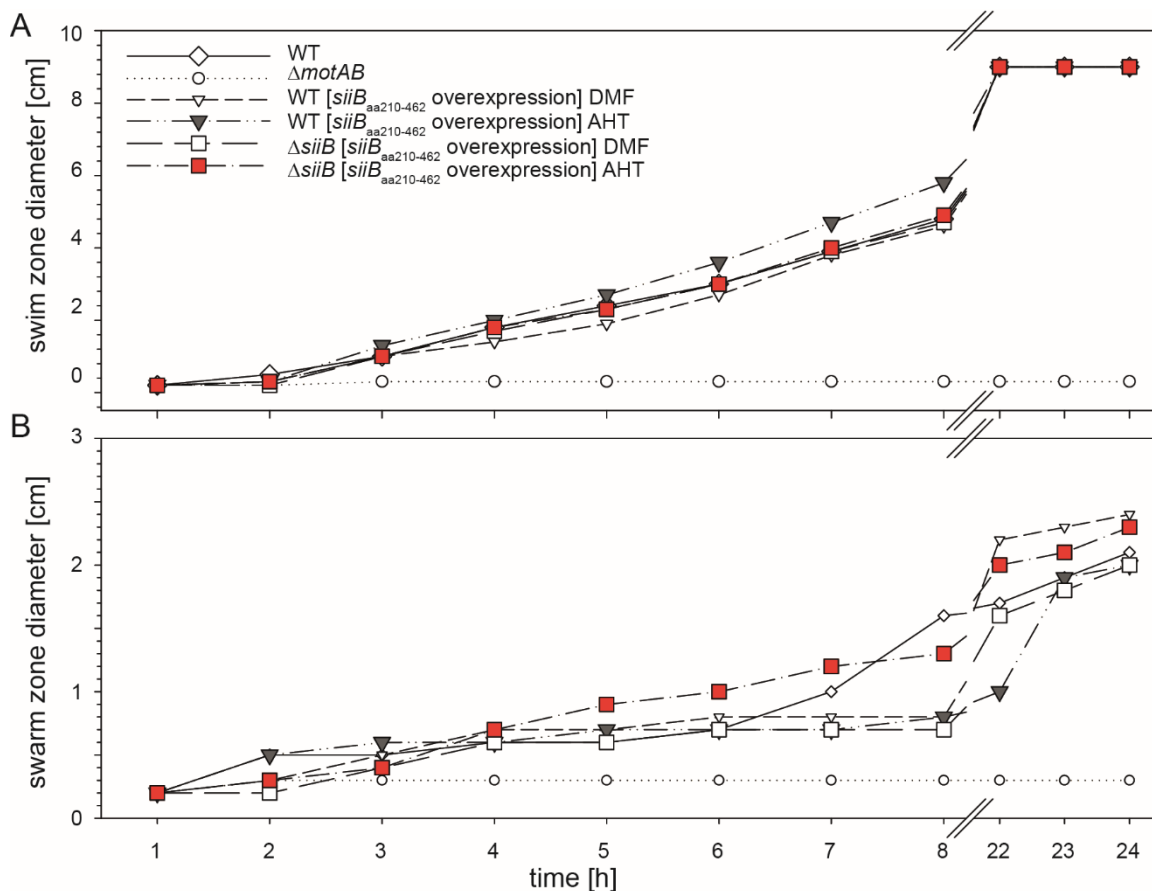


Figure III.2.5. Swim and swarm behavior in dependence of the cytosolic domain of SiiB. Shown are the swim and swarm zone diameters in dependence of the overexpression of the cytosolic domain of SiiB by swim assay. Bacterial subcultures were grown for 2.5 h and inoculated in swim and swarm agar, respectively. Swim and swarm zone diameters were measured every hour, with exception of 9-21 h.

As there are similarities to MotAB described (Kirchweger *et al.*, 2019; Wille *et al.*, 2014) and SiiB is located at the flagellum (unpublished data, PhD thesis Nathalie Sander, 2022c), we decided to analyze a potential role regarding the flagellum (Figure III.2.5). We tested swim (0.3% agar) and swarm agar (0.5% agar). As negative control we used Δ *motAB*. On swim

agar, no difference between the strains was observed (Figure III.2.5 A). Contrary to this, we found an increased swarm diameter after overexpression of the cytosolic domain of SiiB in $\Delta siiB$ (Figure III.2.5 B), especially in the first 8 h. Interestingly, overexpression of the cytosolic domain of SiiB in WT showed no effect after induction in the first 8 h and only a slight decrease after 22 h. Thus, we concluded a potential effect of the cytosolic domain on the flagellum, primarily if SiiB is not expressed.

Taken together, we found potential sites, comparable to critical residues in mechanosensitive channels MscS and YnaI (Figure III.2.2) and not only to MotAB. Furthermore, we demonstrate that the cytosolic domain of SiiB is important for SiiE retention (Figure III.2.4 A) and swarming (Figure III.2.5 B) and potentially affects downstream processes.

III.2.4. Discussion and Outlook

Here, we show that adhesion in a *siiAB* mutant strain, although it retains SiiE on the cell surface (Figure III.2.1 B, C), cannot be increased by forced contact to host cells (Figure III.2.1 E). Thus, we concluded a role of SiiAB for SiiE function, as already described for other adhesive structures and corresponding proton channels like in *Mycoplasma* spp. (Waldo and Krause, 2006). As we already showed that SiiAB play a role for the initial secretion steps of SiiE before it is retained by SiiC in the OM (unpublished data, PhD thesis Nathalie Sander, 2022a), SiiAB potentially influence SiiE conformation or post translationally modify SiiE to increase adhesion.

By multiple sequence alignment and tertiary structure prediction, we found conservation of potential residues and motifs, known to be critical for mechanosensitive channels (Figure III.2.2). Similarities to MotAB were already described for SiiAB (Kirchweiger *et al.*, 2019; Wille *et al.*, 2014). Here, we focused on the predicted, elongated cytosolic domain that is comparable to mechanosensitive channels, MCPs and toxins (data not shown). As we found an effect of the osmotic pressure on SiiE retention and adhesion, we suggest a role in response to a hyperosmotic environment (600 mOsm) (Figure III.2.3). Recent studies revealed that mechanosensitive channels can play essential roles during invasion processes (Edwards *et al.*, 2012; Flegler *et al.*, 2020; Rasmussen and Rasmussen, 2018; Schumann *et al.*, 2010). MscS harbors 3 TMH per subunit whereas other mechanosensitive channels are predicted to have 5 TMH (YnaI, YbdG) or 11 TMH (YbiO, MscK, YjeP). Critical residues are important for channel conductance of mechanosensitive channels like MscS (Wang *et al.*, 2018). For this channel, N117 of TMH3 was shown to interact with a second critical asparagine, N167. We found comparable residues and patterns in the cytosolic domains of SiiB and YnaI (Figure III.2.2, Figure S III.2.2). Hence, comparable functions may be proposed. YbiO was described to be NaCl-specific and stress response-dependent (RpoS) (Edwards *et al.*, 2012). It was already described that SiiF

and SiiB interact (Wille *et al.*, 2014). Potentially, upon a conformational change and opening of SiiF, SiiB senses changes in the IM, connected to proton channel function. As hypoosmotic shock experiments showed no influence on cell viability when *siiAB* were deleted (data not shown), we concluded that SiiAB are not an essential mechanosensitive channel during hypoosmotic shock. There are mechanosensitive channels described, important for infection like YnaI and YbiO, but additionally channels that only have a electrophysiological activity as mutational variant like YbdG (Schumann *et al.*, 2010). This MscM-like channel is important during hyperosmotic stress and not during hypoosmotic stress like MscS-like channels (Amemiya *et al.*, 2019). Thus, further mutations and conditions have to be investigated.

Interestingly, we found an effect of the overexpression of the cytosolic domain of SiiB on SiiE surface retention, but not on adhesion (Figure III.2.4). Furthermore, swarm behavior was influenced (Figure III.2.5). As swarm behavior was explicitly changed, in a next step the flagellation of the bacteria has to be checked. It is possible that an overexpression of the cytosolic domain of SiiB leads to an increased amount of surface structures, as we also observed an increase in SiiE retention. To gain further insights in the function of the cytosolic domain of SiiB, a detailed comparison to other cytosolic domains of IM proteins, like of MotA and others should also be performed.

To conclude, we found evidence that the cytosolic domain of SiiB is of importance and influences proton channel function and that SiiAB can be suggested to be required for SiiE function and motility.

III.2.5. Materials and Methods

III.2.5.1. Bacterial strains and growth conditions

Bacterial strains used in this study are listed in Table III.2.1. Bacteria were grown aerobically in LB or on LB agar plates, if necessary supplemented with carbenicillin (cb, 50 µg/ml). For induction of the Tet-on system encoded on the plasmids used (Table III.2.2), anhydrotetracycline (AHT) was added (10 ng/ml final concentration) 1 h after inoculation of the subculture for additional 1.5 h (1:31).

Table III.2.1. Bacterial strains used in this study.

Designation	Relevant characteristics	Reference
<i>S. Typhimurium</i> NCTC 12023	wild type	NCTC
WRG205	<i>siiA</i> _{D13E} ::FRT	(Wille <i>et al.</i> , 2014)
MvP589	Δ <i>siiA</i> ::FRT	(Gerlach and Hensel, 2007)
MvP1387	Δ <i>siiAB</i> ::FRT	this study
MvP2029	<i>siiE</i> Blg47-52 Type II D→S	(Griessler <i>et al.</i> , 2013)
MvP2168	<i>siiE</i> Blg47-52 Type I D→S	(Griessler <i>et al.</i> , 2013)
MvP2720	Δ <i>motAB</i> ::FRT	lab collection
MvP2778	Δ <i>siiA</i> ::FRT	this study
MvP2807	Δ <i>siiB</i> ::FRT	this study
MvP2779	Δ <i>siiE</i> ::FRT	this study
MvP2780	Δ <i>siiF</i> ::FRT	this study

III.2.5.2. Construction of plasmids

The gene encoding the cytoplasmic domain of SiiB was amplified from genomic DNA of STM WT (NCTC 12023) and introduced into p4251. Oligonucleotides used are listed in Table III.2.3.

Table III.2.2. Plasmids used in this study.

Plasmid	Relevant characteristics, resistance	Reference
p3912	<i>siiB</i> Δ <i>aa231-462</i> -HA	lab collection
p4251	<i>tetR</i> P _{<i>tetA</i>}	lab collection
p5622	<i>tetR</i> P _{<i>tetA</i>} :: <i>siiB</i> _{<i>aa210-462</i>}	this study

Table III.2.3. Oligonucleotides used in this study

Designation	Sequence (3' -> 5')	Purpose
Vr p4251	TTCACCTTTTCTCTATCACTGATAGGGAGTGGTA	amplification p4251
Vf-pWSK29	GAATTCCTGCAGCCCGGGG	amplification p4251
1f PtetA-RBS- siiB	GTGATAGAGAAAAGTGAAAA- TAAAAAGGTGTCAGAATGCGCAGCTCC- TATCCCTTG	insert <i>siiB</i> _{<i>aa210-462</i>}
1r-C-term siiB_lacZ_p42 51	CCGGGCTGCAG- GAATTCTTAATCTTCATTTTTTCTCCTTGT	insert <i>siiB</i> _{<i>aa210-462</i>}

III.2.5.3. Western blot detection for protein biosynthesis

For sample preparation, bacteria were inoculated 1:31 in LB, supplemented with 50 µg/ml cb if necessary, induced with AHT after 1 h after inoculation and grown for 2.5 h. 1 ml was pelleted by centrifugation at 10,000 x g. Pellets were boiled in 1x SDS cracking buffer with volumes adjusted according to OD₆₀₀. SDS-PAGE gels according Laemmli were run for 20 min at 80 V and 75 min with 150 V. Semi-dry Western blot (WB) was performed with 0.45 µm nitrocellulose membrane with 0.8 mA/cm². Following Ponceau S stain, membranes were blocked with 5% skimmed dry milk powder in TBS-T (0.1% Tween20 in TBS) for at least 30 min at RT. Primary antibodies were incubated o/N in blocking solution at 4 °C. The next day, membranes were washed three times with TBS-T and incubated with HRP-conjugated secondary antibody in blocking solution for 1 h at RT. Antibodies, used in this study are mentioned in Table III.2.4 and Table III.2.5. Membranes were washed an additional three times with TBS-T, treated with Pierce™ ECL Western blotting Substrate (Thermo Fisher) after manufacturer's instructions and imaged with ChemiDoc™ Imager (Bio-Rad) and ImageLab software.

Table III.2.4. Primary antibodies used in this study.

Antigen	Host	Dilution	Purpose
GST-SiiE-C	rabbit	1:10,000	WB
GST-SiiE-C	rabbit	1:1,000	IF
<i>Salmonella</i> O Antiserum Group B Factors	rabbit	1:10,000	DB

Table III.2.5. Secondary antibodies used in this study.

Species reactivity	Host	Conjugated with	Dilution	Purpose
rabbit	goat	HRP	1:10,000	WB
rabbit	goat	Alexa488	1:1,000	IF
rabbit	goat	IRDye800CW	1:20,000	DB

III.2.5.4. Dot blot analysis of retained and secreted SiiE

For Dot blot (DB) analysis, subcultures of STM were grown for 2.5 h (SiiE retention maximum, unpublished data, PhD thesis Nathalie Sander) and 6 h (SiiE secretion maximum) (Gerlach *et al.*, 2007b). For analysis of the effect of the osmolarity on SiiE retention and secretion, the cells were incubated for 15 min at 37 °C in PBS with 100 mOsm, 200 mOsm, 400 mOsm and 600 mOsm PBS, adjusted with NaCl. As controls PBS and Milli-Q were used. Additionally, bacteria were fixed during infection assay procedure in PBS, LB for comparison and infection medium

(MEM Earle's). Dot blot was performed as published before (Peters *et al.*, 2017). The antibodies used for the Dot blots are described in Table III.2.4 and Table III.2.5.

III.2.5.5. Flow cytometry of surface-bound SiiE

For analysis of surface retention of SiiE by flow cytometry, 3×10^8 bacteria were fixed with 3% paraformaldehyde in PBS for at least 20 min at RT. Bacteria were blocked with 2% goat serum and 3% BSA in PBS for 30 min and afterwards stained with the specific primary antibody rabbit- α -SiiE (1:1,000) in blocking solution o/N, 4 °C. Staining with second antibody goat- α -rabbit-Alexa488 (1:2,000) occurred for 1 h at RT. Bacteria were diluted 1:10 in cell culture PBS and 50,000 bacteria were measured with the Attune NxT Flow Cytometer (Thermo Fisher) and analyzed using Attune NxT software (Göser *et al.*, 2020; Röder and Hensel, 2020). Bacteria were gated using unstained STM and measured by FSC-H and SSC-H. For gating of the SiiE surface signal, positive control STM WT and negative control Δ siiE were used. All samples were measured under the same conditions (flow rate 12.5 μ l/min).

III.2.5.6. Motility analysis in swim and swarm agar

To further analyze the motility of the strains, subcultures were grown for 2.5 h at 37 °C with AHT induction after 1 h. 5 μ l of the subcultures were inoculated in the center of swim/swarm agar plates (1% tryptone, 0.5% NaCl, 0.3% (swim agar) 0.5% (swarm agar) agar, 1 mM MgSO₄, complemented with carbenicillin (cb, 50 μ g/ml) and AHT, if necessary). The swim and swarm zone diameters were measured hourly for 8 h, and finally after 21 h of incubation at 30 °C.

III.2.5.7. Cell culture

MDCK cells (subline pf, obtained from Prof. Dr. M. Goppelt-Struebe, Med. Klinik 4, Universitätsklinikum Erlangen) were cultured as described before (Gerlach *et al.*, 2008). For adhesion and invasion assays, cells were seeded in 24-well plates at a density of 1×10^5 cells per well 5 days before infection to ensure differentiation of cells. At the day of infection, cell density was 5×10^5 cells per well. Due to the long incubation time, the medium was supplemented with penicillin and streptomycin. The medium was changed to antibiotic-free medium one day before infection (at least 4 h before infection).

III.2.5.8. Adhesion and invasion assay

To determine adhesion, cells were treated with 3 µg/ml Cytochalasin D 1 h before infection, to inhibit actin remodeling and uptake of the pathogen. For infection, 2.5 h subcultures of infecting STM were grown. For analysis of the influence of osmotic active particles in the medium, bacteria were incubated for 15 min at 37 °C in PBS with 100 mOsm, 200 mOsm, 400 mOsm and 600 mOsm PBS. As controls PBS and Milli-Q were used. MDCK cells were infected in technical triplicates at multiplicity of infection (MOI) 5, and incubated for 25 min at 37 °C in an atmosphere of 5% CO₂. The cells were washed three times with prewarmed PBS. To determine adhesion, cells were lysed directly with 0.5% deoxycholate in PBS (freshly prepared). To determine invasion, cells were treated with 500 µl medium containing 100 µg/ml gentamicin per well for 1 h, washed three times with prewarmed PBS and lysed with 0.5% deoxycholate in PBS (freshly prepared). Lysis was performed for 10 min at 37 °C on a shaking platform. Lysates were collected in single tubes and serial dilutions of inoculum and lysates were plated logarithmic on MH plates to determine CFU. Plates were incubated o/N at 37 °C and CFU were counted the next day with Acolyte software. The percentages of adhered and invaded bacteria were calculated.

III.2.5.9. Bioinformatic analyses

Tertiary structure model predictions were performed by Phyre2 algorithm (Kelley *et al.*, 2015) and visualized with Pymol. Multiple sequence alignments were performed with Clustal Omega (Madeira *et al.*, 2019) and T-Coffee, version 11.0 (Notredame *et al.*, 2000).

III.2.6. Acknowledgements

This study was supported by the SFB944.

III.2.7. Supplements

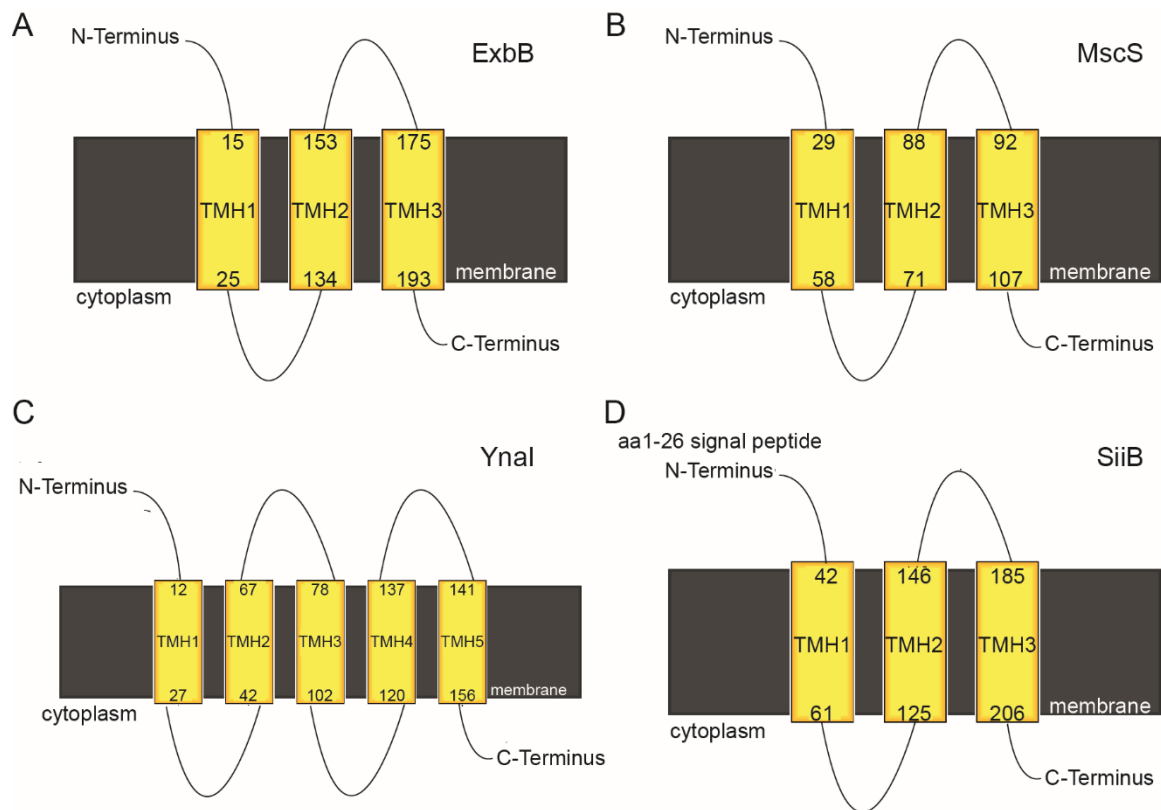


Figure S III.2.1. Transmembrane helix prediction of ExbB, MscS, YnaI and SiiB. Shown are the TMH predictions of ExbB (A), MscS (B), YnaI (C) and SiiB (D) by Phyre2 (Kelley *et al.*, 2015).

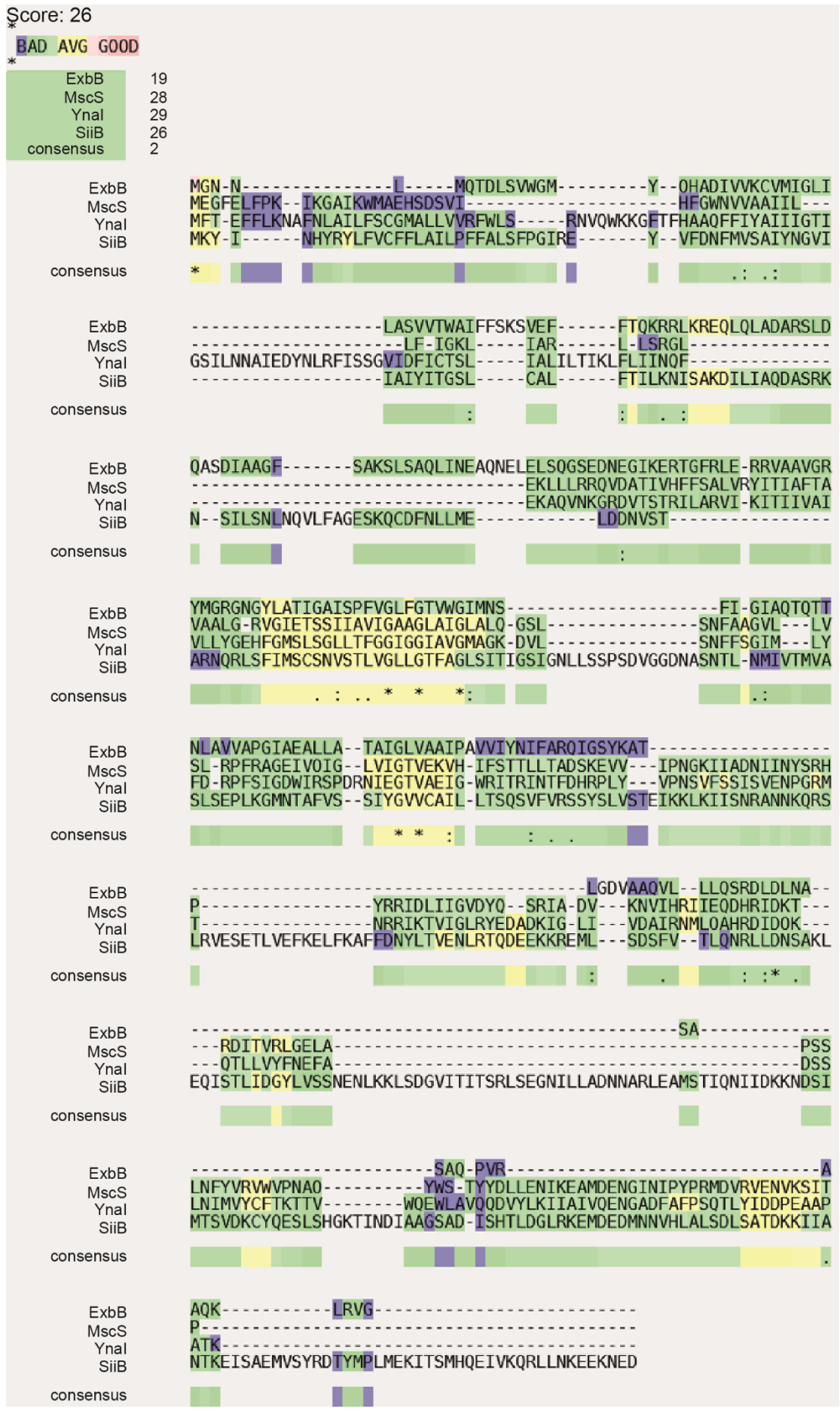


Figure S III.2.2. Full-length multi sequence alignment of proton and mechanosensitive channels in comparison to STM SiiB. A) Shown is the alignment of H⁺-conducting channel ExbB, mechanosensitive channels MscS and YnaI and SiiB of *Salmonella* Typhimurium (STM). Alignment was performed with Clustal Omega (Madeira *et al.*, 2019). Highly conserved regions are depicted as indicated.

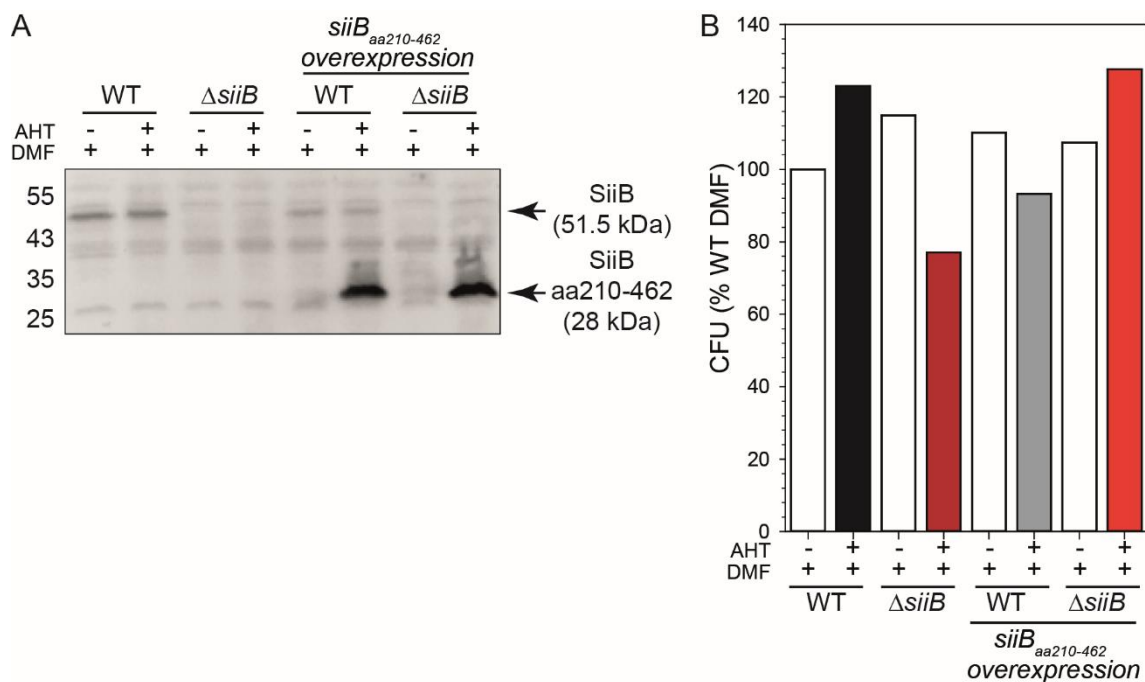


Figure S III.2.3. Protein biosynthesis and toxicity of overexpression of the cytosolic domain of SiiB. A) Western blot against SiiB (51.5 kDa) and cytosolic domain of SiiB (28 kDa), respectively, following induction with 10 ng/ml AHT. Subcultures were grown for 2.5 h with AHT induction after 1 h, pelleted and boiled in SDS-PAGE sample buffer. SDS-PAGE and Western blot with antibodies α -SiiB (1:10,000) and secondary antibody α -rabbit HRP-conjugated (1:10,000) were performed. Protein markers as indicated in kDa. B) Determination of toxicity following overexpression of the cytosolic domain of SiiB. Subcultures were grown for 2.5 h with AHT induction after 1 h, diluted in PBS according to the OD₆₀₀ and plated on LB agar plates (supplemented with cb if necessary). WT without AHT was defined as 100% as indicated.

III.2.8. References

- Almagro Armenteros, J.J., Tsirigos, K.D., Sonderby, C.K., Petersen, T.N., Winther, O., Brunak, S., von Heijne, G., and Nielsen, H. (2019). SignalP 5.0 improves signal peptide predictions using deep neural networks. *Nat Biotechnol* 37, 420-423.
- Amemiya, S., Toyoda, H., Kimura, M., Saito, H., Kobayashi, H., Ihara, K., Kamagata, K., Kawabata, R., Kato, S., Nakashimada, Y., *et al.* (2019). The mechanosensitive channel YbdG from *Escherichia coli* has a role in adaptation to osmotic up-shock. *J Biol Chem* 294, 12281-12292.
- Andersen, C., Hughes, C., and Koronakis, V. (2000). Chunnel vision. Export and efflux through bacterial channel-tunnels. *EMBO Rep* 1, 313-318.
- Barlag, B., and Hensel, M. (2015). The giant adhesin SiiE of *Salmonella enterica*. *Molecules* 20, 1134-1150.
- Blair, D.F., and Berg, H.C. (1991). Mutations in the MotA protein of *Escherichia coli* reveal domains critical for proton conduction. *J Mol Biol* 221, 1433-1442.
- Booth, I.R. (2014). Bacterial mechanosensitive channels: progress towards an understanding of their roles in cell physiology. *Curr Opin Microbiol* 18, 16-22.
- Chenal, A., Guijarro, J.I., Raynal, B., Delepierre, M., and Ladant, D. (2009). RTX calcium binding motifs are intrinsically disordered in the absence of calcium: implication for protein secretion. *J Biol Chem* 284, 1781-1789.
- Dean, G.E., Macnab, R.M., Stader, J., Matsumura, P., and Burks, C. (1984). Gene sequence and predicted amino acid sequence of the motA protein, a membrane-associated protein required for flagellar rotation in *Escherichia coli*. *J Bacteriol* 159, 991-999.
- Deme, J.C., Johnson, S., Vickery, O., Aron, A., Monkhouse, H., Griffiths, T., James, R.H., Berks, B.C., Coulton, J.W., Stansfeld, P.J., *et al.* (2020). Structures of the stator complex that drives rotation of the bacterial flagellum. *Nat Microbiol* 5, 1553-1564.
- Edwards, M.D., Black, S., Rasmussen, T., Rasmussen, A., Stokes, N.R., Stephen, T.L., Miller, S., and Booth, I.R. (2012). Characterization of three novel mechanosensitive channel activities in *Escherichia coli*. *Channels (Austin)* 6, 272-281.
- Flegler, V.J., Rasmussen, A., Rao, S., Wu, N., Zenobi, R., Sansom, M.S.P., Hedrich, R., Rasmussen, T., and Bottcher, B. (2020). The MscS-like channel Ynal has a gating mechanism based on flexible pore helices. *Proc Natl Acad Sci U S A* 117, 28754-28762.
- Gerlach, R.G., Claudio, N., Rohde, M., Jackel, D., Wagner, C., and Hensel, M. (2008). Cooperation of *Salmonella* pathogenicity islands 1 and 4 is required to breach epithelial barriers. *Cell Microbiol* 10, 2364-2376.
- Gerlach, R.G., and Hensel, M. (2007). *Salmonella* pathogenicity islands in host specificity, host pathogen-interactions and antibiotics resistance of *Salmonella enterica*. *Berl Munch Tierarztl Wochenschr* 120, 317-327.
- Gerlach, R.G., Jackel, D., Geymeier, N., and Hensel, M. (2007a). *Salmonella* pathogenicity island 4-mediated adhesion is coregulated with invasion genes in *Salmonella enterica*. *Infect Immun* 75, 4697-4709.
- Gerlach, R.G., Jackel, D., Stecher, B., Wagner, C., Lupas, A., Hardt, W.D., and Hensel, M. (2007b). *Salmonella* Pathogenicity Island 4 encodes a giant non-fimbrial adhesin and the cognate type 1 secretion system. *Cell Microbiol* 9, 1834-1850.
- Goser, V., Kehl, A., Röder, J., and Hensel, M. (2020). Role of the ESCRT-III complex in controlling integrity of the *Salmonella*-containing vacuole. *Cell Microbiol* 22, e13176.
- Griessler, M.H., Schmid, B., Kassler, K., Braunsmann, C., Ritter, R., Barlag, B., Stierhof, Y.D., Sturm, K.U., Danzer, C., Wagner, C., *et al.* (2013). Structural insight into the giant Ca(2+)-binding adhesin SiiE: implications for the adhesion of *Salmonella enterica* to polarized epithelial cells. *Structure* 21, 741-752.
- Guo, S., Stevens, C.A., Vance, T.D.R., Olijve, L.L.C., Graham, L.A., Campbell, R.L., Yazdi, S.R., Escobedo, C., Bar-Dolev, M., Yashunsky, V., *et al.* (2017). Structure of a 1.5-MDa adhesin that binds its Antarctic bacterium to diatoms and ice. *Sci Adv* 3, e1701440.
- Kanonenberg, K., Schwarz, C.K., and Schmitt, L. (2013). Type I secretion systems - a story of appendices. *Res Microbiol* 164, 596-604.

- Kelley, L.A., Mezulis, S., Yates, C.M., Wass, M.N., and Sternberg, M.J. (2015). The Phyre2 web portal for protein modeling, prediction and analysis. *Nat Protoc* *10*, 845-858.
- Kirchweiger, P., Weiler, S., Egerer-Sieber, C., Blasl, A.T., Hoffmann, S., Schmidt, C., Sander, N., Merker, D., Gerlach, R.G., Hensel, M., *et al.* (2019). Structural and functional characterization of SiiA, an auxiliary protein from the SPI4-encoded type 1 secretion system from *Salmonella enterica*. *Mol Microbiol* *112*, 1403-1422.
- Koronakis, V., Koronakis, E., and Hughes, C. (1989). Isolation and analysis of the C-terminal signal directing export of *Escherichia coli* hemolysin protein across both bacterial membranes. *EMBO J* *8*, 595-605.
- Mackman, N., Nicaud, J.M., Gray, L., and Holland, I.B. (1985). Identification of polypeptides required for the export of haemolysin 2001 from *E. coli*. *Mol Gen Genet* *201*, 529-536.
- Madeira, F., Park, Y.M., Lee, J., Buso, N., Gur, T., Madhusoodanan, N., Basutkar, P., Tivey, A.R.N., Potter, S.C., Finn, R.D., *et al.* (2019). The EMBL-EBI search and sequence analysis tools APIs in 2019. *Nucleic Acids Res* *47*, W636-W641.
- Miller, S.S., S. (unpublished). Investigating the Role of the Bacterial Mechanosensitive Channel Ynal in *Salmonella* Pathogenesis.
- Notredame, C., Higgins, D.G., and Heringa, J. (2000). T-Coffee: A novel method for fast and accurate multiple sequence alignment. *J Mol Biol* *302*, 205-217.
- Peters, B., Stein, J., Klingl, S., Sander, N., Sandmann, A., Taccardi, N., Sticht, H., Gerlach, R.G., Muller, Y.A., and Hensel, M. (2017). Structural and functional dissection reveals distinct roles of Ca²⁺-binding sites in the giant adhesin SiiE of *Salmonella enterica*. *PLoS Pathog* *13*, e1006418.
- Rasmussen, T., and Rasmussen, A. (2018). Bacterial Mechanosensitive Channels. *Subcell Biochem* *87*, 83-116.
- Röder, J., and Hensel, M. (2020). Presence of SopE and mode of infection result in increased *Salmonella*-containing vacuole damage and cytosolic release during host cell infection by *Salmonella enterica*. *Cell Microbiol* *22*, e13155.
- Rowe, I., Anishkin, A., Kamaraju, K., Yoshimura, K., and Sukharev, S. (2014). The cytoplasmic cage domain of the mechanosensitive channel MscS is a sensor of macromolecular crowding. *J Gen Physiol* *143*, 543-557.
- Sander, N. (2022). Functional analysis and characterization of the type 1 secretion system and its cognate substrate, the giant adhesin SiiE, of *Salmonella enterica*. University of Osnabrueck
- Schumann, U., Edwards, M.D., Rasmussen, T., Bartlett, W., van West, P., and Booth, I.R. (2010). YbdG in *Escherichia coli* is a threshold-setting mechanosensitive channel with MscM activity. *Proc Natl Acad Sci U S A* *107*, 12664-12669.
- Smith, T.J., Sondermann, H., and O'Toole, G.A. (2018). Type 1 Does the Two-Step: Type 1 Secretion Substrates with a Functional Periplasmic Intermediate. *J Bacteriol* *200*.
- Wagner, C., Polke, M., Gerlach, R.G., Linke, D., Stierhof, Y.D., Schwarz, H., and Hensel, M. (2011). Functional dissection of SiiE, a giant non-fimbrial adhesin of *Salmonella enterica*. *Cell Microbiol* *13*, 1286-1301.
- Waldo, R.H., 3rd, and Krause, D.C. (2006). Synthesis, stability, and function of cytoadhesin P1 and accessory protein B/C complex of *Mycoplasma pneumoniae*. *J Bacteriol* *188*, 569-575.
- Wang, X., Tang, S., Wen, X., Hong, L., Hong, F., and Li, Y. (2018). Transmembrane TM3b of Mechanosensitive Channel MscS Interacts With Cytoplasmic Domain Cyto-Helix. *Front Physiol* *9*, 1389.
- Wille, T., Wagner, C., Mittelstadt, W., Blank, K., Sommer, E., Malengo, G., Dohler, D., Lange, A., Sourjik, V., Hensel, M., *et al.* (2014). SiiA and SiiB are novel type I secretion system subunits controlling SPI4-mediated adhesion of *Salmonella enterica*. *Cell Microbiol* *16*, 161-178.
- Zhou, J., Fazio, R.T., and Blair, D.F. (1995). Membrane topology of the MotA protein of *Escherichia coli*. *J Mol Biol* *251*, 237-242.

III.3. Functional interaction between SPI4-T1SS encoded proton channel SiiAB and the flagellum in *Salmonella enterica*

Nathalie Sander¹, Michael Holtmannspötter² and Michael Hensel^{1,2}

¹Division of Microbiology, University Osnabrueck, Osnabrueck, Germany

²CellNanOs – Center for Cellular Nanoanalytics, University Osnabrueck, Osnabrueck, Germany

III.3.1. Abstract

During infection by *Salmonella enterica* virulence associated secretion systems, like the type 1 secretion system (T1SS), encoded by the *Salmonella* Pathogenicity Island 4 (SPI4) as well as other surface structures like the flagellum play an important role for efficient adhesion and invasion. The flagellar-driven motility is a critical factor during infection for many Gram-negative bacteria like *S. enterica*, *Escherichia coli* or *Pseudomonas aeruginosa* involving biofilm formation, immune system modulations and adhesion to various surfaces. Proton channels such as MotAB power rotation of the flagellum and bacteria lose motility upon deletion of this stator complex of the flagellum. Additionally, it is described that in dependence of environmental changes, alternative stator complexes can associate with the flagella motor, which not only generate more torque, but can also stop the flagellar rotation. The SPI4-T1SS possesses two non-canonical subunits, namely SiiA and SiiB, which form a proton channel in the inner membrane (IM) and show structural similarities to MotAB. SiiAB are required for an efficient adhesion to and invasion of polarized cells. The SPI4-T1SS substrate SiiE mediates the first close contact to the host cell, representing a special microcompartment important for *Salmonella* infection. However, the detailed mechanism and localization of SiiAB during invasion is still not known. Here, we demonstrate that there is a connection between the flagellum and the SPI4-T1SS substrate SiiE. Intriguingly, the synthetic expression of *siiAB* as well as synthetic expression of the flagellar stator unit *motAB* both showed an increase of velocity. By high resolving dual-color 3D dSTORM microscopy and coordinate-based colocalization (CBC) analysis, we could show that SiiAB are not only located at the SPI4-T1SS, but also at the flagellum at the time point of maximal SiiE retention. Thus, we suggest that SiiAB are not only important directly at the SPI4-T1SS, but also for other virulence-associated complexes like the flagellum.

III.3.2. Introduction

Besides a type 3 secretion system (T3SS), encoded by genes on *Salmonella* Pathogenicity Island 1 (SPI1), an important factor for adhesion to and invasion of polarized epithelial cells is the SPI4 type 1 secretion system (T1SS), which is composed of the ATP-binding cassette (ABC) transporter SiiF in the inner membrane (IM), SiiD as periplasmic adaptor protein (PAP), and SiiC as secretin. The giant repetitive 600 kDa substrate SiiE is transported to the IM, recognized by its T1SS and subsequently secreted into the extracellular space, depending on binding of extracellular Ca^{2+} (Barlag and Hensel, 2015; Griessl *et al.*, 2013; Wagner *et al.*, 2011). During secretion, SiiE is retained on the cell-surface and mediates the first close contact to the host cell membrane during invasion (Gerlach *et al.*, 2007b). Additionally, the SPI4 also encodes an accessory non-canonical proton channel, SiiAB, located in the IM (Wille *et al.*, 2014). It was shown that SiiAB play an essential role in adhesion and invasion by transporting ions across the IM (Wille *et al.*, 2014). SiiA and SiiB share similarities regarding composition and structure with the stator complex of the flagellum, MotAB (Kirchweger *et al.*, 2019). SiiA was found to express the conserved critical aspartate residue (D13), comparable to MotB (D33), inhibiting proton channel function after mutation (Wille *et al.*, 2014). Comparable to MotA, SiiB harbors a large cytoplasmic region, which was shown to interact with SiiF as it is postulated for MotA and the rotor (Blair and Berg, 1991; Dean *et al.*, 1984; Deme *et al.*, 2020b; Wille *et al.*, 2014; Zhou *et al.*, 1995). Additionally, a cross correlation between SiiAB and chemotaxis related CheM was recently described (Hoffmann, 2021, under revision). However, the detailed mechanism behind SiiAB function during invasion is still not known.

During invasion, the flagellum, the SPI4-T1SS and the SPI1-T3SS are simultaneously expressed, leading to a most efficient adhesion and invasion (Gerlach *et al.*, 2008; Gerlach *et al.*, 2007a; Holzer *et al.*, 2009; Horstmann *et al.*, 2020). Motility was found to be essential for biofilm development and maturation by *P. aeruginosa*, *Yersinia enterocolitica*, *Listeria monocytogenes* and *E. coli*, but also during infection as described for pathogens like *Campylobacter jejuni* and *S. enterica* (Haiko and Westerlund-Wikstrom, 2013; Kim *et al.*, 2008; Koirala *et al.*, 2014; Lemon *et al.*, 2007; Mertins *et al.*, 2013; Partridge and Harshey, 2013; Sauer *et al.*, 2002; Wood *et al.*, 2006). It was shown that methylation of *S. Typhimurium* (STM) flagella supports adhesion to host cells and hence their invasion (Horstmann *et al.*, 2020). It was shown that the flagellar T3SS can be associated with bacterial pathogenicity and is co-regulated with virulence genes during infection (Duan *et al.*, 2013).

The flagellum consists of a long external filament, built up from flagellin, the hook and a large motor region located in the cell envelope (Berg, 2003; Nakamura and Minamino, 2019). An ion-powered rotor and a ring of a varying number of stator complexes, surrounding the rotor, represent the motor region of the flagellum in different bacteria (Coulton and Murray, 1978;

Khan *et al.*, 1988; Khan *et al.*, 1992; Khan *et al.*, 1991). The rotational direction of the motor can be changed by chemotactic signaling, leading to a higher adaptation to environmental changes (Minamino *et al.*, 2019). MotAB displays the most well studied example for the prokaryotic rotary motor stator unit family that uses energy from the transmembrane (TM) ion gradient instead of ATP in order to generate mechanical work (Kuhlbrandt and Davies, 2016; Lai *et al.*, 2020; Mandadapu *et al.*, 2015). Stator complexes use H⁺ or Na⁺ ion flow across the IM, in turn generating torque in the cytoplasmic region (C-ring) of the rotor complex (Blair and Berg, 1988, 1990; Kojima, 2015; Larsen *et al.*, 1974). These complexes are present in an inactive, plugged form and are activated by motor incorporation and peptidoglycan (PG) binding (Hosking *et al.*, 2006). MotA builds the pore complex in the IM and consists of four TM helices (TMH) and a large cytoplasmic domain between TMH2 and TMH3 that is suggested to directly interact with the rotor (Blair and Berg, 1991; Dean *et al.*, 1984; Deme *et al.*, 2020b; Hu *et al.*, 2021; Zhou *et al.*, 1995). MotB contains one TMH, followed by a plug region and a large periplasmic region, which can bind to peptidoglycan (=peptidoglycan-binding domain, PGB) (Hosking *et al.*, 2006; Kojima *et al.*, 2018; Roujeinikova, 2008). The MotAB stator unit shows homologies to other known stator units of prokaryotic systems coupling proton translocation to force generation in rotary motors (Lai *et al.*, 2020) such as ExbBD (Kojima and Blair, 2001), TolQR (Cascales *et al.*, 2001) and AgIRQS (Sun *et al.*, 2011). A 5:2 stoichiometry was recently confirmed for MotAB and ExbBD, and appears to be a conserved structure across the MotAB/PomAB family (Deme *et al.*, 2020a, b; Santiveri *et al.*, 2020).

It was demonstrated that SiiAB share similarities with MotAB (Kirchweger *et al.*, 2019; Wille *et al.*, 2014) and that not only the flagellum is co-regulated with virulence genes during invasion of STM, but also that different conserved stator complexes were shown to act at the flagellum in dependence of environmental changes. Additionally, we already described a role of SiiAB for invasion (Wille *et al.*, 2014) and now could also show a distinct role in the initial steps of SiiE secretion (unpublished data, PhD thesis Nathalie Sander, 2022a). We concluded that SiiAB are possibly not only involved in SiiE secretion, but additionally at the flagellum to support flagellar rotation or slow it down to increase efficient invasion. Thus, we analyzed possible modes of action of SiiAB and the flagellum during invasion and also the role of SiiAB for movement during infection of STM. Further, we used novel nanobody tags for visualization of SiiAB localization inside STM by dual-color 3D direct stochastic optical reconstruction microscopy (dSTORM) on a single-molecule super-resolution level and coordinate-based colocalization (CBC) analyses. We used MotAB as best-described flagellar-associated proton channel as positive control for our assays.

III.3.3. Results

III.3.3.1. Structure prediction of SPI4-T1SS accessory proton channel SiiAB reveals more consensus with Na⁺-conducting channels than with H⁺-conducting channels

Sequence similarity between SiiA and MotB, and SiiB and MotA have been previously described (Deme *et al.*, 2020b; Kirchweiger *et al.*, 2019; Santiveri *et al.*, 2020; Wille *et al.*, 2014), indicating related functions and mechanisms. Recently, complex structures for MotAB became available, but no structural information are available for SiiAB. We performed tertiary structure analyses using the trRosetta algorithm (Du, 2021; Yang *et al.*, 2020) to compare both channels (Figure III.3.1). The determined TM-scores are indicative of the validity of prediction. The TM-scores in the structure predictions were very high for MotA (0.859) and MotB (0.705), high for SiiA (0.589) and middle for SiiB (0.411). MotA and SiiB share the overall helical structure, although they present a different fold. While SiiB is predicted to possess a long C-terminal domain extending into the cytoplasm, this is not the case for MotA. Based on sequence alignments with *Campylobacter jejuni* MotA (*Cj*MotA), homologous residues critical for FliG binding are conserved in STM MotA to some extent (Hu *et al.*, 2021; Santiveri *et al.*, 2020). For *Cj*MotA, the positively charged residues R89 and R90 and the negatively charged residues E97 and D117 from the adjacent subunit were found to be essential for FliG interaction (Santiveri *et al.*, 2020). These amino acids are present in conserved regions and hence STM MotA shows a comparable positively charged patch (R90/Q91), whereas the negatively charged region is a little less conserved (E98/S135). SiiA and MotB are also anticipated with a very similar fold (Figure III.3.1 A, C). The prediction includes a β -sheet domain in the C-terminal part, consisting of five β -sheets, respectively. The critical aspartate residue essential for the proton channel function is located in the N-terminal region in both cases (Wille *et al.*, 2014; Zhou *et al.*, 1998). Additionally, extended loops at the very N- and C-terminus are predicted for MotB, but not for SiiA. Taken together, the predicted structures for MotA and SiiB and MotB and SiiA are comparable but also show distinct differences. We concluded that these small differences can be explained by their different functions.

As described before, we performed an alignment analysis of not only H⁺-conducting channels, but also Na⁺-conducting channels (Santiveri *et al.*, 2020) and compared them to STM SiiB (Figure III.3.2 and Figure S III.3.1). Besides *Cj*MotA, MotA of *Campylobacter jejuni* (*Cj*), *Salmonella* Typhimurium (STM), *Escherichia coli* (*Ec*), *Helicobacter pylori* (*Hp*), *Bacillus subtilis* (*Bs*), *Shewanella oneidensis* (*So*) and the Na⁺-conducting channels MotP and PomA of *Bs*, *So* and *Vibrio alginolyticus* (*Va*) were analyzed in comparison to STM SiiB (Figure III.3.2 A). The arginine at position 89 was found to be highly conserved among all analyzed channels, independent of the proton specificity. Interestingly, the Na⁺-conducting channels and SiiB all possess a lysine after the critical arginine, which cannot be found in the H⁺-conducting channels.

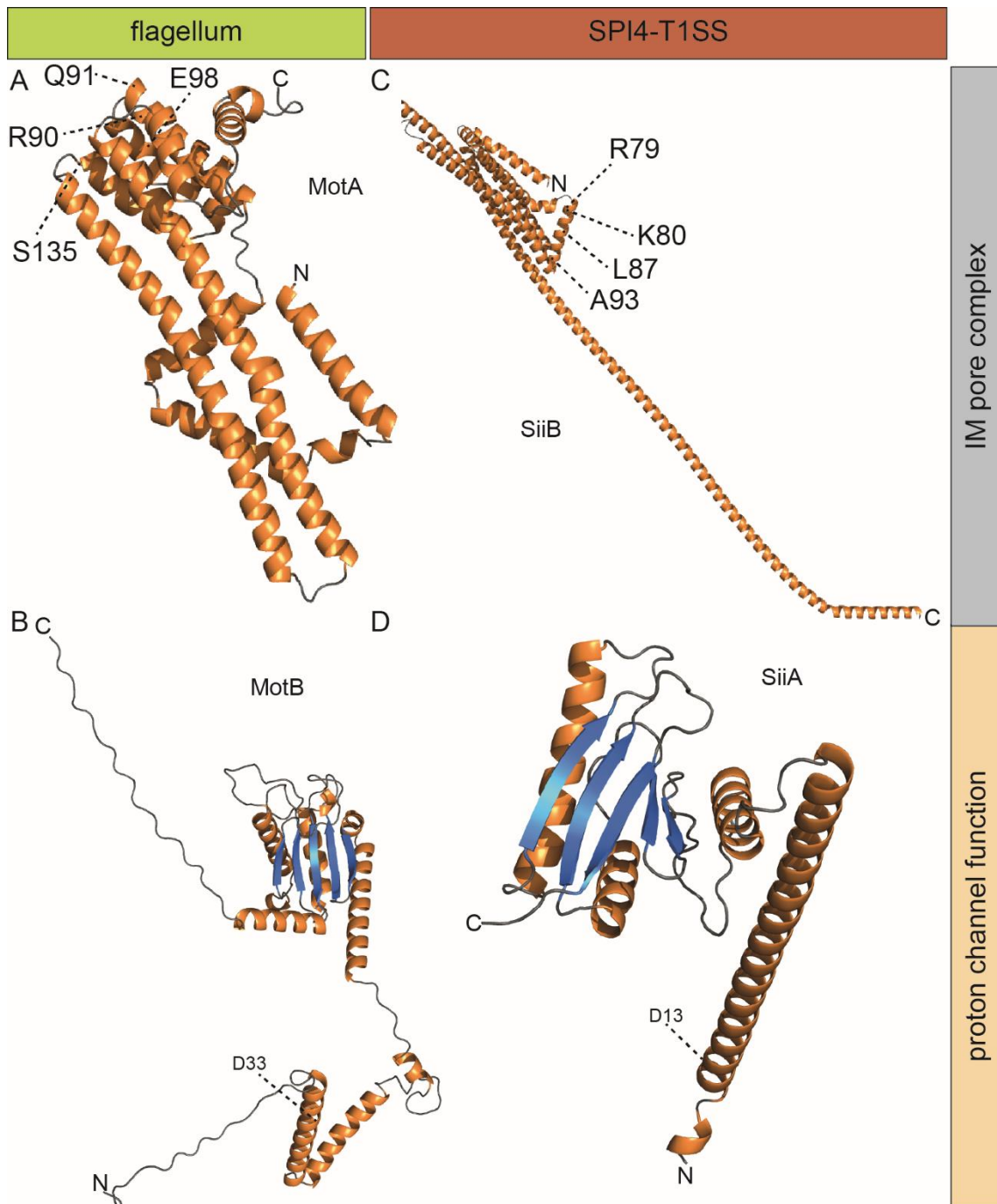


Figure III.3.1 Structural analyses of the proton channels MotAB and SiiAB. Tertiary structure model prediction for MotA (A), MotB (B), SiiB (C) and SiiA (D) by trRosetta (Du, 2021; Yang *et al.*, 2020). Loop, gray; β -sheet, blue; α -helix, orange. TM-score for modelling by trRosetta. TM-Scores: 0.859 (MotA), 0.705 (MotB), 0.589 (SiiA), 0.411 (SiiB). Critical residues as indicated (*). TM-score > 0.4 = middle confidence, TM-score > 0.5 = high confidence, TM-score > 0.7 = very high confidence.

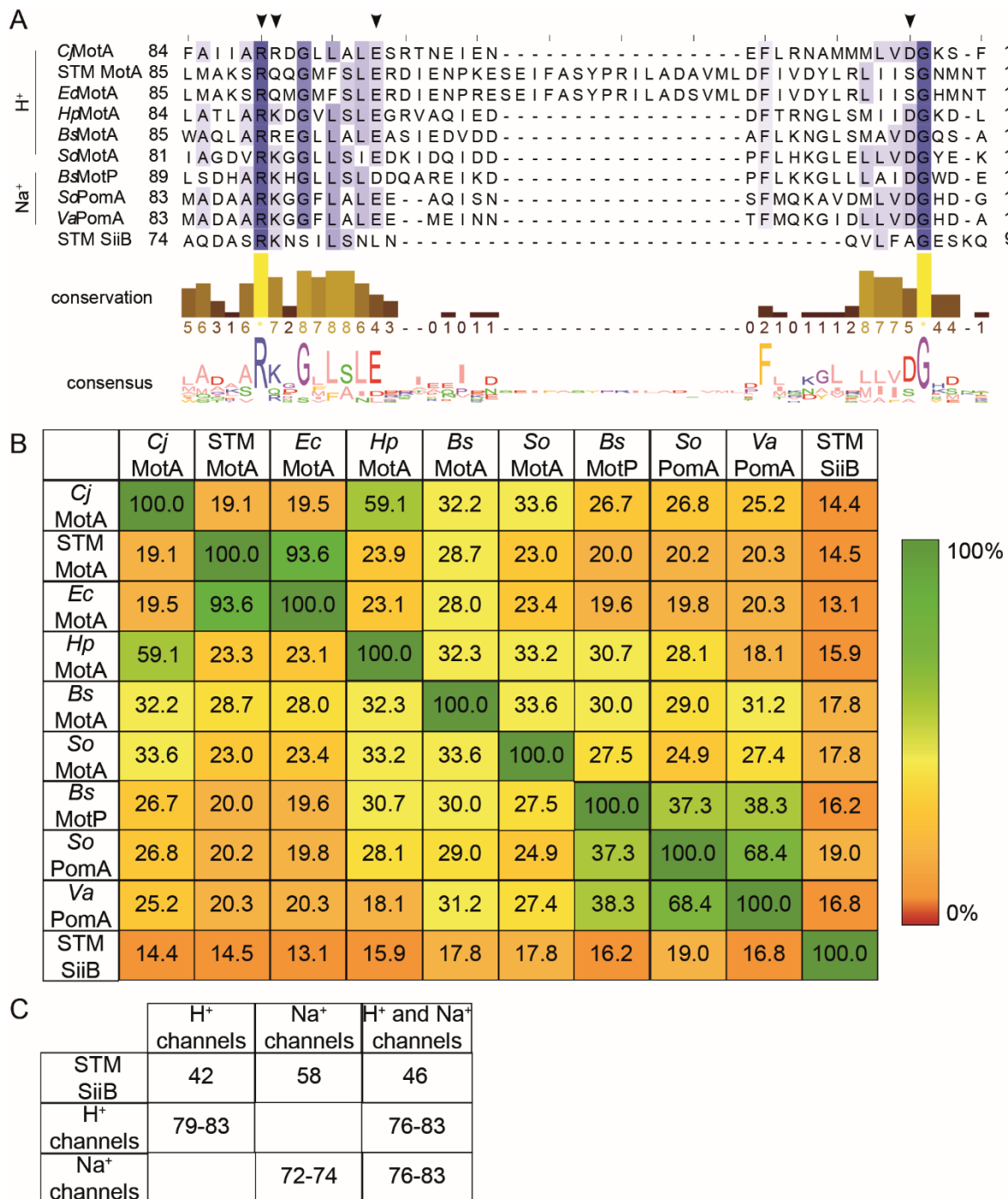


Figure III.3.2. Alignment of various H⁺- and Na⁺-conducting channels in comparison to STM SiiB. A) Shown is the alignment of H⁺-conducting channels (MotA) of *Campylobacter jejuni* (*Cj*), *Salmonella* Typhimurium (STM), *Escherichia coli* (*Ec*), *Helicobacter pylori* (*Hp*), *Bacillus subtilis* (*Bs*), *Shewanella oneidensis* (*So*) and the Na⁺-conducting channels MotP and PomA of *Bs*, *So* and *Vibrio alginolyticus* (*Va*). Alignment was performed with Clustal Omega (Madeira *et al.*, 2019). Highly conserved regions are depicted in dark blue. Arrows indicate the critical *Cj*MotA residues R89, R90, E97 and D117 as published before (Santiveri *et al.*, 2020). B) Percent identity between the analyzed channels as indicated. C) Shown are the total consistency values of the tested channels generated by multiple sequence alignment by T-Coffee algorithm (Notredame *et al.*, 2000).

This patch of higher conservation among the sequences also contains a leucine (*Cj*MotA L94), which was not found in all H⁺-conducting channels, but in all Na⁺-conducting channels. The conserved glutamic acid (*Cj*MotA E98) was found in all analyzed proteins, with exception of *Bs*MotP and STM SiiB. However, *Bs*MotP showed the same charged aspartic acid at this position, which was also not found in STM SiiB (L87), displaying a pattern differing from all tested channels. Additionally, we found a highly conserved glycine (*Cj*MotA G136), indicating an essential role of this residue as well. We additionally analyzed the identity between the different channels (Figure III.3.2 B). Identity of SiiB with the other channels did not reach 20%, whereas H⁺-conducting channels and Na⁺-conducting channels showed higher values between each other, respectively. Between the two groups also only about 20-30% identity was found. SiiB showed less identity with MotA of *Cj*, *Ec*, STM and *Hp* than with MotA of *Bs* and *So*, as well as MotP of *Bs* and PomA of *So* and *Va*. We concluded lower values of overall sequence identity for SiiB compared to the other channels, due to the extended C-terminal part of SiiB (Figure III.3.1 B and Figure S III.3.1), which could not be found in other of the channels (SiiB STM 462aa; STM MotA 295aa). Interestingly, analysis of the total consistency values of the tested channels by multiple sequence alignment by T-Coffee algorithm showed higher scores for SiiB with Na⁺-conducting channels (Score: 58) than with H⁺-conducting channels (Score: 42) (Figure III.3.2 C).

All in all, we confirmed similarities between SiiB with MotA as published before, and additionally observed a higher consensus to Na⁺-conducting channels, shedding new light on the SPI4-T1SS accessory proton channel SiiAB.

III.3.3.2. The flagellar filament directly alters SiiE secretion and function

It was already shown that the non-canonical subunits SiiAB are important during invasion, but their detailed function is still not known (Wille *et al.*, 2014). Interestingly, flagellar-associated proteins can be co-regulated with virulence genes and the flagellum itself plays an important role during invasion (Duan *et al.*, 2013). Furthermore, the flagellum, the SPI1-T3SS and the SPI4-T1SS are simultaneously expressed during invasion (Gerlach *et al.*, 2008; Gerlach *et al.*, 2007a; Holzer *et al.*, 2009; Horstmann *et al.*, 2020). Such a co-regulation is also described for biofilm-forming pathogens as *P. aeruginosa*, which switches between a motile and sessile lifestyle, requiring a defined regulation of associated proteins (Boyd *et al.*, 2014; Cooley *et al.*, 2016; Smith *et al.*, 2018a). Thus, as efficient invasion potentially requires a comparable regulation, we decided to not only investigate the role of SiiAB for the flagellum, but additionally the correlation between the flagellar filament, built from the hook, cap subunit and the major sub-

units flagellins FliC or FljB (Haiko and Westerlund-Wikstrom, 2013), and the SPI4-T1SS, especially the substrate SiiE. In a first attempt to analyze a potential correlation we performed flow cytometry analysis of retained SiiE (Figure III.3.3 A-C) and as a direct functional consequence measured the adhesion to polarized MDCK cells (Figure III.3.3 D).

For flow cytometry analysis, we stained surface-bound SiiE at the time point of maximum retention (2.5 h) (unpublished data, PhD thesis Nathalie Sander, 2022b) with an Alexa488-conjugated antibody. As positive and negative controls, we used STM WT and a *siiE* deletion strain, respectively. We tested a *siiAB* deletion strain, a non-flagellated mutant ($\Delta fliC \Delta fljB$) and a double mutant without filament and proton channel SiiAB ($\Delta fliC \Delta fljB \Delta siiAB$). First, we gated the bacteria (Figure III.3.3 A) with an unstained STM WT sample (not shown). Stained strains behaved like the unstained control and showed no aggregates. In a second step, we gated the SiiE-positive cells with help of the positive and negative control (Figure III.3.3 B, exemplary). We found approximately 20% SiiE-positive cells in WT (20.2%), as well as in $\Delta siiAB$ (20.7%) and $\Delta fliC \Delta fljB$ (22%) (Figure III.3.3 B). Interestingly, $\Delta fliC \Delta fljB \Delta siiAB$ showed twice as many SiiE-positive bacteria (43.9%), but with lower signal intensity per cell (Figure III.3.3 B). The distribution of SiiE-positive events was comparable to $\Delta siiAB$. We analyzed the signal per cell by calculating the mean fluorescence, taking the positive cells and the counted bacteria into account (Figure III.3.3 C). Considering the signal per cell, no difference was observed between WT, $\Delta fliC \Delta fljB$ (95.6%), and $\Delta fliC \Delta fljB \Delta siiAB$ (97%). The *siiAB* deletion strain showed a significantly reduced SiiE signal per cell (48.2%) in comparison to WT. We concluded that *siiAB* actively regulate SiiE retention per cell that – in a deletion of the flagellum – is compensated for by upregulation of the SiiE-positive cells in the whole population. As a direct consequence of SiiE retention, we tested the adhesion to polarized cells (Figure III.3.3 D). Although a *siiAB* deletion strain retains 50% of SiiE on the cell surface, a significant decrease in adhesion, comparable to a *siiE* deletion strain was observed. In comparison to $\Delta fliC \Delta fljB$, $\Delta fliC \Delta fljB \Delta siiAB$ showed a reduced adhesion (67%), indicating that as in a $\Delta siiAB$ strain, SiiE function is reduced despite being retained on the cell surface.

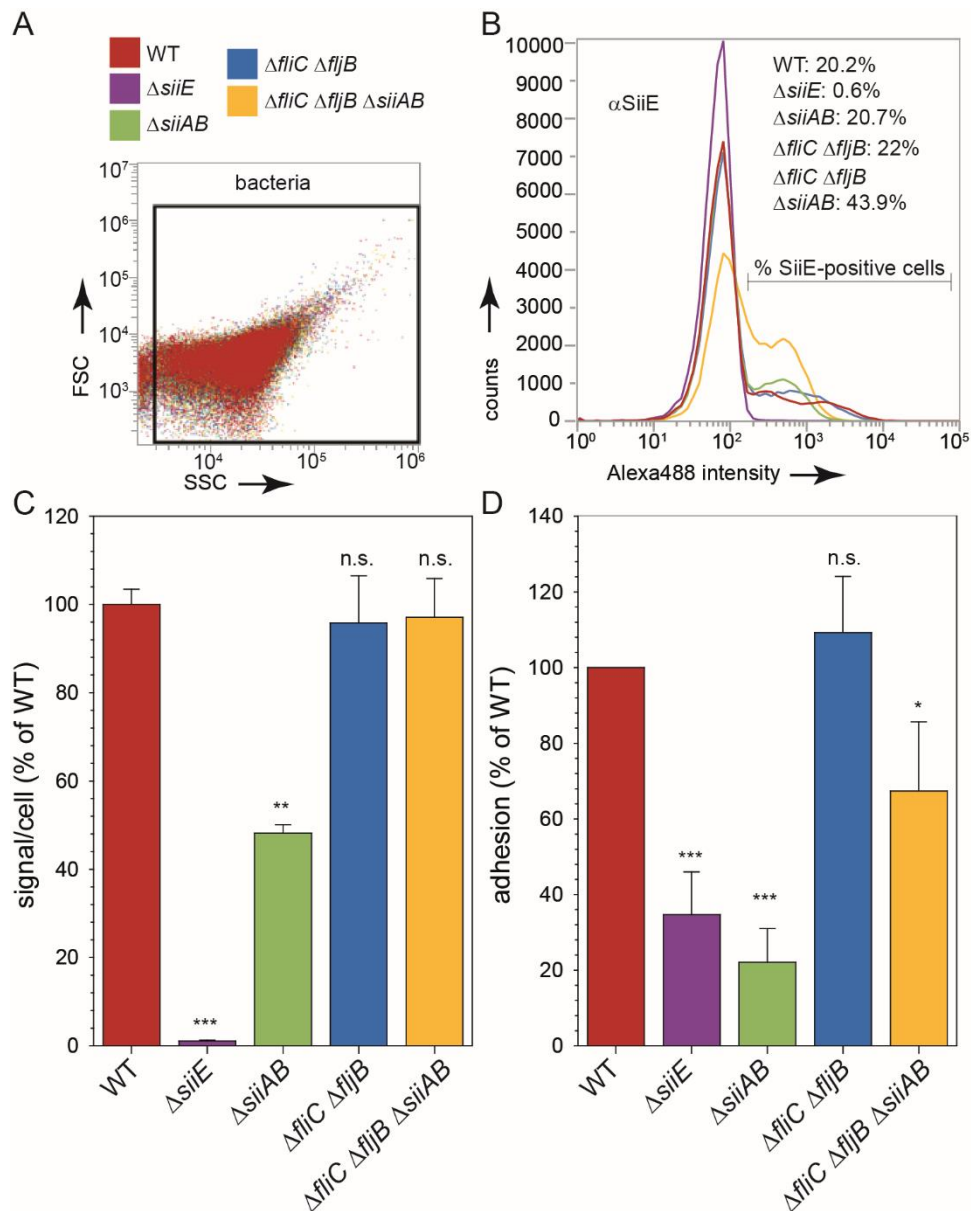


Figure III.3.3. SiiE retention and function in dependence of the flagellum and SiiAB. A-C) Flow cytometry of retained SiiE. Subcultures were grown for 2.5 h, bacteria were pelleted and fixed with 3% PFA in PBS. Retained SiiE was stained with serum against SiiE and Alexa488-conjugated secondary antibody. Bacteria were diluted to OD₆₀₀ of 0.1 and analyzed by flow cytometry. A) Gating for bacteria (FSC, SSC) with unstained WT (not shown). B) Histogram of the Alexa488-positive cells and the counts. WT was used as positive control and $\Delta siiE$ as negative control for gating. SiiE-positive cells as indicated. C) SiiE signal intensities of positive cells. D) Adhesion of STM to polarized MDCK cells in dependence of SiiAB and the flagellum. Subcultures were grown for 2.5 h and MDCK were infected with MOI 5. Statistical analyses compared to WT with at least biological duplicates by two-tailed t-test: ***, $p < 0.001$; **, *, $p < 0.05$; n.s., not significant.

It was postulated that the flagellar filament is important for the adhesion to distinct cell types and the rotation of the flagellum for the invasion (Haiko and Westerlund-Wikstrom, 2013). Therefore, we decided to test the invasion of polarized and non-polarized cells in dependence of the flagellum, MotAB and SiiAB (Figure III.3.4). As functionality of the SPI4-T1SS is not

necessary for invasion of non-polarized cells like HeLa cells (Gerlach *et al.*, 2008), a SPI1-T3SS-deficient strain ($\Delta invC$) was introduced as control. This mutant strain is not able to invade polarized or non-polarized cells (Figure III.3.4). In polarized cells, all SPI4-T1SS mutant strains showed a highly reduced invasion (Figure III.3.4 A). In contrast, only the $\Delta siiE$ strain invaded identical to WT into non-polarized cells (Figure III.3.4 B). The proton channel mutants $siiA_{D13E}$ and $\Delta siiAB$ showed reduced invasion in comparison to WT (53% and 63.5%), indicating a role of the proton channel independent of the canonical T1SS subunits and SiiE for invasion of non-polarized cells. Interestingly, we found that loss of the flagellum leads to a less reduced invasion (77.6%) of polarized cells than deletion of *motAB* (additionally) (33%). Contrary, a deletion of the flagellar filament alone and the proton channels in addition showed the similar phenotype in non-polarized cells (5.5% to 12.4% of WT). We propose that the flagellar-mediated motility of STM is more important for invasion of non-polarized cells than of polarized cells, and that SiiAB contribute to invasion of non-polarized cells independent of SiiE.

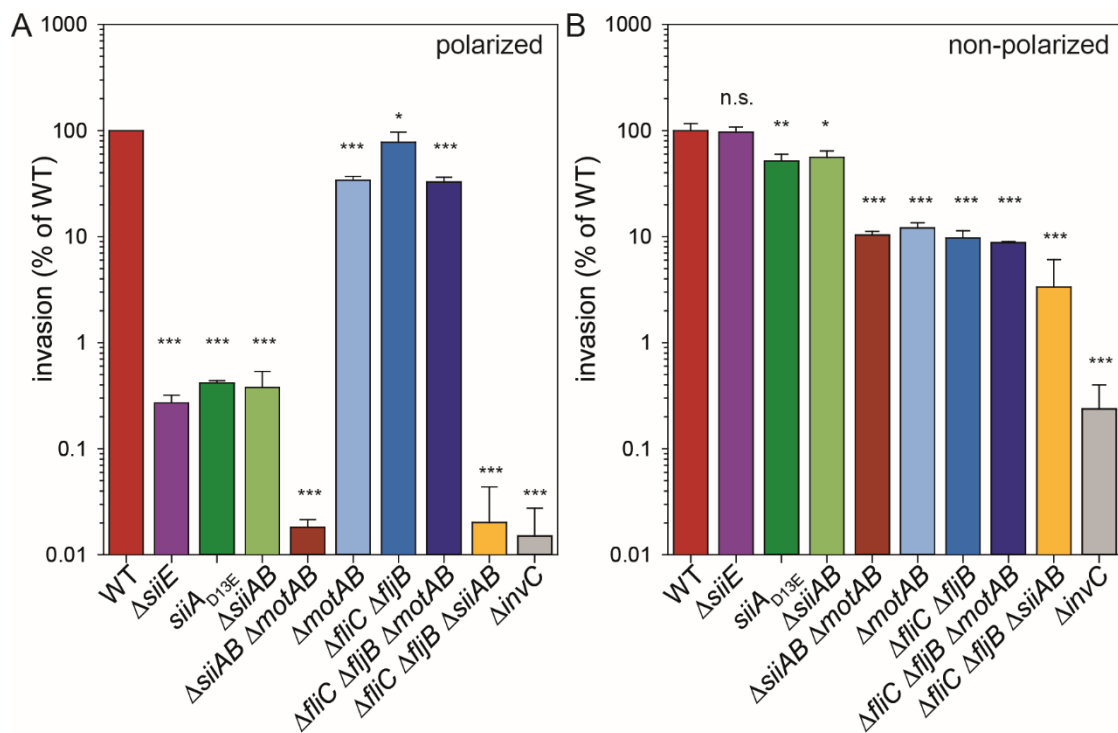


Figure III.3.4. Invasion of polarized or non-polarized cells in dependence of SPI4-T1SS and flagellum associated-proteins. Invasion of polarized MDCK cells (A) or non-polarized HeLa cells (B). Subcultures were grown for 2.5 h and cells were infected at MOI 5. Statistical analyses compared to WT with at least biological triplicates by two-tailed t-test: ***, $p < 0.001$; **, $p < 0.01$; *, $p < 0.05$; n.s., not significant.

III.3.3.3. 3D dSTORM analysis shows localization of SiiB at the flagellum in phases of maximal SiiE retention

Besides similarities between MotAB and SiiAB (Kirchweger *et al.*, 2019; Wille *et al.*, 2014), we additionally found conserved residues in H⁺-conducting and Na⁺-conducting channels, associated with the flagellum (Figure III.3.1, Figure III.3.2). To efficiently invade host cells, a tight control of not only the secretion systems, but also of the flagellum is essential, taking other systems like biofilm-associated systems as in *P. aeruginosa* into account (Smith *et al.*, 2018b), where bacteria change from a motile to a sessile lifestyle, comparable to STM adhesion process. We could already show that the flagellar movement is essential for an increased invasion of polarized and non-polarized cells (Figure III.3.4). Thus, we investigated whether SiiAB are possibly located at the flagellum, actively supporting torque generation or stopping of the flagellum to positively regulate invasion. It was already described for other bacteria and proton channels that MotAB can be exchanged under distinct conditions (Baker and O'Toole, 2017). There are homologies described for MotA and SiiB and MotB and SiiA (Kirchweger *et al.*, 2019), making it conceivable that SiiAB can also play a role directly at the flagellum. We used novel nanobody tags, ALFA-tag and Spot-Tag, and suitable small nanobodies, directly coupled to fluorochromes, to analyze the localization of MotAB and SiiAB by super-resolution microscopy (SRM). By using these small tags and nanobodies, we ensured a minimal distance between the proteins of interest and the fluorochrome, increasing the accuracy of the localization and interpretation of protein colocalization. The fusion proteins were checked for expression and functionality (Figure S III.3.3). For the Spot-Tag system, we were also able to efficiently elute complexes of MotA and MotB via Spot-Trap under endogenous expression conditions (Metterlein, 2018) (data not shown).

In a first attempt, we tested the nanobodies and tags by widefield microscopy (Figure III.3.5). We stained the controls MotA and MotB with nanobodies coupled to Atto565 and Alexa647, respectively. SiiA and SiiB were stained with Alexa647 and Atto565, comparable to the MotAB control. Additionally, we tested specificity of the nanobody binding to our introduced tags (data not shown). Already by using diffraction-limited widefield microscopy we are able to detect specific spots in bacterial envelopes, indicating overlapping signals for MotA and MotB (Figure III.3.5 A). We additionally found signals for SiiA and SiiB (Figure III.3.5 B). We concluded that nanobody tags are compatible with SiiAB and MotAB function and allow specific dual-fluorescence labeling. In a next step, we analyzed colocalization of MotA with the flagellum and of SiiB with the SPI4-T1SS. We labeled FliN and SiiF with a HaloTag and incubated the fixed and stained bacteria with Htl-SiR ligand (Figure III.3.6). FliN is located in the IM and is part of the C-ring of the flagellar rotor, interacting with the stator complexes (Hu *et al.*, 2021).

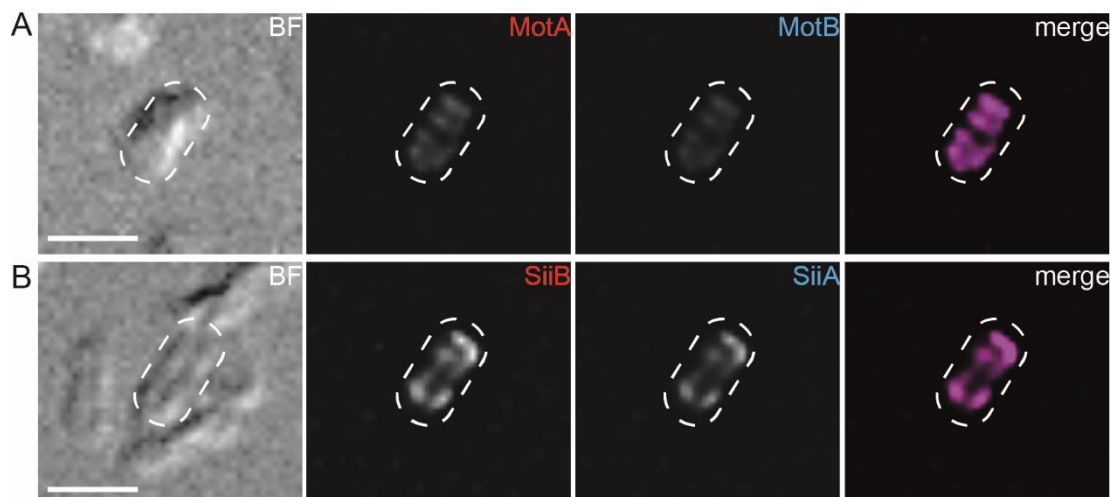


Figure III.3.5. Functionality of ALFA and SPOT tag in MotAB and SiiAB. Microscopic analysis of the controls MotA (ALFA-tag), MotB (Spot-Tag), SiiA (Spot-Tag) and SiiB (ALFA-tag), stained with fluorochrome-coupled nanobodies. Subcultures were grown for 2.5 h, pelleted by centrifugation and fixed with a methanol/acetic acid mix. Cells were permeabilized by treatment with 8 $\mu\text{g}/\text{ml}$ Lysozyme. Bacteria were stained for MotA and SiiB with Atto565-coupled FluoTag-X2 anti-ALFA nanobody, and MotB and SiiA with Alexa647-coupled nanobody against Spot-Tag. For microscopy, a widefield microscope, 100x with oil was used. Images were deconvoluted with Huygens Professional version 19.04 (Scientific Volume Imaging, The Netherlands, <http://svi.nl>). Scale bar, 2 μm .

Furthermore, we checked for localization of SiiB at the flagellum (Figure III.3.6 B, lower panel). For MotA and FliN we found overlapping signals distributed over the cells (Figure III.3.6 A). SiiB and SiiF showed overlapping signals, also potentially located in the membrane regions (Figure III.3.6 B, upper panel). Interestingly, we found spots with a FliN signal only and spots with both proteins, SiiB and FliN, in direct proximity (Figure III.3.6 B, lower panel). We concluded that there is a possibility that SiiB not only localizes at the SPI4-T1SS, but may also be able to localize at the flagellum, as it is described for MotA. After these first tests, we decided to analyze the localization in more detail by using 3D dSTORM SRM.

To analyze localization of subunits with higher spatial resolution, we performed dual-color 3D dSTORM (Huang *et al.*, 2008). We used the tags introduced above and specific controls for our analysis. By addition of a cylindrical lens in a widefield total internal reflection (TIRF) microscope that changes position and ellipticity of the single signals according to its z localization, it is possible to localize single molecules in 3D (Huang *et al.*, 2008). Prior to image acquisition, a calibration curve is generated, thus allowing accurate calculation of the astigmatic signals and determination of the 3D information. In combination with the coordinate-based colocalization (CBC) method, we were not only able to image the proteins (Figure III.3.7), but also to quantify 3D localizations of the proteins of interest (Figure III.3.8).

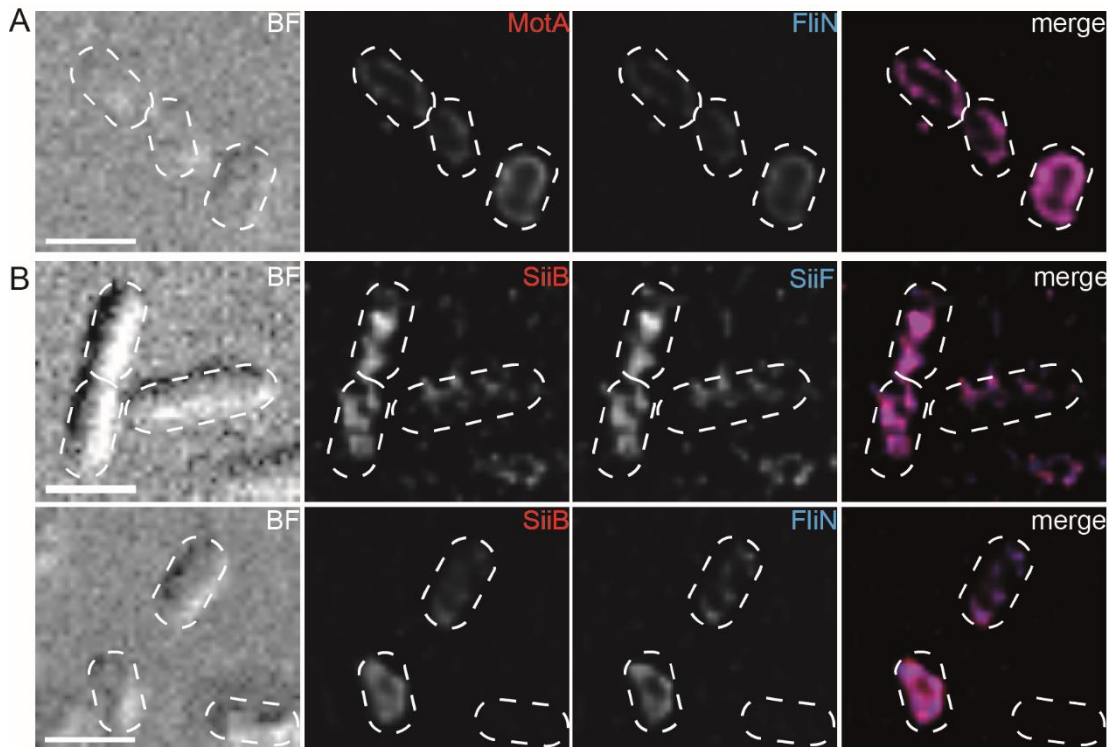
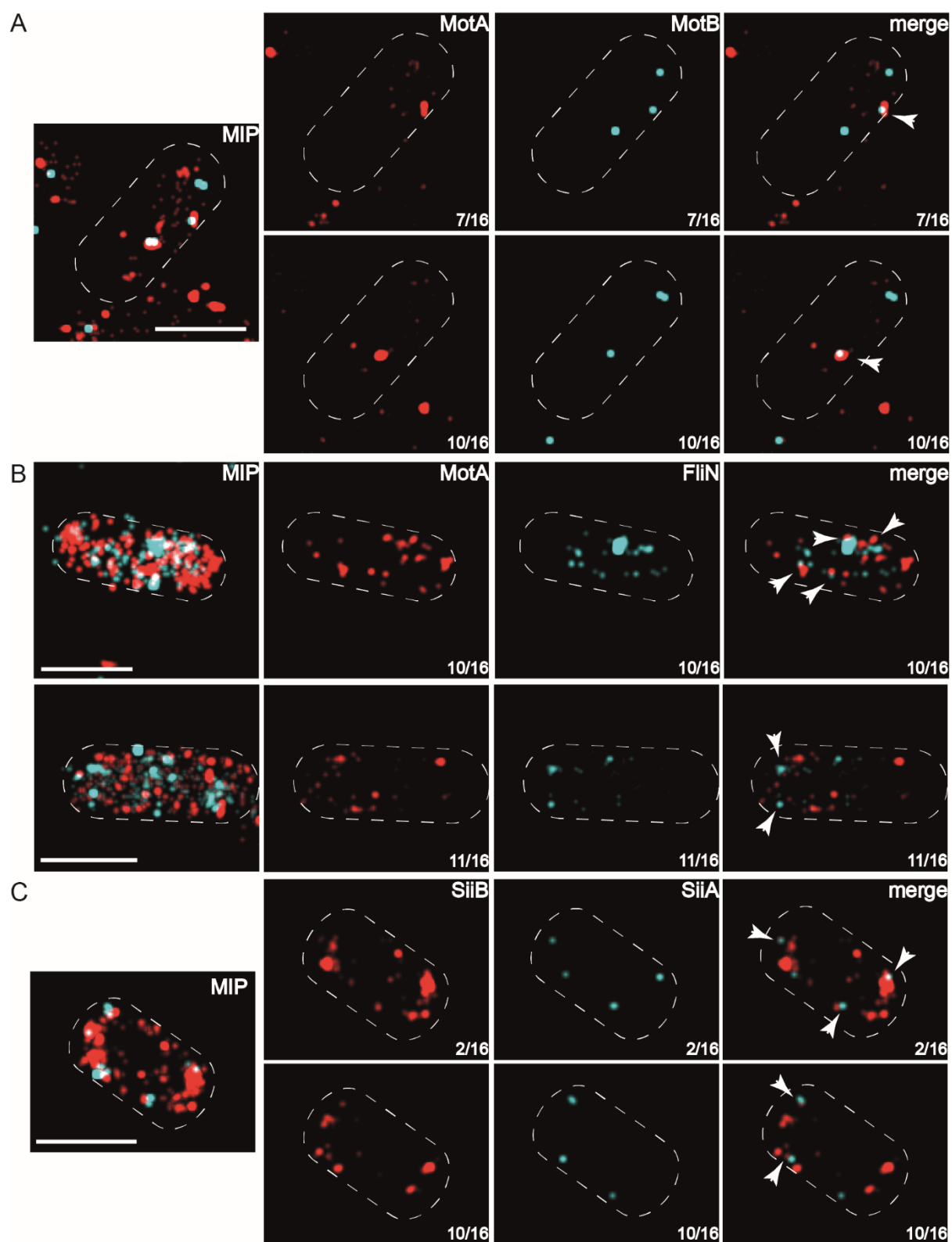


Figure III.3.6. Localization analysis of MotAB, SiiAB, the flagellar rotor, and the SPI4-T1SS. Microscopic analysis of MotA, FliN, SiiB and SiiF, stained with fluorophore-coupled nanobodies and HaloTag® ligand Htl-SiR, respectively. Subcultures were grown for 2.5 h, pelleted by centrifugation and fixed with a methanol/acetic acid mix. Cells were permeabilized by treatment with 8 µg/ml lysozyme. Bacteria were stained for MotA and SiiB with Atto565-coupled FluoTag-X2 anti-ALFA nanobody and FliN and SiiF with HaloTag® ligand Htl-SiR. For microscopy, a widefield microscope, 100x with oil was used. Scale bar, 2 µm.

To exemplarily demonstrate proximity of the proteins we tested, we show distinct evaluated slices of the generated z stacks. The validated images showed overlapping signals of MotB and MotA (Figure III.3.7 A). Additionally, we found MotA adjacent to the C-ring protein FliN (Figure III.3.7 B). We were also able to image SiiB and SiiA in direct proximity and found overlapping signals (Figure III.3.7 C). Interestingly, we found less SiiB located with SPI4-T1SS ATPase subunit SiiF (Figure III.3.7 D), but more frequently associated with the flagellar rotor subunit FliN (Figure III.3.7 E).



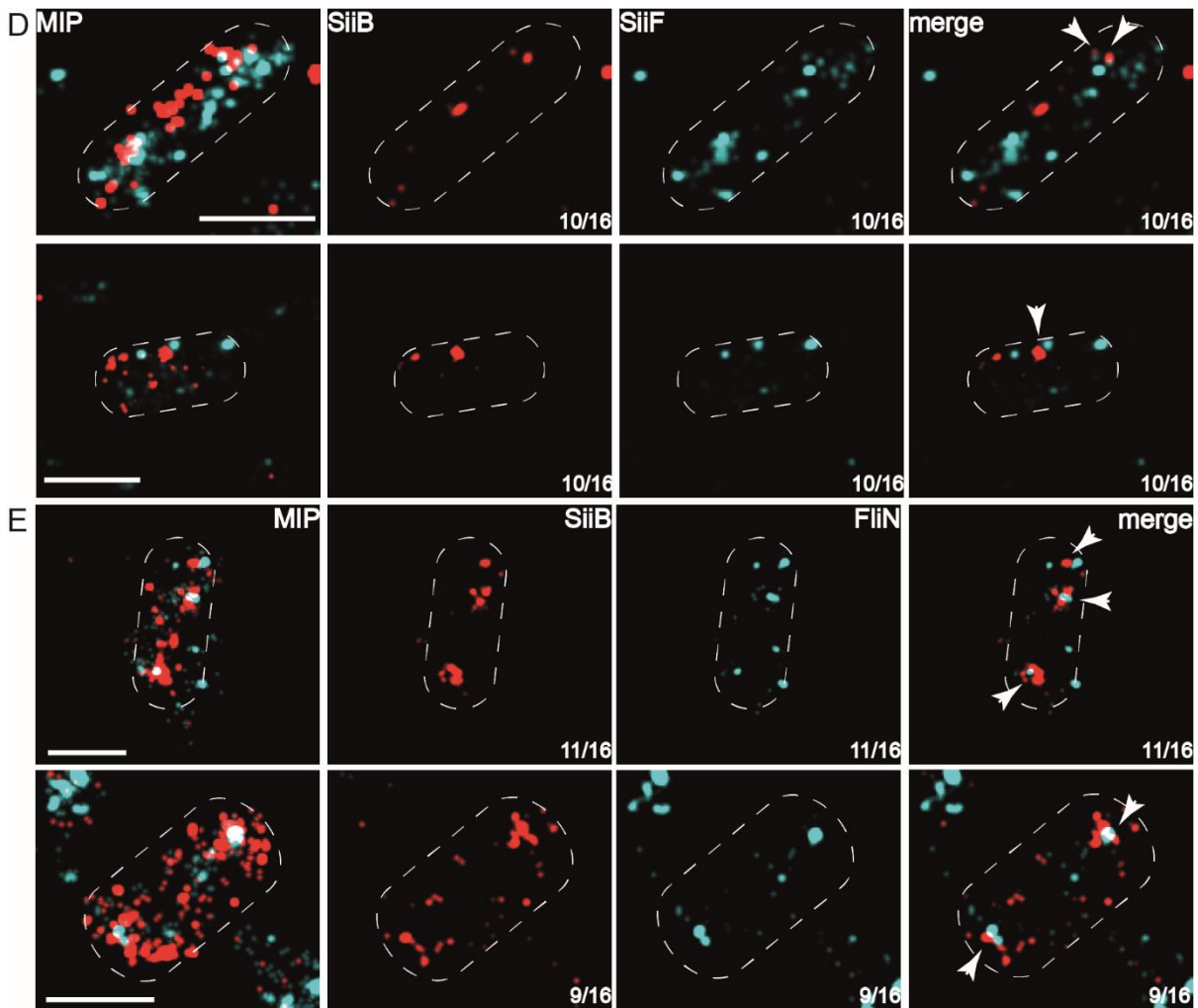


Figure III.3.7. Localization analysis of MotAB and SiiAB by 3D dSTORM microscopy. Shown are representative validated 3D dSTORM SRM images. Subcultures were grown for 2.5 h, pelleted by centrifugation and fixed with a methanol/acetic acid mix. Cells were permeabilized by treatment with 8 $\mu\text{g}/\text{ml}$ Lysozyme. Bacteria were stained for MotA and SiiB with Atto565-coupled FluoTag-X2 anti-ALFA nanobody and FliN and SiiF with HaloTag® ligand Htl-SiR. For SRM by dSTORM imaging, cells were incubated in a buffer containing 15 mM MEA, 4.5 mg/ml D-glucose, 40 $\mu\text{g}/\text{ml}$ catalase and 0.5 mg/ml glucose-oxidase and maximum laser power was used for excitation. The 3D SRM image was rendered from single emitter localizations obtained within at least 2,000 frames and calibrated with TetraSpeck™ Microspheres, recorded under the same conditions. The maximum intensity projection (MIP) of the 3D analysis is shown in the left panel. Scale bars, 1 μm . Numbers in the right corner indicate slice number of the validated z stack. A) Staining of the positive control MotA with α -ALFA-tag nanobody coupled to Atto565 and MotB with α -Spot-Tag nanobody coupled to Alexa647. One representative cell is shown. B) Staining of the positive control MotA with α -ALFA-tag nanobody coupled to Atto565 and FliN with Htl-SiR. C) Staining of SiiB with α -ALFA-tag nanobody coupled to Atto565, and SiiA with α -Spot-Tag nanobody coupled to Alexa647. One representative cell is shown. D) Staining of SiiB with α -ALFA-tag nanobody coupled to Atto565 and SiiF with Htl-SiR. E) Staining of SiiB with α -ALFA-tag nanobody coupled to Atto565 and FliN with Htl-SiR.

These visualizations are supported by our CBC analysis (Figure III.3.8). The CBC is described to be similar to the Spearman correlation (Malkusch *et al.*, 2012). The defined CBC value can reach values from -1 for perfect anti-correlated distribution, described to be difficult to interpret if the Pearson and the Mander's correlation coefficient are taken into account (Adler and

Parmryd, 2010; Zinchuk and Zinchuk, 2008), through 0 for non-correlated distributions (low probability of colocalization), to +1 for perfectly correlated distributions (high probability of colocalization) (Malkusch *et al.*, 2012). The Pearson correlation coefficient (PCC) and the Mander's overlap coefficient (MOC) can be used to quantify the degree of colocalization between two fluorophores (Adler and Parmryd, 2010). As the PCC describes the linear correlation of two characteristics, but the characteristics can also be non-linear, this correlation coefficient is not a good measure for a pure stochastic dependence of two features (Brueckler, 2017). The MOC was introduced to solve these problems with the PCC (Adler and Parmryd, 2010). These coefficients only differ in the use of the intensities. Whereas the PCC uses the deviation from the mean, MOC uses absolute intensities. Contrarily, the introduction of the CBC algorithm was shown to be suitable for single-molecule SRM data (Malkusch *et al.*, 2012). Beside the values ranging from 0.5 to +1 (positive correlation, PC), we additionally defined an anti-correlation range (AC), ranging from -1 to -0.5, as described before (Mass *et al.*, 2020). We found increased AC values for MotA and SiiB with FliN and SiiF (Figure III.3.8 B, D, E) than with MotB and SiiA (Figure III.3.8 A, C), indicating a higher distance than with the other proton channel subunit, as expected. We found comparable amounts of MotA positively correlated with MotB (38.9%, PC: 9%) (Figure III.3.8 A) and with FliN (39.1%, PC: 11.8%) (Figure III.3.8 B). For SiiB and SiiA, colocalization values were slightly smaller in comparison (26.5%, PC: 6.3%) (Figure III.3.8 C). Strikingly, we only found less positive colocalization (11.6%, PC: 2.2%) for SiiB and SiiF along with high AC values, respectively (Figure III.3.8 D), indicating that SiiB (together with SiiA) is not located at the SPI4-T1SS at the time point of maximum SiiE retention. These data are supported by previous results, showing that SiiAB are only important during the initial steps of SiiE secretion prior to retention of SiiE by SiiC in the OM (unpublished data PhD thesis Nathalie Sander, 2022a). Interestingly, we found comparable values for a colocalization of SiiB and FliN (24.3%, PC: 6.5%), as for SiiB and SiiA (Figure III.3.8 E), underlining the above results and further supporting an interplay between SiiAB and the flagellar rotor.

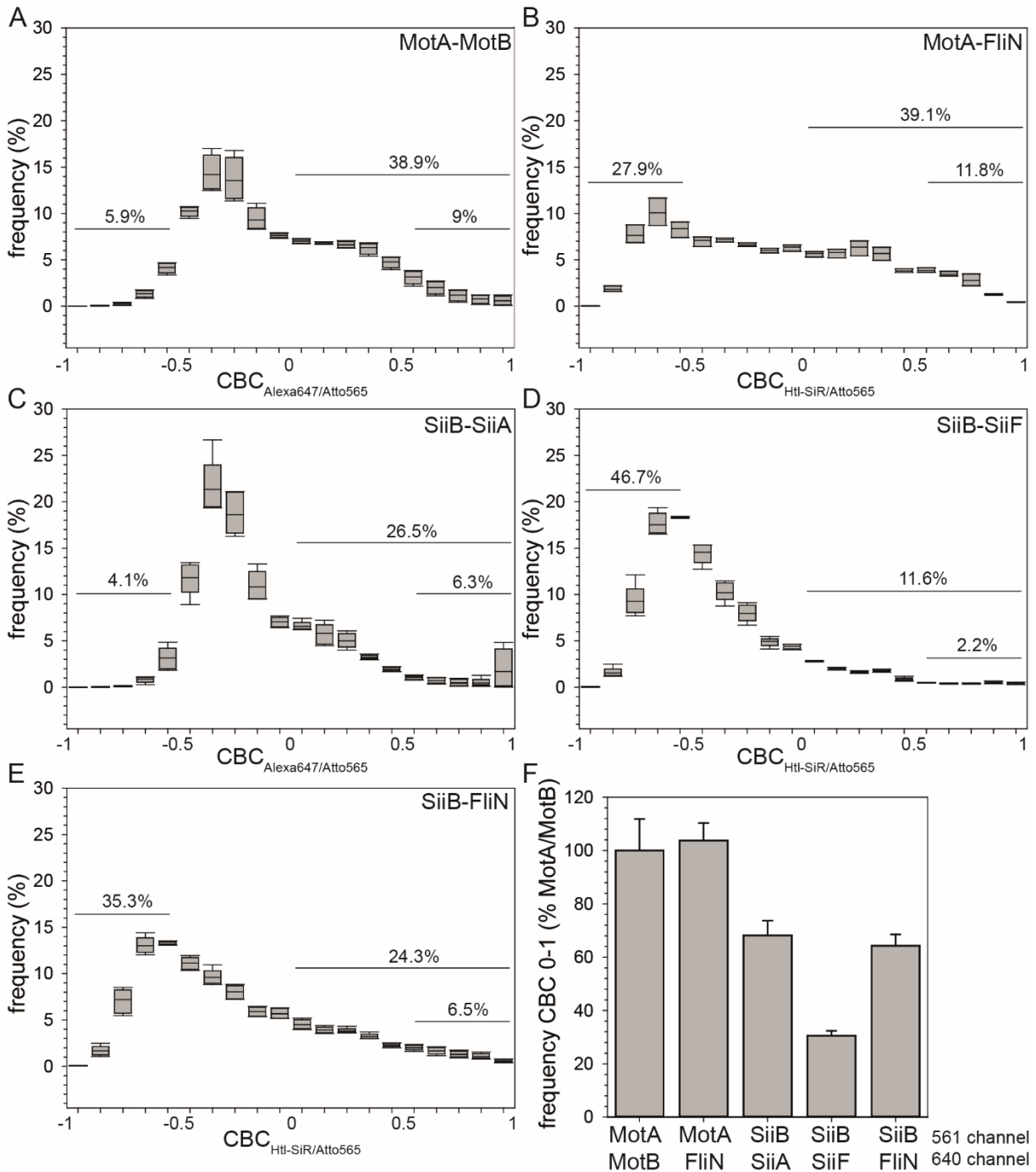


Figure III.3.8. CBC analysis of 3D localizations of MotAB and SiiAB at the flagellum and the SPI4-T1SS. Shown are coupled dual-color 3D-dSTORM localization and quantitative coordinate-based colocalization (CBC) analyses of MotAB and SiiAB with each other (A, C), SiiF (D) or FliN (B, E), respectively. Box plots (A-E) indicate CBC frequencies on the x-axis and show the value distributions. F) Comparison of the colocalization to MotA-MotB control. At least three independent areas with approximately 100 single bacteria were analyzed regarding the localization. Percentages above the box plots indicate AC (-1 to -0.5) and PC ranges (0 to 1; 0.5 to 1).

III.3.3.4. During location at the flagellum, SiiAB potentially alter velocity and stop behavior comparable to MotAB

In a next step, we wanted to investigate whether a deletion of *siiAB* leads to an altered proteomic profile regarding flagellum-associated proteins in comparison to WT (Figure III.3.9) and if SiiAB can influence velocity and stop behavior (Figure III.3.10). It is described that motility mutants can be divided into Mot⁻ and Che⁻ and that there is a cross-correlation between CheM and SiiAB, so other candidates can be of interest (Santiveri *et al.*, 2020) (Hoffmann, 2021, under revision). For the proteomic analysis, we used 2.5 h subcultures and digested the bacteria with trypsin. In both strains we identified strongly related proteins in all replicates (Figure III.3.9 A). We found evidence that not the amount of the flagellin FliC (0.9-fold) is altered, but rather expression of CheA (5.5-fold) and CheZ (7.0-fold) was increased in a *siiAB* mutant (Figure III.3.9 B), regulating the rotational direction of the flagellum (Stock, 1999). Interestingly, both of these proteins act in opposite directions. While CheA phosphorylates CheY after autophosphorylation, resulting in a tumbling movement, CheZ dephosphorylates CheY leading to a direct movement of the bacterium (Stock, 1999). Other flagellum-associated proteins like FljB, FlgG and FliN were only slightly reduced (FljB, 0.6-fold) or increased (FlgG, 1.1-fold; FliN, 1.4-fold). The chemotaxis-associated proteins we found in all replicates, CheW and CheZ, were also slightly decreased (0.6-fold) or increased (1.6-fold). Additionally, we identified two uncharacterized proteins (STM14_3799 and STM14_2852) suggested to be associated with chemotaxis and the flagellum, which were slightly increased in a *siiAB* mutant strain (2.4-fold). STM14_3799 was identified as putative methyl-accepting chemotaxis protein and STM14_2852 as putative chemotaxis signal transduction protein (UniProt, 2021). Thus, we concluded that SiiAB do not significantly influence the chemotaxis-associated proteins in response to environmental signals and decided to analyze the velocity and stop behavior of STM in more detail.

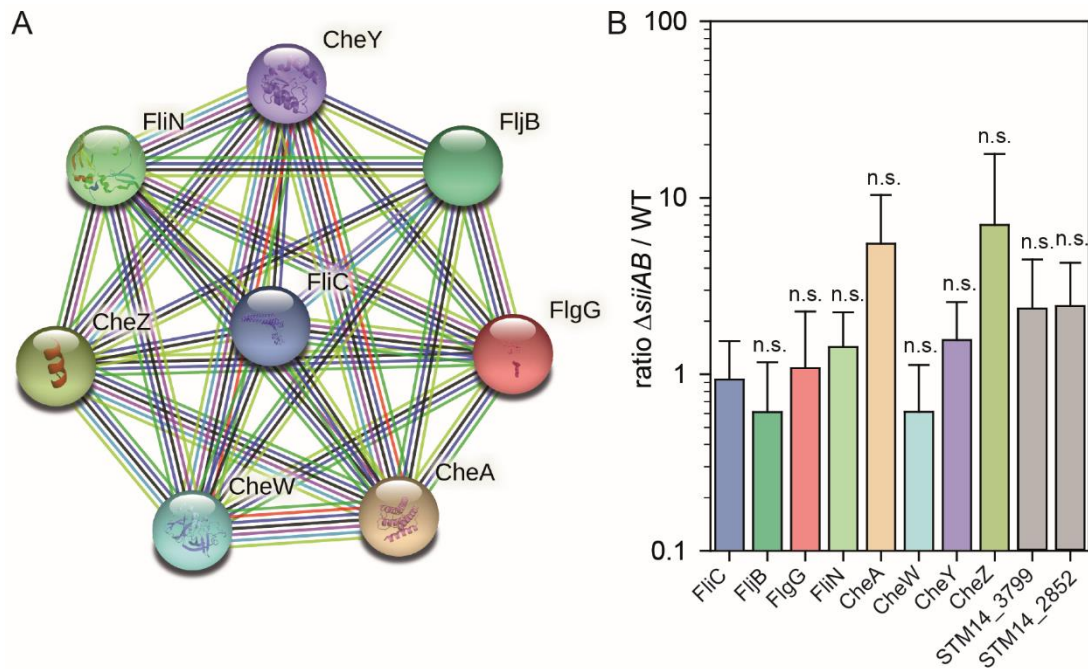


Figure III.3.9. Proteomic analysis of WT and *siiAB* mutant strain. Shown are the chemotaxis and flagellum-associated proteins of the proteome analysis, found in STM WT and Δ *siiAB*. Gene ontology of flagellum-related proteins illustrated by STRING (Szklarczyk *et al.*, 2021). Protein levels were normalized to DnaK, respectively. Statistical analyses compared to FliC with biological triplicates, with exception of FliB and FliG, biological duplicates, by two-tailed t-test: n.s., not significant.

As SiiAB do not significantly influence the chemotaxis-associated proteome of the bacteria, but we found a localization at the flagellum, we decided to analyze the velocity and stop behavior in dependence of the proton channels MotAB and SiiAB. For this purpose, we used STM WT and mutant strains deficient in *motAB* or *siiAB*, as well as STM WT with an additional synthetic expression of *motAB*, *motAB*_{D33E}, *siiAB* and *siiA*_{D13E}*B* and investigated velocity and CCW to CW switch frequency of these strains. First, we confirmed functional expression of the plasmid-encoded proton channels (Figure S III.3.5). We tracked the bacteria in infection medium for the data to be comparable and validated them automatically with TrackMate plugin (Figure III.3.10 A, C) (Ershov *et al.*, 2021). To analyze the swim/tumble switching frequency of the bacteria, we defined a distance <1.5 μ m between two frames as a stop (Figure III.3.10 B, D).

STM WT showed a mean velocity of 19.2 μ m/s (17.8 μ m/s, A) with 0.9 stops/s (0.4 stops/s, B). In contrast, a *motAB*-deficient strain swam with 2.9 μ m/s (4 μ m/s, A) and 4.5 stops/s (4.2 stops/s, B). With *motAB* synthetic expression, the velocity was slightly increased to 22.8 μ m/s (20.6 μ m/s, A), whereas the number of stops was comparable with 0.8 stop/s (0.7 stops/s, B). This phenotype was significantly altered with the expression of *motAB*_{D33E} with 9 μ m/s (9 μ m/s, A) and 2.5 stops/s (2.3 stops/s, B), indicating the requirement for a functional proton channel.

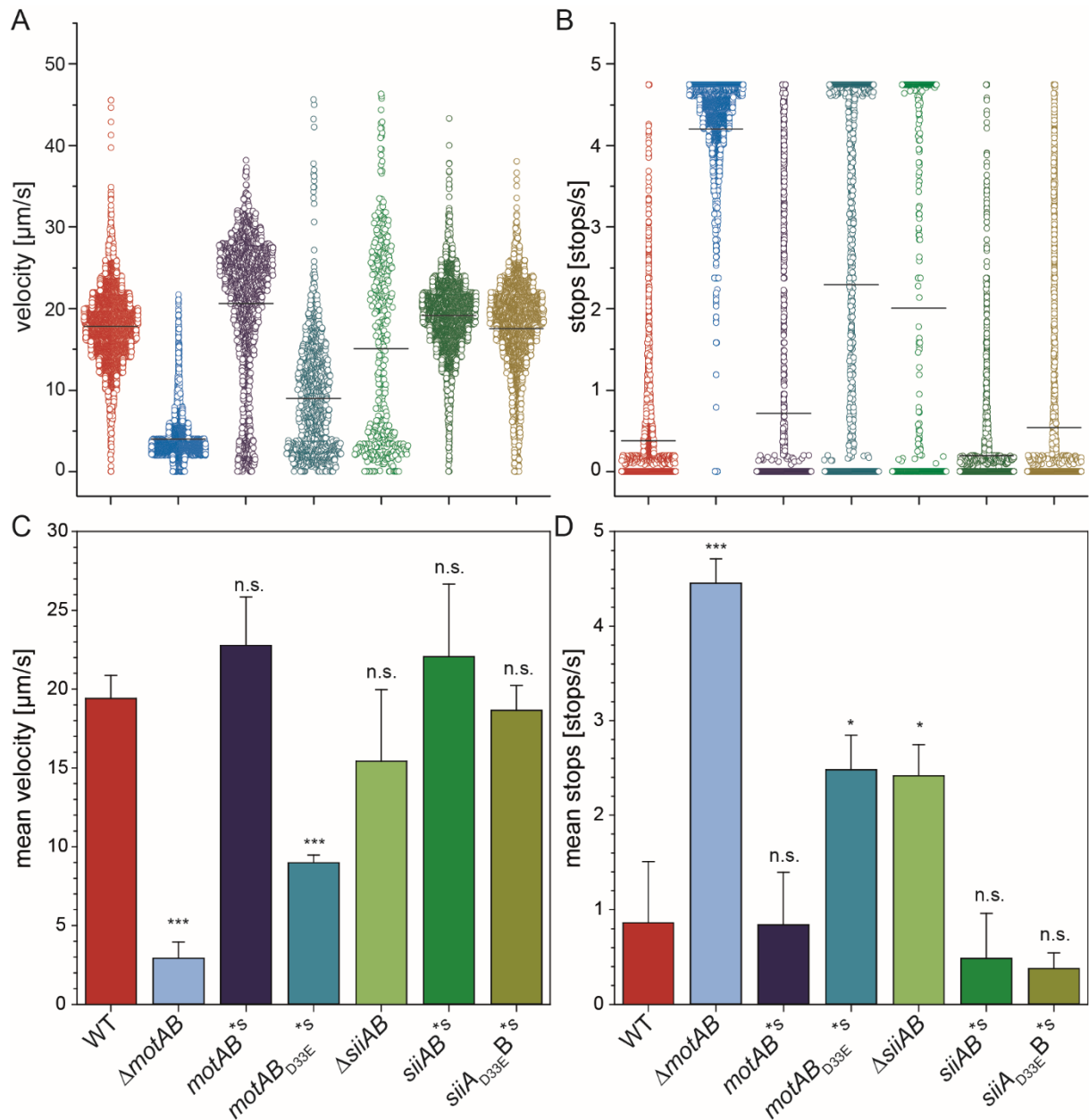


Figure III.3.10. Velocity and stops in dependence of MotAB and SiiAB. Shown are the box plots (25th and 75th percentile) the velocity (A, C) and stops (B, D) of WT in comparison to ΔmotAB , ΔsiiAB and with synthetic expression (^{*S}) of *motAB* and *siiAB* as well as *motAB*_{D33E} and *siiA*_{D13E}*B* in STM WT. Subcultures were grown for 2.5 h and diluted as for infection in 8-well chamber slides. For microscopy, a widefield microscope, 40x magnification with 150 ms exposure time was used (1 min recording per strain). TrackMate plugin for automatic tracking analysis was used (Ershov *et al.*, 2021). A) Exemplary tracking analysis – velocity. Automatic tracking of at least 750 bacteria, with exception of non-motile bacteria (non-motile during recordings), approximately 150 bacteria. B) Exemplary tracking analysis – stops/s. Calculation of the stop frequency by defining distances <1.5 μm between bacterial positions in two frames as a stop. Same bacteria per strain as in A) were calculated. C) Mean velocity of the tested strains. D) Mean number of stops of the tested strains. Statistical analyses of biological triplicates compared to WT by two-tailed t-test: ***, $p < 0.001$; *, $p < 0.05$; n.s., not significant.

We concluded this intermediate phenotype resulted from WT background expression of MotAB. Interestingly, $\Delta siiAB$ tends to show a decreased velocity with 15.4 $\mu\text{m/s}$ (11.8 $\mu\text{m/s}$, A) with a significantly increased stop behavior with 2.4 stops/s (2.5 stops/s, B), comparable to synthetic $motAB_{D33E}$ expression. Furthermore, synthetic expression of $siiAB$ showed a similar increase in velocity like synthetic expression of $motAB$ with 22.1 $\mu\text{m/s}$ (19.1 $\mu\text{m/s}$, A). Thus, we concluded that a distinct maximum of proton channels can be incorporated into the rotor region of the assembled flagella. With synthetic expression of $siiA_{D13E}B$, velocity was comparable to WT again, indicating no insertion into the flagellar rotor or use for it.

Taken together, we here found tendencies that SiiAB can support the torque generation in the rotor region of the flagellum. As the synthetic expression of $siiAB$ showed the same result as the synthetic expression of $motAB$, we concluded that the maximum velocity is limited by the amount of proton channels that can be incorporated.

It was already described that the major stator complex MotAB is important for the rotation of the flagellum (Santiveri *et al.*, 2020). To exclude that $siiAB$ and $motAB$ expression not only led to an altered velocity due to the bacteria showing an altered flagellation, we stained $motAB$ and $siiAB$ background strains against *Salmonella* H antiserum i (flagellum) and SiiB. Additionally, with this staining we can draw conclusions if MotAB also influences SiiAB amounts per cell. We analyzed the flagellation and SiiB distribution (Figure S III.3.6, Figure S III.3.7). As controls we used WT, $\Delta fliC \Delta fljB$ and $\Delta siiAB$, also for background estimation (Figure S III.3.6). As a control for proton channel integrity, we checked for co-localization of SiiAB first (Figure S III.3.6), and used SiiB as indicator for the proton channel in the IM. In none of the strains we found a different pattern of flagellation in comparison to WT which could explain the altered swim behavior (Figure S III.3.7). Most of the bacteria were peritrichous flagellated and some non-flagellated, but no strain was polar flagellated, indicating as expected that neither SiiAB, nor MotAB play a role for the type of flagellation. In course of the analysis of the flagellum and SiiB, we additionally exemplary analyzed the SiiAB amounts per cell, in order to gain first hints for a stoichiometry of the complex (Figure S III.3.7). We stained against SiiA and SiiB and determined the RLU/cell. We found RLU of 0.003 for SiiA and 0.0053 for SiiB in WT, suggesting a comparable stoichiometry as described for ExbBD and MotAB with 5:2 (Celia *et al.*, 2019; Deme *et al.*, 2020a; Santiveri *et al.*, 2020) by only taken the fluorescence signals in the cell into account.

All in all, we showed that during the retention maximum of SiiE, SiiB localizes at the flagellum as shown by 3D dSTORM analysis, where they potentially act in torque generation comparable to MotAB, further supported by our tracking. These new findings give the opportunity to gain more insights inside SiiAB function and mechanisms.

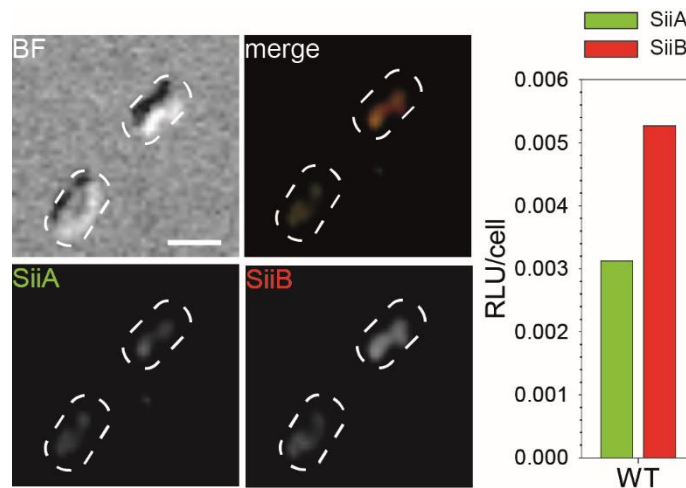


Figure III.3.11. Quantitative analysis of fluorescent signals for SiiA and SiiB. Shown are the ratios of SiiA and SiiB in STM WT. Subcultures were grown for 2.5 h, pelleted by centrifugation and fixed with 3% PFA in PBS. Bacteria were stained for SiiA or SiiB with antibodies against the proteins and secondary antibodies coupled to Alexa488 or Alexa568, respectively. At least 50 single bacteria were analyzed regarding their fluorescence signals. Representative ratios of SiiA and SiiB. Example from supplement (Figure S III.3.6). Scale bar, 2 μ m.

III.3.4. Discussion

We showed that the SPI4-T1SS and the flagellum are interconnected during invasion and additionally observed a localization of the SPI4-T1SS encoded proton channel Sii(A)B at the flagellum. As our proteomic analysis showed that a deletion of *siiAB* did lead to a significantly altered expression profile of some chemotaxis associated proteins like CheZ and CheA (Figure III.3.9, Figure III.3.12 C), we concluded that potentially velocity and stop behavior can be altered by SiiAB.

By dual-color 3D dSTORM analysis we found a two-fold increased localization of SiiB in close proximity to the flagellar C-ring subunit FliN than in proximity to SiiF (Figure III.3.7, Figure III.3.8), although SiiB and SiiF were shown to be linked (Wille *et al.*, 2014). Interestingly, we found this phenotype after 2.5 h, where we already described the maximum of SiiE retention (unpublished data, PhD thesis Nathalie Sander, 2022a, b). In this study, we also showed that SiiAB are only important in steps prior to retention of SiiE in the OM by SiiC (unpublished data, PhD thesis Nathalie Sander, 2022a). Thus, it is possible that SiiAB can change their position during invasion, leading to a more dynamic infection procedure where first adhesion (SiiE) and subsequently invasion (flagellum) is promoted (Figure III.3.12). This conclusion is supported by our new findings, where we can demonstrate the role of the flagellum and motility during

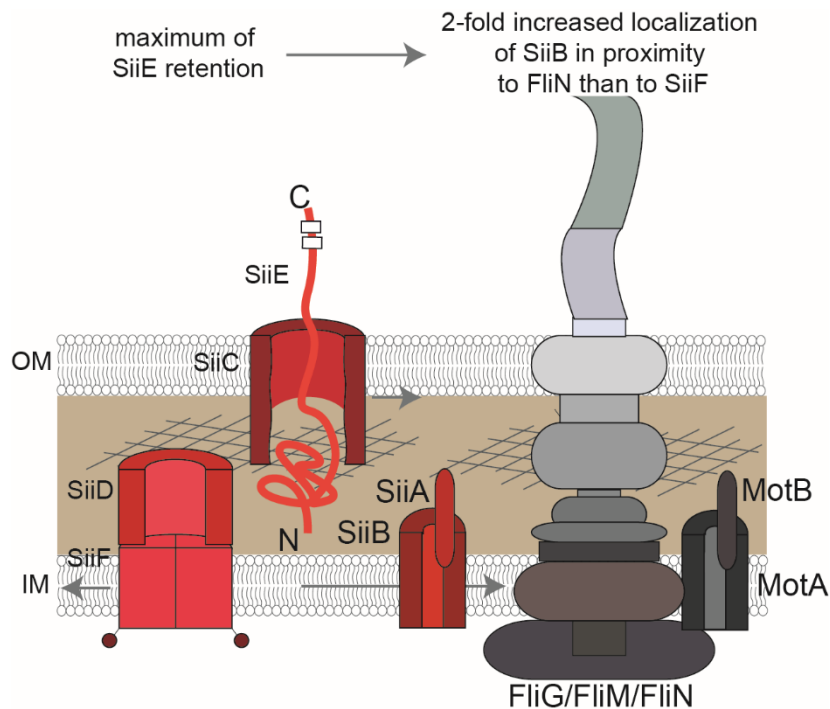


Figure III.3.12. Localization of SiiAB at and the flagellum. Shown is the schematic overview of our new finding that SiiAB show a localization at the flagellum during SiiE retention maximum. By dual-color 3D dSTORM and following CBC analysis, we found two times more SiiB located in closer proximity to the flagellar C-ring subunit FliN than to the SPI4-T1SS ATPase SiiF.

invasion, especially of non-polarized cells (Figure III.3.4). Additionally, we showed that loss of SiiE had no impact on invasion of non-polarized cells as published before (Gerlach *et al.*, 2008), but a *siiAB* deletion and the proton channel mutant led to a decreased invasion (Figure III.3.4 B), indicating a specific role of the proton channel. For further investigations of a potential change of localization for SiiAB during the invasion, it would be of advantage to check for more time points before and after SiiE retention maximum. Especially, because we found evidence that the flagellar filament in combination with SiiAB can alter the SiiE surface retention as well as subsequent adhesion (Figure III.3.3). Additionally, another super-resolution microscopy technique would be of advantage. With single molecule tracking (SMT) we should be able to investigate the potential movement of SiiAB through the membrane. Such a dual occupation of proton channels for the same function is already known from other bacteria like *E. coli* and *P. aeruginosa* (Baker and O'Toole, 2017). It is already described that in dependence of the external load on the flagellum, caused by the heterogeneous environments, *E. coli* can adjust the number of stator units (Lele *et al.*, 2013; Tipping *et al.*, 2013). The mechanism behind this load-dependent stator assembly is still not fully understood. There is evidence that MotB is directly involved in load sensing by its periplasmic domain under light loads (Castillo *et al.*, 2013). By mutations of the critical aspartate residue (D33), they found speed fluctuations under

light loads (Che *et al.*, 2014). The effects of this mutation led to the assumption that the load affects the coupling between the translocation and conformational changes in the stator units for torque generation. Thus, it was concluded that load changes can alter the stator incorporation by triggering conformational changes in MotB (Baker and O'Toole, 2017). While this mechanism is still not understood, the flagellar mechano-sensing itself is a well described mechanism (Belas, 2014). During invasion, STM is also faced with heterogeneous environmental conditions like mucus or cell barriers, thus making potential additional stator complexes like invasion-associated proteins as SiiAB beneficial. Besides the flagellar load, also ion availability and other stimuli are important (Baker and O'Toole, 2017). Thus, many bacteria exploit various proton channels for the same flagellum and rotor incorporation (Baker and O'Toole, 2017; Paulick *et al.*, 2015). However, there are also bacteria described that have two stator sets, both using the same ion, as *P. aeruginosa* (Baker and O'Toole, 2017). It is suggested that these two stator sets are required under different environmental conditions or even play distinct roles for flagellar function. One stator set (MotCD) seem to generate more torque than the other proton channel (MotAB) and is essential during swarming (Doyle *et al.*, 2004; Kuchma *et al.*, 2015; Toutain *et al.*, 2005). It is suggested that MotAB tune the motor for behaviors that are critical for surface attachment and detachment (Baker and O'Toole, 2017; Conrad *et al.*, 2011). With our new findings, gained by a multi sequence alignment, showing SiiB also as a potential Na⁺-conducting channel (Figure III.3.2), further analysis can be performed to narrow down possible modes of action of SiiAB.

Taken this together with our results that SiiAB localizes at the flagellum (Figure III.3.10; Figure III.3.12), we demonstrated that synthetic *siiAB* expression generated the same phenotype as synthetic *motAB* expression and slightly increased velocity. We conclude that there is a limit of proton channels that can be introduced into the rotor region, as even with *motAB* expression velocity was only increased to a distinct maximum. Hence, synthetic expression of *siiAB* under these conditions did neither show a higher increase in velocity. It is possible that under different conditions, e.g. higher amounts of flagella per cell, higher load on the flagellum or tracking analysis during invasion process, an increased amount of incorporated proton channels and thus, increased velocity occurred. By further investigations, critical residues in SiiB required for a potential interaction with FliG should be characterized in more detail to gain insights in the incorporation of SiiAB into the flagellar rotor. Here, we find a new potential proton channel that can be introduced into the flagellar rotor and as a consequence be used for bacterial motility. With further investigations, open questions regarding the exchange of stator complexes in the bacterial rotor may be answered in near future.

III.3.5. Materials and Methods

III.3.5.1. Bacterial strains and growth conditions

Bacterial strains used in this study are listed in Table III.3.1. Bacteria were grown aerobically in LB or on LB agar plates, if necessary supplemented with carbenicillin (cb, 50 µg/ml) or kanamycin (km, 50 µg/ml). For induction of the Tet-on system encoded on the plasmids used (Table III.3.2), anhydrotetracycline (AHT) was added (10 ng/ml final concentration) 1 h after inoculation of the subculture for additional 1.5 h (1:31).

Table III.3.1. Bacterial strains used in this study.

Designation	Relevant characteristics	Reference
S. Typhimurium NCTC 12023	wild type	NCTC
WRG205	<i>siiA</i> _{D13E}	(Wille <i>et al.</i> , 2014)
MvP589	Δ <i>spi4</i> ::FRT	(Gerlach and Hensel, 2007)
MvP818	Δ <i>invC</i> ::FRT	(Gerlach <i>et al.</i> , 2008)
MvP1387	Δ <i>siiAB</i> ::FRT	this study
MvP2720	Δ <i>motAB</i> ::FRT	lab collection
MvP2779	Δ <i>siiE</i> ::FRT	this study
MvP2933	Δ <i>fliC</i> ::FRT Δ <i>fljB</i> ::FRT	this study
MvP2937	Δ <i>siiAB</i> ::FRT Δ <i>motAB</i> ::FRT	this study
MvP2936	Δ <i>fliC</i> ::FRT Δ <i>fljB</i> ::FRT Δ <i>siiAB</i> ::FRT	this study
MvP3006	Δ <i>fliC</i> ::FRT Δ <i>fljB</i> ::FRT Δ <i>motAB</i> ::FRT	this study
MvP3072	Δ <i>motAB</i> :: <i>aph fliN</i> ::HaloTag	this study
MvP3073	Δ <i>siiAB</i> :: <i>aph siiF</i> ::HaloTag	this study
MvP3076	Δ <i>motAB</i> ::FRT <i>fliN</i> ::HaloTag	this study
MvP3077	Δ <i>siiAB</i> ::FRT <i>siiF</i> ::HaloTag	this study
MvP3111	Δ <i>motAB</i> :: <i>aph siiF</i> ::HaloTag	this study
MvP3112	Δ <i>siiAB</i> :: <i>aph fliN</i> ::HaloTag	this study

III.3.5.2. Construction of plasmids and strains

Genes encoding SiiA, SiiB, MotA and MotB were amplified from genomic DNA of STM WT (NCTC 12023) and p5166. For generation of *siiAB* and *motAB* expression plasmid, p4251 under *tetA* promoter control was used. Point mutation in SiiA was inserted into p5216 via Site-directed mutagenesis. Point mutation in MotB was inserted into p5166 via Site-directed mutagenesis, amplified and introduced into p5216. For microscopic analysis of ALFA and SPOT tagged SiiAB and MotAB, *siiAB* and *motAB* were amplified and introduced into pWSK29. Plasmids were generated by Gibson assembly (GA) according to manufacturer's instructions

(NEB) using vectors mentioned below. Oligonucleotides used are listed in Table III.3.3. MvP3072, MvP3073, MvP3111 and MvP3112 were generated by P22 phage transduction, and transductants were selected and cleaned on LB+EGTA+km agar plates. Absence of lysogen was checked by growth on green plates and phage-negative transductants were selected on LB-Km plates. Additionally, colony PCR was performed to confirm proper insertion.

Table III.3.2. Plasmids used in this study. All plasmids conferred resistance to carbenicillin.

Plasmid	Relevant characteristics, resistance	Reference
p4251	<i>tetR</i> P _{tetA}	lab collection
p5166	P _{motA} <i>motAB</i>	lab collection
p5216	<i>tetR</i> P _{tetA} :: <i>siiAB</i>	this study
p5505	<i>tetR</i> P _{tetA} :: <i>siiAD13EB</i>	this study
p5512	<i>tetR</i> P _{tetA} :: <i>motAB</i> _{D33E}	this study
p5517	<i>tetR</i> P _{tetA} :: <i>motAB</i>	this study
p5531	<i>motA</i> ::ALFA tag <i>motB</i> ::3xFLAG tag	this study
p5533	<i>siiA</i> ::ALFA tag <i>siiB</i> ::3xFLAG tag	this study
p5534	<i>siiA</i> ::HA tag <i>siiB</i> ::ALFA tag	this study
p5613	<i>motA</i> ::ALFA tag <i>motB</i> ::SPOT tag	this study
p5620	<i>siiA</i> ::ALFA tag <i>siiB</i> ::SPOT tag	this study
p5731	<i>siiA</i> ::GS linker::SPOT tag <i>siiB</i> ::ALFA tag	this study
p5689	<i>motA</i> ::ALFA <i>motB</i> ::GS linker::SPOT	this study

Table III.3.3. Oligonucleotides used in this study.

Designation	Sequence (3' -> 5')	Purpose
Vf-pWSK29-Pnah	CAGCTTTTGTTCCTTTAGTGA	amplification p4251 for <i>siiAB</i> insertion and p5216 for <i>motAB</i> insertion
Vr-pWSK29-Ptet-rev	TTCACCTTTTCTCTATCACTGATAGGGAGTGG-TAAAATAACTCT	amplification p4251 for <i>siiAB</i> insertion
1f PtetA-siiA	CCCTATCAGTGATAGAGAAAAGTGAAATGTAA-TATCAGGAGACAACatgg	insert <i>siiAB</i> for p4251
1r siiB-pWSK29	TCACTAAAGGGAACAAAA-GCTGTTAATCTTCATTTTTTCTCCT	insert <i>siiAB</i> for p4251
SiiA-D13E-for3	GTTTTGTTGAAACATTCTCTACG	D13E into <i>siiA</i> in p5216
SiiA-D13E-rev3	TAGGCCACGGATTACTTTTCG	<i>siiA</i> D13E into in p5216

Results

MotA-p5216-for	GATAGAGAAAAGTGAAGTGCTTATCTTATTAG	inserts <i>motAB</i> D33E from p5506 and <i>motAB</i> from p5116
MotBD33E-p5216-rev	CTAAAGGGAACAAAAGCTGTCAC-CTCGGTTCCGC	inserts MotAB D33E from p5506 and <i>motAB</i> from p5116
Vr-PtetA	TTCACTTTTCTCTATCACTGATAGGGAGTGGTA	amplification p5216 for insertion <i>motAB</i> D33E and <i>motAB</i>
ALFA-stop FLAG SDM For	CTGCGCCGCCGCCTGACCGAATGAGAC-TACAAAGACCATGACG	insertion of ALFA tag into p5321 and p5367
motA-ALFA SDM Rev	TTCTTCTTCCAGGCGGCTCGGTGCTTCCTCAG-TCGTCTGC	insertion of ALFA tag into p5321
siiB-ALFA SDM Rev	TTCTTCTTCCAGGCGGCTCG-GATCTTCATTTTTTCTCC	insertion of ALFA tag into p5367
siiA-ALFA SDM Rev	TTCTTCTTCCAGGCGGCTCGGCTCTGACAC-CTTTTTATTAATAG	insertion of ALFA tag into p5367
1f pWSK-PsiiA	CTATAGGGCGAATTGGGTACCAAA-GCGTTATTTGCATTTTCG	generation p5620
2r ALFA-siiB	TCTGACAC-CTTTTTATTAATCATTTCGGTCAGGCGGCGGCG	generation p5620
2r SPOT-siiB	TCTGACAC-CTTTTTATTAATCAGCTGCTCCAATGGCTCAC	generation p5620
2r ALFA-motB	CATGCTTCCTCAG-TCGTCTTCATTTCGGTCAGGCGGCGGCGC	generation p5613
2r SPOT-motB	CATGCTTCCTCAG-TCGTCTTCAGCTGCTCCAATGGCTCACCG	generation p5613
3f siiA-siiB	TTAATAAAAAGGTGTCAGAG-TGAAATATATAAATCATTACCG	generation p5620
3f motA-motB	AGACGACTGAGGAA-GCATGAAAAATCAGGCTCATCCCATTG	generation p5613
3r SPOT-pWSK	CACTAAAGGGAACAAAA-GCTGTCAGCTGCTCCAATGGCTCAC	Generation of p5613 and p5620
Vf-p5534_siiB	CATTATTCATCTATTCTTAAAAATATTTTCAG-CAAAAG	amplification p5534 for <i>siiA</i> ::GS linker::SPOT gBlock (Figure S III.3.9)
Vr-p5534_siiA	CATTTCTATCAATAAATACTATTGATTTT-GTCTTCTA	amplification p5534 for <i>siiA</i> ::GS linker::SPOT gBlock
GS-SPOT For	GGTTCTCCGGATCGCGTGCGCGCG	SDM GS linker into p5613
motB-tag Rev	CCTCGGTTCCGCTTTTGGCGATGTG	SDM GS linker into p5613

III.3.5.3. Proteome analysis of WT and *siiAB* deletion strain

Protein extraction

For proteome analyses, subcultures of WT and Δ *siiAB* were grown for 2.5 h and lysates of whole cells were prepared. For cell lysis, the bacteria were pelleted and resuspended in 200 μ l 9.3 M urea in 50 mM TRIS buffer, pH 8.0, and incubated for 1 h at 37 °C with shaking and stored at -80 °C at least for 16 h. The lysates were thawed and cell debris was removed at 20,000 x *g* for 10 min. The resulting supernatant was used for protein digestion and proteomic analyses.

Protein digestion

Protein concentration in samples was determined using an IMPLEN NanoPhotometer® and 100 μ g of total protein were digested, respectively. Following reduction with 5 mM DTT in 50 mM ammonium bicarbonate/NH₃, pH 8.5 buffer for 30 min at 37 °C, samples were alkylated with 15 mM iodoacetamide (in ABC buffer) for 30 min at RT in dark. For digestion, we used 10 μ g protein and 0.3 μ g LysC/Trypsin (Promega) for 3 h at 37 °C. ABC buffer was added to a final volume of 79.2 μ l, incubated o/N at 37 °C and the reaction was stopped by adding 100% formic acid (1% final). After an additional centrifugation for removal of particles, the supernatant was transferred to HPLC vials and 1 μ g digested protein was analyzed by mass spectrometry.

Label-free protein quantification by mass spectrometry

HPLC/MS-MS analysis performed using an Ultimate 3000 Nano HPLC (ThermoFisher). For analyses, a volume of 5-10 μ l were desalted and concentrated using a precolumn (ThermoFisher, C18 PepMap 5 μ m, 100 A with dimension of 300 μ m (id) x 5 mm (length)). The corresponding solvent was 0.1% trifluoroacetic acid TFA in H₂O (flow rate of 25 μ l/min). The loaded and washed precolumn was switched into the 'nano flow line' (250 nl/min) with an Easy Spray column (ThermoFisher, PepMap RSLC C18, 2 μ m, 100 A with dimension of 75 μ m (id) x 500 mm) at the end. Peptides were continuously eluted by 80% acetonitrile ACN and 0.1% in H₂O in 160 min. The electro spray ionization (ESI) was done at 1,500 V (ESI Spray Source, ThermoFisher). A Q-Exactive Plus orbitrap mass spectrometer (ThermoFisher) was used to determine the MS/MS (HCD fragmentation) data under the following conditions (Table III.3.4):

Table III.3.4. Settings for label-free protein quantification by mass spectrometry.

	MS	MS precursor selection	MS/MS
resolution	70,000		17,500
AGC target	3e6	5e2	1e5
max IT	50 ms		80 ms
MS range	375-1,800 m/z		
loop count			10
NCE			27
isolation width			1.4 m/z
charge		2-5	

Data analysis

The resulting data were analyzed by Peaks Studio X and PeaksOnline (Bioinformatics Solution Inc, Canada). *De novo* search was performed for peptide identification by a DB search using a protein database for STM 14028 (*Salmonella* Typhimurium strain 14028s_11_1; 5,372 proteins). Peaks Q (*de novo* assisted Quantification) and Peaks DB (In-depth *de novo* assisted search) were performed. The MS tolerance was adjusted to 20.0 ppm, the MS/MS tolerance to 0.2 Da and two missed cleavages were allowed. The digest mode was set “specific”. Further, carbamido-methylation of cysteines and oxidation of methionine for fixed post translationally modifications and for variable modifications were chosen, respectively. The protein hits were normalized to DnaK, respectively. Only proteins detected in all replicates of both strains were used here. For gene ontology of flagellum-related proteins illustrated by STRING (Szkłarczyk *et al.*, 2021).

III.3.5.4. Western blot for detection protein biosynthesis

For sample preparation, bacteria were inoculated 1:31 in LB, supplemented with 50 µg/ml carbenicillin and induced with AHT after 1 h after inoculation, if necessary, and grown for 2.5 h. 1 ml was pelleted by centrifugation at 10,000 x *g*. Pellet was boiled in 1x SDS cracking buffer according to the OD₆₀₀. SDS Laemmli gels were run for 20 min at 80 V and 75 min with 150 V. Semi-dry Western blot transfer was performed onto 0.45 µm nitrocellulose membranes at 0.8 mA/cm² for 1 h. Following Ponceau S stain, membranes were blocked with 5% skimmed dry milk powder in TBS-T (0.1% Tween20 in TBS) for at least 30 min at RT. Primary antibodies were incubated o/N in blocking solution at 4 °C. The next day, membranes were washed three times with TBS-T and incubated with HRP-conjugated secondary antibody in blocking solution for 1 h at RT. Antibodies used in this study are listed Table III.3.5 and Table III.3.6. Membranes

were washed an additional three times with TBS-T, incubated with Pierce™ ECL Western blotting Substrate (ThermoFisher) following manufacturer's instructions and imaged using a ChemiDoc™ Imager (Bio-Rad) and ImageLab software.

Table III.3.5. Primary antibodies used in this study.

Antigen	Host	Conjugated with	Dilution	Purpose
GST-SiiE-C	rabbit	-	1:10,000	WB
SiiA	rabbit	-	1:10,000	WB
SiiA	rabbit	-	1:1,000	IF
SiiB	rabbit	-	1:10,000	WB
SiiB	rabbit	-	1:1,000	IF
<i>Salmonella</i> H Antiserum i	rabbit	-	1:500	IF
ALFA	rabbit	-	1:1,000	WB
ALFA	llama	Atto565	1:500	IF
SPOT	llama	Atto488	1:1,000	WB/IF
SPOT	llama	Alexa647	1:500	WB/IF
HA tag	rat	-	1:10,000	WB
FLAG tag	mouse	-	1:2,000	WB

Table III.3.6. Secondary antibodies used in this study.

Species reactivity	Host	Conjugated with	Dilution	Purpose
rabbit	goat	HRP	1:10,000	WB
rat	goat	HRP	1:10,000	WB
mouse	goat	HRP	1:10,000	WB
rabbit	goat	Alexa488	1:1,000	IF
rabbit	goat	Alexa568	1:1,000	IF

III.3.5.5. Flow cytometry

For analysis of surface retention of SiiE by flow cytometry, 3×10^8 bacteria were fixed with 3% paraformaldehyde in PBS for at least 20 min at RT. Bacteria were blocked with 2% goat serum and 3% BSA in PBS for 30 min and afterwards stained with the specific primary antibody rabbit- α -SiiE (1:1,000) o/N, 4 °C. Staining with second antibody goat- α -rabbit-Alexa488 (1:2,000) occurred for 1 h at RT. Bacteria were diluted 1:10 in cell culture PBS and measured with a Attune NxT Flow Cytometer (Thermo Fisher) and analyzed using Attune NxT software (Goser *et al.*, 2020; Röder and Hensel, 2020). Bacteria were gated using unstained STM and measured by FSC-H and SSC-H. For gating of the SiiE surface signal, positive control STM WT and negative

control $\Delta siiE$ were used. All samples were measured under the same conditions (flow rate 12.5 $\mu\text{l}/\text{min}$).

III.3.5.6. Tracking analyses in liquid medium

For the microscopic tracking analysis, subcultures were grown for 2.5 h with AHT induction after 1 h. As for infection, bacteria were diluted in PBS to an OD_{600} of 0.2 and further diluted in MEM medium in a 8-well chamber. For microscopy, Zeiss Axio Observer.Z1 was used. The used objective was the LD Plan-Neofluar 40x/0.6 Korr. Imaging with CoolSNAP camera with a camera adapter 1.0x, total magnification 40x, zoom 1.0x. Bacteria were imaged for 60 s with 150 ms exposure time and 2x2 binning. Tracking analysis was performed automatically with ImageJ plugin TrackMate (Ershov *et al.*, 2021). Mean velocity was determined directly by TrackMate. Stops were calculated by analysis of the displacement between single frames. A stop was defined as displacement $<1.5 \mu\text{m}$ between two frames. Same bacteria were analyzed for velocity and stop behavior. Analysis was performed in biological triplicates. Distribution for velocity and stops is exemplary shown (Figure III.3.10 A and B), as well as results of the triplicates (Figure III.3.10 C and D).

III.3.5.7. Swimming motility analysis in swim agar

To further analyze the motility of the strains, subcultures were grown for 2.5 h at 37 °C with AHT induction after 1 h. 5 μl of the subcultures were inoculated in the center of swim agar plates (1% tryptone, 0.5% NaCl, 0.3% agar, 1 mM MgSO_4 , complemented with carbenicillin (cb, 50 $\mu\text{g}/\text{ml}$) and AHT, if necessary) and the swim zone diameters were measured hourly for 8 h, and finally after 21 h of incubation at 30 °C.

III.3.5.8. Fluorescence microscopy

For the microscopic analysis of SiiA, SiiB and the flagellum, subcultures were grown for 2.5 h with AHT induction after 1 h, if necessary. OD_{600} was measured and bacteria were fixed with 3% PFA in PBS for 15 min at RT on Poly-L-Lysine covered coverslips. Afterwards, bacteria on coverslips were centrifuged at 500 x g to further increase the attachment of the bacteria to the coverslips. Following fixation, bacteria were washed three times with PBS and treated with blocking solution (supplemented with 2% goat serum) for at least 30 min at RT. Bacteria were incubated with sera against SiiA, SiiB and the flagellum, respectively, and secondary antibody against rabbit conjugated with Alexa488 or Alexa568 in blocking solution (Table III.1.5 and

Table III.1.6). For microscopy, Zeiss Axio Observer.Z1 was used. The used objective was the alpha Plan-Apochromat 100x/1.46 Oil DIC (UV) M27. Imaging with CoolSNAP camera with a camera adapter 1.0x, total magnification 100x, Zoom 1.0x, 2x2 binning.

III.3.5.9. Dual-color 3D-dSTORM microscopy of MotAB and SiiAB at the flagellum and SPI4-T1SS

Sample preparation

Here, we performed dual-color 3D direct stochastic optical reconstruction microscopy (dSTORM) as single-molecule super-resolution imaging method to visualize structures with a resolution of approximately 20 nm (Huang *et al.*, 2008; Mass *et al.*, 2020). For dSTORM microscopy, subcultures were grown for 2.5 h and bacteria were fixed with same amounts of a methanol and acetic acid mix (4:1) for 20 min at RT and 50 min on ice. Following fixation, bacteria were pelleted for 5 min at 7,000 x g and washed three times with PBS. Afterwards, pellet was resuspended in GTE buffer (50 mM glucose, 25 mM Tris, pH 8.0, 10 mM EDTA) and OD₆₀₀ was measured. Ca. 3×10^8 bacteria were diluted in 4% sucrose in PBS o/N at 4 °C and the other cells were stored in GTE buffer at 4 °C. The next day, bacteria were incubated with 20% sucrose in PBS for 10 min at RT. For permeabilization, the cells were treated with 8 µg/ml lysozyme in GTE buffer for 2 min at RT and 1 h at 4 °C. Bacteria were washed an additional three times with PBS and were incubated with blocking solution for at least 30 min at RT. For staining of SiiA, SiiB, MotA and MotB in various combinations, the samples were incubated with Atto565- and Alexa647-conjugated nanobodies for 1 h at RT. Htl-SiR ligand was used for HaloTag detection (10 nM, 45 min RT). Coverslips for TIRF holder were prepared with 0.01% Poly-L-Lysine and samples were applied to the coverslips.

Dual-color 3D-dSTORM image acquisition

For microscopy, an inverted Olympus IX-81 (Hamburg, Germany) with a motorized filter cassette, revolving nosepiece and z-drive with remote focus handle was used. The microscope was equipped with piezo z-stage (NanoScanZ, NZ100) from Prior, a motorized xy-stage IM 120x80 from Märzhäuser and a mid-long working distance condenser IX2-LWUCD (working distance 27 mm, NA 0.55). An Olympus UAPON 150x/1.45 NA oil objective was used. Oxygen depletion during dSTORM acquisition was inhibited by usage of scavenger buffer (150 mM Tris-HCl, pH 8.8, 0.5 % Glucose (v/w), 0.25 mg/ml Glucose Oxidase, 20 µg/ml Catalase, 15 mM mercaptoethylamine) and at least 2,000 up to 3,000 frames with 10% and 15% laser power and 32 ms exposure time were recorded with cylindrical lens directly in front of the camera for transformation of the point spread functions (PSF) (Thorlabs, Newton, NJ, USA; focal length f

= 500 mm LJ1144RM-A or $f = 1000$ mm LJ1516RM-A). According to their z position, cylindrical lenses transform PSF from the single localizations and add ellipticity and orientation, relative to the focal plane. Thus, to determine the precise z position of each molecule, 3D information can be generated (Huang *et al.*, 2008). Excitation was performed with a 640 nm laser (maximum 500 mW; MPB Communications, Montreal, Quebec, Canada) for AlexaFluor647 (excitation 650 nm/emission 665 nm) and Htt-SiR (excitation 656 nm/emission 677 nm), and a 561 nm laser (maximum 500 mW; MPB Communications) for Atto565 (excitation 564 nm/emission 590 nm) and a 405 nm diode-pumped solid-state laser (maximum 100 mW, BCL-100-405; CrystaLaser, Reno, NV, USA) for activation, connected to a quad-line TIRF condenser (Olympus). Filtering occurred with a Chroma 600/50 ET or 685/50 ET bandpass filter and detection with an Andor iXon Ultra 897 EMCCD camera. To calibrate the images, TetraSpeck™ Microspheres, 0.2 μm (Invitrogen, Waltham, MA, USA; T7280) additionally were recorded in both channels with scavenger buffer. For acquisition of PSF deformations, essential for calibration curve, the focal plane was moved in 10 nm z steps for each recorded frame (130 nm pixel size) with a piezo z -stage (NanoScanZ, NZ100; Prior Scientific, Rockland, MA, USA), usable for imaging and processing of the same day.

Dual-color 3D-dSTORM image processing

For 3D localization analysis with sub-diffraction accuracy ImageJ plugin ThunderSTORM (Ovesny *et al.*, 2014) with an elliptical Gaussian algorithm was used. The wavelet filter (B-spline) with order 3 and scale 2 was used for image filtering. For the approximate localization of the molecules centroid of connected components method with a peak intensity threshold equaling two times the standard deviation of the wavelet filter used for signal processing was performed. Sub-pixel localization was analyzed with elliptical Gaussian (3D astigmatism) algorithm with a fit radius of 15 pixels. Calibration curves were processed with the cylindrical lens calibration command to fit the raw data. Raw data files were processed with similar settings using ThunderSTORM. The corresponding calibration files for each wavelength were used for the data analysis. Results were visualized via the average-shifted histogram option with a magnification of 5, resulting in a lateral pixel size of 20 nm, step size of 50 nm and total axial range of 400 nm.

Coordinate-based colocalization analysis

To quantify the 3D dSTORM data, a coordinate-based colocalization (CBC) analysis was performed. The CBC analysis was also performed by ImageJ plugin ThunderSTORM (Malkusch *et al.*, 2012). The coordinate information from each localization, rather than its intensity for calculation, is used by CBC analysis. The localization of each protein is assigned a CBC value between -1 (anti correlated, low probability of colocalization) and 1 (perfectly correlated, high

probability of colocalization), indicating how well two types of proteins are correlated in 3D. For data analysis, at least 3 different areas with at least 100 bacteria were imaged and arranged in box plots (25th–75th percentile) with a mean line.

III.3.5.10. Cell culture

Polarized MDCK cells (subline pf, obtained from Prof. Dr. M. Goppelt-Struebe, Med. Klinik 4, Universitätsklinikum Erlangen) and non-polarized HeLa cells (obtained from Cell Lines Service CLS, Heidelberg) were cultured as described before (Gerlach *et al.*, 2008). For adhesion and invasion assays, MDCK cells were seeded in 24-well plates at a density 1×10^5 cells per well 5 days prior infection to ensure differentiation of cells. At the day of infection, cell density was 5×10^5 cells per well. Due to the long incubation time, the medium was supplemented with penicillin and streptomycin. The medium was changed to antibiotic-free medium 1 day before infection (at least 4 h before infection). HeLa cells were seeded one day before infection at a density of 1×10^5 cells per well. At the day of infection cell density was 2×10^5 cells per well.

III.3.5.11. Adhesion and invasion assay

To determine adhesion, cells were treated with 3 $\mu\text{g/ml}$ Cytochalasin D 1 h before infection to inhibit actin remodeling and uptake of the pathogen. For infection, 2.5 h subcultures of infecting STM were grown, MDCK and HeLa cells were infected in technical triplicates at multiplicity of infection (MOI) of 5, centrifuged for 5 min at $500 \times g$ and incubated for 25 min at 37°C in an atmosphere of 5% CO_2 . The cells were washed three times with prewarmed PBS. To determine adhesion, cells were lysed directly with 0.5% deoxycholate in PBS (freshly prepared). To determine invasion, cells were treated with 500 μl medium containing 100 $\mu\text{g/ml}$ gentamicin per well for 1 h, washed three times with prewarmed PBS and lysed with 0.5% deoxycholate in PBS (freshly prepared). Lysis was performed for 10 min at 37°C on a shaking platform. Lysates were collected in single tubes and serial dilutions of inoculum and lysates were plated logarithmic on MH plates to determine CFU. Plates were incubated o/N at 37°C and CFU were counted the next day with Acolyte software. The percentages of adhered and invaded bacteria were calculated.

III.3.5.12. Bioinformatics analyses

Tertiary structure model predictions were performed by trRosetta algorithms (Du, 2021; Yang *et al.*, 2020) and visualized with Pymol. TM-score for modelling by trRosetta. TM-score > 0.4 = medium, TM-score > 0.5 = high, TM-score > 0.7 = very high confidence. Multi sequence

alignments were performed with Clustal Omega (Madeira *et al.*, 2019) and T-Coffee algorithm (Notredame *et al.*, 2000).

III.3.6. Acknowledgements

This study was supported by the SFB944.

III.3.7. Supplements

```

CjMotA      1 ---MDLSTILGMVLAVTSISVGDIL-----EG--GNPLHVIHLSSFLIVMPTAAFCAMTSTHK 53
STM MotA    1 ----MLILLGYLVVIGTVFGGYVM-----TG--GHLGALYQPAELVIGGAGIGAFIVGNNG 51
EcMotA      1 ----MLILLGYLVVLTGTVFGGYLM-----TG--GSLGALYQPAELVIGGAGIGSFIVGNNG 51
HpMotA      1 ---MDLSTILGLVLAVASISLGDIL-----ED--GNPLHIHLSSVIVIVPTSLFAAMTGTHA 53
BsMotA      1 ---MDKTSLIGIILAFVALSVGMVL-----KG--VSFSALANPAAIILIIAGTISAVVIAFPT 53
SoMotA      1 ----MSFIGVIVALVFLVGNLI-----EG--GHPSALLDLPAFMVIGGTIGATVAQFPF 50
BsMotP      1 MKRFDYLTVPVGFVLTIIIVIGIIS-----GSGVSGFRSFLDLTSFFIVTGGCAAVFISFPF 58
SoPomA      1 --MDLATIIGLVGSFGFIWSMVI-----S--GGVMMFYDLASVIVFVGSFFVVMKFNL 52
VaPomA      1 ---MDLATLGLIGGFVIMAMVL-----G--GSIGMFVDVTSILIVVGSIFVVLMKFTM 52
STM SiiB    1 ----VKYINHRYLFCVCFLLALPFFALSFPPIREYVFDN--FMVSAIYNGVIAIYITGSLCALFT---- 61

CjMotA      54 KIVKAAKELKIVFKGS-G--VNLPERIAQLIEFAI IARRDGLLALLESRTNEIEN-----EFLR 109
STM MotA    52 KAIKGTMKAIPLFRRSKYTKSMYMDLLALLYLRLMAKSRQGMFSLERDIENPKESI FASYPRILADAVMLDFIV 127
EcMotA      52 KAIKGTMLKALPLFRRSKYTKAMYMDLLALLYLRLMAKSRQGMFSLERDIENPRESEIFASYPRILADSVMLDFIV 127
HpMotA      54 RYVKAAYKEIKIVFLNP-K--INLNETIKNLVELATLARKDQVLSLEGRVAQIED-----DFTR 109
BsMotA      54 KEIKKYPTLFRVLFKENKQ--LTIEELIPMFSEWAQLARREGLLALEASIEDVDD-----AFLK 110
SoMotA      51 SVIIASMKRFKWLIFPL-R--TDLNERAEFLIEIAGDVRKGGLLSIEDKIDQIDD-----PFLH 106
BsMotP      59 SELKKAPSVLKQAFIRQ-E--DNVKDLVKTFSVLSDHARKHGLSLDDQAREIKD-----PFLK 114
SoPomA      53 KQFLGAVKIAAKAFIFK-I--DRPEDLI EQSVTMADAARKGGFLALEE--AQISN-----SFMQ 106
VaPomA      53 QQFFGATKIAGKAFMFK-A--DEPEDLI AKIVEMADAARKGGFLALEE--MEINN-----TFMQ 106
STM SiiB    62 ----ILKN--ISA---KDILIAQDASRKNSILSNLN----- 88

CjMotA      110 NAMMMLVDGKS-FEEIHESMEIQTEQLEEHYKECAEYWIIFGETPTMGLVGA VGLI L----- 167
STM MotA    128 DYLRLLIISGNMNTFEIEALMDEEIEHSEAEVPANSLAMVGDLSLPAFGIVAAMGVVH----- 186
EcMotA      128 DYLRLLIISGHMNTFEIEALMDEEIEHSEAEVPANSLALVGDLSLPAFGIVAAMGVVH----- 186
HpMotA      110 NGLSMIIDGKD-LKSVKESLEISIEEMEYYHGAHYWETAGETAPTMGLVGA VMGLML----- 167
BsMotA      111 NGLSMAVDGQS-AEIRIDIMTEEVEAMEDRHQAGAAIFTAGTYAPTLGLGAVISLIA----- 168
SoMotA      107 KGLELLVDGQYE-KDNIVEILEKEIEFEQHGIEQTVKVEAMGGYCTPMGLVGA VGLI H----- 164
BsMotP      115 KGLLLAIDGWD-EETIRLVMDSEIAAMEERHRKGRVFEKAGFEFAPAWGMIGTLVGLV L----- 172
SoPomA      107 KAVDMLVDGHD-GEVVRAALEKDITLTERHRIGIAIFRAFADVGPAMGMIGTLVGLV A----- 164
VaPomA      107 KGIDLLVDGHD-ADVVRALKDDIALTDRHTQGTGVFRAGDVAPAMGMIGTLVGLV A----- 164
STM SiiB    89 --QVLFAGESKQCDFNLLMELDDNVSTARN-QRLSFI MSCSNVSTLVGLLGTFALESITIGSIGNLLSSPSDVGG 160

CjMotA      168 -----ALKLLDNPQ-AMAAGISGAFTAVTGIIFGAYALFAPWGRKMKANGMDLVKEQIVITEA IKGIAE 230
STM MotA    187 -----ALASADRPAAELGALIAHAMVGTFLGILLAYGFISPLATVLRQKSAETTMMQCVKITLLSNLN 250
EcMotA      187 -----ALGSADRPAAELGALIAHAMVGTFLGILLAYGFISPLATVLRQKSAETSKMMQCVKVTLLSNLN 250
HpMotA      168 -----ALQKLDNPA-EMAAGIAGAFTAVTGIIMCSYAFI GPF GHKLLKAKSKDIKEKTVLLEGLIGIAN 230
BsMotA      169 -----ALSHMDNTD-ELGHAISAAAFVATLLGIFTGYVLWHPFANKLKRKSKQEVKLRVMI EGVL SVLE 231
SoMotA      165 -----AMGLLDAPD-KLGGAI AVAFIAT IYGVAAANIIFL PFGNRYKAF AHQLSLFKEMTLVGTIGIAD 227
BsMotP      173 -----MLKNLNDPH-MLGPNMAIALLTTLYGSLLANMVFNP IAAKLEEKTESEIFIKQVMVEG IIGVQS 235
SoPomA      165 -----MLANMSDPK-SIGPSMAVALLTTLYGAVLANMVCIP IADKLSLRMGEEMLNRNLIMDAVLA IQD 227
VaPomA      165 -----MLSNMDDPK-AIGPAMAVALLTTLYGAILSNMVFFPIADKLSLRDQETLNRRLIMDGVLA IQD 227
STM SiiB    161 DNASNTLNMIVTMVASLSEPL---KGMNTAFVSSIYGVVCAILLTSQSVFVRSSYSLVSTEIKK--LKIISNRA 229

CjMotA      231 GANP-----RDLEAKLFNFLSHDDPRI SQFDKG----- 258
STM MotA    251 GYAP-----PIAVEFGRKTLYSSERPSEIELEEHVRAVRNPNPQQQTTEEA----- 295
EcMotA      251 GYAP-----PIAVEFGRKTLYSSERPSEIELEEHVRAVRNPNPQQQTTEEA----- 295
HpMotA      231 GENP-----RDLENKLLNYIAPGEPKKSQFEG----- 257
BsMotA      232 GQAP-----KVI EQKLLMYLPAKDRLKFAEQGE-----AQNGEKKEEEA----- 270
SoMotA      228 GES P-----QRLQAQLNPYLEH----- 244
BsMotP      236 GKNP-----RNLESQLVVFS SREEWQKPKQVK-----TKKGSVHEA----- 272
SoPomA      228 GQNP-----RVI EGFLKNYLAEKQRK-----ID-----TTDGE----- 255
VaPomA      228 GQNP-----RVIDSYLKNYLNEGKRA-----LE-----IDE----- 253
STM SiiB    230 NNKQRSRLRVESETLVEFKELKFAFFDNYLTVENLR-----TQDEEKKREMLSDSFVTLQNRLLDNSAK 292

CjMotA      -----
STM MotA    -----
EcMotA      -----
HpMotA      -----
BsMotA      -----
SoMotA      -----
BsMotP      -----
SoPomA      -----
VaPomA      -----
STM SiiB    293 LEQISTLIDGYLVSSNENLKKLSDGVITITSR LSEGNILLADNNARLEAMSTIQNIIDKKNDSIMTSVDKCYQESL 368

CjMotA      -----
STM MotA    -----
EcMotA      -----
HpMotA      -----
BsMotA      -----
SoMotA      -----
BsMotP      -----
SoPomA      -----
VaPomA      -----
STM SiiB    369 SHGKTINDIAAGSADISHTLDGLRKEMDEDMNNVHLALSDL SATDKKIANTKEISAEMVSYRDTYMLMEKITSM 444

CjMotA      -----
STM MotA    -----
EcMotA      -----
HpMotA      -----
BsMotA      -----
SoMotA      -----
BsMotP      -----
SoPomA      -----
VaPomA      -----
STM SiiB    445 HQEIVKQRLLNKEEKND----- 462
    
```

Figure S III.3.1. Full-length multi sequence alignment of various H⁺- and Na⁺-conducting channels in comparison to STM SiiB. A) Shown is the alignment of H⁺-conducting channels (MotA) of *Campylobacter jejuni* (Cj), *Salmonella Typhimurium* (STM), *Escherichia coli* (Ec), *Helicobacter pylori* (Hp), *Bacillus subtilis* (Bs), *Shewanella oneidensis* (So) and the Na⁺-conducting channels MotP and PomA of Bs, So and *Vibrio alginolyticus* (Va). Alignment was performed with Clustal Omega (Madeira *et al.*, 2019). Highly conserved regions are depicted in dark blue.

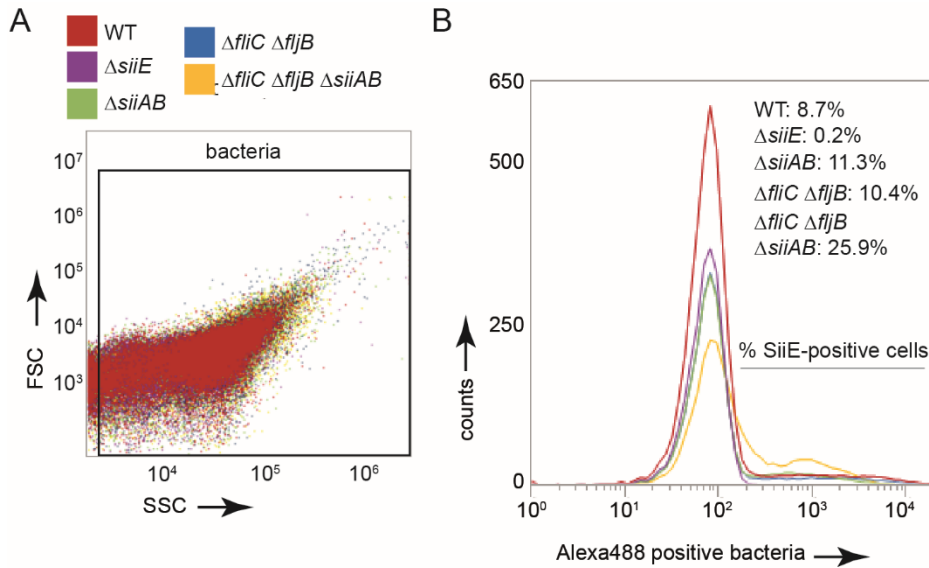


Figure S III.3.2. SiiE retention and function in dependence of the flagellum and SiiAB. Flow cytometry of retained SiiE. Subcultures were grown for 2.5 h, bacteria were pelleted and fixed with 3% PFA in PBS. Retained SiiE was stained with serum against SiiE and Alexa488-conjugated secondary antibody. Bacteria were diluted to OD₆₀₀ of 0.1 and analyzed by flow cytometry. A) Gating for bacteria (FSC, SSC) with unstained WT (not shown). B) Histogram of the Alexa488-positive cells and the counts. WT was used as positive control and $\Delta siiE$ as negative control for gating. SiiE-positive cells as indicated.

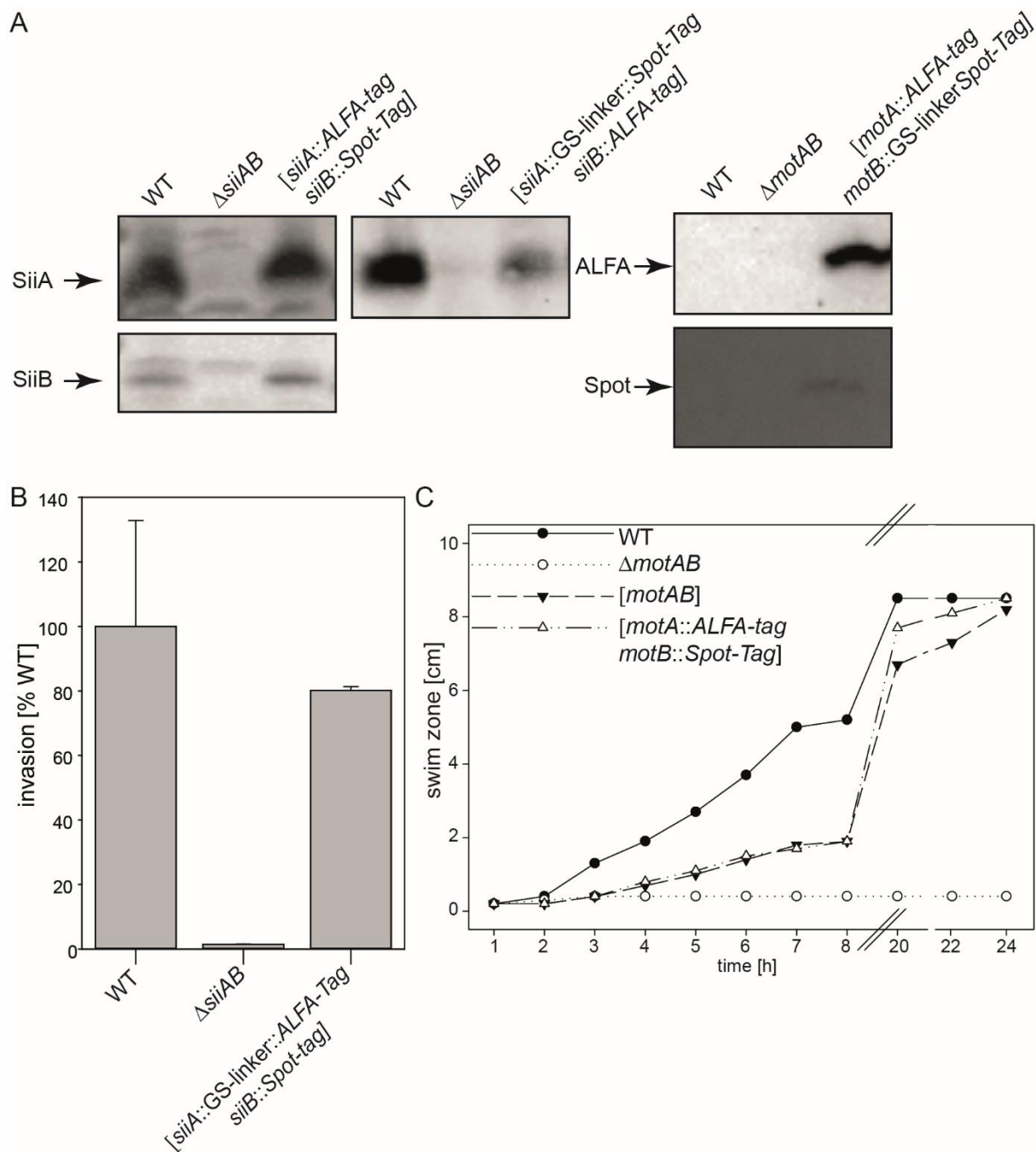


Figure S III.3.3. Analysis of expression and function of the introduced ALFA-tag and Spot-Tag.

A) Shown are protein expression levels for SiiA, SiiB, MotA and MotB with the introduced ALFA- and Spot-Tag. Western blot against SiiA and SiiB. Subcultures were grown for 2.5 h with AHT induction after 1 h, pelleted by centrifugation at 7,000 x g and boiled in SDS cracking buffer according to the OD₆₀₀. SDS-PAGE and Western blot with antibodies α -SiiA (1:10,000), α -SiiB (1:10,000), α -ALFA (1:1,000), α -Spot-Tag, coupled to Atto488, (1:1,000) and α -rabbit HRP-conjugated (1:10,000) were performed. B) Analysis of the functionality of the *siiAB* vector by invasion assay. Invasion of STM of polarized MDCK cells. Subcultures were grown for 2.5 h and MDCK were infected with MOI 5. C) Analysis of the functionality of the *motAB* vector by swim assay. Same vector backbones were used for further constructs.

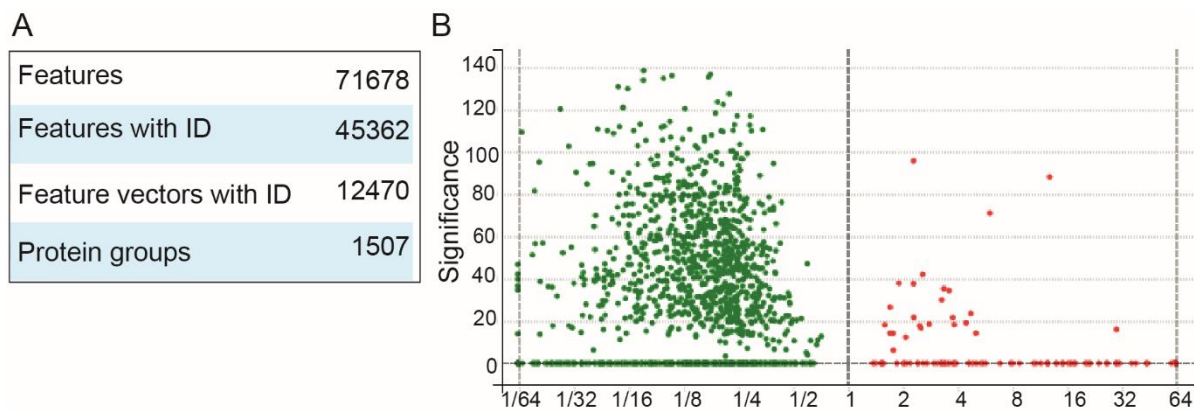


Figure S III.3.4. MS analysis of the proteome of STM WT and Δ *siiAB*. Shown are the hits of the proteomic search for STM WT and Δ *siiAB* (A) and the corresponding volcano plot (B). A detailed list of all hits can be found on the attached CD.

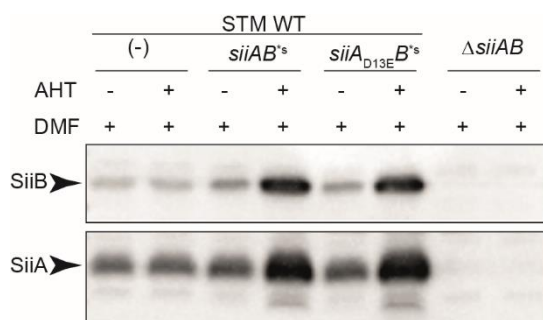


Figure S III.3.5. Analyses of protein levels after *siiAB* synthetic expression in WT. Western blot against SiiA and SiiB to check for synthetic expression (^s) of *siiAB* as well as *siiA*_{D13E}*B*. Subcultures were grown for 2.5 h with AHT induction after 1 h, pelleted by centrifugation at 7,000 x *g* and boiled in SDS cracking buffer according to the OD₆₀₀. SDS-PAGE and Western blot with antibodies α -SiiA (1:10,000), α -SiiB (1:10,000) and α -rabbit HRP-conjugated (1:10,000) were performed. Same vector backbone was used for *motAB* constructs.

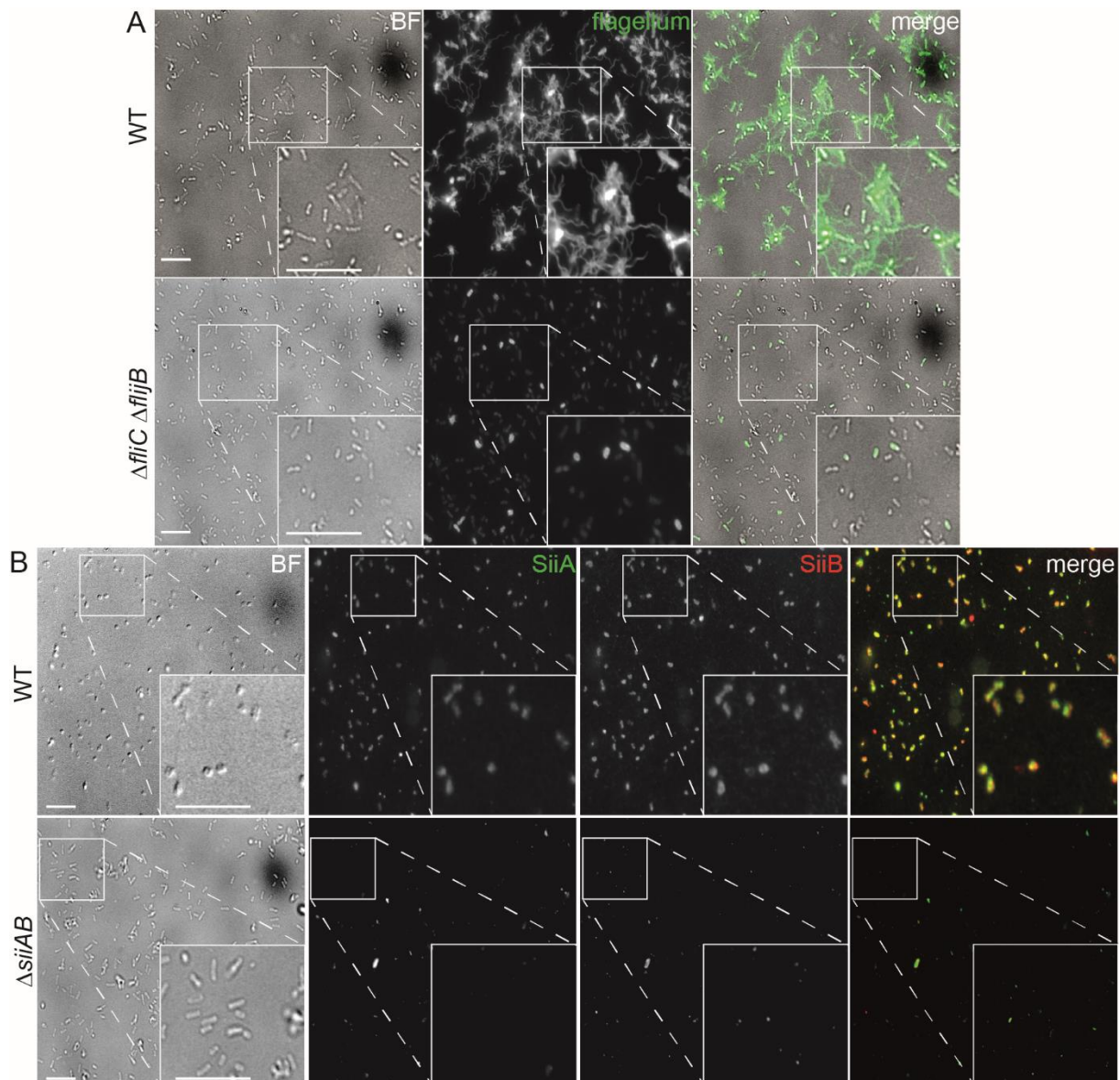


Figure S III.3.6. Microscopic analysis of the flagellum, SiiA and SiiB – controls. Microscopic analysis of flagellum surface signal, SiiA and SiiB. Subcultures were grown for 1 h, induced by addition of AHT, and further cultured for 1.5 h, pelleted by centrifugation and fixed with 3% PFA in PBS. Bacteria were stained for the flagellum, SiiA and SiiB, respectively. For microscopy, a widefield microscope, 100x with oil was used. Scale bar 10 μ m.

Results

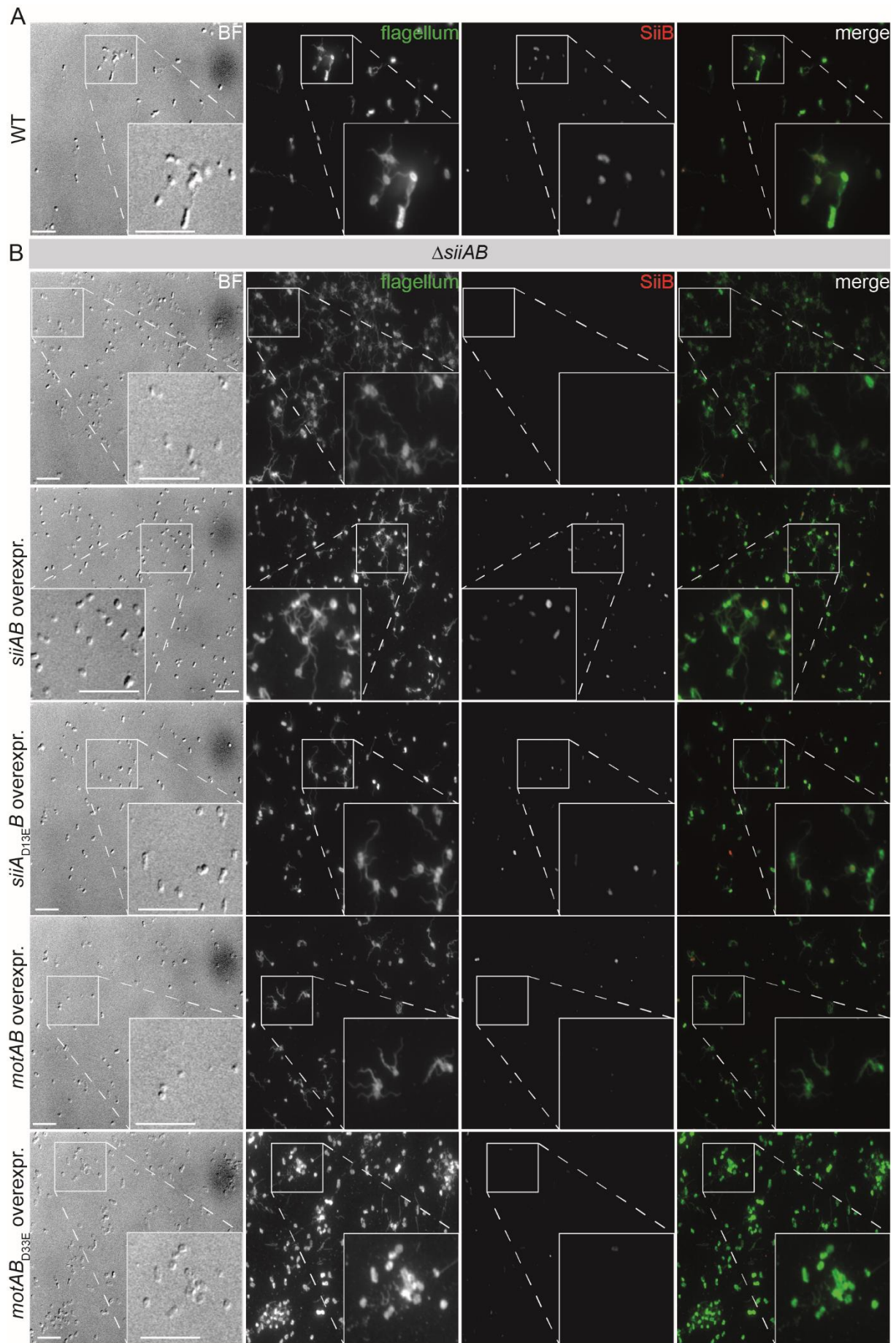


Figure S III.3.7. Presence of flagella and SiiAB. Microscopic analysis of flagellum surface signals and SiiB of WT (A) and Δ *siiAB* (B) strains under different synthetic expression plasmids encoding *siiAB* and *motAB* (B). Subcultures were grown for 1 h, induced by addition of AHT, and further cultured for 1.5 h, pelleted by centrifugation and fixed with 3% PFA in PBS. Bacteria were stained for the flagellum and SiiB, respectively. For microscopy, a widefield microscope with 100x objective with oil was used. Scale bars 10 μ m.

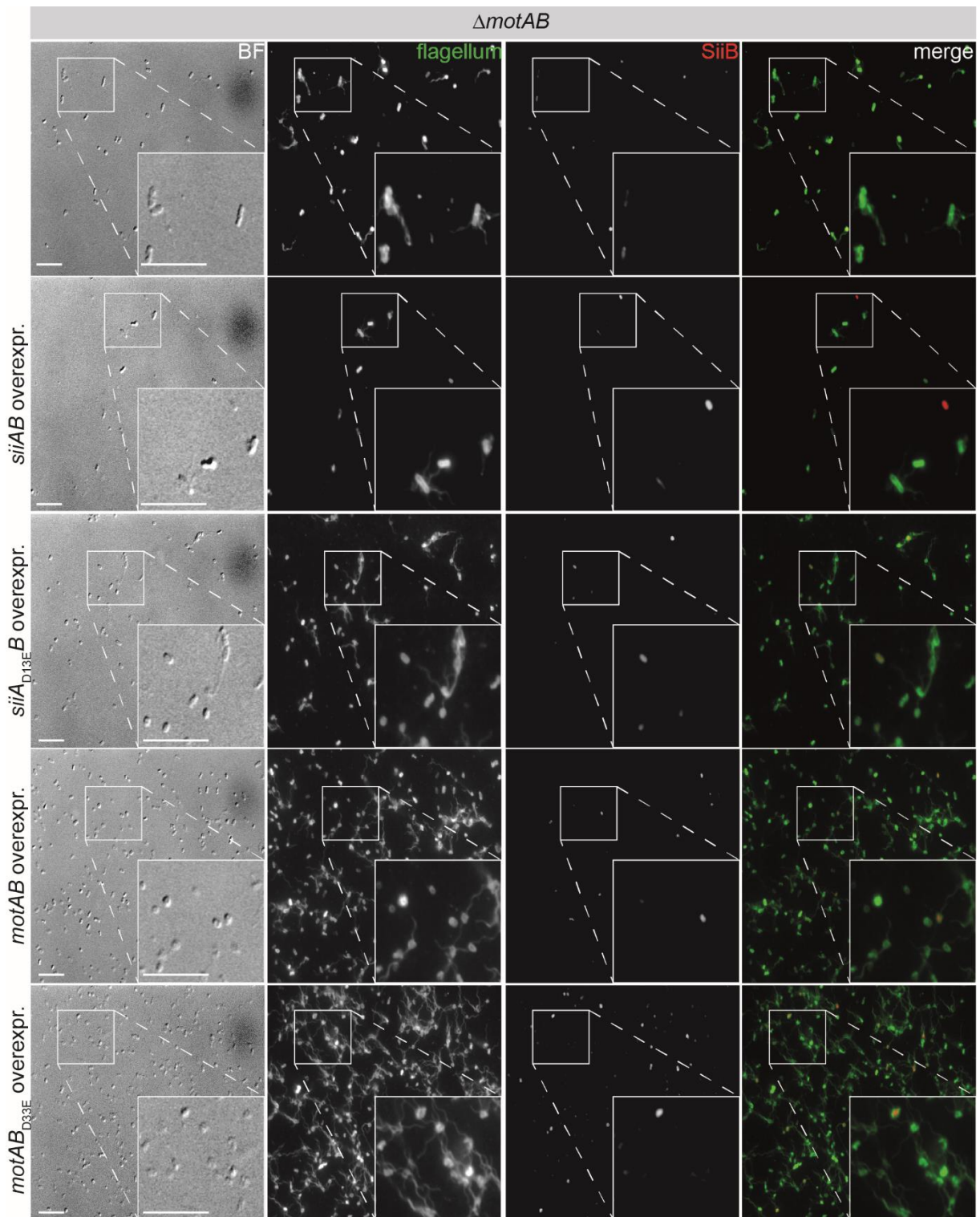


Figure S III.3.8. Presence of flagella and SiiB in $\Delta motAB$ background. Microscopic analysis of flagellum surface signal and SiiB of *motAB* mutant under with various expression plasmids encoding *siiAB* and *motAB*. Subcultures were grown for 1 h, induced by addition of AHT, and further cultured for 1.5 h, pelleted by centrifugation and fixed with 3% PFA in PBS. Bacteria were stained for the flagellum and SiiB, respectively. For microscopy, a widefield microscope, 100x with oil was used. Scale bar, 10 μ m.

```
AATTTATTGATAGAAATGGTTATTCCTCAGGCAGACATCTCTTTCTCTGACTCTCTACGAC
TGGGATATGAACGGGGAATTATTTTGGATGAAAGAGATTAAGAAAATATATCCTGATGTAG
TTATTGACATGAGTGTTAACTCCGCAGCATCAAGTACAACGAGTAAAGCTATTATCACGA
CTATCAACAAGAAAGTCTCGGAAGGTTCTCCGGATCGCGTGCGCGCGGTGAGCCATTG
GAGCAGCTGATTAATAAAAAGGTGTCAGAGTGAAATATATAAATCATTACCGCTATTTGT
TTGTCTGTTTTTTCCTTGCCATACTCCCTTTTTTTGCTTTATCTTTTCCCGGTATAAGAGA
GTATGTTTTTGATAACTTCATGGTTTCTGCAATTTACAATGGAGTCATTATTGCCATTTAT
ATTACAGGTTCTTTGTGTGCATTATTCCTATTCTTAAA
```

Figure S III.3.9. gBlock sequence used for SiiA-Spot-Tag insertion. Shown is the sequence for insertion of *siiA*-GS-linker-*Spot-Tag* ordered at Seqlab.

III.3.8. References

- Adler, J., and Parmryd, I. (2010). Quantifying colocalization by correlation: the Pearson correlation coefficient is superior to the Mander's overlap coefficient. *Cytometry A* 77, 733-742.
- Baker, A.E., and O'Toole, G.A. (2017). Bacteria, Rev Your Engines: Stator Dynamics Regulate Flagellar Motility. *J Bacteriol* 199.
- Barlag, B., and Hensel, M. (2015). The giant adhesin SiiE of *Salmonella enterica*. *Molecules* 20, 1134-1150.
- Belas, R. (2014). Biofilms, flagella, and mechanosensing of surfaces by bacteria. *Trends Microbiol* 22, 517-527.
- Berg, H.C. (2003). The rotary motor of bacterial flagella. *Annu Rev Biochem* 72, 19-54.
- Blair, D.F., and Berg, H.C. (1988). Restoration of torque in defective flagellar motors. *Science* 242, 1678-1681.
- Blair, D.F., and Berg, H.C. (1990). The MotA protein of *E. coli* is a proton-conducting component of the flagellar motor. *Cell* 60, 439-449.
- Blair, D.F., and Berg, H.C. (1991). Mutations in the MotA protein of *Escherichia coli* reveal domains critical for proton conduction. *J Mol Biol* 221, 1433-1442.
- Boyd, C.D., Smith, T.J., El-Kirat-Chatel, S., Newell, P.D., Dufrene, Y.F., and O'Toole, G.A. (2014). Structural features of the *Pseudomonas fluorescens* biofilm adhesin LapA required for LapG-dependent cleavage, biofilm formation, and cell surface localization. *J Bacteriol* 196, 2775-2788.
- Brueckler, F.M. (2017). *Geschichte der Mathematik kompakt. Das Wichtigste aus Analysis, Wahrscheinlichkeitstheorie, angewandter Mathematik, Topologie und Mengenlehre.* Springer-Verlag.
- Cascales, E., Lloubes, R., and Sturgis, J.N. (2001). The TolQ-TolR proteins energize TolA and share homologies with the flagellar motor proteins MotA-MotB. *Mol Microbiol* 42, 795-807.
- Castillo, D.J., Nakamura, S., Morimoto, Y.V., Che, Y.S., Kami-Ike, N., Kudo, S., Minamino, T., and Namba, K. (2013). The C-terminal periplasmic domain of MotB is responsible for load-dependent control of the number of stators of the bacterial flagellar motor. *Biophysics (Nagoya-shi)* 9, 173-181.
- Celia, H., Botos, I., Ni, X., Fox, T., De Val, N., Lloubes, R., Jiang, J., and Buchanan, S.K. (2019). Cryo-EM structure of the bacterial Ton motor subcomplex ExbB-ExbD provides information on structure and stoichiometry. *Commun Biol* 2, 358.
- Che, Y.S., Nakamura, S., Morimoto, Y.V., Kami-Ike, N., Namba, K., and Minamino, T. (2014). Load-sensitive coupling of proton translocation and torque generation in the bacterial flagellar motor. *Mol Microbiol* 91, 175-184.
- Conrad, J.C., Gibiansky, M.L., Jin, F., Gordon, V.D., Motto, D.A., Mathewson, M.A., Stopka, W.G., Zelasko, D.C., Shrout, J.D., and Wong, G.C. (2011). Flagella and pili-mediated near-surface single-cell motility mechanisms in *P. aeruginosa*. *Biophys J* 100, 1608-1616.
- Cooley, R.B., Smith, T.J., Leung, W., Tierney, V., Borlee, B.R., O'Toole, G.A., and Sondermann, H. (2016). Cyclic Di-GMP-Regulated Periplasmic Proteolysis of a *Pseudomonas aeruginosa* Type Vb Secretion System Substrate. *J Bacteriol* 198, 66-76.
- Coulton, J.W., and Murray, R.G. (1978). Cell envelope associations of *Aquaspirillum serpens* flagella. *J Bacteriol* 136, 1037-1049.
- Dean, G.E., Macnab, R.M., Stader, J., Matsumura, P., and Burks, C. (1984). Gene sequence and predicted amino acid sequence of the motA protein, a membrane-associated protein required for flagellar rotation in *Escherichia coli*. *J Bacteriol* 159, 991-999.
- Deme, J.C., Johnson, S., Vickery, O., Aron, A., Monkhouse, H., Griffiths, T., James, R.H., Berks, B.C., Coulton, J.W., Stansfeld, P.J., *et al.* (2020a). Author Correction: Structures of the stator complex that drives rotation of the bacterial flagellum. *Nat Microbiol* 5, 1616.
- Deme, J.C., Johnson, S., Vickery, O., Aron, A., Monkhouse, H., Griffiths, T., James, R.H., Berks, B.C., Coulton, J.W., Stansfeld, P.J., *et al.* (2020b). Structures of the stator complex that drives rotation of the bacterial flagellum. *Nat Microbiol* 5, 1553-1564.
- Doyle, T.B., Hawkins, A.C., and McCarter, L.L. (2004). The complex flagellar torque generator of *Pseudomonas aeruginosa*. *J Bacteriol* 186, 6341-6350.

- Du, S., Wang, Ye, Wei, Peng, Anishchenko, Baker, Yang (2021). The trRosetta server for fast and accurate protein structure prediction. *Nature Protocols*.
- Duan, Q., Zhou, M., Zhu, L., and Zhu, G. (2013). Flagella and bacterial pathogenicity. *J Basic Microbiol* 53, 1-8.
- Ershov, D.M.-S.P., Joanna W. Pylvänäinen, Stéphane U. Rigaud, L.L.B., Arthur Charles-Orszag, Ames R. W. Conway, Romain F. Laine, Nathan H. Roy, Daria Bonazzi, Guillaume Duménil, Guillaume Jacquemet, *et al.* (2021). Bringing TrackMate into the era of machine-learning and deep-learning. *bioRxiv*.
- Gerlach, R.G., Claudio, N., Rohde, M., Jackel, D., Wagner, C., and Hensel, M. (2008). Cooperation of *Salmonella* pathogenicity islands 1 and 4 is required to breach epithelial barriers. *Cell Microbiol* 10, 2364-2376.
- Gerlach, R.G., and Hensel, M. (2007). *Salmonella* pathogenicity islands in host specificity, host pathogen-interactions and antibiotics resistance of *Salmonella enterica*. *Berl Munch Tierarztl Wochenschr* 120, 317-327.
- Gerlach, R.G., Jackel, D., Geymeier, N., and Hensel, M. (2007a). *Salmonella* pathogenicity island 4-mediated adhesion is coregulated with invasion genes in *Salmonella enterica*. *Infect Immun* 75, 4697-4709.
- Gerlach, R.G., Jackel, D., Stecher, B., Wagner, C., Lupas, A., Hardt, W.D., and Hensel, M. (2007b). *Salmonella* Pathogenicity Island 4 encodes a giant non-fimbrial adhesin and the cognate type 1 secretion system. *Cell Microbiol* 9, 1834-1850.
- Goser, V., Kehl, A., Röder, J., and Hensel, M. (2020). Role of the ESCRT-III complex in controlling integrity of the *Salmonella*-containing vacuole. *Cell Microbiol* 22, e13176.
- Griessl, M.H., Schmid, B., Kassler, K., Braunsmann, C., Ritter, R., Barlag, B., Stierhof, Y.D., Sturm, K.U., Danzer, C., Wagner, C., *et al.* (2013). Structural insight into the giant Ca(2)(+)-binding adhesin SiiE: implications for the adhesion of *Salmonella enterica* to polarized epithelial cells. *Structure* 21, 741-752.
- Haiko, J., and Westerlund-Wikstrom, B. (2013). The role of the bacterial flagellum in adhesion and virulence. *Biology (Basel)* 2, 1242-1267.
- Holzer, S.U., Schlumberger, M.C., Jackel, D., and Hensel, M. (2009). Effect of the O-antigen length of lipopolysaccharide on the functions of Type III secretion systems in *Salmonella enterica*. *Infect Immun* 77, 5458-5470.
- Horstmann, J.A., Lunelli, M., Cazzola, H., Heidemann, J., Kuhne, C., Steffen, P., Szefs, S., Rossi, C., Lokareddy, R.K., Wang, C., *et al.* (2020). Methylation of *Salmonella Typhimurium* flagella promotes bacterial adhesion and host cell invasion. *Nat Commun* 11, 2013.
- Hosking, E.R., Vogt, C., Bakker, E.P., and Manson, M.D. (2006). The *Escherichia coli* MotAB proton channel unplugged. *J Mol Biol* 364, 921-937.
- Hu, H., Santiveri, M., Wadhwa, N., Berg, H.C., Erhardt, M., and Taylor, N.M.I. (2021). Structural basis of torque generation in the bi-directional bacterial flagellar motor. *Trends Biochem Sci*.
- Huang, B., Wang, W., Bates, M., and Zhuang, X. (2008). Three-dimensional super-resolution imaging by stochastic optical reconstruction microscopy. *Science* 319, 810-813.
- Khan, S., Dapice, M., and Reese, T.S. (1988). Effects of *mot* gene expression on the structure of the flagellar motor. *J Mol Biol* 202, 575-584.
- Khan, S., Ivey, D.M., and Krulwich, T.A. (1992). Membrane ultrastructure of alkaliphilic *Bacillus* species studied by rapid-freeze electron microscopy. *J Bacteriol* 174, 5123-5126.
- Khan, S., Khan, I.H., and Reese, T.S. (1991). New structural features of the flagellar base in *Salmonella typhimurium* revealed by rapid-freeze electron microscopy. *J Bacteriol* 173, 2888-2896.
- Kim, T.J., Young, B.M., and Young, G.M. (2008). Effect of flagellar mutations on *Yersinia enterocolitica* biofilm formation. *Appl Environ Microbiol* 74, 5466-5474.
- Kirchweiger, P., Weiler, S., Egerer-Sieber, C., Blasl, A.T., Hoffmann, S., Schmidt, C., Sander, N., Merker, D., Gerlach, R.G., Hensel, M., *et al.* (2019). Structural and functional characterization of SiiA, an auxiliary protein from the SPI4-encoded type 1 secretion system from *Salmonella enterica*. *Mol Microbiol* 112, 1403-1422.

- Koirala, S., Mears, P., Sim, M., Golding, I., Chemla, Y.R., Aldridge, P.D., and Rao, C.V. (2014). A nutrient-tunable bistable switch controls motility in *Salmonella enterica* serovar Typhimurium. *mBio* 5, e01611-01614.
- Kojima, S. (2015). Dynamism and regulation of the stator, the energy conversion complex of the bacterial flagellar motor. *Curr Opin Microbiol* 28, 66-71.
- Kojima, S., and Blair, D.F. (2001). Conformational change in the stator of the bacterial flagellar motor. *Biochemistry* 40, 13041-13050.
- Kojima, S., Takao, M., Almira, G., Kawahara, I., Sakuma, M., Homma, M., Kojima, C., and Imada, K. (2018). The Helix Rearrangement in the Periplasmic Domain of the Flagellar Stator B Subunit Activates Peptidoglycan Binding and Ion Influx. *Structure* 26, 590-598 e595.
- Kuchma, S.L., Delalez, N.J., Filkins, L.M., Snavey, E.A., Armitage, J.P., and O'Toole, G.A. (2015). Cyclic di-GMP-mediated repression of swarming motility by *Pseudomonas aeruginosa* PA14 requires the MotAB stator. *J Bacteriol* 197, 420-430.
- Kuhlbrandt, W., and Davies, K.M. (2016). Rotary ATPases: A New Twist to an Ancient Machine. *Trends Biochem Sci* 41, 106-116.
- Lai, Y.W., Ridone, P., Peralta, G., Tanaka, M.M., and Baker, M.A.B. (2020). Evolution of the Stator Elements of Rotary Prokaryote Motors. *J Bacteriol* 202.
- Larsen, S.H., Adler, J., Gargus, J.J., and Hogg, R.W. (1974). Chemomechanical coupling without ATP: the source of energy for motility and chemotaxis in bacteria. *Proc Natl Acad Sci U S A* 71, 1239-1243.
- Lele, P.P., Hosu, B.G., and Berg, H.C. (2013). Dynamics of mechanosensing in the bacterial flagellar motor. *Proc Natl Acad Sci U S A* 110, 11839-11844.
- Lemon, K.P., Higgins, D.E., and Kolter, R. (2007). Flagellar motility is critical for *Listeria monocytogenes* biofilm formation. *J Bacteriol* 189, 4418-4424.
- Madeira, F., Park, Y.M., Lee, J., Buso, N., Gur, T., Madhusoodanan, N., Basutkar, P., Tivey, A.R.N., Potter, S.C., Finn, R.D., *et al.* (2019). The EMBL-EBI search and sequence analysis tools APIs in 2019. *Nucleic Acids Res* 47, W636-W641.
- Malkusch, S., Endesfelder, U., Mondry, J., Gelleri, M., Verveer, P.J., and Heilemann, M. (2012). Coordinate-based colocalization analysis of single-molecule localization microscopy data. *Histochem Cell Biol* 137, 1-10.
- Mandadapu, K.K., Nirody, J.A., Berry, R.M., and Oster, G. (2015). Mechanics of torque generation in the bacterial flagellar motor. *Proc Natl Acad Sci U S A* 112, E4381-4389.
- Mass, L., Holtmannspotter, M., and Zachgo, S. (2020). Dual-color 3D-dSTORM colocalization and quantification of ROXY1 and RNAPII variants throughout the transcription cycle in root meristem nuclei. *Plant J* 104, 1423-1436.
- Mertins, S., Allan, B.J., Townsend, H.G., Koster, W., and Potter, A.A. (2013). Role of *motAB* in adherence and internalization in polarized Caco-2 cells and in cecal colonization of *Campylobacter jejuni*. *Avian Dis* 57, 116-122.
- Metterlein, M.Y., L.; Buchfellner, A.; Ruf, B. (2018). Spot-Tag: a Nanobody-based Peptide-Tag System for Protein Detection, Purification and Imaging.
- Minamino, T., Kinoshita, M., and Namba, K. (2019). Directional Switching Mechanism of the Bacterial Flagellar Motor. *Comput Struct Biotechnol J* 17, 1075-1081.
- Nakamura, S., and Minamino, T. (2019). Flagella-Driven Motility of Bacteria. *Biomolecules* 9.
- Notredame, C., Higgins, D.G., and Heringa, J. (2000). T-Coffee: A novel method for fast and accurate multiple sequence alignment. *J Mol Biol* 302, 205-217.
- Ovesny, M., Krizek, P., Borkovec, J., Svindrych, Z., and Hagen, G.M. (2014). ThunderSTORM: a comprehensive ImageJ plug-in for PALM and STORM data analysis and super-resolution imaging. *Bioinformatics* 30, 2389-2390.
- Partridge, J.D., and Harshey, R.M. (2013). More than motility: *Salmonella* flagella contribute to overriding friction and facilitating colony hydration during swarming. *J Bacteriol* 195, 919-929.
- Paulick, A., Delalez, N.J., Brenzinger, S., Steel, B.C., Berry, R.M., Armitage, J.P., and Thormann, K.M. (2015). Dual stator dynamics in the *Shewanella oneidensis* MR-1 flagellar motor. *Mol Microbiol* 96, 993-1001.

- Röder, J., and Hensel, M. (2020). Presence of SopE and mode of infection result in increased *Salmonella*-containing vacuole damage and cytosolic release during host cell infection by *Salmonella enterica*. *Cell Microbiol* 22, e13155.
- Roujeinikova, A. (2008). Crystal structure of the cell wall anchor domain of MotB, a stator component of the bacterial flagellar motor: implications for peptidoglycan recognition. *Proc Natl Acad Sci U S A* 105, 10348-10353.
- Sander, N. (2022). Functional analysis and characterization of the type 1 secretion system and its cognate substrate, the giant adhesin SiiE, of *Salmonella enterica*. University of Osnabrueck
- Santiveri, M., Roa-Eguiara, A., Kuhne, C., Wadhwa, N., Hu, H., Berg, H.C., Erhardt, M., and Taylor, N.M.I. (2020). Structure and Function of Stator Units of the Bacterial Flagellar Motor. *Cell* 183, 244-257 e216.
- Sauer, K., Camper, A.K., Ehrlich, G.D., Costerton, J.W., and Davies, D.G. (2002). *Pseudomonas aeruginosa* displays multiple phenotypes during development as a biofilm. *J Bacteriol* 184, 1140-1154.
- Smith, T.J., Font, M.E., Kelly, C.M., Sondermann, H., and O'Toole, G.A. (2018a). An N-Terminal Retention Module Anchors the Giant Adhesin LapA of *Pseudomonas fluorescens* at the Cell Surface: a Novel Subfamily of Type I Secretion Systems. *J Bacteriol* 200.
- Smith, T.J., Sondermann, H., and O'Toole, G.A. (2018b). Type 1 Does the Two-Step: Type 1 Secretion Substrates with a Functional Periplasmic Intermediate. *J Bacteriol* 200.
- Stock, A.M. (1999). A nonlinear stimulus-response relation in bacterial chemotaxis. *Proc Natl Acad Sci U S A* 96, 10945-10947.
- Sun, M., Wartel, M., Cascales, E., Shaevitz, J.W., and Mignot, T. (2011). Motor-driven intracellular transport powers bacterial gliding motility. *Proc Natl Acad Sci U S A* 108, 7559-7564.
- Szklarczyk, D., Gable, A.L., Nastou, K.C., Lyon, D., Kirsch, R., Pyysalo, S., Doncheva, N.T., Legeay, M., Fang, T., Bork, P., *et al.* (2021). The STRING database in 2021: customizable protein-protein networks, and functional characterization of user-uploaded gene/measurement sets. *Nucleic Acids Res* 49, D605-D612.
- Tipping, M.J., Delalez, N.J., Lim, R., Berry, R.M., and Armitage, J.P. (2013). Load-dependent assembly of the bacterial flagellar motor. *mBio* 4.
- Toutain, C.M., Zegans, M.E., and O'Toole, G.A. (2005). Evidence for two flagellar stators and their role in the motility of *Pseudomonas aeruginosa*. *J Bacteriol* 187, 771-777.
- UniProt, C. (2021). UniProt: the universal protein knowledgebase in 2021. *Nucleic Acids Res* 49, D480-D489.
- Wagner, C., Polke, M., Gerlach, R.G., Linke, D., Stierhof, Y.D., Schwarz, H., and Hensel, M. (2011). Functional dissection of SiiE, a giant non-fimbrial adhesin of *Salmonella enterica*. *Cell Microbiol* 13, 1286-1301.
- Wille, T., Wagner, C., Mittelstadt, W., Blank, K., Sommer, E., Malengo, G., Dohler, D., Lange, A., Sourjik, V., Hensel, M., *et al.* (2014). SiiA and SiiB are novel type I secretion system subunits controlling SPI4-mediated adhesion of *Salmonella enterica*. *Cell Microbiol* 16, 161-178.
- Wood, T.K., Gonzalez Barrios, A.F., Herzberg, M., and Lee, J. (2006). Motility influences biofilm architecture in *Escherichia coli*. *Appl Microbiol Biotechnol* 72, 361-367.
- Yang, J., Anishchenko, I., Park, H., Peng, Z., Ovchinnikov, S., and Baker, D. (2020). Improved protein structure prediction using predicted interresidue orientations. *Proc Natl Acad Sci U S A* 117, 1496-1503.
- Zhou, J., Fazio, R.T., and Blair, D.F. (1995). Membrane topology of the MotA protein of *Escherichia coli*. *J Mol Biol* 251, 237-242.
- Zhou, J., Sharp, L.L., Tang, H.L., Lloyd, S.A., Billings, S., Braun, T.F., and Blair, D.F. (1998). Function of protonatable residues in the flagellar motor of *Escherichia coli*: a critical role for Asp 32 of MotB. *J Bacteriol* 180, 2729-2735.
- Zinchuk, V., and Zinchuk, O. (2008). Quantitative colocalization analysis of confocal fluorescence microscopy images. *Curr Protoc Cell Biol Chapter 4*, Unit 4 19.

III.4. Establishment of a novel infection model for *Salmonella* adhesion and invasion – human intestinal organoids

Nathalie Sander^{1*}, Felix Scharte^{1*}, Rico Franzkoch², Michael Kim¹, Katherina Psathaki², Guntram Grassl³ and Michael Hensel^{1,2}

*These authors contributed equally to this work.

¹Division of Microbiology, University Osnabrueck, Osnabrueck, Germany

²CellNanOs – Center for Cellular Nanoanalytics, University Osnabrueck, Osnabrueck, Germany

³ Institute for Medical Microbiology and Hospital Epidemiology, Hannover Medical School and German Center for Infection Research, Partner Site Hannover-Braunschweig.

III.4.1. Abstract

Salmonella spp. are classified into typhoidal and non-typhoidal serovars and can cause a range of foodborne illnesses from self-limiting gastroenteritis to life threatening systemic disease. Analyses of host-pathogen interactions is a key requirement for the understanding of bacterial virulence mechanisms. In former studies, cell culture models as HeLa, MDCK and CaCo cell-lines were frequently used to investigate interactions with *Salmonella* in high temporal and spatial resolution. However, these models lack the complex tissue architecture of whole tissues, therefore interpretation of the results and transition to the human host is limited. Thus, the need for a cell culture system, displaying all different cell types of organs, is essential to gain more insights in physiological processes. Most recently, organoids have become a promising tool to study host-pathogen interactions in a setting resembling the *in vivo* situation. Especially the research with human-restricted pathogens like typhoidal *Salmonella* is dependent on human cell culture with a close relation to *in vivo* conditions. In contrast to cell culture with only a single cell population, crypt-derived intestinal organoids mimic tissue characteristics of distinct sections of the gastrointestinal tract. Stem cells of human or murine origin can be differentiated to 3D or 2D tissues with crypt formation, distinct cell populations, polarization and mucus secretion.

Here, we demonstrate the use of murine and human intestinal organoids in 3D and 2D to study virulence mechanisms of both typhoidal and non-typhoidal *Salmonella* regarding adhesion, invasion, and extra- and intracellular lifestyles. We performed infections with *Salmonella enterica* Typhimurium (STM) and Paratyphi A (SPA), quantified invaded bacteria, and imaged infection. For this, we adapted our imaging approaches to analyze *Salmonella* infection with confocal spinning disc microscopy (SDCM), scanning electron microscopy (SEM) and transmission electron microscopy (TEM). Using different labeling techniques, we aimed to identify cell types important in *Salmonella* infection.

Previous investigations in cell culture models led to definition of hallmark virulence functions such as invasion with induction of massive membrane ruffles, formation of *Salmonella*-containing vacuoles (SCV), and remodeling of the endosomal system of host cells, resulting in *Salmonella*-induced filament (SIF) formation. An established organoid model will help to critically analyze if these phenotypes also occur in more tissue-like organoid infection models and also offers options to investigate the cellular mechanisms of pathogen exit from infected host cells.

III.4.2. Introduction

III.4.2.1. Characteristics and cultivation of patient-derived Organoids

The development of a cell culture model, representing all different cell types of an organ or tissue, was shown to be scientifically transformative with various applications in epithelial and cell biology, including tissue polarity, adhesion, growth control and differentiation, pathology and clinical applications (Fujii *et al.*, 2016; Urbischek *et al.*, 2019; van de Wetering *et al.*, 2015). The critical aspect of organoid cultivation is the culture medium, containing defined ingredients, controlling growth, proliferation and differentiation, as R-spondins, potentiating Wnt pathway, and Noggin, inhibiting differentiation signals from the bone morphogenetic protein (BMP) pathway (Urbischek *et al.*, 2019).

Besides tissue development and regeneration, metabolic diseases and other biological processes, intestinal organoids can be used to study host-pathogen interactions as during *Salmonella* infection process. The intestinal epithelium displays an effective barrier against the invasion of microorganisms (Turner, 2009). Simpler cell culture models like Madin-Darby Canine Kidney (MDCK) cells or Henrietta Lacks (HeLa) cells only consist of a single cell type and are derived from tumors, thus they have error-filled genomes and investigations of host-pathogen interactions are more difficult to interpret (Beskow, 2016; Gaush *et al.*, 1966; Ponce de Leon-Rodriguez *et al.*, 2019). The possibility of intestinal organoids that can be isolated from stem cells of the crypts, let scientists now gain insights in infection processes much closer to reality (Figure III.4.1).

The intestine is surrounded by a monolayer of epithelial cells, typically forming villi and crypts to enlarge the surface of the intestine (Figure III.4.1 A). The epithelium consists of four major differentiated cell types (enterocytes, enteroendocrine cells (EEC), goblet cells and Paneth cells), multipotent stem cells, namely Lgr5⁺ crypt based columnar (CBC) cells and +4 cells, and a small population of epithelial cells that include tuft and microfold (M) cells (Beumer and Clevers, 2016; Gerbe and Jay, 2016; Iismaa *et al.*, 2018; Takashima *et al.*, 2013). These different cell types are part of distinct areas of the villus and crypt, respectively. EEC, enterocytes, goblet cells and M cells migrate to the tip of the villus, whereas Paneth cells are located at the bottom of the crypt, involved in stem cell maintenance (Gassler, 2017; Gomez and Boudreau, 2021). Enterocytes are the most abundant cell type here (Egi Kardia, 2020). Goblet cells function in production and secretion of mucus and EEC synthesize hormones and neuropeptides. Absorptive cells are not only involved in metabolic and digestive functions, but also express specific reporters on their surface important for innate immune response (Pott and Hornef, 2012; van der Flier and Clevers, 2009). By the recognition of luminal antigens and microorganisms, M cells are associated with the immunological vigilance and maturation (Peterson

and Artis, 2014). The different cell types of the mammalian intestine are constantly being renewed after reaching the villus tip 4-5 days after their generation (Iismaa *et al.*, 2018). As the intestine has a cellular and molecular complexity, investigating the mechanisms of the regulation of the epithelial homeostasis is difficult and the usage of conventional cell lines was more beneficial (Ponce de Leon-Rodriguez *et al.*, 2019). However, progress in the organoid cultivation now allows the successful growth of intestinal organoids in 3D (Figure III.4.1) and 2D (Figure III.4.15).

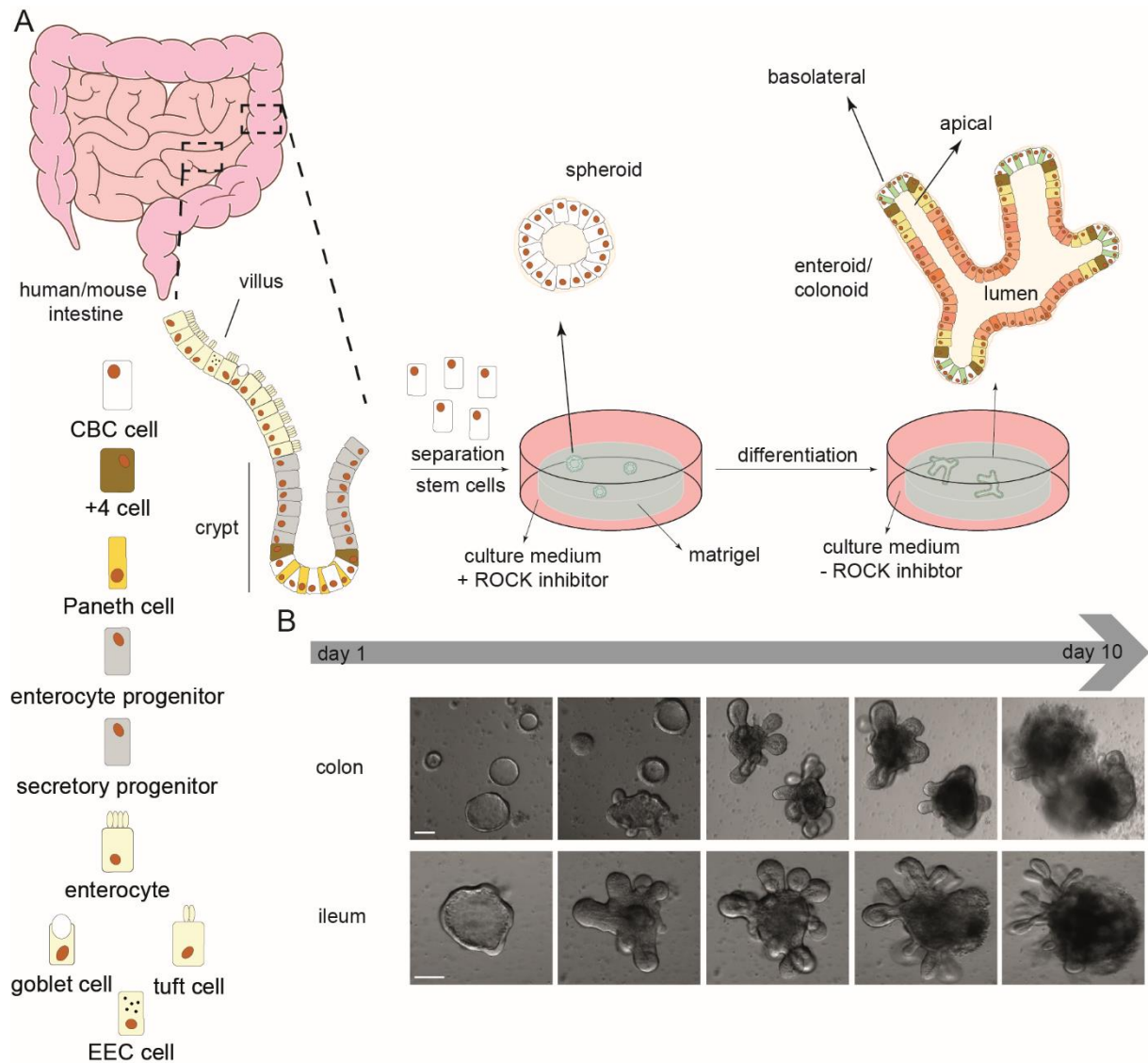


Figure III.4.1. Cultivation of 3D intestinal organoids from biopsy samples. A) Schematic overview of cultivation of 3D intestinal organoids. The epithelial layer of the intestine consists of villi and crypts. The villi are built up from differentiated epithelial cells, including enterocytes, enteroendocrine cells (EEC), tuft cells and goblet cells. The crypts consist of paneth cells, +4 cells and crypt base columnar cells (CBC). Paneth cells represent mature cells that remain in the crypts and influence the stem cell environment. By continuous proliferation of the CBC, new cells are provided during differentiation of the villus. Stem cells are isolated from the crypts of intestinal biopsy samples and seeded in a Matrigel-culture medium mix, allowing growth of 3D cultured cells reproducing the physiology and structure of the intestine. Initially, the culture medium is supplemented with growth factors and 10 μ M Y27623 for inhibition of the Rho-associated, coiled-coil containing protein kinase (ROCK) pathway, improving the survival of stem cells in the initiation of differentiation protocols (Ishizaki *et al.*, 2000; Rezania *et al.*,

2014). Y27623 inhibits stem cell differentiation, so spheroids are formed. For differentiation, the medium is exchanged after 3 days with supplemented medium without Y27623, allowing differentiation. The intestinal organoids form villi and crypts and after 10 days, organoids can be dissociated and seeded again. B) Micrographs of intestinal organoid growth over time. Exemplary shown are murine colonoids and enteroids. Scale bar: 100 μm .

After first cultivation attempts with murine small intestine segments, the approach extended to other parts of the intestine, resulting in growth of colonoids, if colon was used, and enteroids, if the small intestine was used (Sato *et al.*, 2009; Stelzner *et al.*, 2012). One of the most essential cell types during enteroid formation are the Lgr5⁺ CBC cells, which differentiate to enterocytes, goblet cells, EEC and Paneth cells (Sato *et al.*, 2009) (Figure III.4.1 A). These cells initially form spheroids under cultivation conditions with Rho-associated, coiled-coil containing protein kinase (ROCK) pathway inhibitor (Y27623), improving the survival of stem cells in the initiation of differentiation protocols (Ishizaki *et al.*, 2000; Reznia *et al.*, 2014). Following spheroid stadium, protrusions are formed, mimicking crypts and the intestinal architecture (Sato and Clevers, 2013). It was also shown that Paneth cells are crucial for organoids and the maintenance of intestinal stem cells (Sato *et al.*, 2011). Organoids can grow under *in vitro* conditions, but the medium has to be supplemented with factors and molecules normally composing their natural niche (Gomez and Boudreau, 2021). To provide this essential environment, organoids are cultured in semi-viscous medium, enriched with an extracellular matrix (Matrigel) to allow differentiation and interactions of the cells. Additionally, a cocktail of biological enhancers is added to the medium, containing the bone morphogenetic protein inhibitor R-spondin, Wnt3a, Noggin and epidermal growth factors (Ootani *et al.*, 2009; Sato *et al.*, 2011; Sato *et al.*, 2009). Following spheroid assembly, the ROCK inhibitor is removed from the medium and the spheroids break the symmetry, leading to crypt formation. Intestinal organoids form a lumen with an apical side, in which apoptotic cells and metabolites are ejected (Gomez and Boudreau, 2021). In contrast to the gut epithelium, the external milieu is not in touch with the apical side of the organoid, but with the basolateral side (Sato *et al.*, 2009). This organization makes infection models and analyses of host-pathogen interactions more difficult. However, new strategies were devised that allow to reverse this polarity, leading to new infection protocols and analyses of infection processes.

III.4.2.2. Organoids as model for infection biology

Infectious diseases are one of the most common causes of death and represent a major health problem around the world (WHO, 2008). In times of rising infection rates and frequently emerging antibiotic-resistance in pathogenic bacteria as well as newly emerging zoonotic diseases

as SARS-CoV-2, it is of crucial importance to better understand their pathogenesis for development of new strategies to counteract infections or for vaccine development (WHO, 2014).

Organoid systems are one of the major recent advances for biological research across biological research fields including drug treatment, cancer therapy, developmental biology and also infection biology. Organoids can be derived from induced and adult stem cells and are able to reconstitute complex tissues with different cell types and physiological functions. For many diseases, the broader biological context is necessary to elucidate infection routes, disease progression and pathogenesis of the causative agent. With their ability to mimic the *in vivo* context, organoids can therefore serve as model in infection biology (Bartfeld, 2016; Dutta and Clevers, 2017; Rios and Clevers, 2018). Despite being only a recently developed method, numerous bacterial, viral and parasitic pathogens have been analyzed in organoid systems such as *Cryptosporidium*, enterohemorrhagic *Escherichia coli*, *Campylobacter jejuni*, *Clostridium difficile*, *Helicobacter pylori*, *Listeria monocytogenes*, *Shigella flexneri*, *Vibrio cholerae*, *Salmonella enterica*, Zika virus, rotavirus and SARS-CoV-2 (Bartfeld and Clevers, 2015; Finkbeiner *et al.*, 2012; Forbester *et al.*, 2015; Garcez *et al.*, 2016; He *et al.*, 2019; Heo *et al.*, 2018; Lamers *et al.*, 2021; Leslie *et al.*, 2015; Ranganathan *et al.*, 2019; Roodsant *et al.*, 2020; Tse *et al.*, 2018; Zomer-van Ommen *et al.*, 2016). Even formerly, unculturable pathogens like norovirus show the high potential of organoids to become a promising model system for pathogens, especially if they are adapted to the human host (Ettayebi *et al.*, 2016).

Many bacterial pathogens using the intestinal tract as route of entry to deeper tissues and systemic spread in the host (Ribet and Cossart, 2015). Intestinal organoids with their ability to recapitulate infection relevant characteristics such as crypt and microvilli domains, mucus production, defensive and antimicrobial peptide secretion can serve as adequate model system for enteric pathogens (Bartfeld and Clevers, 2015; Dutta and Clevers, 2017). Further systems with gallbladder and liver organoids can help to study specific infection foci in systemic diseases (Caiazza *et al.*, 2021; Sepe *et al.*, 2020). Co-culture models with immune cells in medium could serve as model for microenvironments like the lamina propria (Schreurs *et al.*, 2021). A decent set of methods for infection biology research with organoid systems is available by now which is schematically presented in Figure III.4.2.

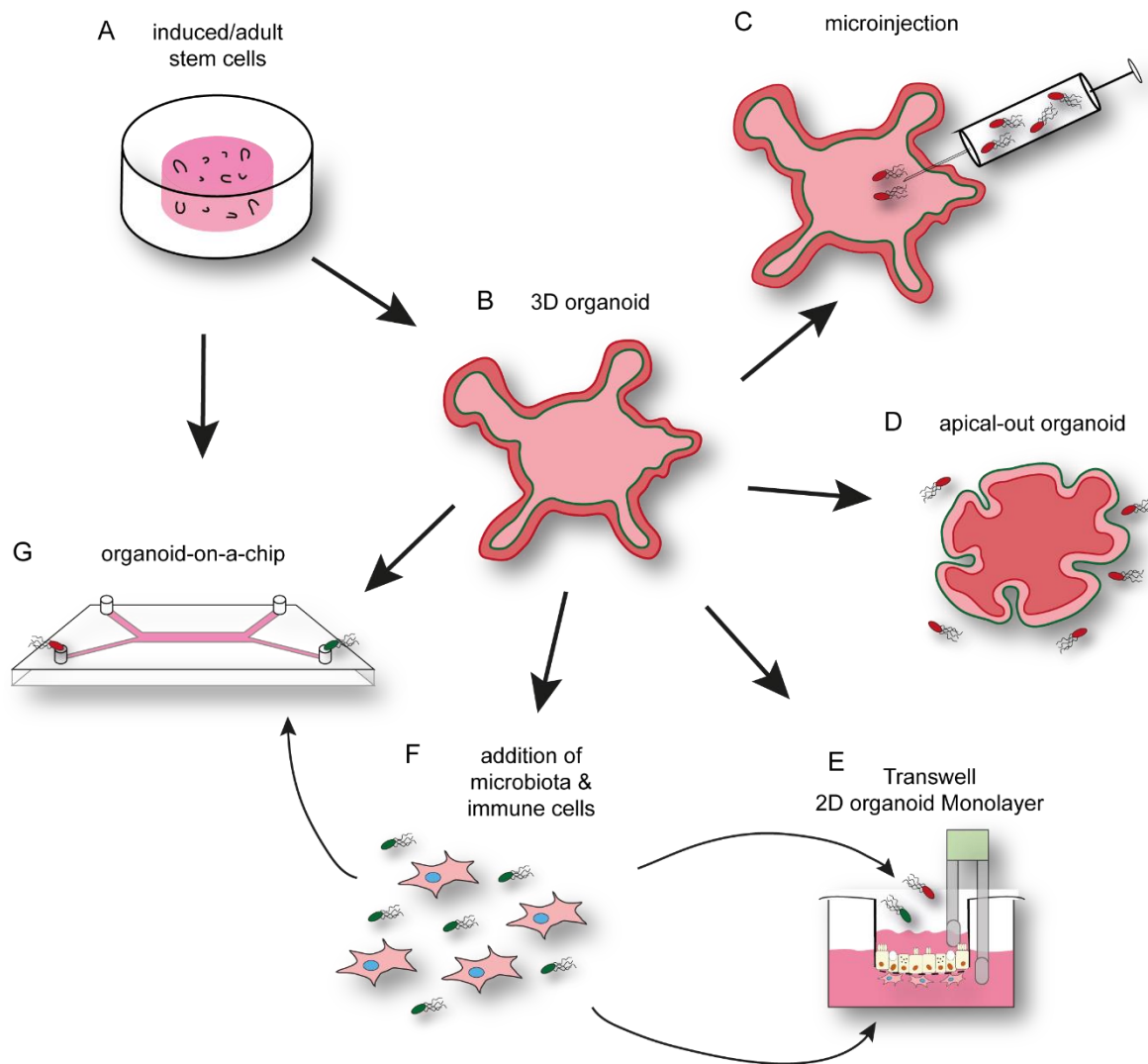


Figure III.4.2. Methods of infection studies with 3D and 2D organoids. A) stem cells are cultured in Matrigel as described in figure III.4.1 until they develop 3D organoids (B). C) To allow pathogens access to the apical side of 3D organoids, microinjection can be performed. D) Generation of apical-out organoids allows infection with pathogens added directly to the culture medium. E) Organoid-derived monolayers allow infection from the apical side in a more defined manner described in figure III.4.15. F) Microbiota and immune cells can be added to organoids grown on transwells (E) and in microfluidic chambers (G).

Salmonella enterica

One of the most prevalent enteropathogens belongs to the family *Salmonella enterica* that can cause diseases ranging from self-limiting gastroenteritis to life-threatening systemic infections (typhoid fever) (Johnson *et al.*, 2018). The pathogenic, Gram-negative bacteria are rod-shaped and live facultative anaerobic. There are over 2,500 serovars within the genus of *Salmonella* which can be highly human-specific like *Salmonella enterica* serovar Typhi (STY) or *S. enterica* serovar Paratyphi A (SPA), or with a broad host range like *S. enterica* serovar Typhimurium (STM) (Pui, 2011). The ability of invasion and subsequent intracellular lifestyle in epithelial and immune cells is a major characteristic of *Salmonella*. The pathogenesis is thereby mediated

by virulence genes which are mainly encoded on *Salmonella* pathogenicity islands (SPI), large chromosomal regions harboring several virulence-associated genes (Gerlach and Hensel, 2007; Hensel, 2004). *Salmonella* is able to actively invade polarized epithelial cells by the so-called trigger mechanism (Gerlach *et al.*, 2008). Prior invasion, the giant non-fimbrial adhesin SiiE mediates first close contact to the apical side of the target cell. SiiE is secreted by the SPI4-encoded type 1 secretion system (SPI4-T1SS). In the further process of the infection, effector proteins are translocated via a SPI1-encoded type 3 secretion system (SPI1-T3SS) into the target cell and thereby induce manipulation of the actin cytoskeleton in enterocytes (Ly and Casanova, 2007). This process leads to membrane protrusions (membrane ruffles) and subsequently the non-phagocytic cells internalize the *Salmonella* in a phagocytic-like manner (Galan and Curtiss, 1989; Gerlach *et al.*, 2008). After invasion, *Salmonella* is present in the *Salmonella*-containing vacuole (SCV), similar to a phagosome. The following intracellular lifestyle with maturation of the SCV and as well as replication is depending on effector proteins which are translocated via a SPI2-encoded T3SS (SPI2-T3SS). Human-specific typhoidal *Salmonella* serovars replicate in immune cells like macrophages and are able to systemic disseminate to gallbladder, lymph nodes, bone marrow and liver as the infection progresses (Dougan and Baker, 2014).

III.4.3. Results

III.4.3.1. 3D imaging of intestinal organoids

Organoids possess complex structures and are embedded in hydrogel that reconstitute an extracellular matrix and allows growth in 3D. These circumstances make microscopy approaches of whole-mount organoids challenging and imaging is highly dependent on specimen preparation, microscope and objective properties. Staining of organoids with fluorescent probes can be performed directly in suitable cell culture chambers or with detached organoids, released from Matrigel. Imaging is then performed in the respective chambered coverslip or after embedding of the detached organoids on conventional microscope slides (Figure III.4.3). Imaging quality is further dependent on working distance, parfocal length and numerical aperture of the used objective and the wavelength of light used to illuminate the specimen.

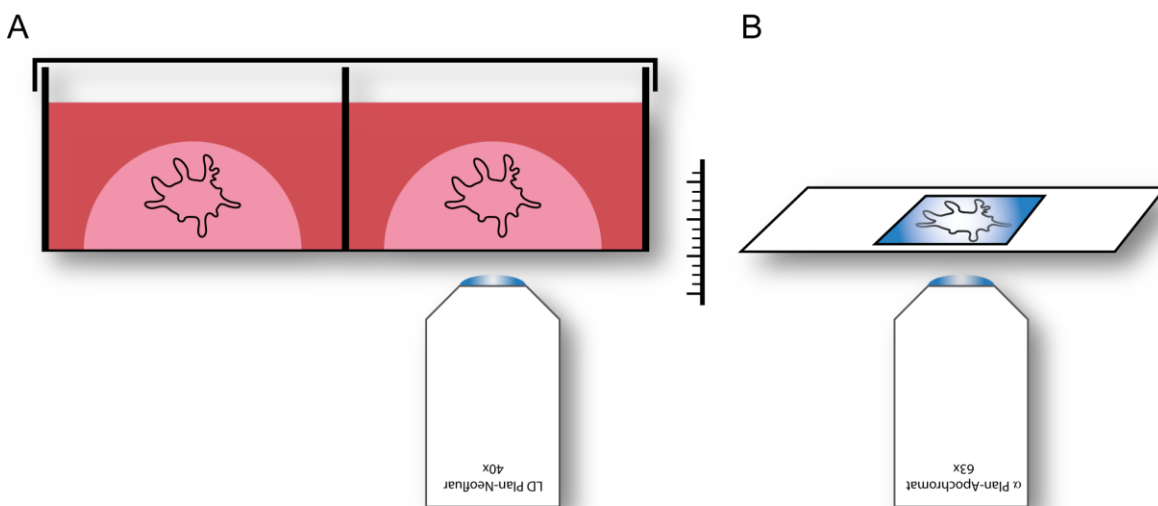


Figure III.4.3. Light microscopy of whole-mount intestinal organoids. A) Distance from specimen to microscope objective is higher in setups with organoids cultured in Matrigel in a μ -slide chambered coverslip (ibidi) than with fixed organoids that were mounted on microscope slides (B).

Scanning electron microscopy (SEM) gives an impression of the dimensions of 3D organoids (Figure III.4.4 A). A side view of 3D enteroids cultured in chambered coverslips reveals how challenging fluorescence microscopy with such large specimen can be (Figure III.4.4 B). With up to 500 μm in diameter, not nearly half of the organoid can be imaged properly in Z dimension with loss of focus and decreasing fluorescence signal with increasing imaging height. Especially the illumination with shorter wavelengths for DAPI or Alexa488 fluorescence samples is problematic as penetration depth in confocal microscopy is typically limited to less than 100 μm (Graf and Boppart, 2010). However, the organoid side near the coverslip bottom and also some crypt domains were imaged in adequate resolution (Figure III.4.4 B, C, C'). Staining with DAPI, phalloidin and CellMask can give an insight into the general organization of a fully differentiated

enteroid. CellMask allowed a uniform staining of the plasma membrane without cell-type differences exhibited by lectins and shows the dimensions of the enteroid. Nuclei staining with DAPI and F-actin staining with phalloidin showed the distribution and orientation of cells in the organoid. High F-actin accumulation was visible at the apical side of the epithelial cells, which showed a high order of polarization with a high number of microvilli that were densely packed on the apical surface. The apical side faced the lumen of the enteroid. DAPI stained nuclei were located at the basolateral side.

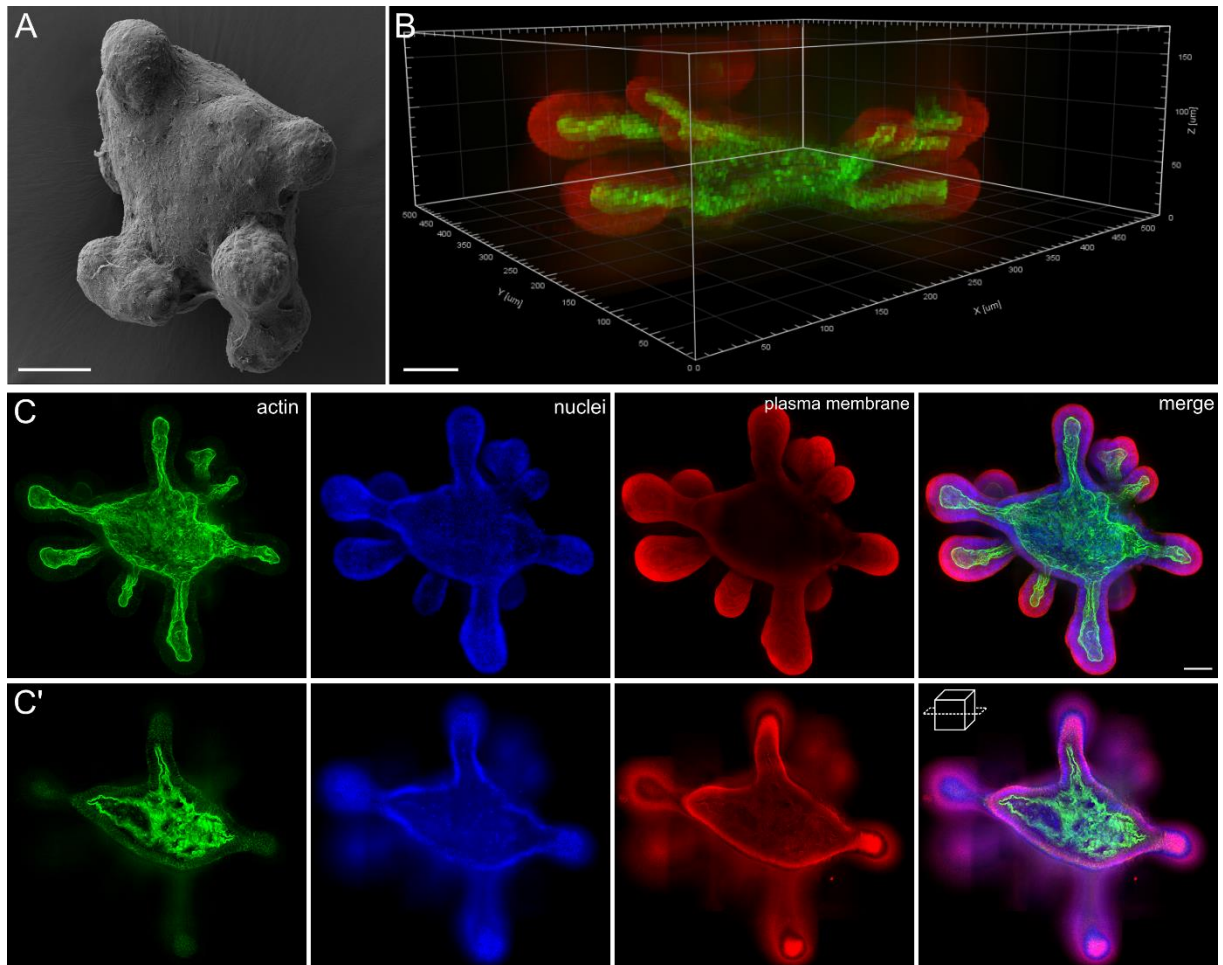


Figure III.4.4. Imaging and fluorescence labeling of 3D enteroids. A) SEM image of mouse intestinal organoid. 3D side view (B), maximum intensity projection (C) and cross-section (C') of whole-mount enteroid. Murine ileum organoids were cultured, fixed and stained with phalloidin-iFluor647 (green), DAPI (blue) and CellMask Deep Red (red) in μ -slide chambered coverslip before imaging. Imaging with 40x objective. Multiple images with overlaps were acquired and stitched. Scale bars: 50 μ m.

Imaging of enteroids released from Matrigel and embedded on microscope slides is easier in terms of microscope prerequisites. Due to flattening of the organoids between microscope slide and coverslip and the resulting lower distance between objective and specimen, imaging of whole organoids in full Z was possible (Figure III.4.5). This allowed imaging with higher

magnifying objectives and detailed characterization of cells e.g. at the apical side of enterocytes (Figure III.4.5 C'). Additionally, the brush border with microvilli structures was visible in detail.

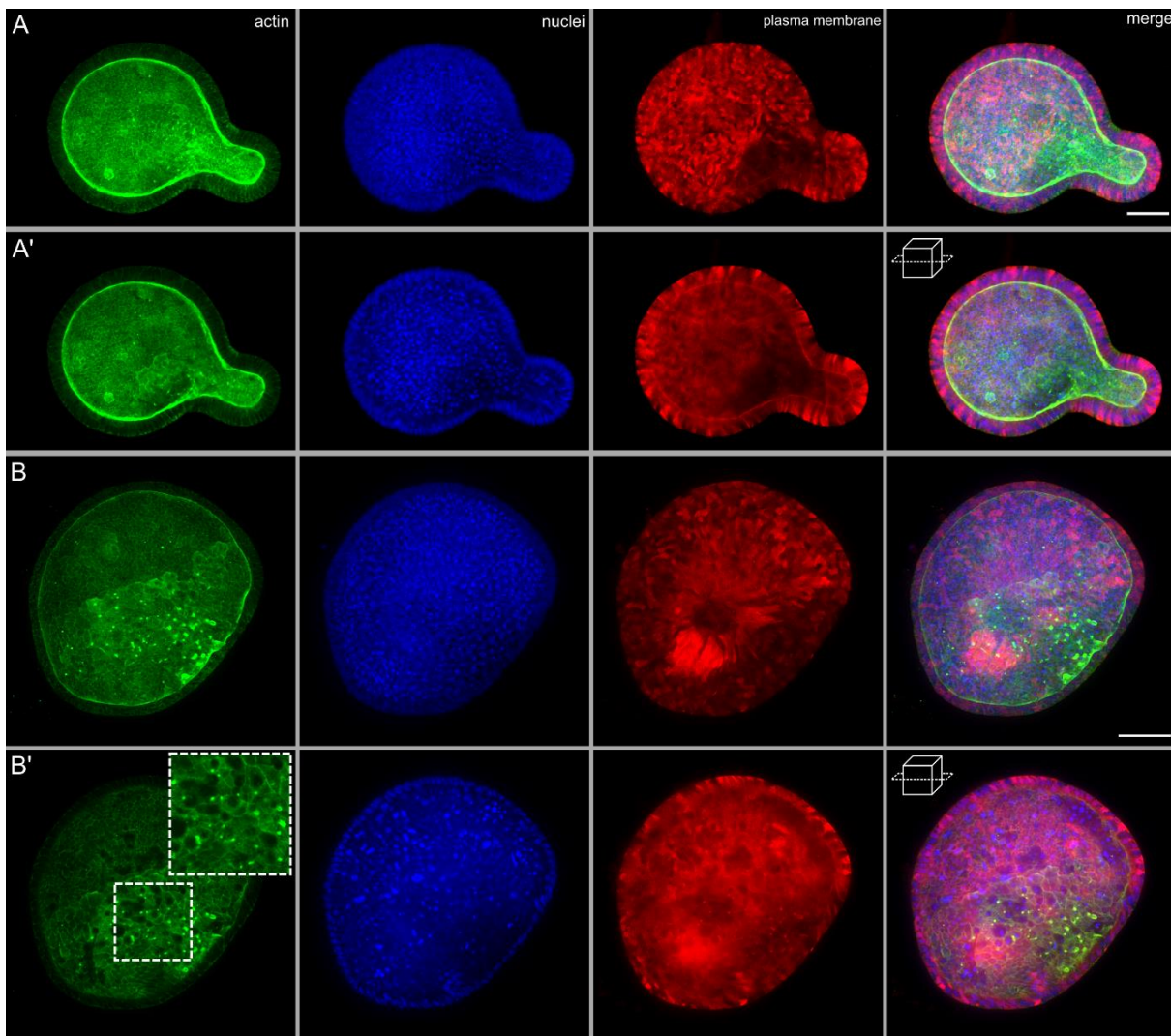


Figure III.4.5. Imaging and fluorescence labeling of 3D enteroids. A and B) Maximum intensity projection and cross-section (A', B') of whole-mount murine ileum organoids that were cultured and fixed in a 24-well, detached and stained with phalloidin-iFluor647 (green), DAPI (blue) and CellMask Deep Red (red) before mounted on microscope slide for imaging. Imaging with 63x objective. Multiple images with overlaps were acquired and stitched. Scale bars: 50 μ m.

Transmission electron microscopy (TEM) of ultrathin sections of a 3D-cultured enteroid revealed differences regarding the ultrastructure of various cell types (Figure III.4.6). The apical side of epithelial cells that are facing the lumen of the enteroid showed highly ordered microvilli structure, which therefore were defined as brush border (Figure III.4.6 A). Goblet cells were easily distinguishable by TEM because of their unique cellular architecture. A large volume of the goblet cell was densely packed with mucus containing secretory vesicles with large glycoproteins called mucins (Figure III.4.6 B). Due to harsh fixation methods necessary for TEM,

the structure of carbohydrate-rich polymeric mucins may be disrupted, yet secretion of it was also visible in Figure III.4.6 B.

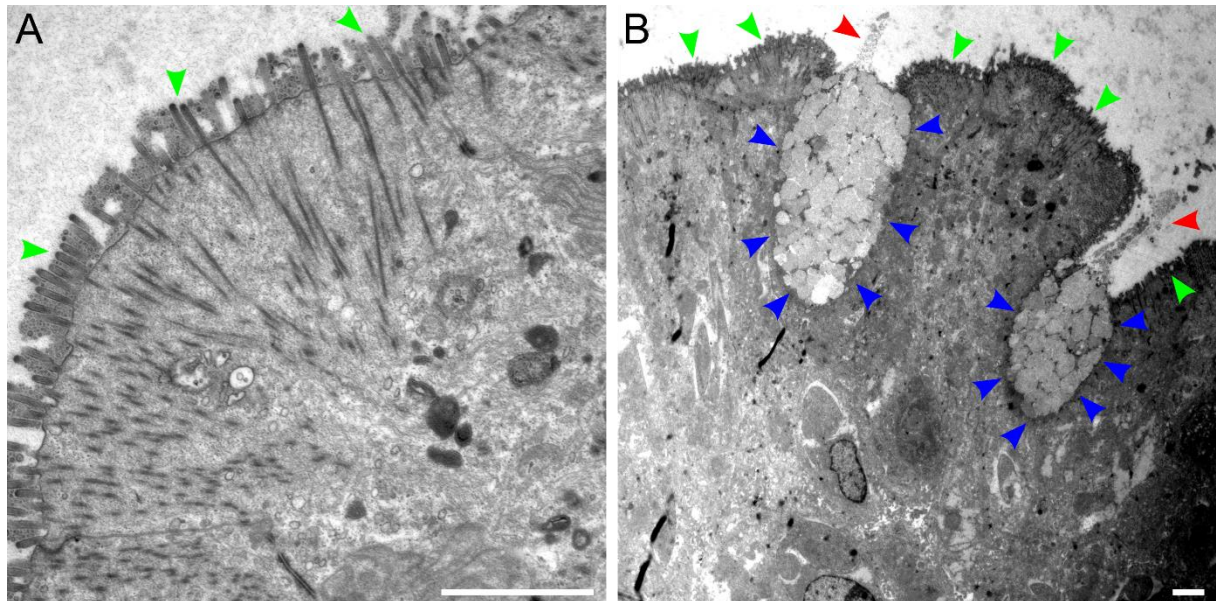


Figure III.4.6. 3D organoids develop multiple cell types with brush border and mucus secretion. TEM image of mouse intestinal organoid. A+B) Green arrowheads indicate microvilli in a brush border. B) Goblet cells with secretory vesicles (blue arrowheads) inside of the cell and secreted mucus (red arrowheads) are shown. Scale bars: 2 μm .

Lectins like wheat germ agglutinin (WGA) with a high affinity for sialic acid and N-acetylglucosamine can be used to distinguish between certain cell types within organoids e.g. goblet and Paneth cells. WGA-stained murine and human enteroids showed expected high WGA signal predominantly in crypt domains (Figure III.4.7 A, B), the area where goblet and Paneth cells are mainly present (Figure III.4.1) (Birchenough *et al.*, 2015). Imaging in higher magnification also revealed single cells with secreted mucus at the apical side of the cell, these cells also showed less F-actin signal (Figure III.4.7 C, C', C*). Note that WGA also stains the nuclear envelope, which was therefore also visible.

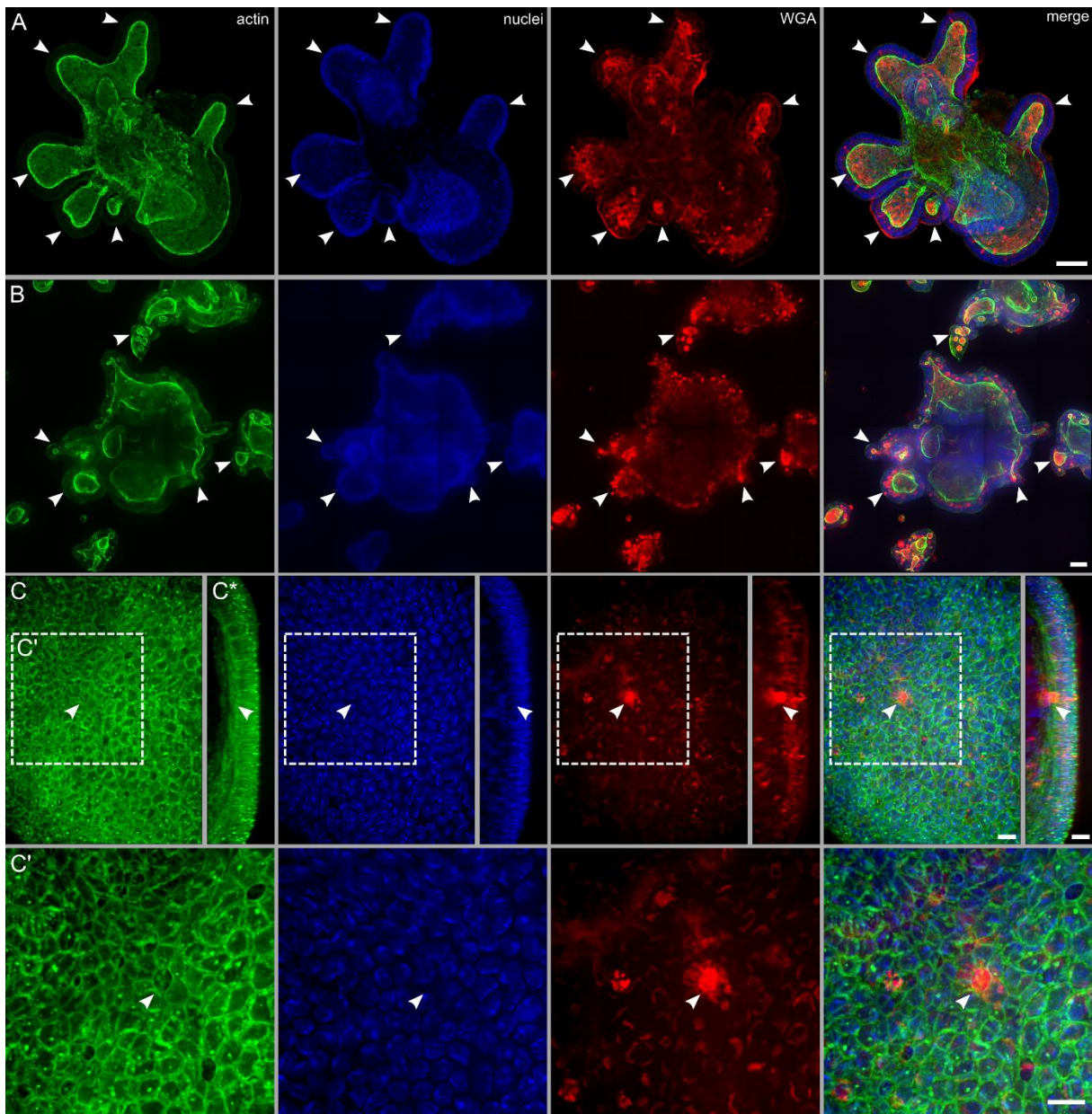


Figure III.4.7. Fluorescence analysis of 3D enteroids with wheat germ agglutinin. Murine (A) and human (B, C, C', C*) enteroids were cultured, fixed and stained with AlexaFluor488-phalloidin (green), DAPI (blue) and CF®640R WGA (red) in μ -slide chambered coverslip before imaging. (C') and (C*) show magnification and side view of a region of interest. Arrowheads indicate accumulation of WGA signal. Images are shown as maximum intensity projection. Imaging with 40x objective (A, B) and 63x objective (C, C', C*). Multiple images with overlaps were acquired and stitched. Scale bars: 50 μ m (A, B), 10 μ m (C, C', C*).

III.4.3.2. Lentiviral transfection

To further analyze host-pathogen interactions without additional staining, we aimed to stably transfect the organoids with LifeAct-GFP by lentiviral transduction as a highly efficient method of gene transfer into mammalian cells (Figure III.4.8) (Miyoshi and Stappenbeck, 2013). The organoids were grown for 2-4 days in 3D organoid medium, supplemented with ROCK inhibitor, to generate as many stem cells as possible. As the lentiviruses interfere with the Matrigel, the organoids were seeded on a thin Matrigel layer. Following this step, we incubated the organoids for 3 days to allow differentiation. After 7 days, we started selection by Blasticidin treatment for 24 h. Blasticidin is a selection antibiotic, acting on eukaryotic and prokaryotic cells. The cell death induced by Blasticidin occurs rapidly and allows selection of transfected cell lines carrying a Blasticidin resistance gene within one week (Miyoshi and Stappenbeck, 2013). Additionally, organoids were selected without Blasticidin treatment (Figure III.4.8) and non-transduced organoids were treated with Blasticidin (not shown).

After selection with Blasticidin, we obtained successfully transfected human colon and ileum organoids with a rate of approximately 50% (Figure III.4.8). We found a varying distribution of the GFP signal among the survived organoids ranging from only one to a few cells, up to nearly all cells of a single organoid. Interestingly, we found partly damaged organoids after Blasticidin treatment (Figure III.4.8). Thus, as the untreated organoids showed less to no damage, the Blasticidin concentration has to be decreased. However, we passaged the successfully transduced organoids and tried to further select for organoids with many positive cells to increase the amount in the population. The stable transfection was tested over several months and could be confirmed for most of the selected organoids. In future attempts, sorting of the stem cells by FACS or by visual inspection during passaging could lead to a monoclonal population of stably transfected organoids (Miyoshi and Stappenbeck, 2013). In a next step, these stably transfected organoids can then be used for 2D analyses or apical-out approaches to gain more insights into STM, SPA or STY infection process under nearly physiological parameters.

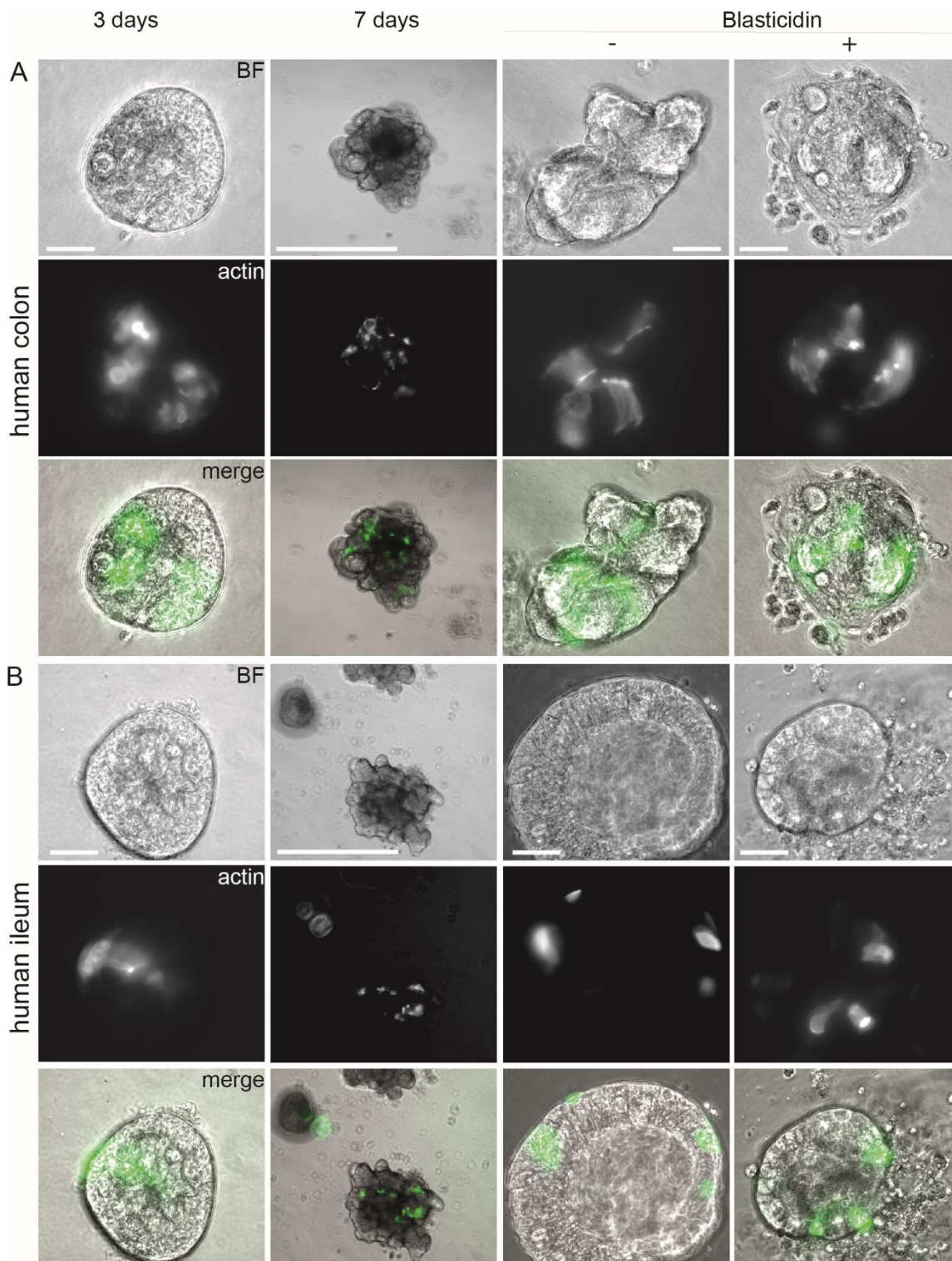


Figure III.4.8. Lentiviral transfection of human organoids with LifeAct-GFP. Microscopic analyses of the lentiviral transduction and following selection. Human organoids were lentiviral transfected for 24 h. After 24 h transduction, medium was exchanged, organoids covered with additional Matrigel and covered with medium. Selection occurred with Blasticidin. Microscopy was performed with the Zeiss Axio Vert.A1. Scale bar: 100 μ m. A) Human colon spheroids (left) and colonoids (center and right). B) Human ileum spheroids (left) and enteroids (center and right).

In addition to human organoids, we successfully transfected murine enteroids (Figure III.4.9). These cell line survived the Blasticidin treatment and showed no damaged organoids.

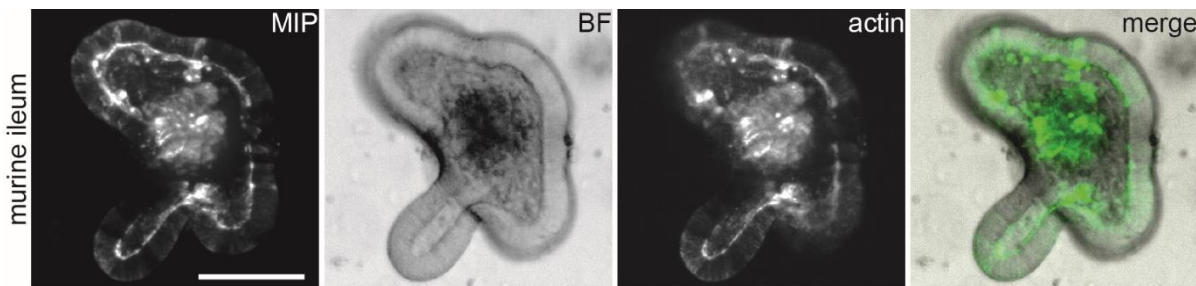


Figure III.4.9. Murine enteroids stably transfected with lentivirus. Microscopic analyses of the lentiviral transduction of murine enteroids. Organoids were transfected with LifeAct-GFP lentiviruses. Procedure as described in Figure III.4.8. Images show maximum intensity projection (MIP), brightfield (BF) and fluorescence microscopy images with LifeAct-GFP (green, actin) of stably transfected enteroids after blasticidin treatment. Scale bar: 100 μ m.

III.4.3.3. Analysis of intestinal organoids microinjected with *Salmonella*

Fluorescence microscopy of human organoids microinjected with Salmonella

One challenge in using organoids to study pathogen-host interactions is the difficulty in accessing the apical, or luminal, surface of the epithelium, which is enclosed by the organoid cell layer. Infection of 3D cultured organoids with *Salmonella* by microinjection is a method to allow apical invasion of the pathogenic bacteria to mimic *in vivo* conditions. Microinjection with a glass micropipette is used to enable *Salmonella* to invade the apical side. Often, not fully differentiated organoids with crypts are used, but mostly round shaped spheroids in early cultivation because microinjection is much easier with these.

Figure III.4.10 shows an exemplary image of a 3D human colonoid microinjected with STM WT carrying a plasmid for constitutive expression of GFP. For microinjection, a fluorescence microscope was used to control injection of STM (Figure III.4.10 B). STM were visible inside the glass micropipette and the round shaped organoid but also leaking out of the injection side. Microinjected human colonoids were fixed for fluorescence imaging, detached, stained with DAPI, phalloidin and CellMask and mounted on microscope slides. Multiple small round shaped organoids were visible as well as a large organoid with approximately 350 μ m in diameter (Figure III.4.10 A). Some STM were visible outside of the organoid and at the basolateral side. A large number of poorly visible individual STM were dispersed in the organoid lumen. At the injection site, tissue damage could be detected as well as a huge accumulation of STM. Invasion sites could not be analyzed in detail because of the tissue damage that occurred during microinjection and the staining and embedding steps. Also, the flattening of the organoid due to mounting on microscope slides hamper the determination of individual infection sites at the bacterial-cell contact site.

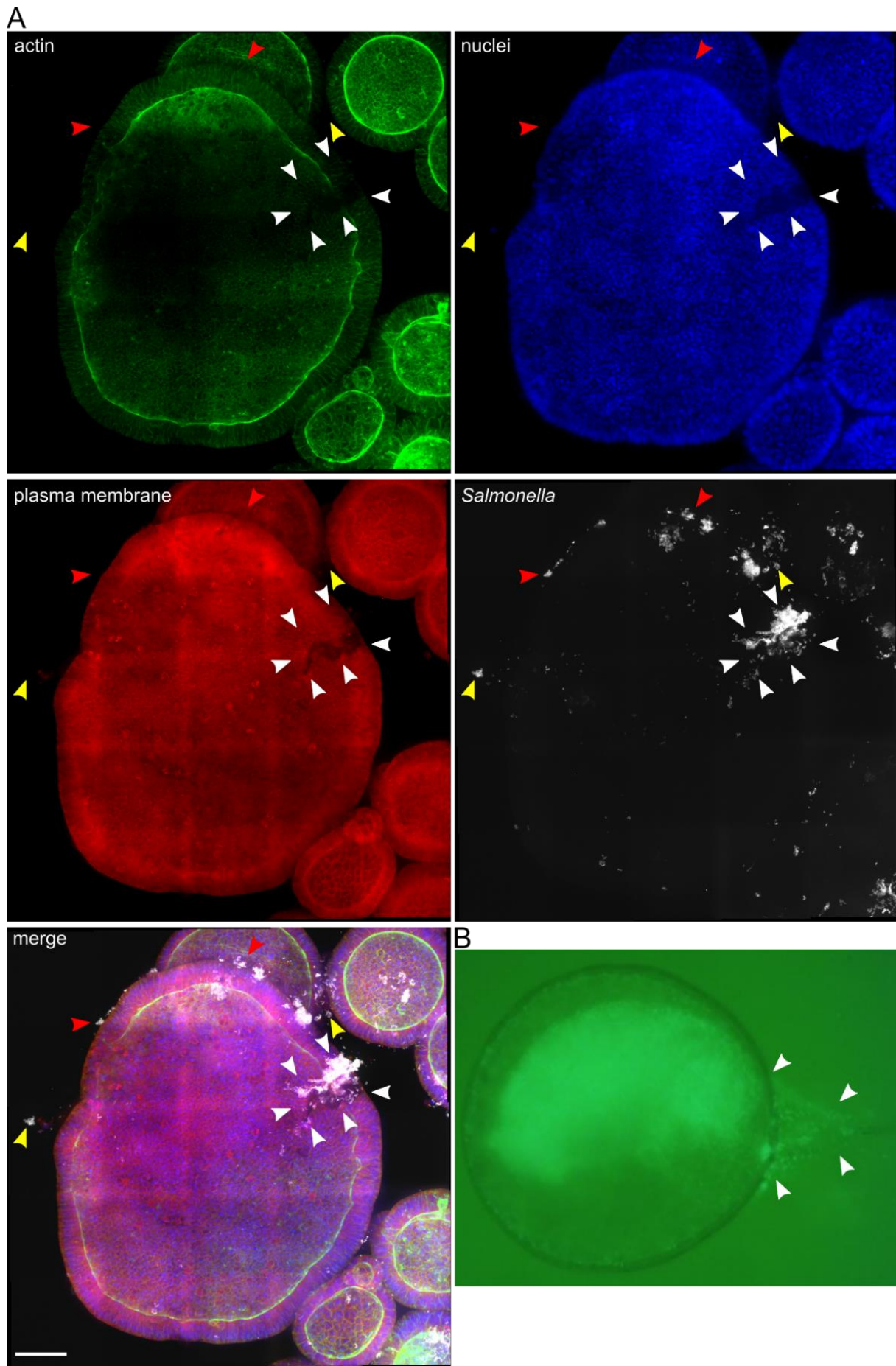


Figure III.4.10. Fluorescence imaging of 3D human colonoid microinjected with *Salmonella Typhimurium*. A) Human colonoids were microinjected with STM WT expressing GFP (white), fixed at 1-1.5 h p.i. and stained with phalloidin-iFluor647 (green), DAPI (blue) and CellMask Deep Red (red) before imaging. Arrowheads indicate STM at injection site inside and outside of the organoid (white) and with and without direct contact to basolateral side of the enteroid (red, yellow, respectively). Images are shown as maximum intensity projection. Imaging with 40x objective. Multiple images with overlaps were acquired and stitched. Scale bar: 50 μm . B) Exemplary image of microinjection process with STM WT expressing GFP (green). Arrowheads indicate injection site with STM leaking off the lumen.

TEM analysis of murine and human organoids microinjected with Salmonella

Murine organoids were fixed 60 to 90 min p.i. with STM WT. The organoid shown in Figure III.4.11 possessed a diameter of approximately 330 μm . It had a round shape and consists of a mixture of monolayers and multilayers, some with different cell types (Figure III.4.11 B), surrounding a large, central lumen (Figure III.4.11 A, B). Both, in the lumen and outside of the organoid, a multitude of *Salmonella* were visible (Figure III.4.11 A, B, C). While there were no microvilli on the basolateral side of the cells, a large amount can be detected on the apical side (Figure III.4.11 E), where also some invading *Salmonella* could be observed (Figure III.4.11 C - F). Two bacteria were already completely enclosed by the plasma membrane of the host cell, and were located in a SCV in the distal area of the cell (Figure III.4.11 C - D). At another site of the organoid, the *Salmonella* were only half-enclosed by the host membrane (Figure III.4.11 E, F). In both cases, however, much of the microvilli around the invasion site were effaced and the cell showed an extensive membrane ruffle around the bacteria (Figure III.4.11 D - F), similar to previously described membrane ruffles in polarized cell culture models (Gerlach *et al.*, 2008).

In another murine organoid, *Salmonella* had already fully invaded both from basolateral and apical side and were located in an area near the nucleus, and possess a SCV (Figure III.4.12). Possibly, due to the embedding protocol, the SCV were no longer completely preserved. It seems that in this organoid sample mainly basolateral invasion happened. A high number of *Salmonella* and also most of the invasion events were detected at the basolateral side, which could indicate that invasion happened primarily at this side (Figure III.4.12 A).

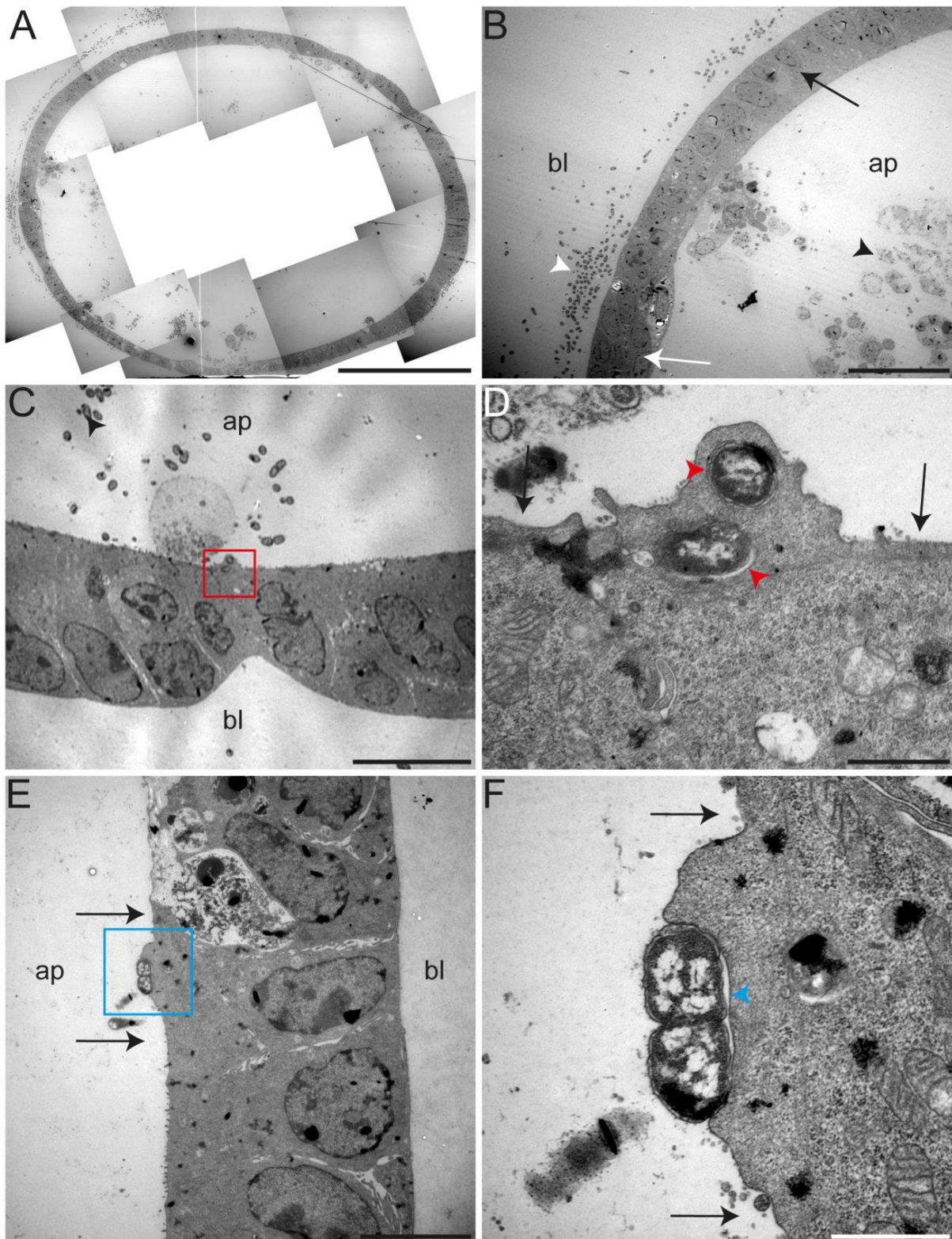


Figure III.4.11. TEM images of a murine colonoid microinjected with *Salmonella Typhimurium*. Murine colonoids were microinjected with STM WT and fixed for TEM 1-1.5 h p.i. A) Overview image of the murine colonoid. B) Magnified area from (A) showing presence of STM on the basolateral side (bl) outside of the organoid (white arrowhead), the monolayer (black arrow) and multilayer (white arrow) surrounding the lumen (ap), and the cellular debris located in the lumen (black arrowhead). C) Section of the cell layer surrounding the lumen. Some STM are located on the apical side (ap) (black arrowhead); bl (basolateral). D) Detailed view of two invading STM with SCVs partially present (red arrowheads) and microvilli effacement (black arrows). E) Section of cell layer of an intestinal organoid showing apical (ap) and basolateral (bl) sides and absence of microvilli (black arrows). F) A detailed view shows dividing

invading STM that trigger membrane protrusion but that have not yet formed an SCV (blue arrowhead). No microvilli are present in the vicinity of the invasion site (black arrows). Scale bars: 100 μm (A), 25 μm (B), 10 μm (C), 1 μm (D, F), 5 μm (E).

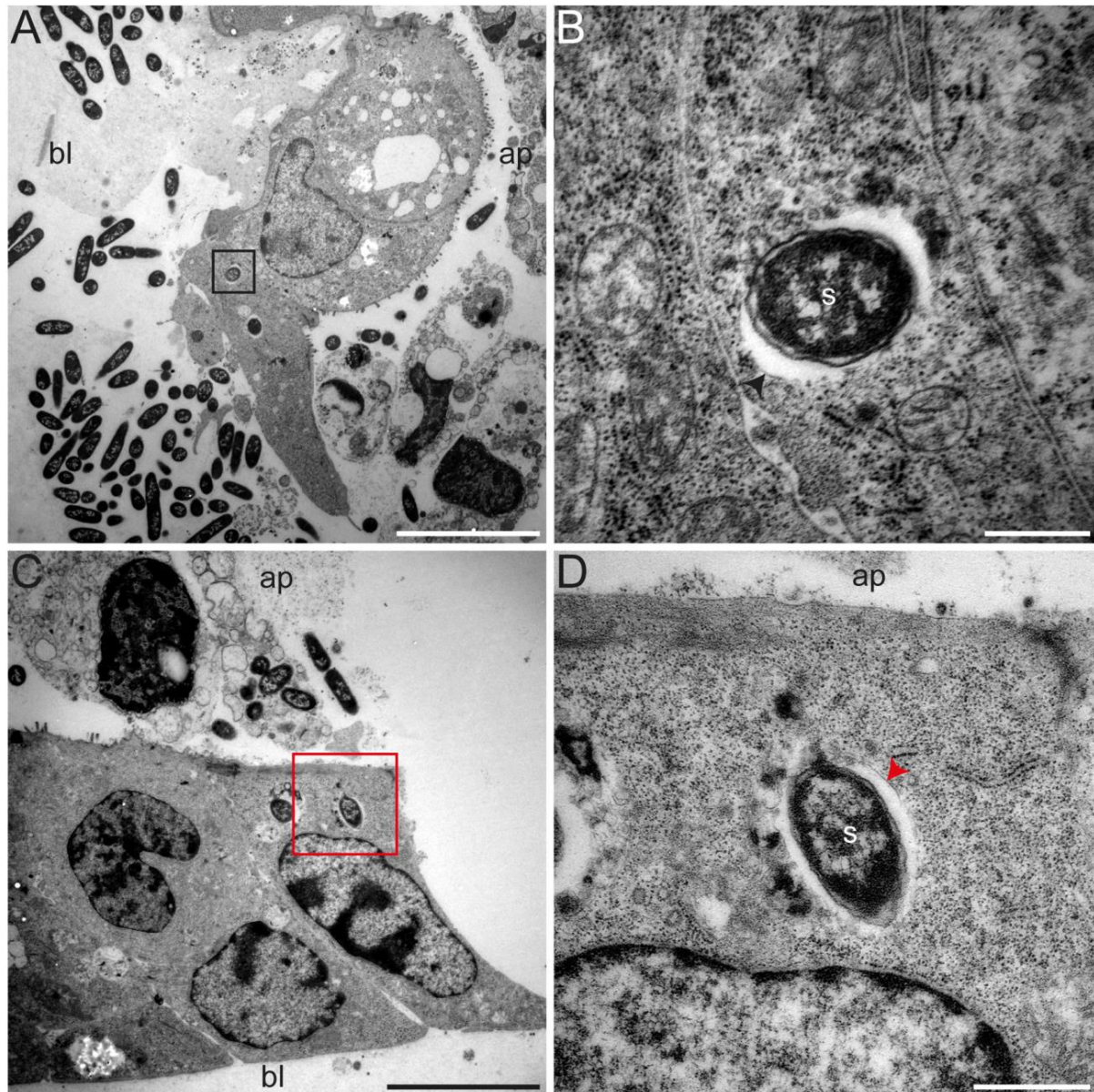


Figure III.4.12. TEM images of a murine colonoids microinjected with *Salmonella Typhimurium*. Murine colonoids were microinjected with STM WT and fixed for TEM 1-1.5 h p.i. A) Overview image of the murine colon organoid showing apical (ap), basolateral (bl) side and several intracellular STM, one is located near the nucleus (black box). B) Detailed view from A shows STM (s) is located within an SCV with a single membrane (black arrowhead). C) Overview image from another area of the organoid showing apical (ap) and basolateral (bl) sides, as well as intracellular STM on the basolateral side near the nucleus. D) Detailed view from C showing intracellular STM (s) enclosed by an SCV with a single membrane (red arrowhead). Scale bars: 7 μm (A), 500 nm (B), 5 μm (C), 750 nm (D).

The human intestinal organoids were microinjected as mentioned above, but they were fixed for TEM already 30 min after injection. The organoid shown in Figure III.4.13 A had a diameter of approximately 540 μm at its widest point, and again *Salmonella* were present both outside (Figure III.4.13 A) and inside of the organoid (Figure III.4.13 E). With an alternation between monolayer and multilayer, with partly different cell types, a similar organization as in the murine variant was observed (Figure III.4.13 B). Several invading *Salmonella* could be recognized, which just contact the host cell membrane, so that a membrane ruffle was formed (Figure III.4.13 G, I). In the posterior part of this protrusion, fine elongated structures could be observed, which have morphological similarity to cytoskeletal components (Figure III.4.13 G). In close vicinity to the invading *Salmonella*, small round structures were visible and the microvilli of the apical side of the cells were still present (Figure III.4.13 I). Furthermore, *Salmonella* were observed to be located, together with other materials, in an electron-light compartment enclosed by a membrane (Figure III.4.13 F).

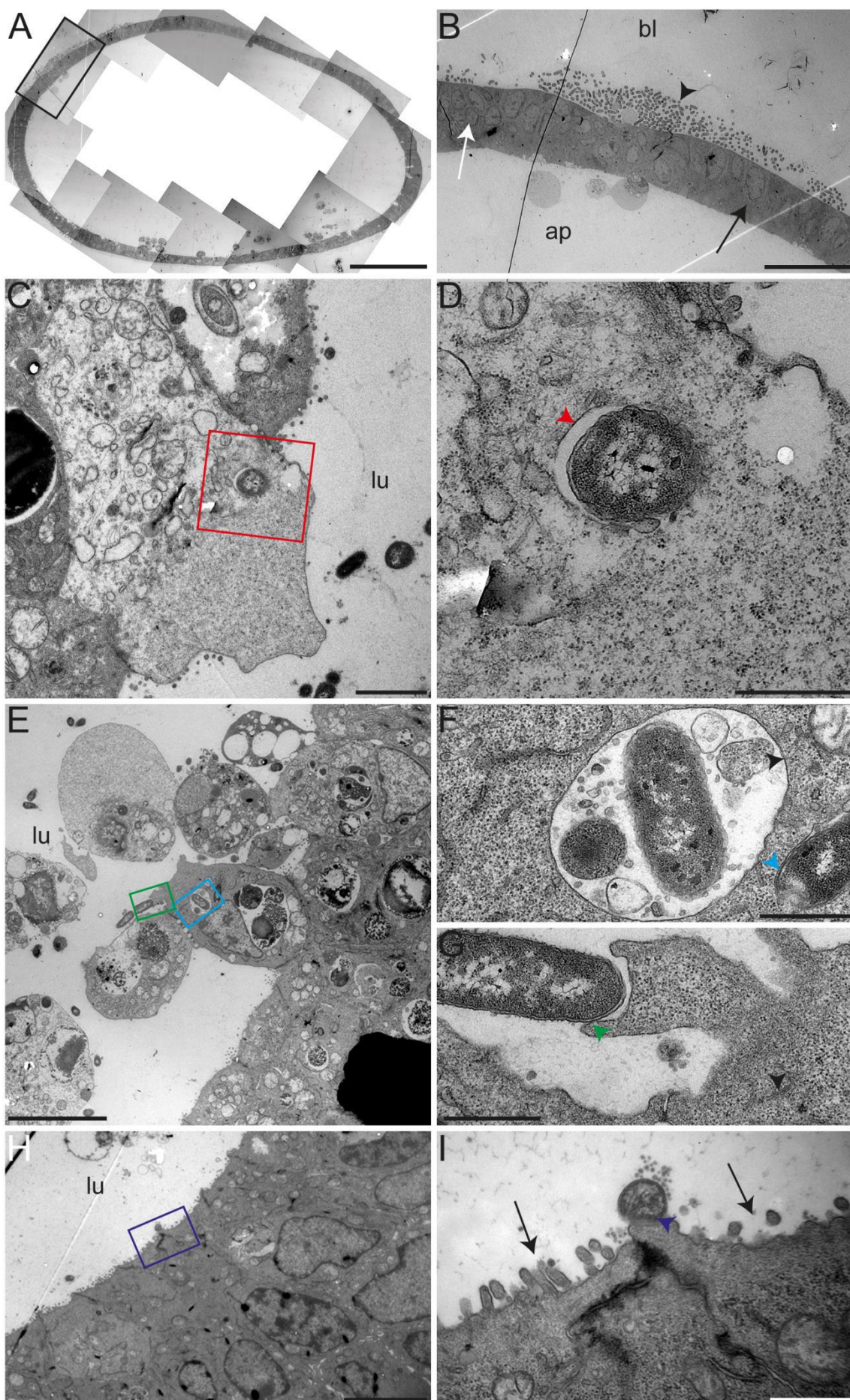


Figure III.4.13. TEM images of a human colon organoid microinjected with *Salmonella Typhimurium*. Human colonoids were microinjected with STM WT and fixed for TEM 30 min p.i. A) Overview image of the human colon organoid. B) Magnified area from (A) shows presence of STM (black arrowhead) on the basolateral (bl) side, the apical (ap) side, and the monolayer (black arrow) and multilayer (white arrow) surrounding the lumen. C) Overview of a possibly apoptotic cell with intracellular STM near the lumen (lu). D) Detailed view of STM from C shows enclosure within an SCV with a single membrane (red arrowhead). E) Detail of another area of the organoid showing cells in the luminal region (lu). F, G) Detail from E. F) Detail of two STM located along with other unknown structures within a single membrane compartment (black arrowhead) and STM in an SCV (blue arrowhead). G) A close-up shows STM in contact with a membrane protrusion (green arrow), but not invaded. H) Overview of a part of the cell layer of the organoid. I) Detailed view of invading STM with contact to a membrane protrusion (purple arrow) and surrounding microvilli (black arrows). Scale bars: 100 μm (A), 25 μm (B), 3 μm (C), 750 nm (D, F, G, I), 7 μm (E), 5 μm (H).

III.4.3.4. Generation of apical-out intestinal organoids

Another method to infect 3D organoids without physical injury is the generation of apical-out organoids (Co *et al.*, 2019). The reversal of the polarity of 3D organoids enables analyses of pathogen-host interactions at the apical side without microinjection. For the generation of apical-out organoids, murine enteroids were cultured as regular for 7-10 days in Matrigel. These normal 3D basal out enteroids were dislodged and solubilized to remove the Matrigel. The solubilized enteroids were re-seeded in medium without Matrigel in low-attachment plates or with a minimal amount of Matrigel to immobilize the organoids at the bottom of the chambered coverslips. In first attempts, mostly enteroids with mixed polarity could be observed (Figure III.4.14 A, B). Mixed-polarity enteroids were fixed and stained with DAPI, phalloidin and CellMask whereas high F-actin signal indicates the apical side. In cross-sections of mixed polarity enteroids both apical-out and basal out areas were visible (Figure III.4.14 A'). The formation of apical-out organoids is highly heterogenic; however, it allows to infect multiple 3D organoids directly within the medium without microinjection.

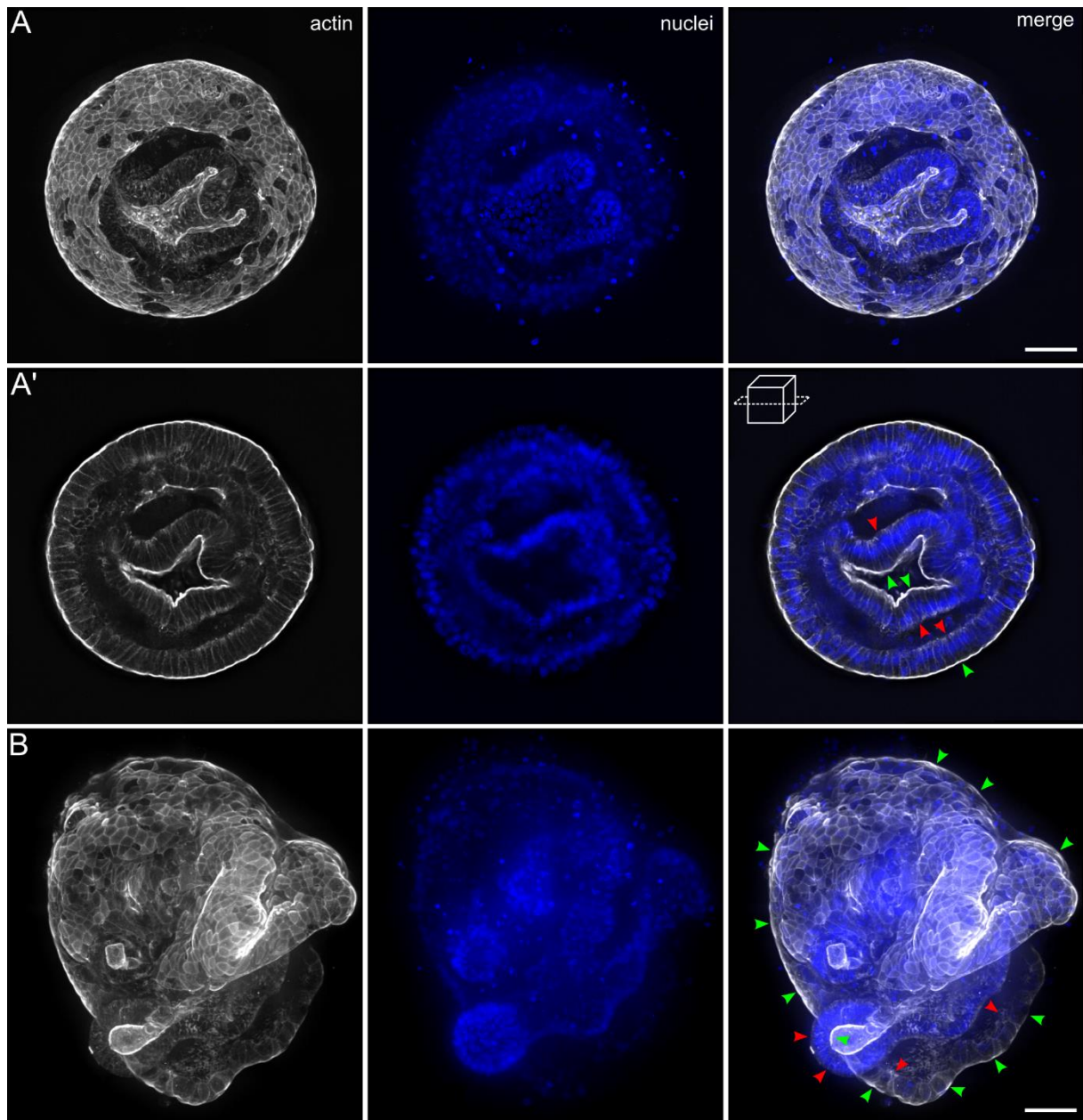


Figure III.4.14. Fluorescence imaging of 3D apical-out enteroids. Maximum intensity projection (A, B) and cross-section (A') of induced mixed polarity murine ileum organoids. Murine ileum organoids were cultured with minimal amount of Matrigel. Arrowheads indicate apical (green) and basal (red) regions. Cultivation, fixation and staining with phalloidin-iFluor647 (white) and DAPI (blue) in μ -slide chambered coverslip before imaging. Imaging with 40x objective. Multiple images with overlaps were acquired and stitched. Scale bars: 50 μ m.

III.4.3.5. 2D cultivation, characterization and infection

Organoid cultivation on transwells – from 3D to 2D

In addition to 3D cultivated organoids, enzymatic dissected organoids can be seeded on a flat plastic surface or transwells (Figure III.4.15). The attachment of the organoid fragments or single cells requires coating with complex matrices, e.g. Matrigel, or gelatin, collagen or fibronectin (Aguilar *et al.*, 2021). The complex matrix on the one hand provides a suitable coating surface, but on the other hand has several disadvantages like the presence of growth factors and other components like gentamicin with batch-to-batch variability (Aguilar *et al.*, 2021). To obtain a confluent cell layer, parameters as seeded cell number and medium composition has to be considered. With the medium composition, cell differentiation can be inhibited or induced for example. The advantages of organoid-derived monolayers are the access to the apical side without the need of special equipment. Pathogens can easily be added or removed, as well as cell debris and waste products. Additionally, due to the usually flat monolayer, microscopic analysis should be also more straightforward. Single cells can easily be analyzed by high-throughput screenings. However, cell characteristics like differentiation and intercellular connections can differ between organoids and organoid-derived monolayers (Aguilar *et al.*, 2021).

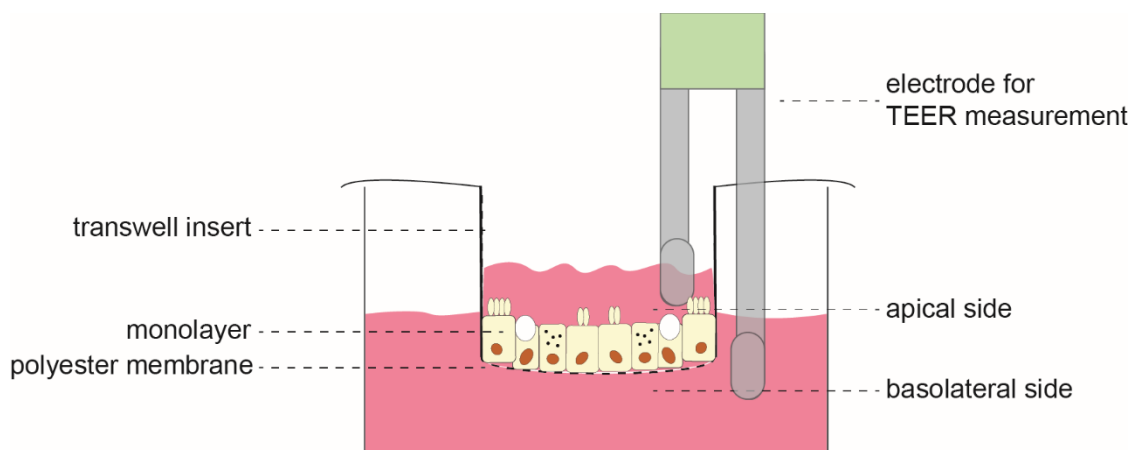


Figure III.4.15. Cultivation of organoid-derived monolayers on transwells. The organoids are enzymatically dissected and single cells are seeded on a matrix-coated membrane (here polyester). Growth is dependent on the cell number seeded, medium composition as well as the coating matrix. The cells of the monolayer have access to nutrients from both cellular surfaces, enabling a more physiological growth. To assess monolayer confluence, transepithelial electrical resistance (TEER) is measured.

Transwells or other permeable inserts can be used to get access to both sides of the epithelium, increasing the possibilities of investigations. Thus, the cells are able to take up molecules from both cellular surfaces, leading to a more physiological metabolic activity. The confluence of transwell monolayers is assessed by measuring the transepithelial electrical resistance

(TEER). The confluent layer then can be used for specific staining, e.g. PAS staining or immunostaining, and infections.

PAS staining of murine tissue and 2D cultured intestinal organoids

The periodic acid Schiff (PAS) reaction is one of the most frequently used chemical methods in histology. As unstained structures are low in contrast under the light microscope, staining with peroxide solution and Schiff's reagent increases contrast and can help to distinguish forms and structures. This method was already used for other biopsy samples and scientific approaches (Adams and Dilly, 1989; Lauren and Sorvari, 1969; Nikiforou *et al.*, 2016; Osho *et al.*, 2017; Spicer, 1960). During the PAS reaction, the samples are treated with periodic acid, resulting in the oxidation of the 1,2-glycols into aldehyde groups. Following oxidation, fuchsin-sulfuric acid (Schiff's reagent) is added to the samples, causing a reaction of the aldehydes to form a red color. Thus, this reaction yields a specific color reaction with unsubstituted polysaccharides, neutral mucopolysaccharides, muco- and glycoproteins, and glyco- and phospholipids and can be used as evidence for mucus production. We wanted to investigate potential mucus production of our human 2D monolayers (Figure III.4.16 A and B) before infection to get a better insight and result interpretation. Additionally, for comparison, we stained freshly prepared and embedded murine gut samples (Figure III.4.16 D). As a control, we performed a toluidine staining (Richart, 1963; Sridharan and Shankar, 2012) (Figure III.4.16 C). Besides nucleic acids, toluidine blue also stains mucins, amyloids and granules from mast cells and endocrine cells and is described for epoxy resin embedded thin sections (Sridharan and Shankar, 2012).

We stained the human organoid monolayers after 3 days and 11 days, directly before infection (Figure III.4.16 A and B). We were able to find smaller areas high in contrast, as exemplarily indicated. After 3 days, the amount of these spots was less than after 11 days, indicating a differentiation of the cells also in our 2D monolayers. Thus, we concluded that infections can be performed under mucus producing conditions with these cells. Additionally, we found an increased mucus production and potential goblet cells in colon monolayers in comparison to ileum monolayers. Furthermore, epoxy resin embedded thin sections of murine gut samples showed an increased signal in toluidine stain (Figure III.4.16 C) and also PAS reaction (Figure III.4.16 D). Hence, we performed infections for 30 min and 60 min and demonstrated that usage of organoid cell culture can lead to a more complex result in comparison to conventional and simpler cell culture models (Figure III.4.18).

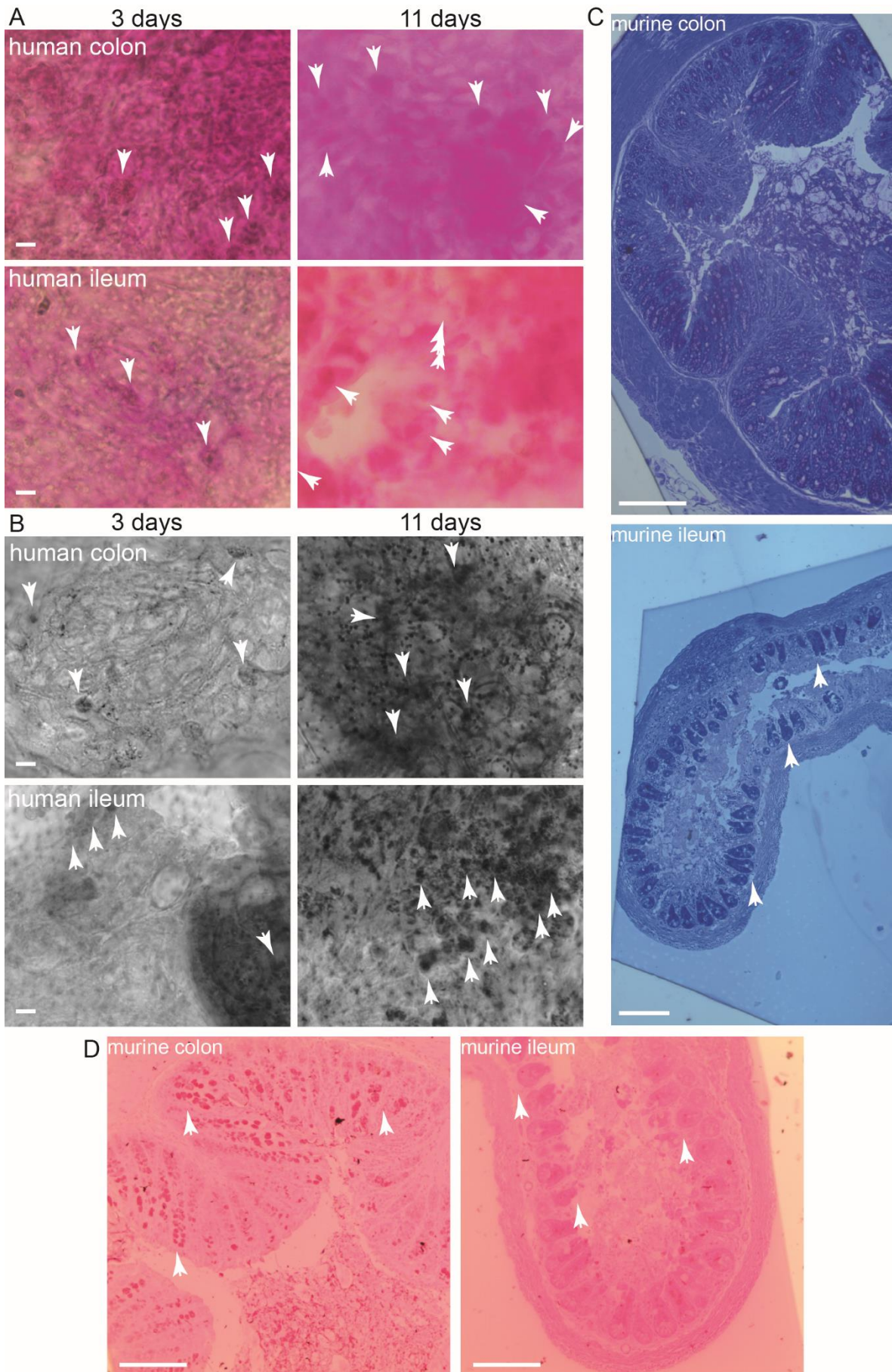


Figure III.4.16. PAS analysis of human organoid monolayer and murine biopsy samples. PAS staining of human colonoids and enteroids (A and B), as well as toluidine stained murine biopsy samples (C) and PAS stained murine biopsy samples (D). Arrows indicate stained structures. A and B) Monolayers were fixed with 3% PFA in PBS and incubated with periodic acid solution (10%). After washing, samples were incubated with Schiff's reagent. Following these preparations, the samples were fixed on microscope slides. For microscopy, 10x and 20x magnification were used, respectively. Scale bars: A) and B) 10 μm , C) 50 μm , D) 100 μm .

2D infections – TEER measurements

Various cells can be cultured on porous filters. However, due to optical properties of the filter material and cell shape, the quality of the cell monolayer is difficult to evaluate (Chen *et al.*, 2015). However, the TEER measurement can be used as an indicator of the polarization level quality for the cultivation. It is described that completely differentiated cell cultures possess a stable TEER between 500 and 1,100 Ω/cm^2 (Chen *et al.*, 2015).

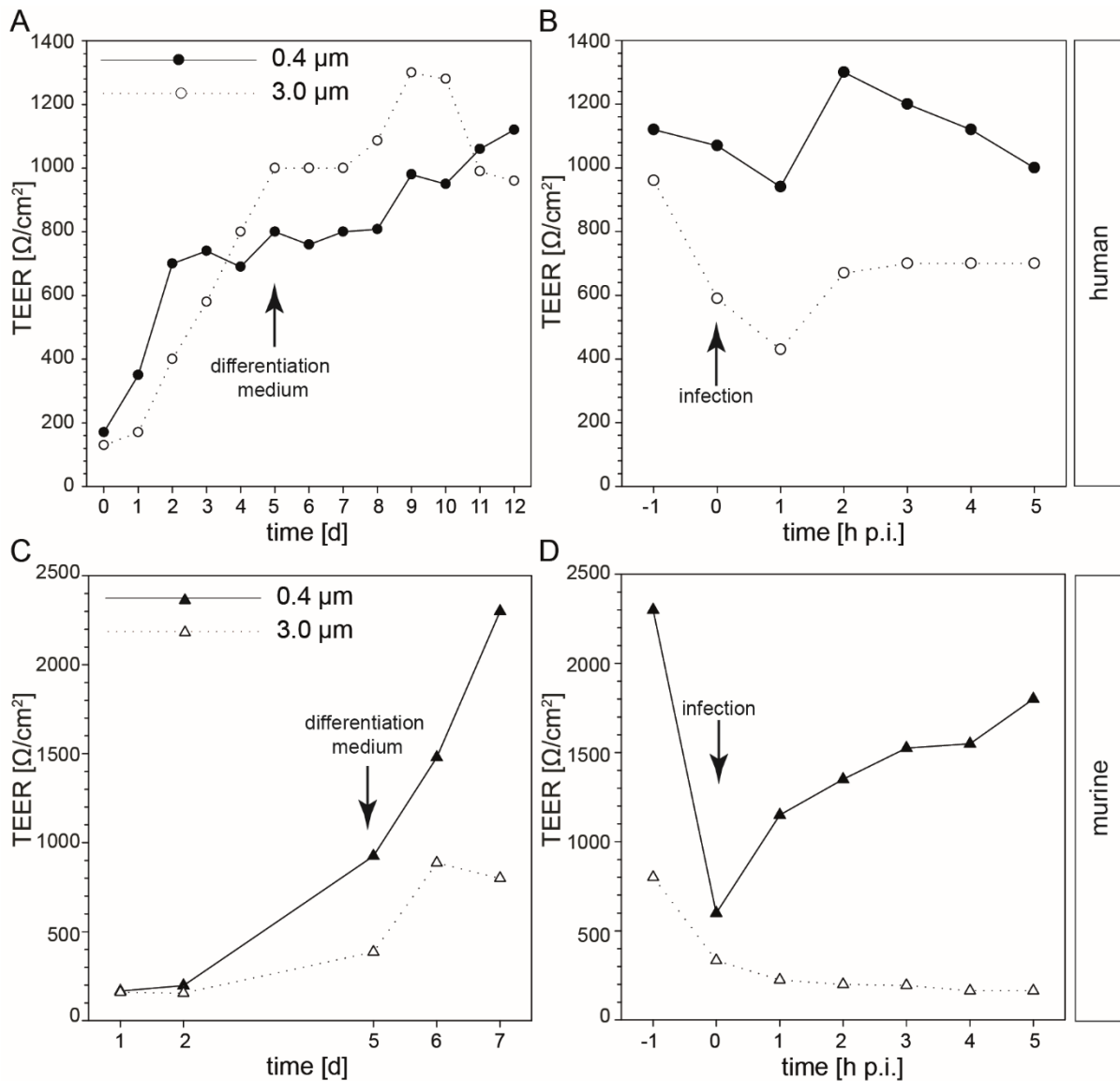


Figure III.4.17. TEER measurement during infection process of intestinal organoid monolayers. Shown are TEER measurements during growth (A, C) and infection of human- and mouse-derived monolayers (B, D). The transepithelial electrical resistance (TEER) was measured every day after seeding the cells (A) or every hour post infection (p.i.) (B). A) 1×10^5 cells/well were seeded in 2D monolayer medium at day 0. At day 5, medium was changed to differentiation medium as indicated. Monolayers were grown for 12 days before infection. B) For infection, 2.5 h subcultures of infective STM were grown and organoid monolayers were infected at MOI of 50 for 60 min. The cells were treated with 100 $\mu\text{g/ml}$ gentamicin per well for 1 h, washed three times with prewarmed PBS and incubated with 10 $\mu\text{g/ml}$ gentamicin per well for additional 4 h. C) Growth of murine-derived monolayer. Set-up as described for human-derived monolayer, with exception of 1.5×10^5 cells/well were seeded. TEER measurement as indicated. D) Infection of mouse-derived monolayer as described for human-derived monolayer.

During cultivation of our 2D monolayers of murine and human organoids, we measured the TEER daily, (Figure III.4.17 A, C) whereas during infection, it was determined every hour (Figure III.4.17 B, D), respectively. We used transwells with polyester membranes with a pore size 0.4 μm (= 0.4 μm transwell) and 3.0 μm (= 3.0 μm transwell), respectively, to investigate growth (Figure III.4.17 A) and also behavior of the cell layer during infection (Figure III.4.17 B). 3.0 μm transwells were tested, because potential exit strategies were aimed to be analyzed, allowing the bacteria to cross the filter more easily after passaging the 2D monolayer. In the first growth phase with 2D monolayer medium, TEER of human-derived monolayers increased almost exponentially from day 0 (170 Ω/cm^2) to day 3 (740 Ω/cm^2) on 0.4 μm transwells and from day 0 (130 Ω/cm^2) to day 5 (1,000 Ω/cm^2) on 3.0 μm transwells. For the mouse-derived monolayer we measured a TEER of Ω/cm^2 on 0.4 μm transwells and 387 Ω/cm^2 on 3.0 μm transwells after 5 days (Figure III.4.17 B). The growth curve of the human-derived monolayers on 0.4 μm filter flattened earlier than on 3.0 μm transwells, indicating an earlier saturation regarding cell-cell contacts and differentiation. At day 5 we changed the medium to differentiation medium and observed a saturation of the human-derived monolayers up to day 7 (1,000 Ω/cm^2) on the 3.0 μm transwells, whereas TEER of the monolayer continuously increased on 0.4 μm transwells to 1,120 Ω/cm^2 . Between day 7 and 10, TEER increased up to 1,300 Ω/cm^2 on the 3.0 μm transwells and decreased back to 960 Ω/cm^2 . Thus, on both transwells we were able to reach an optimal TEER for the human-derived monolayers, indicating a confluent and differentiated monolayer. In contrast to this, mouse-derived monolayers at day 7 with a TEER of 800 Ω/cm^2 (3.0 μm) and 2,967 Ω/cm^2 (0.4 μm) were infected (Figure III.4.17 D).

In a next step, we infected the monolayers with STM WT and measured the TEER during infection over 5 h (Figure III.4.17 B, D). Directly at the point of infection, the TEER of the monolayer on the 3.0 μm transwells decreased to 590 Ω/cm^2 (human) and 335 Ω/cm^2 (murine), whereas TEER of the monolayer on the 0.4 μm transwells remained stable at 1,070 Ω/cm^2 (human). Contrary, the TEER of the mouse-derived monolayer decreased to 820 Ω/cm^2 on 0.4 μm transwells. After 1 h, a minimum for human-derived monolayers was measured on both filters (3.0 μm : 430 Ω/cm^2 ; 0.4 μm : 940 Ω/cm^2) (Figure III.4.17 B). Whereas the TEER of the

mouse-derived monolayer on 0.4 μm transwells was slightly increasing (1,300 Ω/cm^2), TEER on 3.0 μm transwells was still decreasing until the end of the measurement (Figure III.4.17 D). At 2 h p.i. the TEER of the human-derived monolayer on the 3.0 μm transwells reached 700 Ω/cm^2 , not fully recovering to its initial value of 960 Ω/cm^2 , indicating a loss of barrier integrity. In contrast to this, the TEER of the monolayer on the 0.4 μm transwells reached a maximum of 1,300 Ω/cm^2 2 h p.i., slowly decreasing to 1,000 Ω/cm^2 after 5 h p.i., similar to the starting TEER. Thus, we concluded a full recovery of the monolayer on 0.4 μm transwells. Comparably, the TEER of the mouse-derived monolayer also increased on 0.4 μm transwells to 2,200 Ω/cm^2 , not reaching fully recovered start TEER 5 h p.i. (Figure III.4.17 D). This loss of barrier integrity and recovery during invasion of STM is already described and we concluded that the selected parameters are compatible with the chosen system and can be used for further investigations on infection of mutant strains (Figure III.4.18) and also of STY/SPA. Additionally, in combination with lentiviral transfected organoids, a microscopic analysis of the infection process and actin remodeling can be possible in a next step.

2D infections – quantification of invasion

As there are known described phenotypes regarding the SPI1 and SPI4 in cell lines as HeLa, MDCK and CaCo2 (Gerlach and Hensel, 2007; Gerlach *et al.*, 2007), in a next step we aimed to investigate the invasion of cells in human organoid monolayers. It was already shown that distinct SPI are important for different stages of infection (Gerlach and Hensel, 2007). Whereas the SPI4 and its giant substrate SiiE are essential for adhesion and invasion of polarized cells by supporting translocation of the SPI1-T3SS effector proteins, SPI4 function is not required for invasion of non-polarized cells (Gerlach *et al.*, 2008; Wagner *et al.*, 2011). In contrast to this, the SPI1-encoded T3SS is essential for a successful invasion of polarized and non-polarized cells. Thus, we decided to analyze these known phenotypes in monolayers of human enteroid- and colonoid-derived cells. As we demonstrated mucus production of the cells (Figure III.4.16), these monolayers differ from simple tumor-based cell culture lines like polarized MDCK and non-polarized HeLa cells. We infected the human monolayers for 30 and 60 min, lysed the cells, plated lysates onto agar plates and determined colony-forming units to quantify invasion (Figure III.4.18) of STM WT, $\Delta spi4$ and $\Delta invC$ strains. Because of co-regulation of the SPI with other systems, important during invasion, it was shown that *invC* deletion specifically inhibits SPI1-T3SS assembly (Gerlach *et al.*, 2008; Gerlach *et al.*, 2007).

Interestingly, we found a 9-fold higher invasion of WT of colon cells 30 min p.i. in comparison to ileum (Figure III.4.18 A), whereas invasion of colon cells was slightly lower 60 min p.i. (76.5%) (Figure III.4.18 C). At both time points and for both types of organoids, the $\Delta invC$ strain showed the most decrease in invasion compared to WT and $\Delta spi4$ (Figure III.4.18 B, D). An

exception to this is the invasion of colon cells after 30 min, indicating the essential role of the SPI1-T3SS for invasion as already described. With an invasion of 2.2% of WT (Figure III.4.18 B), $\Delta spi4$ showed an even more decreased invasion of colon cells after 30 min in comparison to $\Delta invC$ (10% of WT). Invasion of ileum cells was less influenced by a $spi4$ deletion 30 min p.i. (65% of WT) than 60 min p.i. (27.4% of WT). Thus, we concluded a higher invasion of ileum cells by the WT over time, which is not possible if $spi4$ is deleted, as invasion of ileum cells by the WT was increased 13-fold of 60 min p.i. in comparison to 30 min p.i. In contrast to this, $\Delta spi4$ invasion of colon cells 60 min p.i. was increased in comparison to 30 min infection (43.7%). Hence, we assumed that invasion of colon cells is partly possible after 1 h, even if only the SPI1-T3SS is expressed. If the SPI4-T1SS is not expressed for mediating adhesion to the apical side, SPI1-T3SS is possibly affected in the efficient translocation of the effector proteins into the host cell. Thus, we gained first insights in the SPI1- and SPI4-dependent invasion of human-derived cells 30 min p.i. and 60 min p.i., showing distinct differences and making further investigations favorable.

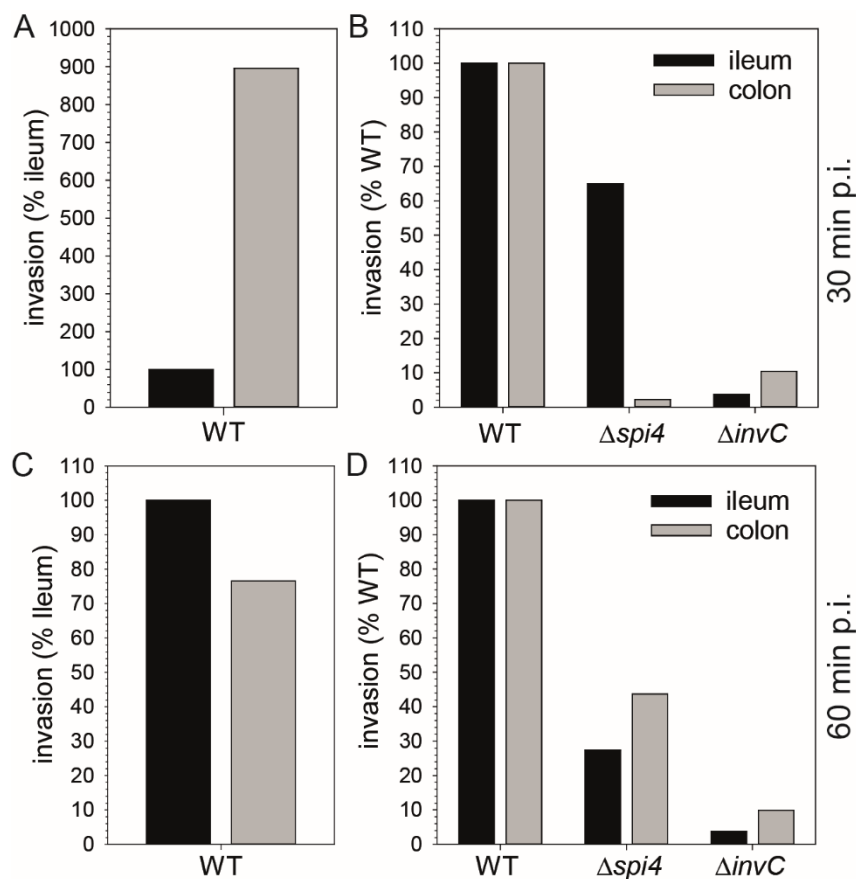


Figure III.4.18. Infection of intestinal organoid monolayers with STM. Shown are representative infections of exemplary chosen human enteroid and colonoid monolayers on 0.4 μm transwells as indicated with STM WT, $\Delta spi4$ and $\Delta invC$. Infection occurred as described above for 30 min or 60 min at MOI 50. To determine invasion, cells were treated with 100 $\mu\text{g}/\text{ml}$ gentamicin per well for 1 h, washed thrice with prewarmed PBS and lysed with 0.5% deoxycholate in PBS (freshly prepared) for 10 min. The samples of inoculum and lysates were diluted and plated to determine CFU. The percentages of invaded bacteria were calculated. A) Comparison of the invasion of ileum and colon monolayers by STM WT 30 min p.i. B) Invasion of ileum and colon monolayers by $\Delta spi4$ and $\Delta invC$ in comparison to STM WT 30 min p.i. C) Comparison of the invasion of ileum and colon monolayers by STM WT 60 min p.i. D) Invasion of ileum and colon monolayers by $\Delta spi4$ and $\Delta invC$ in comparison to STM WT 60 min p.i.

30 min p.i. C) Comparison of the invasion of ileum and colon monolayers by STM WT 60 min p.i. B) Invasion of ileum and colon monolayers by $\Delta spi4$ and $\Delta invC$ in comparison to STM WT 60 min p.i.

In conclusion, we were able to establish a way to quantify the invasion of 2D cultured intestinal organoids by STM. As the typhoidal serovars STY and SPA are pathogens that are highly adapted to the human host, analysis of these will be of great interest.

2D cultivation and infection – microscopy

Imaging of cells grown on transwells is challenging due to the high position of the cells in the well and the transwell membrane interfering with illumination. For microscopic analysis, the cell culture inserts have to be taken out of the culture well and transwell membranes have to be punched out. This makes live cell imaging nearly impossible. However, microscopy of fixed membranes, embedded on microscope slides or taped on SEM stubs is possible and analysis is described below.

After fixation and preparation of 2D cultured intestinal organoids for SEM, monolayers could be analyzed in highest magnification (Figure III.4.19). Ultrastructural analysis of monolayers of human colon, human ileum and murine ileum organoids show adjacent growing cells with a densely packed apical brush border that is also intact at the cell borders (Figure III.4.19A, B, C, D). A detailed view of the brush border shows microvilli in a high order with almost identical length (D). Some areas of the monolayer show higher heterogeneity regarding the morphology of cells (Figure III.4.19 E, E'). This may indicate the successful cultivation of distinct cell types, e.g. goblet cells that possess less microvilli on their apical side and a large secretion pore on their apical side in the center of the cell. (Figure III.4.19 E') similarly shown in the side-view TEM image above (Figure III.4.6 B).

Monolayers infected with STM and SPA WT were also analyzed (Figure III.4.20). The *Salmonella*-induced rearrangement of the actin cytoskeleton into membrane ruffles during the invasion process has been studied in detail in our lab (Gerlach *et al.*, 2008; Kommnick and Hensel, 2021; Kommnick *et al.*, 2019; Lorkowski *et al.*, 2014). We identified *Salmonella*-induced membrane ruffles at adhesion and invasion sites on 2D cultured murine enteroid-derived monolayers (Figure III.4.20). STM WT induced the formation of small membrane pedestals at adhesion sites (Figure III.4.20 A) and small bulky membrane ruffles at invasion sites with multiple bacteria inside (Figure III.4.20 B, B', B''). First infection experiments with human-adapted typhoidal SPA showed less invasiveness and almost no invasion sites at cells with dense brush border. Membrane ruffles were only observed at cell borders and cells largely lacking microvilli (Figure III.4.20 C, C').

Fluorescence microscopy of STM-infected monolayers was performed (Figure III.4.21). The murine enteroid monolayers show adjacent growing cells with high F-actin accumulation at the apical site, indicating a densely packed brush border. Multiple invasion sites with microvilli effacement are visible at low and high magnification (Figure III.4.21 A, B, C).

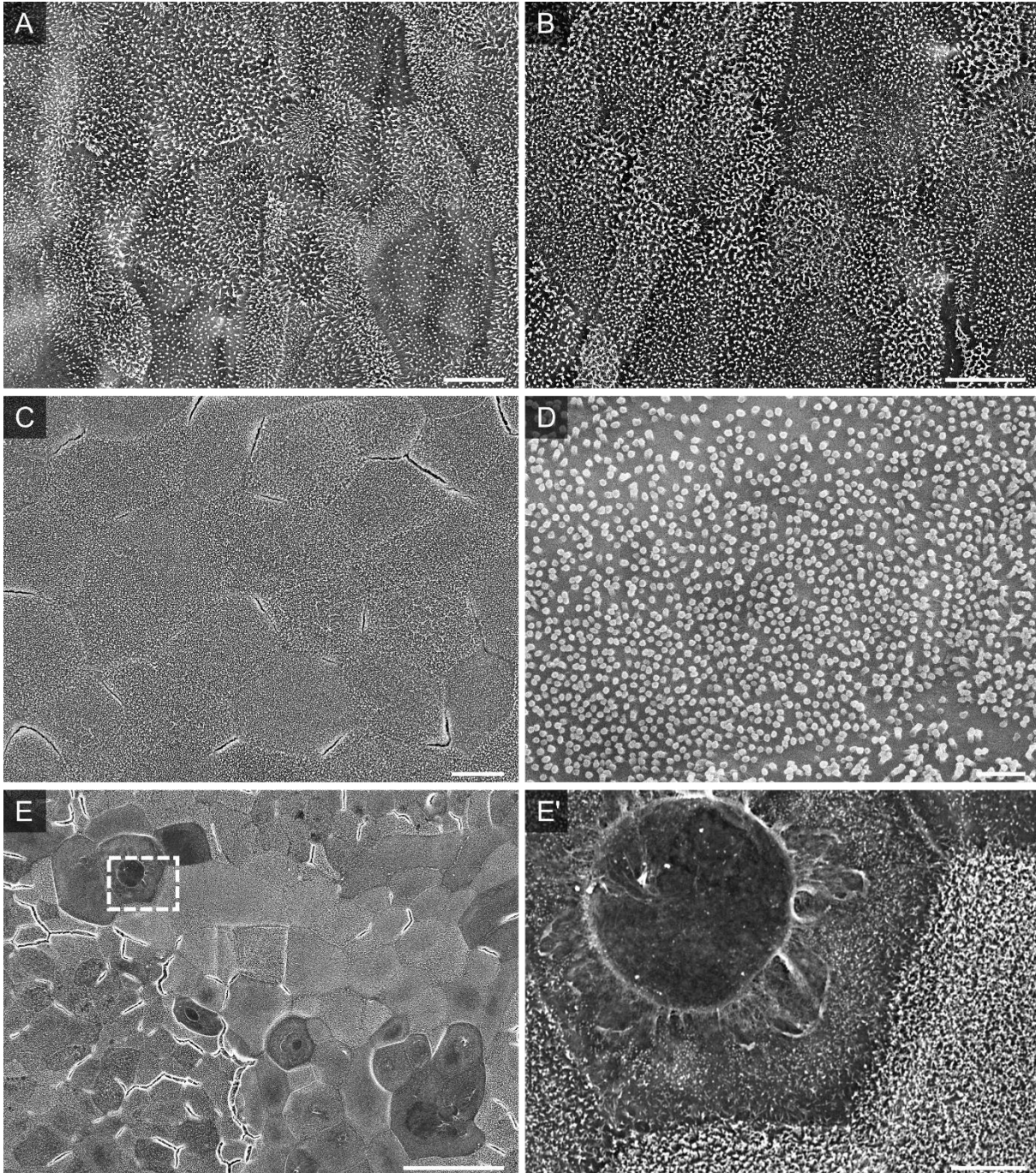


Figure III.4.19. SEM imaging of 2D cultured organoids. Organoids were cultured on transwell cell culture inserts and fixed for SEM. Overview of 2D cultured human colon (A), human ileum (B) and murine (C, D, E, E') enteroids. Inset (E') shows a possible goblet cell. Scale bars: 10 μm (A, B, C), 50 μm (E), 1 μm (E').

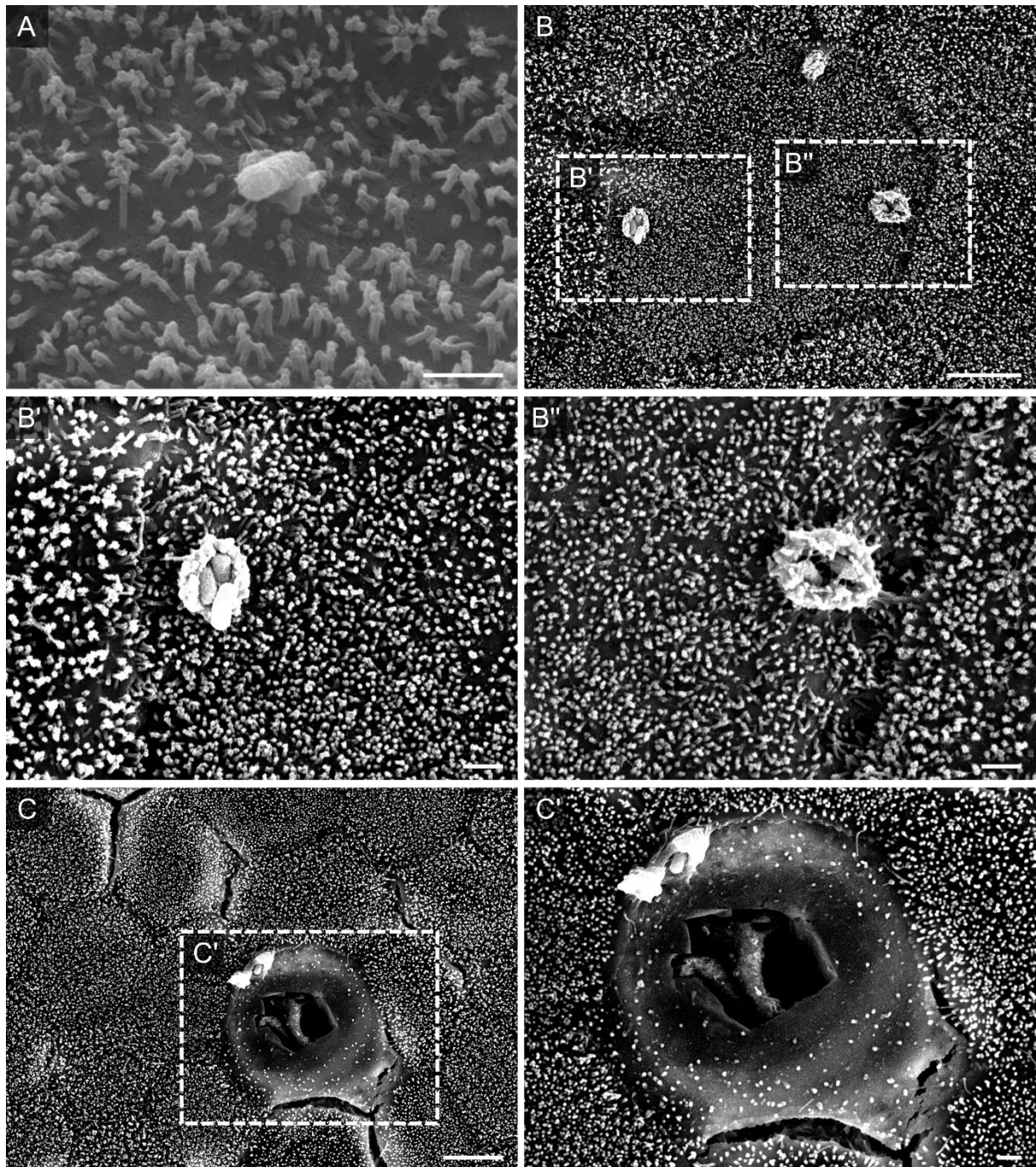


Figure III.4.20. SEM imaging of 2D cultured STM and SPA infected organoids. Murine ileum enteroids were cultured on transwell cell culture inserts and fixed 30-60 p.i. for SEM. Adhesion (A) and invasion sites (B, B', B'') of STM WT on apical side of enterocytes. Invasion site of SPA WT at a cell with less prominent brush border (C, C') Scale bars: 1 μm (A, B', B'', C'), 5 μm (B, C).

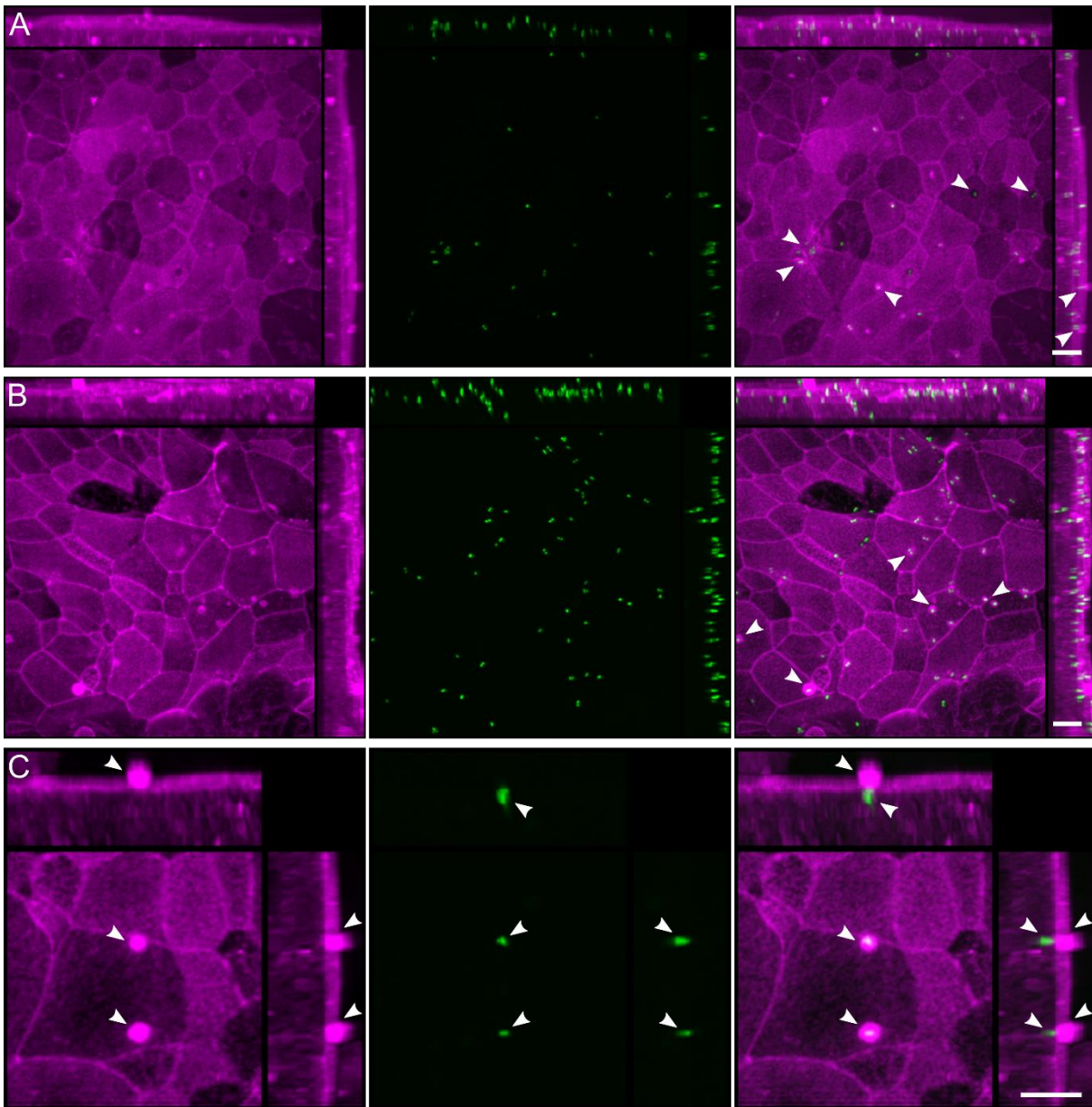


Figure III.4.21. Fluorescence imaging of 2D cultured STM infected organoids. Murine ileum enteroids were cultured on transwell cell culture inserts and fixed 30-60 min p.i. for fluorescence microscopy and stained with phalloidin-iFluor647 for actin visualization (magenta). Adhesion and invasion sites of STM WT expressing GFP (green) on apical side of enterocytes with membrane ruffles are indicated with arrowheads. Images are shown as maximum intensity projection of X-Y, X-Z and Y-Z plane. Scale bars: 10 μm .

All in all, we established intestinal organoids in 2D and 3D as infection models for *S. enterica*. Here, we demonstrated a wide range of methods, possible to use for investigation of STM and SPA infection.

III.4.4. Discussion

Frequently used cell culture models were over several years the tool to unravel virulence mechanisms in host-pathogen interactions. However, the experimental design was restricted to one cell type for most of the cell culture-based assays. While it was possible to investigate cellular interactions of pathogens with high temporal and spatial resolution, these experiments lacked complex tissue architecture and were not suitable to reflect *in vivo* relevant settings. Most recently, organoid systems have been established in a wide field of biological research, including infection biology. Stem-cell derived organoids are capable to reconstitute a certain degree of multicellular complexity with a close relation to *in vivo* conditions in a 3D environment. But still, organoid culture remains complex, expensive and time consuming with some issues in reproducibility between labs because of the highly heterogenic nature.

The results presented here show uninfected and infected 3D and 2D grown organoids of human and murine origin that were labeled and imaged across scales as well as analyzed regarding their behavior during infection. Organoids are difficult to image because of their dimensions in X, Y and Z. Imaging in Z is limited, which is dependent on working distance, parfocal length and numerical aperture of the used objectives and the wavelength of light used to illuminate the specimen (Figure III.4.3). SDCM of 3D organoids revealed the overall architecture with enterocytes facing inward with their apical side but imaging of higher Z planes resulted in blurry images with loss of focus and high background (Figure III.4.4). The penetration depth of confocal microscopy is roughly limited to less than 100 μm (Graf and Boppart, 2010). Multiphoton microscopy can improve penetration depth at least 2-fold (Centonze and White, 1998), but lateral resolution is worse and it may lead to photo toxic and bleaching effects due to higher light intensities (Hopt and Neher, 2001). Recently developed methods like light sheet-based microscopy offer live cell imaging well suited for large specimens with more photons and less photo damage (Reynaud *et al.*, 2008). Dipping objectives could be used to reduce distance to specimens (Rakotoson *et al.*, 2019). Matrigel may interfere with fluorescence excitation and emission and may result in higher background.

Better resolution and less background can be achieved by releasing organoids from Matrigel and mounting them on microscope slides (Figure III.4.5). This method may simplify imaging approaches but could create artefacts because of the treatment of the organoids. Detachment and preparation with multiple staining and washing steps in solution could damage the specimens. Large, complex organoids may disrupt during this procedure and in result, only round shaped spheroids are being analyzed. Flattening of the organoids between coverslip and microscope slide can also falsify the interpretation of infection sites. However, imaging of organoids mounted on microscope slides allows analyses of cell structures in more detail.

Immunostaining and other labeling techniques are commonly used to identify structures of interest. Also in the context of organoids as infection model, these methods can help to shed light on the cell types important in infection processes. Frequently used antibodies and fluorescent probes are e.g. villin (polarized epithelium), mucin 2 (goblet cells), MMP7 (Paneth cells), chromogranin A (enteroendocrine cells), Ki67 (dividing cells), lysozyme (Paneth cells), ZO1 (tight-junctions), wheat germ agglutinin (goblet cells, Paneth cells, mucus), ulex europaeus agglutinin I (goblet cells, Paneth cells, mucus, M cells), phalloidin (F-actin) and also histological staining like PAS are used to determine certain cell types and structures (Broguiere *et al.*, 2018; Farin *et al.*, 2016; Fatehullah *et al.*, 2013; Noel *et al.*, 2017a, b). Through WGA staining we also could identify regions of interest with secretory granules inside cells and mucus in crypt domains in enteroids and colonoids as well as the general structure with a combination of phalloidin, DAPI and CellMask staining (Figure III.4.7). However, it was difficult to analyze staining with first and secondary antibodies due to high background. The used methods have to be improved for further experimental procedures. Flow cytometry, especially if combined with reporters that provide information about the physiological state of *Salmonella* (SPI1-T3SS & SPI2-T3SS activity, induced stress, and metabolic pathways), could also represent a powerful tool to investigate cell types targeted by *Salmonella* in single cell-based studies (Reuter *et al.*, 2021; Röder *et al.*, 2021a, b; Schulte *et al.*, 2021a, b).

To investigate infection processes in organoids, it is crucial to allow pathogens access to the apical side of organoids. One of the techniques to facilitate that is the microinjection of pathogens into the lumen of the organoids. This method has been used successfully with *Helicobacter pylori*, *Clostridium difficile*, *Escherichia coli*, *Salmonella enterica* and even SARS-CoV-2 (Aguilar *et al.*, 2021; Bartfeld and Clevers, 2015; Hentschel *et al.*, 2021; Lamers *et al.*, 2021; Ramirez-Flores and Knoll, 2021; Tindle *et al.*, 2021). Technical limitations such as the highly heterogenic nature of organoids and the labor- and cost-intensive infection are drawbacks of this method. Further, the penetration with an injection needle can damage cell layers and spillage of pathogens into the medium could favor unwanted infections at the basal site of the organoid. Our microinjection experiments showed exactly these injuries at the injection site (Figure III.4.10) and *Salmonella* infection sites at the basolateral side of intestinal organoids (Figure III.4.10, Figure III.4.11, Figure III.4.12, Figure III.4.13). We could observe *Salmonella*-containing compartments in microinjected intestinal organoids (Figure III.4.11, Figure III.4.12, Figure III.4.13) with a localization near the nucleus as described before (Abrahams and Hensel, 2006; Salcedo and Holden, 2003) and in an electron-light- compartment which probably represents a phago-lysosome with subsequent degradation of the pathogen (Buchmeier and Heffron, 1991; Carrol *et al.*, 1979). Due to the early fixation time points, no *Salmonella*-induced tubular structures such as SIF could be observed (Krieger *et al.*, 2014; Yin and Zhou, 2018a,

b). Krieger *et al.* (2014) described these tubular structures in detail with a CLEM approach in epithelial cell culture. However, no CLEM compatible methods have been yet developed for such large specimens as organoids.

Another method to circumvent physical injury of the organoids is the addition of the pathogens directly to the culture medium. To prevent infection processes from happening at the basolateral side it is possible to control the epithelial polarity to generate apical-out organoids (Co *et al.*, 2019; Co *et al.*, 2021) (Figure III.4.22). We were indeed able to reproduce this recently published method to generate organoids with mixed polarity (Figure III.4.14). As in all the other 3D-based methods, the generated apical-out organoids are highly heterogenic which could hamper experimental design and reproducibility. However, apical-out organoids could represent a possibility of a 3D infection model without the drawbacks of microinjection.

All the 3D-based methods described above are difficult to combine with live cell imaging techniques. Lentiviral transfected organoids may help to develop live cell imaging approaches in the future (Maru *et al.*, 2016). Interpretation of fixed samples is often hard to analyze e.g. time and location of invasion sites (apical or basal side) and also fixation with aldehydes may interfere with surface structures such as mucus. It was also reported that invasion of *Salmonella* is higher in secretory cells, but for some methods as microinjection, not fully differentiated spheroids are utilized which possess only a low number of these cell types (Gagnon *et al.*, 2013; Yin and Zhou, 2018a, b). TEM analyzes are also challenging due to the sheer size of the specimen with several hundred micrometers in contrast to the ultrathin sections with a thickness of about 70 nm used for TEM. Also interactions with cell debris that accumulates inside of 3D organoids. Newly developed organoid-on-a-chip models could represent a future technique to address this issue, even in combination with a defined microbiota applied to the organoid tissue (May *et al.*, 2017; Wang *et al.*, 2021).

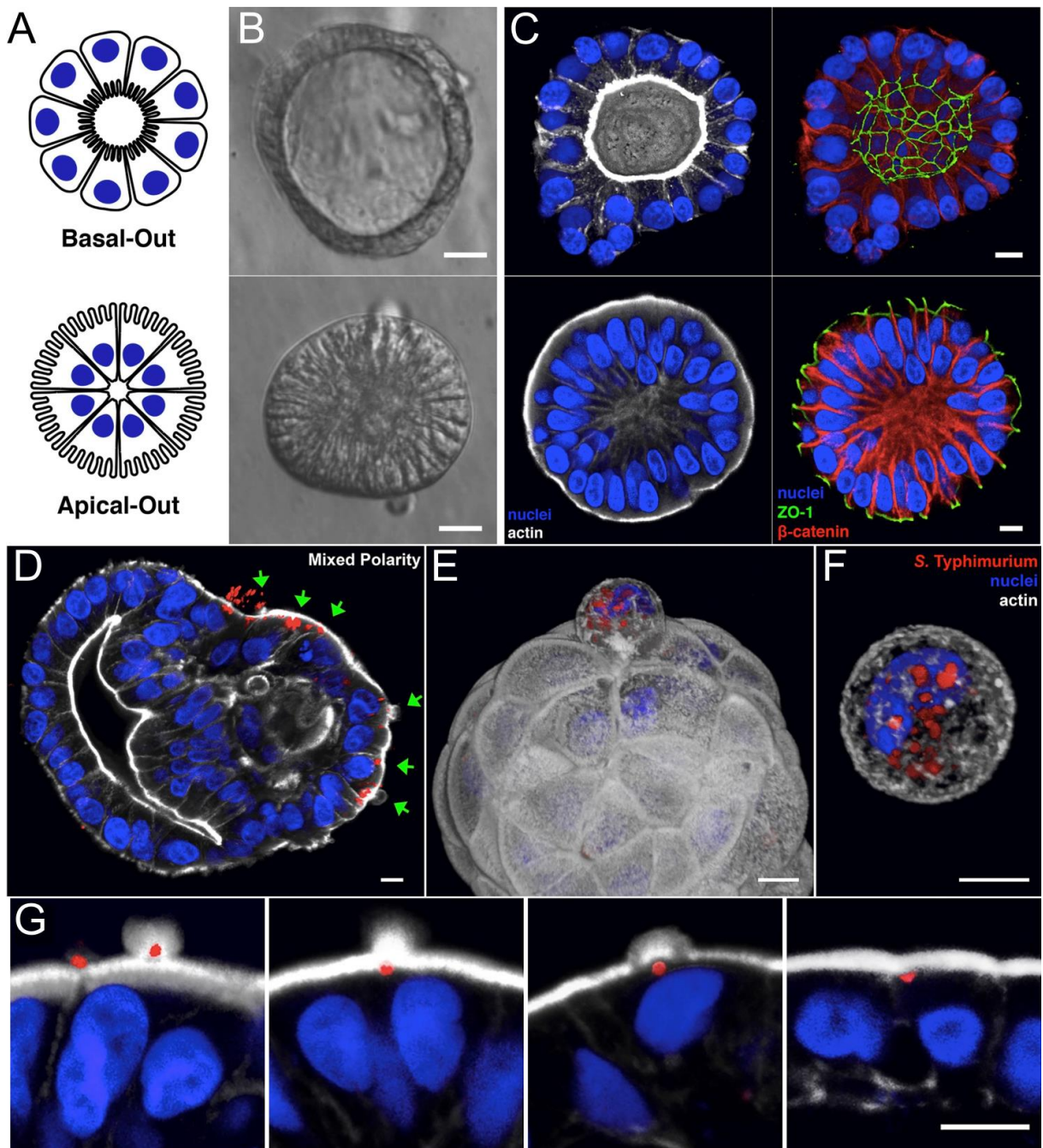


Figure III.4.22. Generation and Infection of apical-out enteroids. A-E) Basal-out enteroids and apical-out enteroids are depicted schematically (A), imaged using modulation contrast microscopy (B) and imaged using confocal microscopy (C). D) STM selectively invades the exposed apical surface (green arrows) of a mixed polarity enteroid. E-F) 3D confocal reconstruction of STM within an epithelial cell in the process of extruding from the apical enteroid surface (E) or within a fully extruded cell after 6 h of infection (F). G) STM at different stages of invasion of apical-out enteroid. Nuclei in blue, actin in white, ZO-1 in green, β -catenin/STM in red. Scale bars 10 μ m (B, C). Figure adapted from Co *et al.* under CC BY license.

To investigate host-pathogen interactions, organoid-derived monolayers can have many advantages in comparison to 3D organoids as they provide access to the apical side of the cells (Aguilar *et al.*, 2021). Thus, pathogens, debris and solutes can be added or removed and a

microscopic analysis is even better possible and single cells can be analyzed by high-throughput screening. 2D monolayers were already successfully used for analysis of infections, including *Helicobacter pylori* (Bartfeld and Clevers, 2015; Boccellato *et al.*, 2019; Schlaermann *et al.*, 2016), *Escherichia coli* (VanDussen *et al.*, 2015), norovirus (Ettayebi *et al.*, 2016; Hosmillo *et al.*, 2020) and Epstein Barr virus (EBV) (Wallaschek *et al.*, 2021) infections. Here, we demonstrated the possibility of 2D cultivation of human- and murine-derived organoids (Figure III.4.16-Figure III.4.21). By high-resolution SEM, we were able to image the intestinal brush border on the apical side and conclude a high number of enterocytes in intestinal 2D monolayers (Figure III.4.19, Figure III.4.20). Together with TEER measurements, we can assess cell integrity and differentiation of the cells. In contrast to 3D approaches, no further equipment, e.g. for microinjections, is necessary and growth and infection parameters can be controlled more easily as already described (Aguilar *et al.*, 2021). Additionally, TEER measurement allows assessment of the cell integrity during infection (Figure III.4.17). With the calculated number of cells or staining, we are now able to calculate the MOI and are consequently able to quantify the adhesion, invasion and intracellular replication, not possible in 3D organoids. For comparison and also further applications, mucine-producing cell line HT29 can be used, which is an adherent epithelial cell line, derived from human colon cancer tumor. This cell line was already used to determine viral titers of the human parechovirus (Abed and Boivin, 2006) and to analyze *Bifidobacterium* and *Lactobacillus* strains counteraction to the toxic effect of *Clostridium difficile* (Boonma *et al.*, 2014; He *et al.*, 2002; Wang *et al.*, 2014). In future investigations, we are now able to combine infections with specific staining and/or transfected organoid-derived cells, to analyze if different *Salmonella* serovars preferentially invade distinct cell types. Experimental setups can easily be adjusted, like disadvantageous growth of 2D monolayers on transwells on complex matrices like Matrigel, which can be bypassed by using alternatives as collagen (Aguilar *et al.*, 2021). Growth on collagen was already shown to be a good alternative for stomach and intestinal organoids (Hosmillo *et al.*, 2020; Kayisoglu *et al.*, 2021; Lulla *et al.*, 2019; Schlaermann *et al.*, 2016). Furthermore, it is possible to grow cells in an air-liquid interface, where the cells are in contact with the culture medium only from the basolateral side, whereas the apical side is exposed to air (Aguilar *et al.*, 2021). This model showed a higher cell differentiation induced by the air exposure (Boccellato *et al.*, 2019; Li *et al.*, 2014a; Li *et al.*, 2014b; Sachs *et al.*, 2019; Sepe *et al.*, 2020).

Besides the microscopic analysis, we were also able to quantify STM infection in human-derived organoid monolayers (Figure III.4.18). Interestingly, STM WT showed reduced invasion of organoid-derived monolayers than in other published cell lines (Gerlach *et al.*, 2008; Gerlach *et al.*, 2007; Kommnick and Hensel, 2021). Invasion increased 60 min p.i. Thus, we concluded that the mucus layer, we stained by PAS stain, slowed down the invasion of the cells. Whereas

invasion of colon 30 min p.i. was 9-fold higher in comparison to ileum, invasion was comparable 60 min p.i., indicating that invasion of STM of colon cells is faster than ileum cells. $\Delta spi1$ could not invade, as published before, indicating mucus and different cell types do not alter invasion depletion. Interestingly, $\Delta spi4$ showed different phenotypes in ileum and colon monolayers, as well as 30 min p.i. and 60 min p.i. No invasion of colon cells was observed 30 min p.i., but approximately 70% invasion of WT of ileum cells, indicating a more important role of the SPI4 for invasion of colon-derived monolayers. 60 min p.i. invasion of $\Delta spi4$ was comparable to slightly increased invasion of colon-derived monolayers. We concluded that invasion of colon cells without SPI4-T1SS is more difficult. Thus, we were able to gain new insights in STM infection by using human organoid-derived monolayers.

III.4.5. Outlook

Organoids have advanced infection research, leading to better understanding of host-pathogen interactions and diseases. During cellular and molecular pathways triggered by pathogen interactions, the organoids maintain tissue architecture. By combining infections with stained and transfected organoids, we can gain further insights into host-pathogen interactions and preferred cell types for invasion and proliferation. Thus, this knowledge will allow us to treat *Salmonella* infections more targetedly or prevent them, especially those of typhoidal serovars. As the typhoidal serovars are highly adapted to the human host, the analysis of their infection process is of great interest. As STY during infection influences and reprograms host functions and protection mechanisms as immune response to evade immune defense in intestinal human organoids (Nickerson *et al.*, 2018), further details about *Salmonella* infection can provide new input into future vaccine development. Furthermore, M cell differentiation by addition of Receptor Activator of NF- κ B Ligand (RANKL) could be of great importance as M cells represent a common portal for pathogen invasion (Jepson and Clark, 1998) and controlled testing of these cells will lead to a better understanding of *Salmonella* infection.

Infection process can be analyzed in intestinal organoids, but to analyze the systemic infection of typhoidal *Salmonella* also other organoids, e.g. derived from gall bladder or liver, can shed new light on *Salmonella* infection. In general, first insights of the typhoidal serovars were already gained in intestinal and gallbladder organoids in 3D and 2D (Nickerson *et al.*, 2018; Scanu *et al.*, 2015). Scanu *et al.* found indications that STY can be a causative agent of gallbladder cancer by transforming genetically predisposed cells (Scanu *et al.*, 2015). STM was also already shown to be able to induce tumor growth in those predisposed cells in primary mouse fibroblast model (Scanu *et al.*, 2015). Sepe *et al.* observed host cell DNA damages in invaded epithelial cells, where double-strand breaks are induced by the CdtB subunit of the

typhoid toxin also in neighboring non-infected cells (Sepe *et al.*, 2020). However, the typhoid toxin was found to be not involved in initial cell cycle arrest during air-liquid infection of polarized monolayers. Thus, with help of the constantly growing field of different organoids, we gain more and more insights in *Salmonella* and other infections and by optimizing growth and infection conditions get closer to processes induced in the human body.

III.4.6. Materials and Methods

III.4.6.1. Bacterial strains and growth conditions

Bacterial strains used in this study are listed in Table III.4.1. Bacteria were grown aerobically in LB or on LB agar plates, if necessary supplemented with carbenicillin (cb, 50 µg/ml). Subcultures were grown for 2.5 h (1:31).

Table III.4.1. Bacterial strains used in this study.

Designation	Relevant characteristics	Reference
S. Typhimurium ATCC14028s	wild type	<i>Salmonella</i> genetic stock center, University of Calgary
MvP589	$\Delta spi4::FRT$	(Gerlach and Hensel, 2007)
MvP818	$\Delta invC::FRT$	(Gerlach and Hensel, 2007)
S. Paratyphi A 45157	wild type, clinical isolate, 2009 Nepal outbreak	(Gal-Mor <i>et al.</i> , 2012)

III.4.6.2. Plasmids used in this study

Plasmids used in this study are listed in Table III.4.2.

Table III.4.2. Plasmids used in this study.

Plasmid	Relevant characteristics, resistance	Reference
pFPVmCherry	const. mCherry	(Drecktrah <i>et al.</i> , 2008)
pFPV25.1	const. GFP	(Valdivia and Falkow, 1996)
p4878	pLX304 LifeAct::GFP, 3 rd generation lentivirus vector	based on Addgene #25890
pMD2.G	2 nd generation lentiviral packaging plasmid	Addgene #12259
psPAX2	VSV-G envelope expressing plasmid	Addgene #12260

III.4.6.3. Cell culture

Murine and human organoids and protocols were kindly provided by Guntram Grassl. The organoids were cultured in defined medium, mentioned in Table III.4.3. The organoids were incubated at 37 °C with 5% CO₂. Every 7 to 10 days after seeding, the enteroids were passaged. For passaging, the medium was removed and 1 ml ice-cold DPBS was added to each well. The Matrigel was broken up by pipetting back and forth (20x with P-1000 tip + 15x with P-1000 + P-200 µL tip on top). All wells were collected in one 15 ml conical tube on ice, filled up with ice-cold PBS and centrifuged for 5 min at 4 °C at 250 x *g*. The supernatant was discarded and the dissociated organoids were resuspended in an organoid medium-Matrigel mix (50:50). 50 µl were spotted in each well and overlaid with 500 µl organoid medium (3D). Every other day, medium was replaced. The first two days, the medium additionally was conditioned with 10 µM Y27623.

Table III.4.3. Ingredients for organoid medium.

	2D monolayer medium	2D differentiation medium	3D medium
L-WRN conditioned supernatant	50%	5%	50%
DMEM F-12/Glutamax			
Y27623	10 µM		10 µM (only early culture)
Pen/Strep	100 µg/ml		100 µg/ml
FCS	20%	20%	
rm-EGF	50 ng/ml	50 ng/ml	50 ng/ml
DAPT		5 µM	
Gastrin I			10 nM
HEPES			10 mM
A83-01			500 nM
SB202190			10 µM
ACC			1 mM
B27			1x

For infections, we also used monolayers of intestinal murine and human organoids. Matrigel was mixed with cold DPBS and 200 µl were filled into the transwells and incubated for at least 1.5 h at 37 °C, 5% CO₂. The medium was removed from all wells with 3D crypt organoids and

2 wells were resuspended with 1 ml cold DPBS. As described above, organoids were resuspended and collected in 15 ml tubes, pre-filled with cold DPBS. The tubes were centrifuged at 500 x g. Following centrifugation, supernatant was discarded and the pellet was resuspended in 1 ml warm 0.05% Trypsin/EDTA and incubated for 5 min at 37 °C in a water bath. Cells were then resuspended 20x with P-1000 tip + 15x with P-1000 + P-200 µL tip on top. We added 10 ml cold DMEM with 10% FCS and centrifuged an additional time for 5 min at 4 °C for at 500 x g. Supernatant was discarded and the pellet was resuspended in monolayer medium (Table III.4.3). For human organoids 1×10^5 cells/well and for murine organoids 1.5×10^5 cells/well were seeded. Every other day medium was replaced and transepithelial electrical resistance (TEER) was measured every day. At approximately day 5 (TEER 500-1000), medium was changed to differentiation medium (Table III.4.3).

III.4.6.4. Lentiviral transfection

For microscopic analysis, we transfected organoids with third generation lentivirus system (Table III.4.2) (Miyoshi and Stappenbeck, 2013). The organoids were cultured in 24-well plates in 3D for 10 days. The organoids were resuspended as described above and centrifuged for 5 min at 4 °C at 400 x g and then trypsinized for 5-10 min in 1 ml PBS. Trypsin digestion was stopped by addition of 5 ml cold DPBS and cells were centrifuged again for 5 min at 4 °C at 400 x g. Cells were resuspended in 3D organoid medium, supplemented with 10 µM Y27623. Organoid solution was spotted on Matrigel, prepared before. After 16 h, the medium was discarded and organoids were coated with additional Matrigel (incubation for 20 min) and 3D organoid medium, supplemented with 10 µM Y27623. The organoids were incubated 2-4 days to generate many stem cells. In the following, the organoids were extracted with medium and Matrigel and transferred into 15 ml tubes. The organoids were centrifuged for 5 min at 400 x g and supernatant was carefully removed and were resuspended in 1 ml warm 0.05% Trypsin/EDTA and incubated for 5 min at 37 °C in a water bath. We added 5 ml cold DPBS and centrifuged an additional time. Cells were resuspended in 3D organoid medium, supplemented with 10 µM Y27623. Organoids were adhered to a thin layer of Matrigel for 15 min at 37 °C, prepared before, because of the interference of the lentiviruses with the Matrigel. Lentiviral particles were prepared by C. Kommnick and V. Göser. We added lentivirus and 8 µg/mL polybrene to the cells on hardened Matrigel in a 12-well plate. We incubated the organoids 24 h with the lentivirus-polybrene mix, discarded the supernatant and coated the cells with additional Matrigel and added 3D organoid medium, supplemented with 10 µM Y27623. We incubated the organoids for 3 days, changed the medium to 3D organoid medium without ROCK inhibitor and started selection with 10 µg/ml Blasticidin (LpLX304 p4878_5) after 7 days for 24 h.

III.4.6.5. Fluorescence labeling of murine and human organoids

For microscopic analysis of uninfected and infected 3D and 2D cultured organoids, we washed the cells thrice with DPBS and fixed them with 3% PFA in PBS for 25 min at RT. Organoids grown on transwells were stamped out with the membrane before staining. Fixed cells were washed thrice with DPBS and incubated in blocking solution (2% goat serum, 2% bovine serum albumin) with 0.5% Triton-X100 for 30 min. For staining, the samples were incubated within the respective reagents, diluted in blocking solution with 0.2% Triton-X100 and incubated for 1 h at RT. Following this step, the samples were washed thrice with DPBS and were mounted on microscope slides, using Fluorshield (Sigma) and Entellan (Merck).

fluorescence excitation	Reagent	concentration	reference
488	AlexaFluor488-phalloidin	1:100	Molecular Probes
405	DAPI	1:1000	Sigma
588	CellMask Deep Red	2 µg/ml	ThermoFisher Scientific
642	CF®640R WGA	5 µg/ml	Biotium
647	phalloidin-iFluor647	1:100	AAT Bioquest

III.4.6.6. PAS staining of intestinal organoid monolayers and mouse tissue

As the PAS (periodic acid Schiff) reaction is one of the most frequently used chemical methods for histology, we used this method to investigate the mucus layer of our intestinal organoid monolayers. First, the fixed monolayers (3% PFA in PBS) were washed with MQ for 1 min. In a next step, periodic acid solution (10%) was added and incubated for 5 min. The samples were washed for 3 min with MQ. Schiff's reagent was added and samples were incubated for 15 min. The washing step was repeated for 3 min. Following this step, the samples were fixed on microscope slides, using Entellan. Mouse ileum and colon tissue was acquired from C57BL/6 mouse kindly provided by the division Neurobiology (University Osnabrueck). The dissected tissue was cut in 0.5 cm pieces and fixed for 24 h in 10% formaldehyde. Dehydration was done with ethanol series at RT with 10% for 15 min, 30% for 30 min, 50% for 1 h, 70% for 2 h, 70% for 72 h, 80% for 4 h, 80% for 16h, 90% for 24 h and two steps with 100% ethanol for 24 h each. Samples were embedded with Technovit 8100 according to manufacturer instructions (1:1 ethanol:Technovit step for at least 2 h at 4 °C, Technovit and hardener 1 for 72 h at 4 °C, Technovit and hardener 1+2 for 48 h at 4 °C under anerobic conditions). Trimming and semithin sectioning (5 µm) was done with conventional microtome. Toluidine staining was performed with one drop of filtered toluidine blue stain solution and let dry. Excess stain was rinsed gently with water and dried before microscopy. PAS staining with mouse tissue was

performed as described in manufacturer protocol from Roth. Briefly, semithin sections were rinsed with distilled water, incubated in 1% periodic acid solution for 10 min and rinsed with tap water afterwards for 10 min. After two short 2 min washing steps with distilled water, sections were stained with Schiff's reagent for 10-20 min and rinsed with warm tap water afterwards for 5 min. For microscopy, Zeiss Axio Observer.Z1 was used. with LD Plan-Neofluar 20x/0.6 objective. Imaging with CoolSNAP camera with a camera adapter 1.0x, total magnification 20x, zoom 1.0x. Additionally, a Zeiss Axio lab A1 with 10x and 20x objectives and Bresser Micro-Cam SP 3.1 was used. Images were further processed with MicroCamLab II, version x64, 3.7.8752.

III.4.6.7. Invasion assay of human organoid monolayers

For infection, 2.5 h subcultures of infecting STM were grown, intestinal organoids on 0.4 μm porous filters were infected at multiplicity of infection (MOI) of 50, and incubated for 30 min or 60 min at 37 °C in an atmosphere of 5% CO₂. The cells were washed three times with pre-warmed PBS. To determine invasion, cells were treated with 200 μl medium containing 100 $\mu\text{g/ml}$ gentamicin per well for 1 h, washed three times with prewarmed PBS and lysed with 0.5% deoxycholate in PBS (freshly prepared). Lysis was performed for 10 min at 37 °C on a shaking platform. Lysates were collected in single tubes and serial dilutions of inoculum and lysates were plated logarithmic on MH plates to determine CFU. Plates were incubated o/N at 37 °C and CFU were counted the next day with Acolyte software. The percentages of invaded bacteria were calculated. Additionally, single wells were fixed with PFA and stained for microscopy as described above. For microscopy, Zeiss Axio Observer.Z1 was used. The used objective was the LD Plan-Neofluar 40x/0.6 Korr. Imaging with CoolSNAP camera with a camera adapter 1.0x, total magnification 40x, zoom 1.0x. Bacteria were imaged for 60 s with 150 ms exposure time and 2x2 binning.

III.4.6.8. Infection of organoid monolayers for microscopy

For imaging of infections, Organoids were cultured in 2D as described above. STM infection was carried out as described above. SPA WT strain was grown for 8 h under aerobic conditions, subcultured (1:100) in fresh LB medium to stationary phase for 16 h under microaerophilic conditions as described in (Elhadad *et al.*, 2015). Bacteria were adjusted to an optical density of 0.2 at 600 nm in PBS, used for infection with MOI 50 and incubated for 30-60 min at 37 °C. After washing thrice with PBS or HEPES, cells were fixed for fluorescence or scanning electron microscopy, respectively.

III.4.6.9. 3D Organoid cultivation for imaging

Ileum and colon organoids of murine and human origin were seeded on surface-treated μ -slide 8-well chamber slides. 8-wells were cooled during seeding to prevent solidification of Matrigel and allow organoids to settle near the polymer coverslip bottom of the chamber. Imaging was performed with Cell Observer microscope (Zeiss) equipped with Yokogawa Spinning Disc Unit CSU-X1a5000, an incubation chamber, two ORCA Flash 4.0 V3 cameras (Hamamatsu) and appropriate filters for the respective fluorescence dyes. The following objectives were used: 40x (LD-Plan-Neofluar, NA 0.6), 40x (Plan-Apochromat, NA 1.4) and 63x (α -Plan-Apochromat, NA 1.4). For imaging of large areas of 3D organoids, multiple images with overlaps were acquired and stitched.

III.4.6.10. Microinjection of 3D cultured organoids

For microinjection, STM WT was cultured under microaerobic conditions as described above. Organoids were microinjected with Zeiss Axio Observer A1 with Eppendorf FemtoJet combined with InjectMan N12. Organoids were fixed at desired time points either 30 min (human colon) or between 60-90 min p.i. (murine colon).

III.4.6.11. Generation of immobilized apical-out enteroids for microscopy

Immobilized apical-out enteroids for microscopy were prepared as described in (Co *et al.*, 2019). In brief, enteroids were grown as described above for 7-10 days, dislodged with sterile spatula and solubilized in 5 mM EDTA in PBS for 1 h at 4°C on a rotating platform. 10 μ l Matrigel was spread in a cooled μ -slide as described above to form a thin layer and polymerized for 10 min at 37 °C. Enteroids were centrifuged at 200 x g for 3 min at 4 °C and supernatant was removed. Enteroids were re-suspended in 30 μ l organoid medium, spotted on solidified Matrigel and incubated for 15 min at 37 °C before organoid medium was added to well for cultivation. Fixation, staining and imaging was performed 1-3 days after seeding as described above.

III.4.6.12. Sample preparation for electron microscopy

Sample preparation for SEM

After the desired incubation time, cells were washed thrice with 0.2 M HEPES and fixed with 2.5% Glutaraldehyde (Sciences Services, Germany) in 0.2 M HEPES for 20 min at 37 °C. Dehydration was done with ethanol series at RT with 10%, 30% and 50% ethanol once for 10

min each step and 70%, 90% and 100% ethanol twice for 10 min each step. For chemical drying, hexamethyldisilazane (HMDS), diluted with pure ethanol in ratios of 1:3, 1:1, 1:3 was used for 15 min for each step and 100% HMDS for 20 min at RT. After the final step, samples were air dried until HMDS has completely evaporated. Transwell membrane was stamped out with biopsy punch and taped on aluminum SEM pin stubs with leit-taps before they were coated with 6 nm gold with sputter coater Leica EM ACE600. For imaging, Jeol SEM JSM-IT200 was used.

3D organoids were fixed for 2 h at room temperature (RT) in 2.5% glutaraldehyde in 0.1 M cacodylate buffer pH 7.4 (Sciences Services, Germany) subsequently washed twice in 0.1 M cacodylate buffer pH 7.4 and dehydrated stepwise in a graded ethanol series. Samples were critical point dried in 100% ethanol with a critical point drying machine (CPD300, Leica) and mounted on aluminum stubs as described above. Samples were sputter-coated with a 10 nm thin gold layer and imaged with Zeiss SEM Auriga at 4 kV

Sample preparation for TEM

For TEM, organoids were fixed for 2 h at room temperature (RT) in 2.5% glutaraldehyde in 0.1 M cacodylate buffer pH 7.4, subsequently washed in 0.1 M cacodylate buffer pH, 7.4, post-fixed for 2 h at RT in 1% osmium tetroxide in 0.1 M cacodylate buffer pH 7.4, dehydrated stepwise in a graded ethanol series and embedded in Epon 812 (Fluka, Buchs, Switzerland). Ultrathin sections (70 nm, ultramicrotome EM UC7, Leica, Wetzlar, Germany) were afterwards stained for 30 min with 1% uranyl acetate (Leica, Germany) and 20 min in 3% lead citrate (Leica, Germany). Sections were analyzed in a transmission electron microscope with a Zeiss TEM 902 (Oberkochen, Germany) at 80 kV.

For TEM analysis of microinjected organoids, specimens were fixed with 2.5% glutaraldehyde in 0.2 M HEPES buffer for 1 h at RT. Samples were washed thrice with buffer and incubated in 2% osmium tetroxide (Electron Microscopy Sciences) in 0.2 M HEPES buffer with 0.1% ruthenium red and 1.5% potassium ferrocyanide for 1 h at 4 °C in the dark. After five rinses with buffer, organoids were gradually dehydrated with 30%, 50%, 70%, 80%, 90%, 100% ethanol at 4 °C with one incubation in 100% anhydrous ethanol and two rinses in anhydrous acetone at RT for 10 min each step. For infiltration, samples were incubated in mixtures of EPON 812 (Sigma-Aldrich) and acetone. Namely 25% and 75% EPON for 1 h each, 100% EPON overnight and 100% EPON for 8 h. Polymerization of the resin was conducted for 72 h at 60 °C. Ultrathin sectioning (70 nm) was performed with a Leica EM UC7 (Leica, Wetzlar, Germany) and sections were collected on formvar-coated copper slot grids. Sections were contrasted with 2% uranyl acetate and 3% lead citrate using a Leica EM AC20 (Leica, Wetzlar, Germany) and analyzed with a Zeiss TEM 902 A, operated at 80 kV and equipped with a 2K

wide-angle slow-scan CCD camera (TRS, Moorenweis, Germany). Images were collected using the software ImageSP (TRS image SysProg, Moorenweis, Germany).

III.4.7. Acknowledgements

We thank Christian Meyer from the division of Zoology for help with embedding of murine tissue.

III.4.8. References

- Abed, Y., and Boivin, G. (2006). Human parechovirus types 1, 2 and 3 infections in Canada. *Emerg Infect Dis* 12, 969-975.
- Abrahams, G.L., and Hensel, M. (2006). Manipulating cellular transport and immune responses: dynamic interactions between intracellular *Salmonella enterica* and its host cells. *Cell Microbiol* 8, 728-737.
- Adams, G.G., and Dilly, P.N. (1989). Differential staining of ocular goblet cells. *Eye (Lond)* 3 (Pt 6), 840-844.
- Aguilar, C., Alves da Silva, M., Saraiva, M., Neyazi, M., Olsson, I.A.S., and Bartfeld, S. (2021). Organoids as host models for infection biology - a review of methods. *Exp Mol Med* 53, 1471-1482.
- Bartfeld, S. (2016). Modeling infectious diseases and host-microbe interactions in gastrointestinal organoids. *Dev Biol* 420, 262-270.
- Bartfeld, S., and Clevers, H. (2015). Organoids as Model for Infectious Diseases: Culture of Human and Murine Stomach Organoids and Microinjection of Helicobacter Pylori. *J Vis Exp*.
- Beskow, L.M. (2016). Lessons from HeLa Cells: The Ethics and Policy of Biospecimens. *Annu Rev Genomics Hum Genet* 17, 395-417.
- Beumer, J., and Clevers, H. (2016). Regulation and plasticity of intestinal stem cells during homeostasis and regeneration. *Development* 143, 3639-3649.
- Birchough, G.M., Johansson, M.E., Gustafsson, J.K., Bergstrom, J.H., and Hansson, G.C. (2015). New developments in goblet cell mucus secretion and function. *Mucosal Immunol* 8, 712-719.
- Boccellato, F., Woelffling, S., Imai-Matsushima, A., Sanchez, G., Goosmann, C., Schmid, M., Berger, H., Morey, P., Denecke, C., Ordemann, J., et al. (2019). Polarised epithelial monolayers of the gastric mucosa reveal insights into mucosal homeostasis and defence against infection. *Gut* 68, 400-413.
- Boonma, P., Spinler, J.K., Venable, S.F., Versalovic, J., and Tumwasorn, S. (2014). *Lactobacillus rhamnosus* L34 and *Lactobacillus casei* L39 suppress *Clostridium difficile*-induced IL-8 production by colonic epithelial cells. *BMC Microbiol* 14, 177.
- Broguiere, N., Isenmann, L., Hirt, C., Ringel, T., Placzek, S., Cavalli, E., Ringnalda, F., Villiger, L., Zullig, R., Lehmann, R., et al. (2018). Growth of Epithelial Organoids in a Defined Hydrogel. *Adv Mater* 30, e1801621.
- Buchmeier, N.A., and Heffron, F. (1991). Inhibition of macrophage phagosome-lysosome fusion by *Salmonella typhimurium*. *Infect Immun* 59, 2232-2238.
- Caiazza, C., Parisi, S., and Caiazza, M. (2021). Liver Organoids: Updates on Disease Modeling and Biomedical Applications. *Biology (Basel)* 10.
- Carrol, M.E., Jackett, P.S., Aber, V.R., and Lowrie, D.B. (1979). Phagolysosome formation, cyclic adenosine 3':5'-monophosphate and the fate of *Salmonella typhimurium* within mouse peritoneal macrophages. *J Gen Microbiol* 110, 421-429.
- Centonze, V.E., and White, J.G. (1998). Multiphoton excitation provides optical sections from deeper within scattering specimens than confocal imaging. *Biophys J* 75, 2015-2024.
- Chen, S., Einspanier, R., and Schoen, J. (2015). Transepithelial electrical resistance (TEER): a functional parameter to monitor the quality of oviduct epithelial cells cultured on filter supports. *Histochem Cell Biol* 144, 509-515.
- Co, J.Y., Margalef-Catala, M., Li, X., Mah, A.T., Kuo, C.J., Monack, D.M., and Amieva, M.R. (2019). Controlling Epithelial Polarity: A Human Enteroid Model for Host-Pathogen Interactions. *Cell Rep* 26, 2509-2520 e2504.
- Co, J.Y., Margalef-Catala, M., Monack, D.M., and Amieva, M.R. (2021). Controlling the polarity of human gastrointestinal organoids to investigate epithelial biology and infectious diseases. *Nat Protoc* 16, 5171-5192.
- Dougan, G., and Baker, S. (2014). *Salmonella enterica* serovar Typhi and the pathogenesis of typhoid fever. *Annu Rev Microbiol* 68, 317-336.

- Drecktrah, D., Levine-Wilkinson, S., Dam, T., Winfree, S., Knodler, L.A., Schroer, T.A., and Steele-Mortimer, O. (2008). Dynamic behavior of *Salmonella*-induced membrane tubules in epithelial cells. *Traffic* 9, 2117-2129.
- Dutta, D., and Clevers, H. (2017). Organoid culture systems to study host-pathogen interactions. *Curr Opin Immunol* 48, 15-22.
- Egi Kardia, M.F., Tanja Strive, Xi-Lei Zeng, Mary Estes, Robyn N. Hall (2020). Isolation, culture and maintenance of rabbit intestinal organoids, and organoid-derived cell monolayers.
- Elhadad, D., Desai, P., Rahav, G., McClelland, M., and Gal-Mor, O. (2015). Flagellin Is Required for Host Cell Invasion and Normal *Salmonella* Pathogenicity Island 1 Expression by *Salmonella enterica* Serovar Paratyphi A. *Infect Immun* 83, 3355-3368.
- Ettayebi, K., Crawford, S.E., Murakami, K., Broughman, J.R., Karandikar, U., Tenge, V.R., Neill, F.H., Blutt, S.E., Zeng, X.L., Qu, L., *et al.* (2016). Replication of human noroviruses in stem cell-derived human enteroids. *Science* 353, 1387-1393.
- Farin, H.F., Jordens, I., Mosa, M.H., Basak, O., Korving, J., Tauriello, D.V., de Punder, K., Angers, S., Peters, P.J., Maurice, M.M., *et al.* (2016). Visualization of a short-range Wnt gradient in the intestinal stem-cell niche. *Nature* 530, 340-343.
- Fatehullah, A., Appleton, P.L., and Nathke, I.S. (2013). Cell and tissue polarity in the intestinal tract during tumorigenesis: cells still know the right way up, but tissue organization is lost. *Philos Trans R Soc Lond B Biol Sci* 368, 20130014.
- Finkbeiner, S.R., Zeng, X.L., Utama, B., Atmar, R.L., Shroyer, N.F., and Estes, M.K. (2012). Stem cell-derived human intestinal organoids as an infection model for rotaviruses. *mBio* 3, e00159-00112.
- Forbester, J.L., Goulding, D., Vallier, L., Hannan, N., Hale, C., Pickard, D., Mukhopadhyay, S., and Dougan, G. (2015). Interaction of *Salmonella enterica* Serovar Typhimurium with Intestinal Organoids Derived from Human Induced Pluripotent Stem Cells. *Infect Immun* 83, 2926-2934.
- Fujii, M., Shimokawa, M., Date, S., Takano, A., Matano, M., Nanki, K., Ohta, Y., Toshimitsu, K., Nakazato, Y., Kawasaki, K., *et al.* (2016). A Colorectal Tumor Organoid Library Demonstrates Progressive Loss of Niche Factor Requirements during Tumorigenesis. *Cell Stem Cell* 18, 827-838.
- Gagnon, M., Zihler Berner, A., Chervet, N., Chassard, C., and Lacroix, C. (2013). Comparison of the Caco-2, HT-29 and the mucus-secreting HT29-MTX intestinal cell models to investigate *Salmonella* adhesion and invasion. *J Microbiol Methods* 94, 274-279.
- Gal-Mor, O., Suez, J., Elhadad, D., Porwollik, S., Leshem, E., Valinsky, L., McClelland, M., Schwartz, E., and Rahav, G. (2012). Molecular and cellular characterization of a *Salmonella enterica* serovar Paratyphi a outbreak strain and the human immune response to infection. *Clin Vaccine Immunol* 19, 146-156.
- Galan, J.E., and Curtiss, R., 3rd (1989). Cloning and molecular characterization of genes whose products allow *Salmonella typhimurium* to penetrate tissue culture cells. *Proc Natl Acad Sci U S A* 86, 6383-6387.
- Garcez, P.P., Loiola, E.C., Madeiro da Costa, R., Higa, L.M., Trindade, P., Delvecchio, R., Nascimento, J.M., Brindeiro, R., Tanuri, A., and Rehen, S.K. (2016). Zika virus impairs growth in human neurospheres and brain organoids. *Science* 352, 816-818.
- Gassler, N. (2017). Paneth cells in intestinal physiology and pathophysiology. *World J Gastrointest Pathophysiol* 8, 150-160.
- Gaush, C.R., Hard, W.L., and Smith, T.F. (1966). Characterization of an established line of canine kidney cells (MDCK). *Proc Soc Exp Biol Med* 122, 931-935.
- Gerbe, F., and Jay, P. (2016). Intestinal tuft cells: epithelial sentinels linking luminal cues to the immune system. *Mucosal Immunol* 9, 1353-1359.
- Gerlach, R.G., Claudio, N., Rohde, M., Jackel, D., Wagner, C., and Hensel, M. (2008). Cooperation of *Salmonella* pathogenicity islands 1 and 4 is required to breach epithelial barriers. *Cell Microbiol* 10, 2364-2376.
- Gerlach, R.G., and Hensel, M. (2007). *Salmonella* pathogenicity islands in host specificity, host pathogen-interactions and antibiotics resistance of *Salmonella enterica*. *Berl Munch Tierarztl Wochenschr* 120, 317-327.

- Gerlach, R.G., Jackel, D., Geymeier, N., and Hensel, M. (2007). *Salmonella* pathogenicity island 4-mediated adhesion is coregulated with invasion genes in *Salmonella enterica*. *Infect Immun* 75, 4697-4709.
- Gomez, D.P., and Boudreau, F. (2021). Organoids and Their Use in Modeling Gut Epithelial Cell Lineage Differentiation and Barrier Properties During Intestinal Diseases. *Front Cell Dev Biol* 9, 732137.
- Graf, B.W., and Boppart, S.A. (2010). Imaging and analysis of three-dimensional cell culture models. *Methods Mol Biol* 591, 211-227.
- He, D., Sougioultzis, S., Hagen, S., Liu, J., Keates, S., Keates, A.C., Pothoulakis, C., and Lamont, J.T. (2002). *Clostridium difficile* toxin A triggers human colonocyte IL-8 release via mitochondrial oxygen radical generation. *Gastroenterology* 122, 1048-1057.
- He, Z., Gharaibeh, R.Z., Newsome, R.C., Pope, J.L., Dougherty, M.W., Tomkovich, S., Pons, B., Mirey, G., Vignard, J., Hendrixson, D.R., *et al.* (2019). *Campylobacter jejuni* promotes colorectal tumorigenesis through the action of cytolethal distending toxin. *Gut* 68, 289-300.
- Hensel, M. (2004). Evolution of pathogenicity islands of *Salmonella enterica*. *Int J Med Microbiol* 294, 95-102.
- Hentschel, V., Arnold, F., Seufferlein, T., Azoitei, N., Kleger, A., and Muller, M. (2021). Enteropathogenic Infections: Organoids Go Bacterial. *Stem Cells Int* 2021, 8847804.
- Heo, I., Dutta, D., Schaefer, D.A., Iakobachvili, N., Artegiani, B., Sachs, N., Boonekamp, K.E., Bowden, G., Hendrickx, A.P.A., Willems, R.J.L., *et al.* (2018). Modelling *Cryptosporidium* infection in human small intestinal and lung organoids. *Nat Microbiol* 3, 814-823.
- Hopt, A., and Neher, E. (2001). Highly nonlinear photodamage in two-photon fluorescence microscopy. *Biophys J* 80, 2029-2036.
- Hosmillo, M., Chaudhry, Y., Nayak, K., Sorgeloos, F., Koo, B.K., Merenda, A., Lillestol, R., Drumright, L., Zilbauer, M., and Goodfellow, I. (2020). Norovirus Replication in Human Intestinal Epithelial Cells Is Restricted by the Interferon-Induced JAK/STAT Signaling Pathway and RNA Polymerase II-Mediated Transcriptional Responses. *mBio* 11.
- Iismaa, S.E., Kaidonis, X., Nicks, A.M., Bogush, N., Kikuchi, K., Naqvi, N., Harvey, R.P., Husain, A., and Graham, R.M. (2018). Comparative regenerative mechanisms across different mammalian tissues. *NPJ Regen Med* 3, 6.
- Ishizaki, T., Uehata, M., Tamechika, I., Keel, J., Nonomura, K., Maekawa, M., and Narumiya, S. (2000). Pharmacological properties of Y-27632, a specific inhibitor of rho-associated kinases. *Mol Pharmacol* 57, 976-983.
- Jepson, M.A., and Clark, M.A. (1998). Studying M cells and their role in infection. *Trends Microbiol* 6, 359-365.
- Johnson, R., Mylona, E., and Frankel, G. (2018). Typhoidal *Salmonella*: Distinctive virulence factors and pathogenesis. *Cell Microbiol* 20, e12939.
- Kayisoglu, O., Weiss, F., Niklas, C., Pierotti, I., Pompaiah, M., Wallaschek, N., Germer, C.T., Wiegering, A., and Bartfeld, S. (2021). Location-specific cell identity rather than exposure to GI microbiota defines many innate immune signalling cascades in the gut epithelium. *Gut* 70, 687-697.
- Kommnick, C., and Hensel, M. (2021). Correlative Light and Scanning Electron Microscopy to Study Interactions of *Salmonella enterica* with Polarized Epithelial Cell Monolayers. *Methods Mol Biol* 2182, 103-115.
- Kommnick, C., Lepper, A., and Hensel, M. (2019). Correlative light and scanning electron microscopy (CLSEM) for analysis of bacterial infection of polarized epithelial cells. *Sci Rep* 9, 17079.
- Krieger, V., Liebl, D., Zhang, Y., Rajashekar, R., Chlanda, P., Giesker, K., Chikkaballi, D., and Hensel, M. (2014). Reorganization of the endosomal system in *Salmonella*-infected cells: the ultrastructure of *Salmonella*-induced tubular compartments. *PLoS Pathog* 10, e1004374.
- Lamers, M.M., van der Vaart, J., Knoop, K., Riesebosch, S., Breugem, T.I., Mykytyn, A.Z., Beumer, J., Schipper, D., Bezstarosti, K., Koopman, C.D., *et al.* (2021). An organoid-derived bronchioalveolar model for SARS-CoV-2 infection of human alveolar type II-like cells. *EMBO J* 40, e105912.

- Lauren, P.A., and Sorvari, T.E. (1969). The histochemical specificity of mucicarmine staining in the identification of epithelial mucosubstances. *Acta Histochem* 34, 263-272.
- Leslie, J.L., Huang, S., Opp, J.S., Nagy, M.S., Kobayashi, M., Young, V.B., and Spence, J.R. (2015). Persistence and toxin production by *Clostridium difficile* within human intestinal organoids result in disruption of epithelial paracellular barrier function. *Infect Immun* 83, 138-145.
- Li, X., Nadauld, L., Ootani, A., Corney, D.C., Pai, R.K., Gevaert, O., Cantrell, M.A., Rack, P.G., Neal, J.T., Chan, C.W., *et al.* (2014a). Oncogenic transformation of diverse gastrointestinal tissues in primary organoid culture. *Nat Med* 20, 769-777.
- Li, Y., Xu, C., and Ma, T. (2014b). In vitro organogenesis from pluripotent stem cells. *Organogenesis* 10, 159-163.
- Lorkowski, M., Felipe-Lopez, A., Danzer, C.A., Hansmeier, N., and Hensel, M. (2014). *Salmonella enterica* invasion of polarized epithelial cells is a highly cooperative effort. *Infect Immun* 82, 2657-2667.
- Lulla, V., Dinan, A.M., Hosmillo, M., Chaudhry, Y., Sherry, L., Irigoyen, N., Nayak, K.M., Stonehouse, N.J., Zilbauer, M., Goodfellow, I., *et al.* (2019). An upstream protein-coding region in enteroviruses modulates virus infection in gut epithelial cells. *Nat Microbiol* 4, 280-292.
- Ly, K.T., and Casanova, J.E. (2007). Mechanisms of *Salmonella* entry into host cells. *Cell Microbiol* 9, 2103-2111.
- Maru, Y., Orihashi, K., and Hippo, Y. (2016). Lentivirus-Based Stable Gene Delivery into Intestinal Organoids. *Methods Mol Biol* 1422, 13-21.
- May, S., Evans, S., and Parry, L. (2017). Organoids, organs-on-chips and other systems, and microbiota. *Emerg Top Life Sci* 1, 385-400.
- Miyoshi, H., and Stappenbeck, T.S. (2013). *In vitro* expansion and genetic modification of gastrointestinal stem cells in spheroid culture. *Nat Protoc* 8, 2471-2482.
- Nickerson, K.P., Senger, S., Zhang, Y., Lima, R., Patel, S., Ingano, L., Flavahan, W.A., Kumar, D.K.V., Fraser, C.M., Faherty, C.S., *et al.* (2018). *Salmonella* Typhi Colonization Provokes Extensive Transcriptional Changes Aimed at Evading Host Mucosal Immune Defense During Early Infection of Human Intestinal Tissue. *EBioMedicine* 31, 92-109.
- Nikiforou, M., Jacobs, E.M., Kemp, M.W., Hornef, M.W., Payne, M.S., Saito, M., Newnham, J.P., Janssen, L.E., Jobe, A.H., Kallapur, S.G., *et al.* (2016). Intra-amniotic *Candida albicans* infection induces mucosal injury and inflammation in the ovine fetal intestine. *Sci Rep* 6, 29806.
- Noel, G., Baetz, N.W., Staab, J.F., Donowitz, M., Kovbasnjuk, O., Pasetti, M.F., and Zachos, N.C. (2017a). Erratum: A primary human macrophage-enteroid co-culture model to investigate mucosal gut physiology and host-pathogen interactions. *Sci Rep* 7, 46790.
- Noel, G., Baetz, N.W., Staab, J.F., Donowitz, M., Kovbasnjuk, O., Pasetti, M.F., and Zachos, N.C. (2017b). A primary human macrophage-enteroid co-culture model to investigate mucosal gut physiology and host-pathogen interactions. *Sci Rep* 7, 45270.
- Ootani, A., Li, X., Sangiorgi, E., Ho, Q.T., Ueno, H., Toda, S., Sugihara, H., Fujimoto, K., Weissman, I.L., Capecchi, M.R., *et al.* (2009). Sustained in vitro intestinal epithelial culture within a Wnt-dependent stem cell niche. *Nat Med* 15, 701-706.
- Osho, S.O., Wang, T., Horn, N.L., and Adeola, O. (2017). Comparison of goblet cell staining methods in jejunal mucosa of turkey poults. *Poult Sci* 96, 556-559.
- Peterson, L.W., and Artis, D. (2014). Intestinal epithelial cells: regulators of barrier function and immune homeostasis. *Nat Rev Immunol* 14, 141-153.
- Ponce de Leon-Rodriguez, M.D.C., Guyot, J.P., and Laurent-Babot, C. (2019). Intestinal in vitro cell culture models and their potential to study the effect of food components on intestinal inflammation. *Crit Rev Food Sci Nutr* 59, 3648-3666.
- Pott, J., and Hornef, M. (2012). Innate immune signalling at the intestinal epithelium in homeostasis and disease. *EMBO Rep* 13, 684-698.
- Pui, C.F., Wong, W. C., Chai, L. C., Tunung, R., Jeyaletchumi, P., Noor Hidayah, M. S., Ubong, A., Farinazleen, M. G., Cheah, Y. K. and Son, R (2011). *Salmonella*: A foodborne pathogen. *International Food Research Journal* 18, 465-473.

- Rakotoson, I., Delhomme, B., Djian, P., Deeg, A., Brunstein, M., Seebacher, C., Uhl, R., Ricard, C., and Oheim, M. (2019). Fast 3-D Imaging of Brain Organoids With a New Single-Objective Planar-Illumination Two-Photon Microscope. *Front Neuroanat* 13, 77.
- Ramirez-Flores, C.J., and Knoll, L.J. (2021). Breakthroughs in microbiology made possible with organoids. *PLoS Pathog* 17, e1010080.
- Ranganathan, S., Doucet, M., Grassel, C.L., Delaine-Elias, B., Zachos, N.C., and Barry, E.M. (2019). Evaluating *Shigella flexneri* Pathogenesis in the Human Enteroid Model. *Infect Immun* 87.
- Reuter, T., Scharte, F., Franzkoch, R., Liss, V., and Hensel, M. (2021). Single cell analyses reveal distinct adaptation of typhoidal and non-typhoidal *Salmonella enterica* serovars to intracellular lifestyle. *PLoS Pathog* 17, e1009319.
- Reynaud, E.G., Krzic, U., Greger, K., and Stelzer, E.H. (2008). Light sheet-based fluorescence microscopy: more dimensions, more photons, and less photodamage. *HFSP J* 2, 266-275.
- Rezania, A., Bruin, J.E., Arora, P., Rubin, A., Batushansky, I., Asadi, A., O'Dwyer, S., Quiskamp, N., Mojibian, M., Albrecht, T., *et al.* (2014). Reversal of diabetes with insulin-producing cells derived in vitro from human pluripotent stem cells. *Nat Biotechnol* 32, 1121-1133.
- Ribet, D., and Cossart, P. (2015). How bacterial pathogens colonize their hosts and invade deeper tissues. *Microbes Infect* 17, 173-183.
- Richart, R.M. (1963). A clinical staining test for in vivo delineation of Dysplasia and Carcinoma *in Situ*. *Am J Obst Gynecol*, 703.
- Rios, A.C., and Clevers, H. (2018). Imaging organoids: a bright future ahead. *Nat Methods* 15, 24-26.
- Röder, J., Felgner, P., and Hensel, M. (2021a). Comprehensive Single Cell Analyses of the Nutritional Environment of Intracellular *Salmonella enterica*. *Front Cell Infect Microbiol* 11, 624650.
- Röder, J., Felgner, P., and Hensel, M. (2021b). Single-cell analyses reveal phosphate availability as critical factor for nutrition of *Salmonella enterica* within mammalian host cells. *Cell Microbiol* 23, e13374.
- Roodsant, T., Navis, M., Aknouch, I., Renes, I.B., van Elburg, R.M., Pajkrt, D., Wolthers, K.C., Schultsz, C., van der Ark, K.C.H., Sridhar, A., *et al.* (2020). A Human 2D Primary Organoid-Derived Epithelial Monolayer Model to Study Host-Pathogen Interaction in the Small Intestine. *Front Cell Infect Microbiol* 10, 272.
- Sachs, N., Papaspyropoulos, A., Zomer-van Ommen, D.D., Heo, I., Bottinger, L., Klay, D., Weeber, F., Huelsz-Prince, G., Iakobachvili, N., Amatngalim, G.D., *et al.* (2019). Long-term expanding human airway organoids for disease modeling. *EMBO J* 38.
- Salcedo, S.P., and Holden, D.W. (2003). SseG, a virulence protein that targets *Salmonella* to the Golgi network. *EMBO J* 22, 5003-5014.
- Sato, T., and Clevers, H. (2013). Growing self-organizing mini-guts from a single intestinal stem cell: mechanism and applications. *Science* 340, 1190-1194.
- Sato, T., Stange, D.E., Ferrante, M., Vries, R.G., Van Es, J.H., Van den Brink, S., Van Houdt, W.J., Pronk, A., Van Gorp, J., Siersema, P.D., *et al.* (2011). Long-term expansion of epithelial organoids from human colon, adenoma, adenocarcinoma, and Barrett's epithelium. *Gastroenterology* 141, 1762-1772.
- Sato, T., Vries, R.G., Snippert, H.J., van de Wetering, M., Barker, N., Stange, D.E., van Es, J.H., Abo, A., Kujala, P., Peters, P.J., *et al.* (2009). Single Lgr5 stem cells build crypt-villus structures in vitro without a mesenchymal niche. *Nature* 459, 262-265.
- Scanu, T., Spaapen, R.M., Bakker, J.M., Pratap, C.B., Wu, L.E., Hofland, I., Broeks, A., Shukla, V.K., Kumar, M., Janssen, H., *et al.* (2015). *Salmonella* Manipulation of Host Signaling Pathways Provokes Cellular Transformation Associated with Gallbladder Carcinoma. *Cell Host Microbe* 17, 763-774.
- Schlaermann, P., Toelle, B., Berger, H., Schmidt, S.C., Glanemann, M., Ordemann, J., Bartfeld, S., Mollenkopf, H.J., and Meyer, T.F. (2016). A novel human gastric primary cell culture system for modelling *Helicobacter pylori* infection in vitro. *Gut* 65, 202-213.

- Schreurs, R., Baumdick, M.E., Drewniak, A., and Bunders, M.J. (2021). In vitro co-culture of human intestinal organoids and lamina propria-derived CD4(+) T cells. *STAR Protoc* 2, 100519.
- Schulte, M., Olschewski, K., and Hensel, M. (2021a). Fluorescent protein-based reporters reveal stress response of intracellular *Salmonella enterica* at level of single bacterial cells. *Cell Microbiol* 23, e13293.
- Schulte, M., Olschewski, K., and Hensel, M. (2021b). The protected physiological state of intracellular *Salmonella enterica* persists reduces host cell-imposed stress. *Commun Biol* 4, 520.
- Sepe, L.P., Hartl, K., Iftexhar, A., Berger, H., Kumar, N., Goosmann, C., Chopra, S., Schmidt, S.C., Gurumurthy, R.K., Meyer, T.F., *et al.* (2020). Genotoxic Effect of *Salmonella* Paratyphi A Infection on Human Primary Gallbladder Cells. *mBio* 11.
- Spicer, S.S. (1960). A correlative study of the histochemical properties of rodent acid mucopolysaccharides. *J Histochem Cytochem* 8, 18-35.
- Sridharan, G., and Shankar, A.A. (2012). Toluidine blue: A review of its chemistry and clinical utility. *J Oral Maxillofac Pathol* 16, 251-255.
- Stelzner, M., Helmraath, M., Dunn, J.C., Henning, S.J., Houchen, C.W., Kuo, C., Lynch, J., Li, L., Magness, S.T., Martin, M.G., *et al.* (2012). A nomenclature for intestinal in vitro cultures. *Am J Physiol Gastrointest Liver Physiol* 302, G1359-1363.
- Takashima, S., Gold, D., and Hartenstein, V. (2013). Stem cells and lineages of the intestine: a developmental and evolutionary perspective. *Dev Genes Evol* 223, 85-102.
- Tindle, C., Fuller, M., Fonseca, A., Taheri, S., Ibeawuchi, S.R., Beutler, N., Katkar, G.D., Claire, A., Castillo, V., Hernandez, M., *et al.* (2021). Adult stem cell-derived complete lung organoid models emulate lung disease in COVID-19. *Elife* 10.
- Tse, C.M., In, J.G., Yin, J., Donowitz, M., Doucet, M., Foulke-Abel, J., Ruiz-Perez, F., Nataro, J.P., Zachos, N.C., Kaper, J.B., *et al.* (2018). Enterohemorrhagic *E. coli* (EHEC)-Secreted Serine Protease EspP Stimulates Electrogenic Ion Transport in Human Colonoid Monolayers. *Toxins (Basel)* 10.
- Turner, J.R. (2009). Intestinal mucosal barrier function in health and disease. *Nat Rev Immunol* 9, 799-809.
- Urbischek, M., Rannikmae, H., Foets, T., Ravn, K., Hyvonen, M., and de la Roche, M. (2019). Organoid culture media formulated with growth factors of defined cellular activity. *Sci Rep* 9, 6193.
- Valdivia, R.H., and Falkow, S. (1996). Bacterial genetics by flow cytometry: rapid isolation of *Salmonella typhimurium* acid-inducible promoters by differential fluorescence induction. *Mol Microbiol* 22, 367-378.
- van de Wetering, M., Francies, H.E., Francis, J.M., Bounova, G., Iorio, F., Pronk, A., van Houdt, W., van Gorp, J., Taylor-Weiner, A., Kester, L., *et al.* (2015). Prospective derivation of a living organoid biobank of colorectal cancer patients. *Cell* 161, 933-945.
- van der Flier, L.G., and Clevers, H. (2009). Stem cells, self-renewal, and differentiation in the intestinal epithelium. *Annu Rev Physiol* 71, 241-260.
- VanDussen, K.L., Marinshaw, J.M., Shaikh, N., Miyoshi, H., Moon, C., Tarr, P.I., Ciorba, M.A., and Stappenbeck, T.S. (2015). Development of an enhanced human gastrointestinal epithelial culture system to facilitate patient-based assays. *Gut* 64, 911-920.
- Wagner, C., Polke, M., Gerlach, R.G., Linke, D., Stierhof, Y.D., Schwarz, H., and Hensel, M. (2011). Functional dissection of SiiE, a giant non-fimbrial adhesin of *Salmonella enterica*. *Cell Microbiol* 13, 1286-1301.
- Wallaschek, N., Reuter, S., Silkenat, S., Wolf, K., Niklas, C., Kayisoglu, O., Aguilar, C., Wiegering, A., Germer, C.T., Kircher, S., *et al.* (2021). Ephrin receptor A2, the epithelial receptor for Epstein-Barr virus entry, is not available for efficient infection in human gastric organoids. *PLoS Pathog* 17, e1009210.
- Wang, S.M., Zhang, L.W., Fan, R.B., Han, X., Yi, H.X., Zhang, L.L., Xue, C.H., Li, H.B., Zhang, Y.H., and Shigwedha, N. (2014). Induction of HT-29 cells apoptosis by lactobacilli isolated from fermented products. *Res Microbiol* 165, 202-214.

-
- Wang, Y., Wang, P., and Qin, J. (2021). Microfluidic Organs-on-a-Chip for Modeling Human Infectious Diseases. *Acc Chem Res* 54, 3550-3562.
- WHO (2008). The global burden of disease: 2004 update.
- WHO (2014). Antimicrobial resistance: global report on surveillance 2014.
- Yin, Y., and Zhou, D. (2018a). Corrigendum: Organoid and Enteroid Modeling of *Salmonella* Infection. *Front Cell Infect Microbiol* 8, 257.
- Yin, Y., and Zhou, D. (2018b). Organoid and Enteroid Modeling of *Salmonella* Infection. *Front Cell Infect Microbiol* 8, 102.
- Zomer-van Ommen, D.D., Pukin, A.V., Fu, O., Quarles van Ufford, L.H., Janssens, H.M., Beekman, J.M., and Pieters, R.J. (2016). Functional Characterization of Cholera Toxin Inhibitors Using Human Intestinal Organoids. *J Med Chem* 59, 6968-6972.

III.5. Contributions of Co-Authors

Conserved secretion mechanisms of the giant adhesin SiiE of *Salmonella enterica* and other two-step secreted adhesins

Sander N. and Hensel M.

N.S. performed experimental work, analyzed the data and wrote the manuscript

M.H. analyzed the data, wrote the manuscript

The extended cytosolic domain of SiiB is critical for SiiAB proton channel function of *Salmonella enterica*

Sander N. and Hensel M.

N.S. performed experimental work, analyzed the data and wrote the manuscript

M.H. analyzed the data, wrote the manuscript

Functional interaction between SPI4-T1SS encoded proton channel SiiAB and the flagellum in *Salmonella enterica*

Sander N., Holtmannspötter M. and Hensel M.

N.S. performed experimental work, performed 3D dSTORM microscopy and image analysis, analyzed the data and wrote the manuscript

M.H. performed 3D dSTORM microscopy and image analysis

M.H. analyzed the data, wrote the manuscript

Establishment of a novel infection model for *Salmonella* adhesion and invasion – human intestinal organoids

Sander N., Scharte F., Franzkoch R., Kim M., Psathaki K., Grassl G. and Hensel M.

Sander N.: Conceptualization, Data curation, Formal analysis, Investigation, Methodology, Validation, Visualization, Writing – original draft parts: abstract, introduction part 1, lentiviral transfection, 2D cultivation, PAS staining of 2D organoids, TEER measurements and plate assays, discussion part 2, outlook and associated methods

Scharte F.: Conceptualization, Data curation, Formal analysis, Investigation, Methodology, Validation, Visualization, Writing – original draft parts: abstract, introduction part 2, 3D imaging,

microinjection, apical out, PAS staining of murine tissue, microscopy of 2D cultured organoids, discussion part 1, outlook and associated methods

Franzkoch R.: provided data and text for part TEM of microinjected intestinal organoids and associated methods

Kim M.: provided data for lentiviral transfection and TEER measurements

Psathaki K.: provided data for SEM and TEM of 3D organoids

Grassl G: provided material and methods for cultivation of intestinal organoids and provided microinjected, fixed organoids for TEM and LM analyses

Michael Hensel: Conceptualization, Funding acquisition, Project administration, Resources, Supervision, Writing – review & editing

IV. Discussion

The SPI4-T1SS of STM is essential for the invasion of polarized epithelial cells by mediating the first close contact to the host cells apical side (Gerlach *et al.*, 2008). To convey adhesion, SiiE is retained on the cell surface during secretion, prior its release into the extracellular space (Gerlach *et al.*, 2007b). However, the detailed mechanism of SiiE secretion and function of the

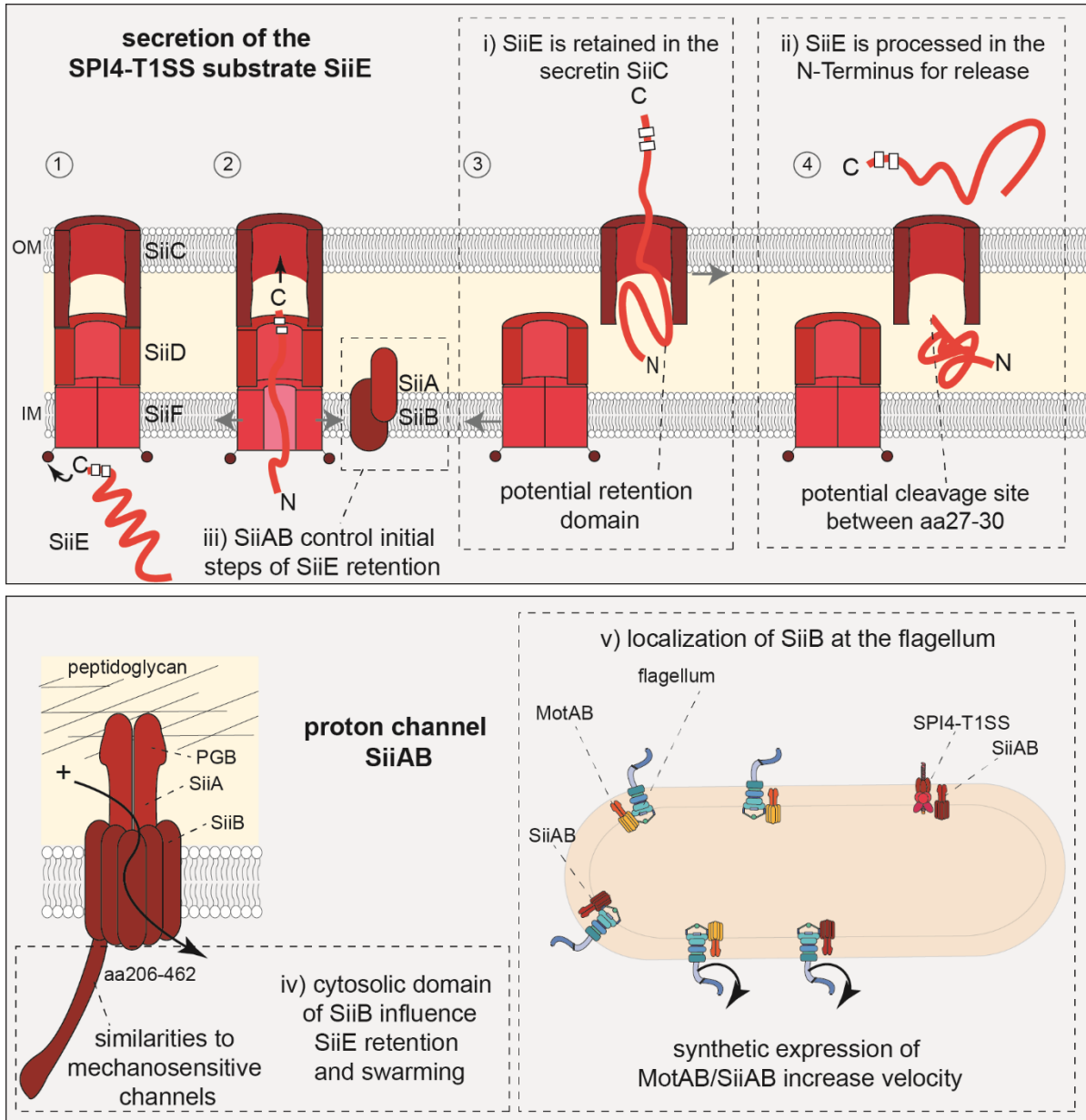


Figure IV.1. Main results of this work. i) SiiE is retained in the OM by SiiC and possesses a potential retention domain in the N-terminal part. ii) For release, SiiE is post-translationally modified and a possible cleavage site is located between aa27-30. iii) The accessory proton channel, SiiAB, is involved in initial steps of SiiE secretion and not needed for release of SiiE. iv) The cytosolic domain (aa206-462) of SiiB shows similarities to mechanosensitive channels and there are hints that this domain influence SiiE retention, but not adhesion, and swarming behavior. v) SiiB was found to localize at the flagellar subunit FliN, more than at the SPI4-T1SS during SiiE retention maximum. Additionally, synthetic expression of *siiAB* or *motAB* both lead to an increased velocity. By bioinformatics analyses of SiiB, I found similarities to Na⁺-conducting channels, rather than to H⁺-conducting channels.

subunits are only partly understood. As the SPI4-T1SS displays a special member of a large family of substrates and their cognate T1SS, a better understanding of this system can reveal new insights in *Salmonella* infection and function of other T1SS and thus pave the way to new anti-infective drugs and virulence blockers.

In this work, I uncovered new details of the SiiE secretion mechanism and the role of specific subunits, in particular SiiA, SiiB and SiiC. The main conclusions gained in this thesis are shown in Figure IV.1. Additionally, I successfully established methods to culture murine and human intestinal organoids for microscopic and quantitative analysis of STM and SPA infection, as organoids were recently reported to be complex organized versatile model system close to processes in the human body.

IV.1. SiiE belongs to a new family of T1SS substrates

IV.1.1. Adhesive T1SS substrates are retained on the cell surface

Adherence is an important virulence factor of pathogens, required for biofilm-formation or infection processes among others. Even if T1SS are highly conserved regarding their structure and function, new data revealed T1SS substrates that are not secreted in one, but rather in two steps with a periplasmic intermediate (Guo *et al.*, 2017; Smith *et al.*, 2018b). The subfamily of RTX/BTLCP-linked adhesins for example, consisting of large adhesins with aa repeat sequences, Ca²⁺-binding RTX sequences and a T1SS secretion signal, was only recently described (Satchell, 2011). It is intriguing that especially large substrates like the 900 kDa biofilm-associated substrate LapA or the unusual giant 1.5 MDa ice-binding protein *MplBP* show this intermediate step in their secretion process (Guo *et al.*, 2017; Smith *et al.*, 2018b). Typically, ice-binding proteins are small soluble proteins (Bar Dolev *et al.*, 2016). Only 34 kDa of the giant *MplBP* attach the bacterium to the ice to keep it in the region, where oxygen and nutrients are available (Bar Dolev *et al.*, 2016). This subfamily contains a range of various adhesins like LapA of *P. putida*, important for adhesion to corn seeds and root colonization (Espinosa-Urgel *et al.*, 2000; Yousef-Coronado *et al.*, 2008); FrhA of *Vibrio cholerae*, involved in hemagglutination and adhesion to epithelial cells, biofilm formation and chitin binding (Syed *et al.*, 2009); RtxA of *Legionella pneumophila*, required for adhesion to and uptake by macrophages and amoebae (Cirillo *et al.*, 2002) and the biofilm-promoting factor BpfA in *Shewanella oneidensis* (Theunissen *et al.*, 2010). In accordance with RTX/BTLCP-linked adhesins, the SPI4-T1SS substrate SiiE also possesses repetitive Blg domains with Ca²⁺-binding sites, a C-terminal secretion signal, is retained on the cell surface during secretion and mediates adhesion (Gerlach

et al., 2007b; Griessl *et al.*, 2013; Wagner *et al.*, 2014; Wagner *et al.*, 2011). Thus, it is very likely that SiiE is also a member of this new subfamily of T1SS substrates.

IV.1.2. SiiE is retained in the OM

Although, SiiE is known to be retained during secretion process, retention mechanism was poorly understood. Other T1SS substrates like LapA and *MplBP* are retained by the respective secretin - LapE and TolC - to mediate adhesion (Guo *et al.*, 2018; Smith *et al.*, 2018a). Here, I demonstrated that SiiE interacts with SiiC in the OM during retention process (Figure IV.1 i) and that a controlled expression of *siiC* regulates the amount of SiiE retained on the cell surface (III.1.). Interestingly, a trimeric state of SiiC, as is the case for TolC, could not be shown. One could postulate that SiiC oligomers are not as stably associated as TolC trimers, since SiiC is only needed for a short period of time during invasion.

A mechanism by which SiiE is retained by the SiiCDF complex can be excluded now. This becomes even more obvious, when structural modeling and TEM analysis of mini SiiE are taken into account. TEM images showed potential mini SiiE structures on the cell surface (III.1). Determination of length indicated, such structures would not be visible on the cell surface, as the N-terminus (aa1-236) was modelled to extend over approximately 20 nm (III.1). Consequently, the Blg domains with the Ca²⁺-binding sites would be located within the channel, if SiiE is retained by parts of the channel in the IM and OM. Various recombinant SiiE fusion proteins with different length were tested on monolayers of polarized cells and it was demonstrated that the longer the fragment, the more binding was observed (Wagner *et al.*, 2014). This is indicative of every Blg domain being able to bind target structures on the host cell, resulting in the most efficient adherence. SiiE regions also showed similar structures to the regions described for *MplBP*, where Ca²⁺-binding sites are located outside the OM and not in the periplasm, as was also described for other RTX adhesins (Guo *et al.*, 2018; Guo *et al.*, 2017; Guo *et al.*, 2019b) (III.1). Additionally, for *MplBP*, distinct interaction surfaces of the RIM and RIC with the secretin TolC were shown. WT SiiE cannot mediate adhesion anymore, if more than 5 Blg domains are deleted and mini SiiE is not able to mediate adhesion anymore. In contrast to non-covalently linked subunits of fimbrial proteins, large non-fimbrial adhesins, consisting of one polypeptide with covalently linked Blg domains, have a robust structure with no alterations in length (Barlag and Hensel, 2015). Thus, protrusion of the LPS is essential for adhesion to the host cell (Barlag and Hensel, 2015; Griessl *et al.*, 2013; Wagner *et al.*, 2011) and the more Blg domains protrude the LPS (maximal 5 Blg domains), the more efficient SiiE binds to the host cell to allow SPI1-T3SS effector protein translocation. *Salmonella* also possesses a biofilm-associated related T1SS adhesin, namely BapA (Latasa *et al.*, 2005). The

associated T1SS is composed of the ABC transporter BapC, the PAP BapD and the secretin BapB (Guttula *et al.*, 2019). As SiiE, BapA contains Blg domains (28) with Ca^{2+} -binding sites, important for folding of the substrate (Guttula *et al.*, 2019). However, in contrast to SiiE, BapA is not expressed under laboratory growth conditions (Latasa *et al.*, 2005). BapA is known to be involved in formation of pellicles on air-liquid interphase (Latasa *et al.*, 2005). Comparable to SiiE, BapA is also retained on the cell surface, but not surface exposed anymore upon deletion of some Blg domains (Elpers *et al.*, 2020), indicating the critical role of LPS protrusion for adhesion. Interestingly, Bap of *Acinetobacter baumannii* was shown to not only be involved in biofilm-formation, but also in adherence to human bronchial epithelial cells and normal human neonatal keratinocytes (Brossard and Campagnari, 2012). As BapA is also involved in invasion, it displays a further member of surface-exposed adhesins involved in pathogenesis (Latasa *et al.*, 2005).

To be retained in the OM, a periplasmic retention domain in the N-terminus is essential, as described for LapA and MplBP (Guo *et al.*, 2018; Guo *et al.*, 2017; Smith *et al.*, 2018a; Smith *et al.*, 2018b). This domain is too bulky to pass through the secretin and hence the substrates can only be released if this domain is proteolytically cleaved. Here, by bioinformatic analysis, a potential retention domain was identified in the N-terminal region of SiiE (III.1). With a width of ~ 27 Å, this β -sheet domain was modelled to have comparable dimensions to MplBP and LapA and thus is too bulky to pass through SiiC. For TolC a pore diameter of 20 Å in an open state is published (Guo *et al.*, 2018). Consequently, it is likely that SiiC possesses a comparable diameter, as also modelled sizes were comparable to TolC (III.1). With a lower sequence identity ($\sim 20\%$), the 3D fold of the retention domain is conserved in RTX adhesins, including pathogens as *V. cholera*, *P. aeruginosa* and *Shewanella oneidensis* (Guo *et al.*, 2019b; Smith *et al.*, 2018a). The N-terminal retention domain, in contrast to the Blg domains, is structured and folded independent of Ca^{2+} (Guo *et al.*, 2019a; Smith *et al.*, 2018a). This supports the results of SiiE being retained in the OM and not the whole T1SS (Figure IV.1 i). As SiiE lacks cysteine residues, a retention by a cysteine hook, as it is described for the non-RTX adhesin CdrA of *P. aeruginosa*, can be excluded here. CdrA like SiiE lacks the T(P)-A-A-G site for proteolysis (Borlee *et al.*, 2010; Cooley *et al.*, 2016). Bioinformatic analyses of the N-termini of several BTLCP-linked adhesins predicted short poly-glycine regions following the di-alanine cleavage site (Smith *et al.*, 2018b). By mutational analysis of LapA N-terminal mutant strains lacking residues D31 to A95, the first 125 aa, including the poly-glycine linker, were found to be the LapA retention region (Smith *et al.*, 2018a). This mechanism of surface anchoring was found to be quite common as a LapA chimera harboring the retention domain from a predicted

BTLCP-linked adhesin expressed by *Vibrio cholerae*, was found to be retained on the cell surface (Smith *et al.*, 2018a). Thus, it would be very interesting to analyze chimeras of SiiE with LapA, MplBP, BapA or further predicted retention modules.

All in all, the subfamily of RTX adhesins that mediate attachment of a range of microorganisms is growing and SiiE seems to be its latest member.

IV.1.3. SiiE is post-translationally modified for release

Proteolytic cleavage of proteins is a common and irreversible PTM, whereby endoproteases cleave specific residues within sequence motifs and exoproteases cleaving from the N- or C-termini (Forrest and Welch, 2020). To release biofilm-associated RTX adhesins into the extracellular space, often a conserved T(P)-A-A-G motif is cleaved (Guo *et al.*, 2019b; Smith *et al.*, 2018a). Such a di-alanine motif is located at positions 144 and 145 in SiiE (III.1). Strikingly, this di-alanine motif was found in the secreted SiiE, excluding a proteolytic cleavage at this site. However, MS analyses revealed a potential cleavage site between aa27-30 (III.1) (Figure IV.1 ii). Thus, another new potential cleavage motif is postulated. This area is now interesting for further mutations and investigations. At position 28 an alanine and at position 29 a lysine can be found. However, less proteases cleave alanine (Fulop *et al.*, 1998) and lysine is the preferable cleavage site. Nevertheless, proline-endopeptidases also accept alanine in position P1 and in most cases lysine in position P2 (Fulop *et al.*, 1998). An additional interesting site was Val46-Ile47-Ile48-Val49, a motif cleaved by periplasmic Clp proteases (Mo *et al.*, 2006) (III.1). Clp proteases degrade accumulated proteins in the periplasm under stress conditions (Bass *et al.*, 1996; Waller and Sauer, 1996) and non-specific proteolysis of folded proteins is inhibited as only unfolded proteins without disulfide bonds are cleaved (Strauch and Beckwith, 1988; Strauch *et al.*, 1989). The protease DegP for example is known to act on at least partially unfolded substrates and the cleavage site is normally between a pair of hydrophobic residues like Val and Ile (Jones *et al.*, 2002). SiiE lacks cysteine residues and consequently disulfide bonds, making it to a potentially target of such periplasmic proteases (Figure IV.2). Thus, two peptides are in focus for further investigations of a proteolytic cleavage and its cognate protease.

However, there are further PTM like acylation of the RTX toxin HlyA, leading to the mature substrate form (Nicaud *et al.*, 1985). Contrary to SiiE and other RTX adhesins, acylation of HlyA is not needed for secretion *per se*, but rather for activation of the toxin (Ludwig *et al.*, 1996). In general, a variety of PTM, ranging from methylation and phosphorylation to addition of complex moieties like lipids and glycans (Cain *et al.*, 2014) can affect conformation, activity,

stability and localization as well as protein interactions (Forrest and Welch, 2020). Phosphorylation was shown as a commonly used PTM also in surface-exposed proteins like the flagellar protein FliC of *P. aeruginosa* (Kelly-Wintenberg *et al.*, 1993; Suriyanarayanan *et al.*, 2016) or type IV pilus protein PilE of *Neisseria gonorrhoeae* (Forest *et al.*, 1999). Interestingly, this phosphorylation of FliC does not alter motility, but rather increases T2SS-dependent biofilm-formation (Suriyanarayanan *et al.*, 2016). There are OMPs from *Klebsiella pneumoniae*, *H. pylori* and *Shigella flexneri* that are also multi-phosphorylated, but the importance behind this is not known (Lai *et al.*, 2020; Standish *et al.*, 2016). PTM like methylation is already described for surface-exposed structures like the flagellum (Horstmann *et al.*, 2020). These modifications however, occur on the outside, difficult to be transferred to the periplasmic located N-terminus of SiiE as a possible release mechanism. Maybe an additional effect has to be investigated in more detail in the secreted parts, with less abundant N-terminus. However, a PTM is more unlikely for SiiE release, also in comparison to other RTX adhesins, especially taken the results of this work into account. Here, besides others, we demonstrated with a very sensitive method distinct aa were less found in secreted SiiE than in cytosolic SiiE. Acetylation and succinylation are commonly applied PTM that occur predominantly at the N-terminus of the proteins (Cain *et al.*, 2014; Christensen *et al.*, 2019). In STM, the protein acetyltransferase (Pat) and deacetylase (CobB) were already described to be involved in cell survival during growth following acidic stress, invasion of the host and replication within macrophages. Mutants unable to acetylate proteins showed reduced host inflammation. However, the relation to specific virulence factors is currently unclear and it is suggested that this PTM is related to SPI1 expression (Sang, 2016). Potentially, retention can be achieved by a PTM in the periplasmic located N-terminus of SiiE, which is again reversed by an antagonist to release SiiE into the extracellular space. As proteolytic cleavage is a commonly used mechanism to release two-step secreted substrates into the extracellular space, a comparable situation can be assumed for SiiE, although the specific mechanism and cleavage site are not clear yet. Nonetheless, in contrast to other RTX/BTLCP-linked adhesins, a role of the accessory proton channel SiiAB can be excluded here (Figure IV.1).

IV.2. SiiAB – a promiscuous all-rounder?

SiiAB are the accessory proton channel of the SPI4-T1SS, located in the IM and important for the invasion process of polarized cells (Wille *et al.*, 2014). Thus, a role for the SPI4-T1SS and SiiE function seems obvious. Here, a role of SiiAB as proton channel for invasion of non-polarized cells was found, comparable to MotAB (III.2). SiiAB share similarities with the well-described flagellar stator unit MotAB as well as ExbBD and TolQR (Kirchweger *et al.*, 2019;

Wille *et al.*, 2014). A 5:2 stoichiometry was recently published for ExbBD and MotAB (Deme *et al.*, 2020b; Santiveri *et al.*, 2020). I found a comparable ratio for SiiA and SiiB by measurement of fluorescence signal intensities (III.2). This has to be confirmed by further controls in more sensitive assays as Blue native PAGE and MS.

IV.2.1. Proton channel SiiAB play an important role for the initial steps of SiiE secretion and not for release

In a *siiAB* mutant strain, although it retains SiiE on the cell surface, no adhesion and invasion was detected (III.1). The phenotype observed by controlled overexpression of *siiC* with an increased SiiE retention, adhesion and invasion, could not be examined in *siiAB* mutants with overexpression of *siiC* (III.1), indicating a role of SiiAB in the initial steps of SiiE secretion (Figure IV.1 iii). There are different accessory proton channels described that either transfer energy of the IM PMF to ion transports in the OM like ExbBD, or transduce energy for processes in the IM like MotAB, PomAB and TolQR (Minamino *et al.*, 2018; Ollis *et al.*, 2009; Zhu *et al.*, 2014). FRET and two-hybrid analysis demonstrated homo- and heterotypic protein interactions of SiiAB (Wille *et al.*, 2014). Additionally, SiiB interacts with the Walker A box of SiiF and is required for SiiF dimerization. Taken this together with the results of my work, there are evidences that SiiAB promote initial steps of secretion by interacting with SiiF in the IM (Figure IV.2). Various classes of T1SS substrates require accessory proteins for their function, like the RTX toxin HlyA, or release, like LapA. This family of accessory proteins important for release of the substrate, was described as BTLCPs with invariant Cys-His-Asp catalytic triads (Ginalska *et al.*, 2004). In former studies, the exact role of this group of proteins was unclear, although a modification of the target proteins (T1SS substrates) by transamidase, acetylase or hydrolase activity has already been postulated (Ginalska *et al.*, 2004). LapG and LapD for instance, responsible for LapA release, were shown to belong to this group of accessory proteins (Boyd and O'Toole, 2012; Navarro *et al.*, 2011; Newell *et al.*, 2011). LapG is the periplasmic calcium-dependent cysteine protease, responsible for the posttranslational cleavage of the giant T1SS RTX adhesion LapA at an N-terminal di-alanine motif, and is in turn regulated by the IM c-di-GMP receptor LapD (Boyd and O'Toole, 2012). Homologues of LapG and LapD were found in the genomes of over 1,300 bacterial species, spanning 120 genera of *Proteobacteria* (Smith *et al.*, 2018a) and identifying this as a commonly used strategy for regulation of adhesin-localization. Such LapD/LapG homologues were found in multiple bacterial species, including *B. bronchiseptica* (Ambrosio *et al.*, 2016), *Shewanella* spp. (Zhou *et al.*, 2015), *Pectobacterium atrosepticum* (Perez-Mendoza *et al.*, 2011), *Desulfovibrio vulgaris* (De Leon *et al.*, 2017), *P. putida* (Gjermansen *et al.*, 2010), and *P. aeruginosa* (Cooley *et al.*, 2016; Rybtke *et al.*, 2015). The results obtained in this work combined with previous investigations basically exclude a

proteolytic cleavage of SiiE by SiiAB in a similar manner, as SiiAB are not homologous to LapG and LapD. Nonetheless, SiiAB potentially display a new subgroup of accessory proteins that have not been described yet, but are as well involved in secretion regulation of a T1SS substrate. The release mechanism and potential protease of SiiE have to be further investigated (Figure IV.2).

In addition, the *siiABC* overexpression did not show higher amounts of SiiE retained on cell surface, controlled by SiiC in the OM, but nonetheless lead to higher adhesion and invasion rates than a *siiC* overexpression alone. As I also showed that the flagellum and its rotation by MotAB, as well as SiiAB play a role during invasion of polarized cells and also SPI4-T1SS independent invasion of non-polarized cells, we concluded a role of SiiAB for the flagellum. As a consequence, the maximum amounts of SiiE retained on the cell surface are defined by availability of SiiC in the OM. An additional overexpression of *siiAB* supports motility during invasion, as motility was found to be an important factor during invasion (III.3).

IV.2.2. The cytosolic domain of SiiB has effects on SiiE and the flagellum

Mechanosensitive channels possess an extended cytosolic domain, important for sensing IM tension changes and emergency release of osmolytes (Edwards *et al.*, 2012; Rasmussen and Rasmussen, 2018; Wang *et al.*, 2018). By multiple sequence alignment and tertiary structure predictions, I found conservation of potential residues and motifs known to be critical for mechanosensitive channels also in SiiB (III.2). As I demonstrated an effect of the osmotic pressure on SiiE retention and adhesion in dependence of the deletion of the cytosolic domain of SiiB in response to a hyperosmotic environment (600 mOsm), I suggest an important role here (III.2) (Figure IV.1 iv). Recent studies revealed that mechanosensitive channels can play essential roles during invasion processes (Edwards *et al.*, 2012; Flegler *et al.*, 2020; Rasmussen and Rasmussen, 2018; Schumann *et al.*, 2010). This cytoplasmic domain was further shown to sense macromolecular crowding in the cytoplasm (Rowe *et al.*, 2014) and the mechanosensitive channel YnaI is important during invasion of *Salmonella* (Edwards *et al.*, 2012; Miller, unpublished). Without YnaI, STM showed an increased internalization in macrophages and epithelial cells (Asogwa, 2019). As *siiAB* mutants show no adhesion and invasion of polarized epithelial cells, this possibly describes a new way of regulation during infection process and a new member of the recently described group of mechanosensitive channels involved in STM infection. However, not much is known about this new described group of mechanosensitive channels important for invasion and further experiments in distinct osmotic environments have to be performed and analyzed to verify this phenotype and put it into context of STM infection. Furthermore it already has been suggested that SiiAB may form a complex that senses the

PMF and transmits this information about the physiological state of the cell to other components of the T1SS, instead of providing energy for a coupled function, which has to be proofed in future investigations (Wille *et al.*, 2014) (Figure IV.2).

SiiB additionally was predicted to possess a signal peptide, ranging from aa1-26, which has not been shown before (III.2). Typically OM proteins possess such N-terminal secretion signals, which are cleaved during or after translocation over the IM and varying in their aa sequence (Jackson *et al.*, 1985). Nonetheless, SiiB was shown to be located in the IM (Wille *et al.*, 2014). However, also some IM proteins are described to possess N-terminal signal peptides and that they have a precursor form with a higher molecular weight in comparison to the membrane integrated protein (Jackson *et al.*, 1985). OmpF of *E. coli* as a hybrid form combined with the N-terminus of the IM protein DacA can also be inserted in the OM. Thus, an N-terminal signal sequence was postulated for this IM protein. As this signal sequence in SiiB was predicted with a very low probability and with no clear result of a potential translocation way, it might be used by chaperones or is no signal sequence at all. This has to be confirmed by molecular weight analysis of cytosolic and membrane integrated SiiB, as well as MS analysis.

Interestingly, we gained hints that overexpression of the cytosolic domain of SiiB alone has an effect on SiiE surface retention, but not on adhesion (III.2). Further, the swarm behavior was altered following overexpression of the cytosolic domain (III.2) (Figure IV.1 iv). Thus, the cytosolic domain alone might trigger processes at the SPI4-T1SS regarding SiiE secretion, as well as at the flagellum regarding torque generation. This indicates a new potential role of this domain, only by interaction with SiiF or the C-ring and not by actively pumping protons (Figure IV.2). MotA also contains a large cytoplasmic domain that is proposed to interact with the rotor (Blair and Berg, 1991; Dean *et al.*, 1984; Zhou *et al.*, 1995).

IV.2.3. Possible SiiAB integration in and interaction with the flagellar rotor

Here, we demonstrated an important role not only of the flagellum and motility during invasion, especially of non-polarized cells, but also the proton channels MotAB and SiiAB (III.3). Interestingly, SiiB was found to localize at the flagellar subunit FliN during SiiE retention maximum (III.3) (Figure IV.1 v). Taken this together with the results described above, a promiscuous role of SiiAB for the initial steps of SiiE secretion and subsequently as an additional stator unit at the flagellum is proposed (III.3). The C-terminal domain of FliG, containing a torque helix, directly interacts with the stator units MotA and PomA (Lee *et al.*, 2010; Santiveri *et al.*, 2020). In both MotA and FliG, critical charged residues necessary for this interaction are described (Lloyd and Blair, 1997; Zhou and Blair, 1997; Zhou *et al.*, 1998). By mutant phenotypes it was found that charge is the most important feature of these residues. Interestingly, the charged

residues in each protein were shown to function redundantly. In FliG, Arg-281, Asp-288, and Asp-289 are essential for interaction and function, whereas residues Lys-264 and Arg-297 were proposed to have secondary roles. In MotA, the important residues for function are Arg-90 and Glu-98, whereas Glu-150 was suggested to have a secondary role. These residues and homologues in FliG, SiiF, MotA and SiiB, respectively, in future experiments can be of interest to investigate comparable functions, interactions and mechanisms in STM. Additionally, as I found an effect on the swarm behavior of the cytosolic domain of SiiB only (IV.2.2), a possible direct interaction of this domain with the flagellar C-ring can be postulated (Figure IV.1 v). In further analyses, the cytosolic domain of MotA and other members of the proton channel family, as well as chimeric constructs have to be tested in addition to gain further insights into this novel phenotype. Further, this is supported by tracking analysis, where synthetic expression of *motAB* and *siiAB* both showed an increased velocity (III.3). As membrane ruffle formation is more induced during invasion of polarized cells than of non-polarized cells (Kommnick, 2021), the support of the flagellar rotation by additional SiiAB integration in the flagellar rotor during invasion of non-polarized cells is conclusive (Figure IV.2). It is already described that in dependence of the external load on the flagellum, caused by the heterogeneous environments, *E. coli* can adjust the number of stator units (Berg, 2003; Macnab, 2004; Minamino *et al.*, 2008; Morimoto and Minamino, 2014). There are evidences that MotB is directly involved in load sensing by its PG domain (Castillo *et al.*, 2013), and that mutations of the aspartate residue (D33) were found to be critical (Che *et al.*, 2014). The effects of this mutation led to the assumption that the load affects the coupling between the translocation and conformational changes in the stator units for torque generation. Thus, it was concluded that load changes can alter the stator incorporation by triggering conformational changes in MotB (Baker and O'Toole, 2017). Thereupon now, on the one hand SiiAB incorporation following MotB mutation should be checked, as well as mutations in SiiA PG domain and the effects on the motility and stop behavior, as MotB was shown to interact with FliG by cross-linking (Hizukuri *et al.*, 2010). For control and comparison, further potential proton channels have to be included in these experiments.

Interestingly, SiiB has a higher identity with Na⁺-conducting channels than with H⁺-conducting channels and possesses specific residues, conserved among Na⁺-conducting channels (III.3). These results shed new light on possible functions and mechanisms of SiiAB, apart from former described similarities to proton channels like MotAB (Kirchweger *et al.*, 2019). At the flagellum, also Na⁺-conducting stator complexes like PomAB are described (Yonekura *et al.*, 2011). PomAB for instance shows structural and functional similarities to MotAB, comparable to SiiAB. Thus, it is also possible that Na⁺-conducting channels share similarities with H⁺-con-

ducting channels, supporting our prediction results for SiiB. Besides the flagellar load, ion availability is an important factor (Baker and O'Toole, 2017). Consequently, many bacteria exploit different proton channels for the same flagellum and rotor incorporation, using H⁺ as well as Na⁺ (Baker and O'Toole, 2017; Paulick *et al.*, 2015). Paulick *et al.* demonstrated that in *S. oneidensis* the number of MotAB stators incorporated in the motor region decreases as the Na⁺ concentration increases. Both types of stators changed between the motor region and a pool of stator complexes located in the IM and exchange of PomAB and not MotAB occurred in dependence of environmental Na⁺. Based on these microscopic and swimming analyses, the role and function of SiiAB for the flagellum can be further investigated and might reveal a novel Na⁺-conducting channel in STM (Figure IV.2). However, there are also bacteria described that have two stator sets, both using the same ion, as for *P. aeruginosa* (Baker and O'Toole, 2017). It still remains unclear if SiiAB use H⁺ or Na⁺, which is an interesting topic for future experiments. As described above, homologues and further proton channels should be used for control and comparison here, in order to analyze swim behavior and localization by using SRM.

IV.2.4. 3D dSTORM is capable for localization of proton channels in the IM of STM

Since we found evidence that SiiAB contribute to flagellar movement, we investigated the localization of this proton channel in the IM at the SPI4-T1SS and the flagellum in comparison to MotAB (III.3). To bypass the diffraction limit of 200 nm for conventional light microscopy, by which it is not possible to resolve protein complexes in the IM of bacteria, we used SRM (Hensel *et al.*, 2013). In the past, in order to stain IM proteins in Gram-negative bacteria tagged at their cytosolic side, the bacteria had to be permeabilized for the large antibodies conjugated to fluorophores to be able to cross the membranes. Self-labeling enzyme (SLE) tags revolutionized the field, as small ligands with increased photostability and emission of more photons than fluorophores, can be used for labeling of the SLE tags (Keppler *et al.*, 2003; Klein *et al.*, 2011; Los and Wood, 2007). The size of 20-33 kDa of the SLE tags is a limiting factor for protein expression, labeling and staining in the IM (Keppler *et al.*, 2004; Los and Wood, 2007). To get in closer proximity between tag and fluorophore, new small ALFA-tag and Spot-Tag can be used (II.6.2). These can be inserted at both termini and the corresponding optimized nanobodies show very high affinities for the tags (Gotzke *et al.*, 2019; Metterlein, 2018; Virant *et al.*, 2018). A further advantage is the small size of the nanobodies, which can more easily cross the membranes and further reduce distances between protein and fluorophore. By dual-color 3D dSTORM analysis and with novel small tags and corresponding nanobodies, I was able to label and image MotA, MotB, SiiA and SiiB and combined these with already described Halo-Tag fusions (Barlag *et al.*, 2016) to the flagellar subunit FliN or SPI4-T1SS SiiF, respectively (III.3). This was one of the first investigations using this method combined with the novel tags

to localize proton channels in the IM of Gram-negative bacteria like STM. For comparison and as a positive control we used MotAB, which as the stator unit of the flagellum should localize there. Following expression and functional checks, localization of MotA and MotB, tagged with ALFA-tag and Spot-Tag, respectively, was analyzed in order to validate labeling and usage of MotA in further imaging as a representative for MotAB proton channel. The same was done for SiiAB, due to similarities between MotA and SiiB, and MotB and SiiA. The same tags were introduced based on the homologies. The best combination we found was the fusion of the ALFA-tag to MotA and SiiB, respectively, as well as the Spot-Tag – including a linker – to MotB and SiiA, respectively. In our approaches, labeling with Spot-Tag in general was more difficult than with ALFA-tag (III.3). Along with further development, this hurdle can also be overcome. To determine the co-localization of the proton channels with secretion systems, the CBC method, directly utilizing the single coordinate information whilst retaining SR information, was used (III.3). As MotAB is not only incorporated in the rotor, but rather there is also a pool of stator units located in the IM, depending on the load on the flagellum, (Paulick *et al.*, 2015) we found MotA not only located near FliN. Comparable amounts of MotA were associated with MotB and with FliN, validating our control. Interestingly, SiiB was less associated with SiiF during SiiE retention maximum, but in comparable amounts with SiiA and FliN (Figure IV.1 v). We concluded, together with the results that SiiAB are important for initial steps of SiiE secretion that SiiAB possibly promiscuously function at the SPI4-T1SS and the flagellum. However, function at the flagellum has to be further investigated as described above (Figure IV.2). To improve our results gained here, we need further controls. As described before, to test the quantification potential of this colocalization approach in our experimental setting, at least one of the subunits has to be simultaneously investigated with two tags at once (Mass *et al.*, 2020). For the best result, ALFA-tag and Spot-Tag as well as Halo-Tag with one of the other tags, respectively, have to be tested to determine the degrees of colocalization. If possible, fluorophores should be tested *vice versa* and additionally the CBC values should be calculated in a bidirectional fashion in further applications, as described before (Malkusch *et al.*, 2012; Mass *et al.*, 2020). With these last improvements left, in the near future we will be able to validate SiiAB localization at the flagellum and extend our analysis, even to different time points of retention.

IV.3. The future is now – tissues and organs in a dish

Standard cell culture models have been used over several years to unravel virulence mechanisms in host-pathogen interactions, but due to their origin, they often consist of a single cell

type with an error-filled genome. On the one hand, it was possible by microscopy and quantitative analysis to easily generate results, but on the other hand, complex tissue and organ structures, leading to a completely different host-pathogen interaction, were missing. Recently, a new stem cell-derived cell culture model emerged: the organoids. They reconstitute a certain degree of multicellular complexity with a close relation to *in vivo* conditions. However, organoid cultivation remains complex, expensive and time consuming and additionally reproducibility is affected between labs because of their highly heterogenic nature. Nevertheless, we were able to establish one of the complex organoid models, murine and human intestinal organoids, in our division (III.4).

Here, we demonstrated uninfected and infected 3D and 2D grown organoids of human and murine origin, which we successfully labeled and imaged as well as analyzed regarding their behavior during infection of STM and SPA (III.4). A disadvantage for imaging of the 3D organoids was the immense size of the 3D organoids in X, Y and Z direction. Especially in Z direction, imaging was limited, depending on working distance, parfocal length and numerical aperture of the used microscope. Thus, beside other reasons, it is difficult to follow infections in 3D organoids. Live imaging is only possible with certain limitations. Light sheet-based microscopy potentially offers a live cell imaging technique well suited for large specimens with more photons and less photo damage that can be used in future applications (Reynaud *et al.*, 2008). Furthermore, Matrigel, required for cultivation, can interfere with fluorescence excitation and emission and may result in higher background. By releasing the organoids from the Matrigel, we potentially obtain a better resolution and less background, but due to the treatment of the organoids, artefacts can make result interpretation difficult or even false. As along infection processes different cell types can be of interest, depending on the pathogen, we tested different staining protocols and labeling (III.4). Staining and imaging were difficult and our applied protocols have to be further improved to gain better insights in *Salmonella* and possibly other pathogens infection. Nevertheless, high-throughput methods like flow cytometry of single organoid-derived cells, especially combined with reporters, can provide information about infection processes as published before (Röder *et al.*, 2021a, b; Schulte *et al.*, 2021a, b). During growth of the intestinal organoids in the Matrigel, they also grow a lumen, outlined with the apical side of the cells and with the basolateral side facing outward. To infect the apical side, often used for entry by intestinal pathogens, different methods can be applied. On the one hand microinjections can be performed, on the other hand apical-out organoids can be used. Here, we successfully demonstrated both techniques (III.4). Disadvantages during microinjections are the technical limitations due to the highly heterogenic nature of organoids and the labor- and cost-intensive infections, as well as the penetration with an injection needle can potentially damage cell layers and spillage of pathogens into the medium could favor unwanted

infections at the basal site of the organoids. In contrast to this, by using apical-out organoids, pathogens can directly be added to the cell culture medium and infect the apical side of the host cell. However, this form of 3D organoids also has the disadvantage that they are highly heterogenic, which possibly makes experimental design and reproducibility difficult. All in all, we demonstrated that 3D growth and also infection as well as imaging is possible, but that at the moment 3D cultured organoids are not, or only less compatible with currently used live cell imaging techniques. Furthermore, fixed infections are difficult to image by fluorescence microscopy as well as electron microscopy. In the future, maybe stably transfected organoids can open the door to live cell imaging applications.

In comparison to 3D organoids, organoid-derived monolayers can have many advantages but also come with some drawbacks (III.4). Here, we demonstrated the successful 2D cultivation of human- and murine-derived organoids. We were able to differentiate and check for cell integrity of the monolayers by TEER measurements, as well as to infect and image them by electron and fluorescence microscopy. However, transwells also have some disadvantages: imaging with an inverted microscope through the transwell membrane is not feasible and punching out the membrane and placing it between a microscope slide and coverslip is a harsh treatment that could alter infection events or falsify analyses. Furthermore, differentiation of the cell layer may vary in comparison to 3D cultured organoids. Nevertheless, in future investigations, we are now able to combine infections with specific staining and/or transfected organoid-derived cells, to analyze if different *Salmonella* serovars preferentially invade distinct cell types. The advantages of organoid-derived monolayers are that experimental setups can easily be adjusted. It is possible to grow cells in an air-liquid interface, where the cells are in contact with the culture medium only from the basolateral side, whereas the apical side is exposed to air (Aguilar *et al.*, 2021), which was shown to induce a higher cell differentiation (Boccellato *et al.*, 2019; Li *et al.*, 2014a; Li *et al.*, 2014b; Sachs *et al.*, 2019; Sepe *et al.*, 2020). We were able to investigate a loss of cell integrity during infection, as well as to quantify invading STM WT, $\Delta spi4$ and $\Delta invC$ (III.4). Interestingly, we found another invasion phenotype of $\Delta spi4$ than of polarized and non-polarized cell culture models, where invasion also differed between ileum-derived and colon-derived monolayers. We concluded a distinct role of the mucus layer, which we stained by PAS stain (III.4), especially for the SPI4-T1SS. Also, in organoids $\Delta invC$ showed no invasion as it is already published, underlining the role of the SPI1-T3SS. Thus, we are able to further define the SPI4-T1SS phenotype in more detail by using murine- and human-derived intestinal monolayers. Furthermore, STM, SPA and STY related phenotypes now can be validated in a cell culture dish. Additionally, taken the results from the tracking analysis of this work into account, velocity and stop behavior of *motAB* and *siiAB*

phenotypes under the aspect of mucus production and infection conditions will be of further interest here (Figure IV.2).

All in all, with the help of organoids we are now closer to the human body and its intricate processes than ever, but due to heterogeneity and difficult growth, we are also faced with variations. However, as this is a fast growing, lucrative niche to not only investigate host-pathogen interactions, but also to analyze diseases and processes, protocols for a more stable handling will emerge fast. Maybe, in future investigations it is possible to combine different organoid types to build up a whole connected system, e.g. for analysis of systemic SPA or STY infections as well as other pathogens and viruses, or even drug development.

IV.4. Conclusions and Outlook

This thesis focused on the SPI4-T1SS and its giant substrate SiiE, essential for invasion of polarized cells. I was able to gain new insights in the function and mechanism of the SPI4-T1SS related canonical subunits SiiCDF, the non-canonical subunits SiiAB and their substrate SiiE. I could show that during secretion mechanism of SiiE, SiiAB are important in the initial steps, prior to retention of SiiE on the cell-surface by the secretin SiiC. Future investigations in this direction should focus on the detailed function of SiiAB during this initial phase of secretion. Further of interest is, whether SiiE is indeed held back by a retention domain, as proposed here, and what the interaction surface with SiiC looks like. We have to validate the proteolytic cleavage of SiiE for its release and to uncover an exact cleavage site as well as the responsible protease in the periplasm. Intriguingly, we found SiiAB located at the flagellum. In a next step, we have to figure out the distinct role of SiiAB in this relationship, also in comparison to other known proton channels. As a consequence of the new evidences gained here, we have to define if SiiB belongs to the H⁺- or Na⁺-conducting channels. Further, I was able to establish intestinal organoids, important for disease investigations, drug development and host-pathogen interaction analysis. The mechanism behind SPI4-T1SS mediated adhesion was poorly understood, I was now able to gain new insights, leading to a better understanding of the host-pathogen microenvironment during adhesion and invasion, transferrable to other pathogens invading host cells and replicating within them. Even though we have taken a few steps forward, there are still unanswered questions and ways to go (Figure IV.2.).

Interaction surface between SiiE and SiiC and retention domain

T1SS were first described to secrete their substrate in one step, like bacteriocins and RTX toxins. A new family was recently uncovered, in which the substrate is retained on the cell surface in an intermediate step, though a cognate TolC-like OM pore. These RTX adhesins

and their secretins have distinct interaction surfaces. As there are many conserved mechanisms and structures among the RTX adhesins (Smith *et al.*, 2018b), we can now, based on homology investigations and experiments done by Smith *et al.* (2018) and Guo *et al.*, design new experiments to further resolve domains and areas responsible for this interaction. In the future, high-resolution Cryo-TEM analyses of bacteria and published mini cells (Kawamoto *et al.*, 2013) can potentially reveal new insights in structures and interactions directly in the membrane.

SiiE release by proteolytic cleavage

The release following proteolytic cleavage is a commonly used mechanism for RTX adhesins, especially for biofilm-associated substrates (Smith *et al.*, 2018b). Here, we performed published assays and homology analyses to demonstrate potential cleavage sites in SiiE. In a next step, we will investigate the role of various residues for SiiE retention and release, by mutation of the potential cleavage sites determined in the N-terminus of SiiE in frame of this work. If we are able to clearly identify a cleavage site, a next step could be the analysis of potential proteases in the IM or periplasm. During STM SPI4-T1SS adhesion, second messengers like c-di-GMP may also play a role, especially after the Lasa group found that mutants not able to synthesize c-di-GMP were attenuated in a systemic murine infection model (Latasa *et al.*, 2016).

Localization and function of SiiAB for SiiE

Following recognition of SiiE by the T1SS, the ABC transporter SiiF dimerizes and SiiE is introduced into the secretion channel (Gerlach *et al.*, 2007b; Smith *et al.*, 2018b; Wille *et al.*, 2014). SiiAB, the non-canonical subunits of the SPI4-T1SS, are located in the IM, where they translocate protons, have an effect on STM adhesion and invasion and are associated with SiiF. We demonstrated that SiiAB are not necessary for release of SiiE, but for initial steps of SiiE secretion and could limit possible modes of action. By further mutational analyses we have to investigate the precise role of SiiAB here. As they potentially display a new mechanism of accessory proteins involved in T1SS substrate secretion, we have to search for novel approaches. Based on this work, possible steps during secretion with an involvement of SiiAB include the recognition, the introduction into the channel or the transfer of SiiE from the SiiDF complex to SiiC. With further analyses of the PG domain of SiiA we possibly find comparable effects on the SPI4-T1SS, SiiE, adhesion and invasion like MotB PG domain on the stator incorporation of the flagellum (Baker and O'Toole, 2017). By cross-linking experiments, we also can investigate further interaction partners in the periplasm as well as the OM. In another possible model described bei Wille *et al.* (2014), the PMF would not provide energy for a coupled function, but rather provide information about the state of the cell. This would be in line

with results already published were the external pH had an effect on SiiE surface expression and that SiiE surface expression is reduced when STM enters stationary growth phase (Wagner *et al.*, 2011). The purification of SiiAB complexes in comparison to published MotAB complexes (Deme *et al.*, 2020b; Santiveri *et al.*, 2020) and following analysis by Blue native PAGE or Cryo-TEM imaging, can possibly reveal new insights.

Localization and function of SiiAB for the flagellum

Motility is an important factor for bacteria, not only towards nutrients, but also during invasion process. We demonstrated a cross-correlation of the flagellum and the SPI4-T1SS during invasion and a distinct role of motility and the proton channels MotAB and SiiAB for invasion of polarized and also non-polarized cells. In our dSTORM analysis, we found SiiB located at the flagellum and now want to analyze the detailed function, incorporation and interactions. As we performed our tracking analyses in medium without host cells, experiments should also be performed with different cell culture cell lines. With the now established intestinal organoids, which were shown to produce mucus, we will gain further insights in the role of SiiAB at the flagellum. Additionally, SiiAB incorporation following MotB mutation should be checked, as well as mutations in SiiA PG domain and the effects on the motility and stop behavior. MotB was shown to interact with Flgl by cross-linking and that MotB is important for exchange of stators in the rotor region (Baker and O'Toole, 2017; Hizukuri *et al.*, 2010). For control and comparison, further potential proton channels have to be included in these experiments. Further constructs with TolQR and other proton channels as well as chimeric proteins can be tested in tracking and also invasion. Thus, we will be able to find conserved structures among different proton channels. We were able to localize SiiAB and MotAB in the IM and in close contact with the flagellum and the SPI4-T1SS, but we need further improvement of the technique, also for validation as described above. Besides further optimization of the validated ALFA-tag and Spot-Tag here, we should exchange the Halo-Tag in SiiF and FliN with ALFA-tag and Spot-Tag, respectively, to minimize the distances between proteins and fluorophores as well as between the localized proteins. Also, additional subunits of the SPI4-T1SS and the flagellum can be tested. Another small tag, the EPEA-Tag is a further option to label three proteins per bacterium, which will allow triple-color 3D dSTORM imaging. To gain further insights into the ultrastructure of the processes in the IM, correlative light and electron microscopy (CLEM) could be performed in addition to dSTORM (Krieger *et al.*, 2014).

Is SiiAB a H⁺-conducting channels or a Na⁺-conducting channel?

I showed that SiiB has a higher conservation of certain regions with Na⁺-conducting channels and possesses residues that seem specific for them. These results together with the localization of SiiB at the flagellum, shed new light on possible functions and mechanisms of SiiAB,

apart from former described similarities to proton channels like MotAB (Kirchweger *et al.*, 2019). At the flagellum, not only H⁺, but also Na⁺-conducting stator complexes like PomAB are described, which also share similarities to MotAB (Yonekura *et al.*, 2011). As many bacteria exploit different proton channels for the same flagellum and rotor incorporation, using H⁺ as well as Na⁺, this could also be postulated for STM (Baker and O'Toole, 2017; Paulick *et al.*, 2015). Based on experiments of Yonekura *et al.* (2011), Baker and O'Toole (2017) and Paulick *et al.* (2015), we now can design new experiments to potentially show new ways of understanding SiiAB structure and function.

Role of the cytosolic domain of SiiB for SiiE and the flagellum?

A new field of mechanosensitive channels important for invasion of STM recently emerged (Asogwa, 2019; Miller, unpublished; Rasmussen and Rasmussen, 2018). SiiB possesses an extended cytosolic domain, interacting with SiiF (Wille *et al.*, 2014). By bioinformatic analyses, we found similarities to mechanosensitive channels, which as well harbor long cytosolic domains. In the results obtained in this work, there are hints that a deletion or overexpression of this domain affects SiiE retention and function. Thus, by further analyses of critical residues already published for mechanosensitive channels and experiments already published for YnaI, we will gain more insights in SiiB conduction and function.

While this study answers a lot of open questions in understanding SPI4-T1SS mediated adhesion, there are still many exciting experiments to be done to get to the bottom of things. The complete understanding of *Salmonella* adhesion and invasion will give important evidences for the development of new therapies to prevent initial steps of diseases also for other related pathogens. Particularly in today's situation with increasingly adapted pathogens and the spread of antibiotic resistances among them, research of invasion processes is of great importance for understanding of infection processes, development of anti-infective drugs, virulence inhibitors and therapies as well as transfer to other pathogens and diseases.

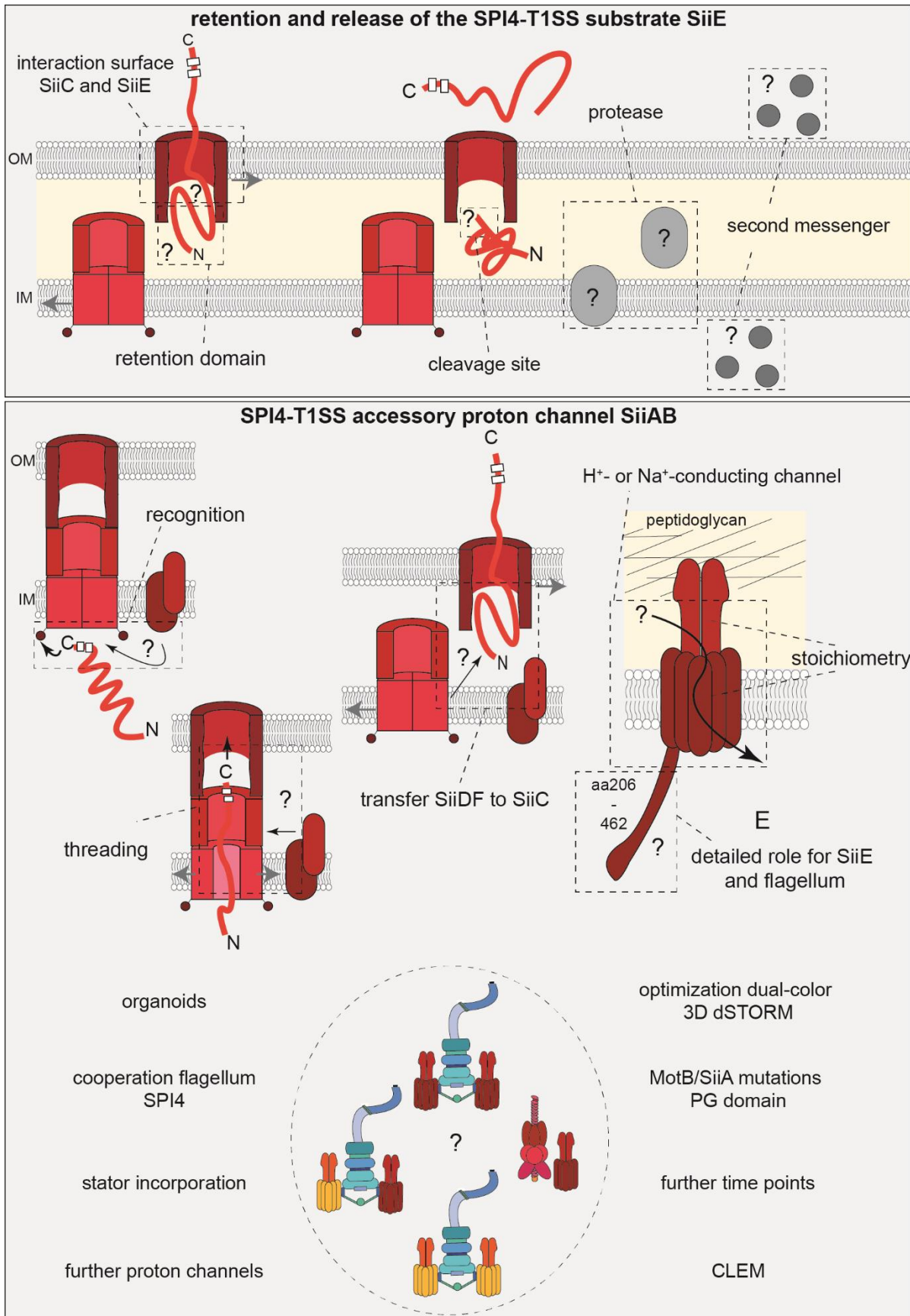


Figure IV.2. Outlook and open questions. Shown is the schematic overview of the open questions and further investigations.

V. References

- Aguilar, C., Alves da Silva, M., Saraiva, M., Neyazi, M., Olsson, I.A.S., and Bartfeld, S. (2021). Organoids as host models for infection biology - a review of methods. *Exp Mol Med* 53, 1471-1482.
- Ahmer, B.M., van Reeuwijk, J., Watson, P.R., Wallis, T.S., and Heffron, F. (1999). *Salmonella* SirA is a global regulator of genes mediating enteropathogenesis. *Mol Microbiol* 31, 971-982.
- Ambrosio, N., Boyd, C.D., GA, O.T., Fernandez, J., and Sisti, F. (2016). Homologs of the LapD-LapG c-di-GMP Effector System Control Biofilm Formation by *Bordetella bronchiseptica*. *PLoS One* 11, e0158752.
- Andersen, C., Hughes, C., and Koronakis, V. (2000). Chunnel vision. Export and efflux through bacterial channel-tunnels. *EMBO Rep* 1, 313-318.
- Asogwa, M.M., S.; Spano, S.; Stevens, M. (2019). Investigating the role of the bacterial mechanosensitive channel YnaI in *Salmonella* pathogenesis.
- Azar, J., Bahmad, H.F., Daher, D., Moubarak, M.M., Hadadeh, O., Monzer, A., Al Bitar, S., Jamal, M., Al-Sayegh, M., and Abou-Kheir, W. (2021). The Use of Stem Cell-Derived Organoids in Disease Modeling: An Update. *Int J Mol Sci* 22.
- Baker, A.E., and O'Toole, G.A. (2017). Bacteria, Rev Your Engines: Stator Dynamics Regulate Flagellar Motility. *J Bacteriol* 199.
- Bar Dolev, M., Bernheim, R., Guo, S., Davies, P.L., and Braslavsky, I. (2016). Putting life on ice: bacteria that bind to frozen water. *J R Soc Interface* 13.
- Barlag, B., Beutel, O., Janning, D., Czarniak, F., Richter, C.P., Kommnick, C., Goser, V., Kurre, R., Fabiani, F., Erhardt, M., *et al.* (2016). Single molecule super-resolution imaging of proteins in living *Salmonella enterica* using self-labelling enzymes. *Sci Rep* 6, 31601.
- Barlag, B., and Hensel, M. (2015). The giant adhesin SiiE of *Salmonella enterica*. *Molecules* 20, 1134-1150.
- Bartfeld, S. (2016). Modeling infectious diseases and host-microbe interactions in gastrointestinal organoids. *Dev Biol* 420, 262-270.
- Bass, S., Gu, Q., and Christen, A. (1996). Multicopy suppressors of *prc* mutant *Escherichia coli* include two HtrA (DegP) protease homologs (HhoAB), DksA, and a truncated R1pA. *J Bacteriol* 178, 1154-1161.
- Bates, M., Huang, B., Dempsey, G.T., and Zhuang, X. (2007). Multicolor super-resolution imaging with photo-switchable fluorescent probes. *Science* 317, 1749-1753.
- Berg, H.C. (2003). The rotary motor of bacterial flagella. *Annu Rev Biochem* 72, 19-54.
- Berg, H.C., and Anderson, R.A. (1973). Bacteria swim by rotating their flagellar filaments. *Nature* 245, 380-382.
- Beskow, L.M. (2016). Lessons from HeLa Cells: The Ethics and Policy of Biospecimens. *Annu Rev Genomics Hum Genet* 17, 395-417.
- Beumer, J., and Clevers, H. (2016). Regulation and plasticity of intestinal stem cells during homeostasis and regeneration. *Development* 143, 3639-3649.
- Blair, D.F., and Berg, H.C. (1988). Restoration of torque in defective flagellar motors. *Science* 242, 1678-1681.
- Blair, D.F., and Berg, H.C. (1990). The MotA protein of *E. coli* is a proton-conducting component of the flagellar motor. *Cell* 60, 439-449.
- Blair, D.F., and Berg, H.C. (1991). Mutations in the MotA protein of *Escherichia coli* reveal domains critical for proton conduction. *J Mol Biol* 221, 1433-1442.
- Blokzijl, F., de Ligt, J., Jager, M., Sasselli, V., Roerink, S., Sasaki, N., Huch, M., Boymans, S., Kuijk, E., Prins, P., *et al.* (2016). Tissue-specific mutation accumulation in human adult stem cells during life. *Nature* 538, 260-264.
- Boccellato, F., Woelffling, S., Imai-Matsushima, A., Sanchez, G., Goosmann, C., Schmid, M., Berger, H., Morey, P., Denecke, C., Ordemann, J., *et al.* (2019). Polarised epithelial monolayers of the gastric mucosa reveal insights into mucosal homeostasis and defence against infection. *Gut* 68, 400-413.

- Borlee, B.R., Goldman, A.D., Murakami, K., Samudrala, R., Wozniak, D.J., and Parsek, M.R. (2010). *Pseudomonas aeruginosa* uses a cyclic-di-GMP-regulated adhesin to reinforce the biofilm extracellular matrix. *Mol Microbiol* 75, 827-842.
- Boyd, C.D., and O'Toole, G.A. (2012). Second messenger regulation of biofilm formation: breakthroughs in understanding c-di-GMP effector systems. *Annu Rev Cell Dev Biol* 28, 439-462.
- Braun, M.B., Traenkle, B., Koch, P.A., Emele, F., Weiss, F., Poetz, O., Stehle, T., and Rothbauer, U. (2016). Peptides in headlock--a novel high-affinity and versatile peptide-binding nanobody for proteomics and microscopy. *Sci Rep* 6, 19211.
- Braun, V., Gaisser, S., Herrmann, C., Kampfenkel, K., Killmann, H., and Traub, I. (1996). Energy-coupled transport across the outer membrane of *Escherichia coli*: ExbB binds ExbD and TonB in vitro, and leucine 132 in the periplasmic region and aspartate 25 in the transmembrane region are important for ExbD activity. *J Bacteriol* 178, 2836-2845.
- Brossard, K.A., and Campagnari, A.A. (2012). The *Acinetobacter baumannii* biofilm-associated protein plays a role in adherence to human epithelial cells. *Infect Immun* 80, 228-233.
- Bumba, L., Masin, J., Macek, P., Wald, T., Motlova, L., Bibova, I., Klimova, N., Bednarova, L., Veverka, V., Kachala, M., *et al.* (2016). Calcium-Driven Folding of RTX Domain beta-Rolls Ratchets Translocation of RTX Proteins through Type I Secretion Ducts. *Mol Cell* 62, 47-62.
- Cain, J.A., Solis, N., and Cordwell, S.J. (2014). Beyond gene expression: the impact of protein post-translational modifications in bacteria. *J Proteomics* 97, 265-286.
- Casadevall, A., and Pirofski, L. (2001). Host-pathogen interactions: the attributes of virulence. *J Infect Dis* 184, 337-344.
- Casadevall, A., and Pirofski, L.A. (1999). Host-pathogen interactions: redefining the basic concepts of virulence and pathogenicity. *Infect Immun* 67, 3703-3713.
- Castillo, D.J., Nakamura, S., Morimoto, Y.V., Che, Y.S., Kami-Ike, N., Kudo, S., Minamino, T., and Namba, K. (2013). The C-terminal periplasmic domain of MotB is responsible for load-dependent control of the number of stators of the bacterial flagellar motor. *Biophysics (Nagoya-shi)* 9, 173-181.
- Celia, H., Botos, I., Ni, X., Fox, T., De Val, N., Lloubes, R., Jiang, J., and Buchanan, S.K. (2019). Cryo-EM structure of the bacterial Ton motor subcomplex ExbB-ExbD provides information on structure and stoichiometry. *Commun Biol* 2, 358.
- Chakravorty, D., Hansen-Wester, I., and Hensel, M. (2002). *Salmonella* pathogenicity island 2 mediates protection of intracellular *Salmonella* from reactive nitrogen intermediates. *J Exp Med* 195, 1155-1166.
- Che, Y.S., Nakamura, S., Morimoto, Y.V., Kami-Ike, N., Namba, K., and Minamino, T. (2014). Load-sensitive coupling of proton translocation and torque generation in the bacterial flagellar motor. *Mol Microbiol* 91, 175-184.
- Chen, Y.W., Huang, S.X., de Carvalho, A., Ho, S.H., Islam, M.N., Volpi, S., Notarangelo, L.D., Ciancanelli, M., Casanova, J.L., Bhattacharya, J., *et al.* (2017). A three-dimensional model of human lung development and disease from pluripotent stem cells. *Nat Cell Biol* 19, 542-549.
- Christensen, D.G., Xie, X., Basisty, N., Byrnes, J., McSweeney, S., Schilling, B., and Wolfe, A.J. (2019). Post-translational Protein Acetylation: An Elegant Mechanism for Bacteria to Dynamically Regulate Metabolic Functions. *Front Microbiol* 10, 1604.
- Cirillo, S.L.G., Yan, L., Littman, M., Samrakandi, M.M., and Cirillo, J.D. (2002). Role of the *Legionella pneumophila* rtxA gene in amoebae. *Microbiology (Reading)* 148, 1667-1677.
- Cooley, R.B., Smith, T.J., Leung, W., Tierney, V., Borlee, B.R., O'Toole, G.A., and Sondermann, H. (2016). Cyclic Di-GMP-Regulated Periplasmic Proteolysis of a *Pseudomonas aeruginosa* Type Vb Secretion System Substrate. *J Bacteriol* 198, 66-76.
- Cornelis, G.R. (2006). The type III secretion injectisome. *Nat Rev Microbiol* 4, 811-825.
- Coulton, J.W., and Murray, R.G. (1978). Cell envelope associations of *Aquaspirillum serpens* flagella. *J Bacteriol* 136, 1037-1049.
- De Leon, K.B., Zane, G.M., Trotter, V.V., Krantz, G.P., Arkin, A.P., Butland, G.P., Walian, P.J., Fields, M.W., and Wall, J.D. (2017). Unintended Laboratory-Driven Evolution Reveals Genetic Requirements for Biofilm Formation by *Desulfovibrio vulgaris* Hildenborough. *mBio* 8.

- De Maayer, P., and Cowan, D.A. (2016). Flashy flagella: flagellin modification is relatively common and highly versatile among the *Enterobacteriaceae*. *BMC Genomics* 17, 377.
- Dean, G.E., Macnab, R.M., Stader, J., Matsumura, P., and Burks, C. (1984). Gene sequence and predicted amino acid sequence of the motA protein, a membrane-associated protein required for flagellar rotation in *Escherichia coli*. *J Bacteriol* 159, 991-999.
- Deme, J.C., Johnson, S., Vickery, O., Aron, A., Monkhouse, H., Griffiths, T., James, R.H., Berks, B.C., Coulton, J.W., Stansfeld, P.J., *et al.* (2020a). Author Correction: Structures of the stator complex that drives rotation of the bacterial flagellum. *Nat Microbiol* 5, 1616.
- Deme, J.C., Johnson, S., Vickery, O., Aron, A., Monkhouse, H., Griffiths, T., James, R.H., Berks, B.C., Coulton, J.W., Stansfeld, P.J., *et al.* (2020b). Structures of the stator complex that drives rotation of the bacterial flagellum. *Nat Microbiol* 5, 1553-1564.
- Duan, Q., Zhou, M., Zhu, L., and Zhu, G. (2013). Flagella and bacterial pathogenicity. *J Basic Microbiol* 53, 1-8.
- Dutta, D., Heo, I., and Clevers, H. (2017). Disease Modeling in Stem Cell-Derived 3D Organoid Systems. *Trends Mol Med* 23, 393-410.
- Edwards, M.D., Black, S., Rasmussen, T., Rasmussen, A., Stokes, N.R., Stephen, T.L., Miller, S., and Booth, I.R. (2012). Characterization of three novel mechanosensitive channel activities in *Escherichia coli*. *Channels (Austin)* 6, 272-281.
- Egi Kardia, M.F., Tanja Strive, Xi-Lei Zeng, Mary Estes, Robyn N. Hall (2020). Isolation, culture and maintenance of rabbit intestinal organoids, and organoid-derived cell monolayers.
- Elpers, L., Kretzschmar, J., Nuccio, S.P., Baumler, A.J., and Hensel, M. (2020). Factors Required for Adhesion of *Salmonella enterica* Serovar Typhimurium to Corn Salad (*Valerianella locusta*). *Appl Environ Microbiol* 86.
- Espinosa-Urgel, M., Salido, A., and Ramos, J.L. (2000). Genetic analysis of functions involved in adhesion of *Pseudomonas putida* to seeds. *J Bacteriol* 182, 2363-2369.
- Espósito, D., and Chatterjee, D.K. (2006). Enhancement of soluble protein expression through the use of fusion tags. *Curr Opin Biotechnol* 17, 353-358.
- Ettayebi, K., Crawford, S.E., Murakami, K., Broughman, J.R., Karandikar, U., Tenge, V.R., Neill, F.H., Blutt, S.E., Zeng, X.L., Qu, L., *et al.* (2016). Replication of human noroviruses in stem cell-derived human enteroids. *Science* 353, 1387-1393.
- Evan, G.I., Lewis, G.K., Ramsay, G., and Bishop, J.M. (1985). Isolation of monoclonal antibodies specific for human c-myc proto-oncogene product. *Mol Cell Biol* 5, 3610-3616.
- Field, J., Nikawa, J., Broek, D., MacDonald, B., Rodgers, L., Wilson, I.A., Lerner, R.A., and Wigler, M. (1988). Purification of a RAS-responsive adenylyl cyclase complex from *Saccharomyces cerevisiae* by use of an epitope addition method. *Mol Cell Biol* 8, 2159-2165.
- Finkbeiner, S.R., Zeng, X.L., Utama, B., Atmar, R.L., Shroyer, N.F., and Estes, M.K. (2012). Stem cell-derived human intestinal organoids as an infection model for rotaviruses. *mBio* 3, e00159-00112.
- Flegler, V.J., Rasmussen, A., Rao, S., Wu, N., Zenobi, R., Sansom, M.S.P., Hedrich, R., Rasmussen, T., and Bottcher, B. (2020). The MscS-like channel Ynal has a gating mechanism based on flexible pore helices. *Proc Natl Acad Sci U S A* 117, 28754-28762.
- Forbester, J.L., Lees, E.A., Goulding, D., Forrest, S., Yeung, A., Speak, A., Clare, S., Coomber, E.L., Mukhopadhyay, S., Kraiczy, J., *et al.* (2018). Interleukin-22 promotes phagolysosomal fusion to induce protection against *Salmonella enterica* Typhimurium in human epithelial cells. *Proc Natl Acad Sci U S A* 115, 10118-10123.
- Forest, K.T., Dunham, S.A., Koomey, M., and Tainer, J.A. (1999). Crystallographic structure reveals phosphorylated pilin from *Neisseria*: phosphoserine sites modify type IV pilus surface chemistry and fibre morphology. *Mol Microbiol* 31, 743-752.
- Forrest, S., and Welch, M. (2020). Arming the troops: Post-translational modification of extracellular bacterial proteins. *Sci Prog* 103, 36850420964317.
- Fulop, V., Bocskei, Z., and Polgar, L. (1998). Prolyl oligopeptidase: an unusual beta-propeller domain regulates proteolysis. *Cell* 94, 161-170.
- Gassler, N. (2017). Paneth cells in intestinal physiology and pathophysiology. *World J Gastrointest Pathophysiol* 8, 150-160.

- Gaush, C.R., Hard, W.L., and Smith, T.F. (1966). Characterization of an established line of canine kidney cells (MDCK). *Proc Soc Exp Biol Med* 122, 931-935.
- Gerbe, F., and Jay, P. (2016). Intestinal tuft cells: epithelial sentinels linking luminal cues to the immune system. *Mucosal Immunol* 9, 1353-1359.
- Gerlach, R.G., Claudio, N., Rohde, M., Jackel, D., Wagner, C., and Hensel, M. (2008). Cooperation of *Salmonella* pathogenicity islands 1 and 4 is required to breach epithelial barriers. *Cell Microbiol* 10, 2364-2376.
- Gerlach, R.G., Jackel, D., Geymeier, N., and Hensel, M. (2007a). *Salmonella* pathogenicity island 4-mediated adhesion is coregulated with invasion genes in *Salmonella enterica*. *Infect Immun* 75, 4697-4709.
- Gerlach, R.G., Jackel, D., Stecher, B., Wagner, C., Lupas, A., Hardt, W.D., and Hensel, M. (2007b). *Salmonella* Pathogenicity Island 4 encodes a giant non-fimbrial adhesin and the cognate type 1 secretion system. *Cell Microbiol* 9, 1834-1850.
- Ginalski, K., Kinch, L., Rychlewski, L., and Grishin, N.V. (2004). BTLCP proteins: a novel family of bacterial transglutaminase-like cysteine proteinases. *Trends Biochem Sci* 29, 392-395.
- Gjermansen, M., Nilsson, M., Yang, L., and Tolker-Nielsen, T. (2010). Characterization of starvation-induced dispersion in *Pseudomonas putida* biofilms: genetic elements and molecular mechanisms. *Mol Microbiol* 75, 815-826.
- Gomez, D.P., and Boudreau, F. (2021). Organoids and Their Use in Modeling Gut Epithelial Cell Lineage Differentiation and Barrier Properties During Intestinal Diseases. *Front Cell Dev Biol* 9, 732137.
- Gotzke, H., Kilisch, M., Martinez-Carranza, M., Sograte-Idrissi, S., Rajavel, A., Schlichthaerle, T., Engels, N., Jungmann, R., Stenmark, P., Opazo, F., *et al.* (2019). The ALFA-tag is a highly versatile tool for nanobody-based bioscience applications. *Nat Commun* 10, 4403.
- Griessl, M.H., Schmid, B., Kassler, K., Braunsmann, C., Ritter, R., Barlag, B., Stierhof, Y.D., Sturm, K.U., Danzer, C., Wagner, C., *et al.* (2013). Structural insight into the giant Ca²⁺(+)-binding adhesin SiiE: implications for the adhesion of *Salmonella enterica* to polarized epithelial cells. *Structure* 21, 741-752.
- Gunn, J.S. (2011). *Salmonella* host-pathogen interactions: a special topic. *Front Microbiol* 2, 191.
- Guo, S., Langelaan, D.N., Phippen, S.W., Smith, S.P., Voets, I.K., and Davies, P.L. (2018). Conserved structural features anchor biofilm-associated RTX-adhesins to the outer membrane of bacteria. *FEBS J* 285, 1812-1826.
- Guo, S., Stevens, C.A., Vance, T.D.R., Olijve, L.L.C., Graham, L.A., Campbell, R.L., Yazdi, S.R., Escobedo, C., Bar-Dolev, M., Yashunsky, V., *et al.* (2017). Structure of a 1.5-MDa adhesin that binds its Antarctic bacterium to diatoms and ice. *Sci Adv* 3, e1701440.
- Guo, S., Vance, T.D.R., Stevens, C.A., Voets, I., and Davies, P.L. (2019a). RTX Adhesins are Key Bacterial Surface Megaproteins in the Formation of Biofilms. *Trends Microbiol* 27, 453-467.
- Guo, S., Vance, T.D.R., Stevens, C.A., Voets, I.K., and Davies, P.L. (2019b). RTX Adhesins are Key Bacterial Surface Megaproteins in the Formation of Biofilms. *Trends Microbiol* 27, 470.
- Guttula, D., Yao, M., Baker, K., Yang, L., Goult, B.T., Doyle, P.S., and Yan, J. (2019). Calcium-mediated Protein Folding and Stabilization of *Salmonella* Biofilm-associated Protein A. *J Mol Biol* 431, 433-443.
- Haiko, J., and Westerlund-Wikstrom, B. (2013). The role of the bacterial flagellum in adhesion and virulence. *Biology (Basel)* 2, 1242-1267.
- Haraga, A., Ohlson, M.B., and Miller, S.I. (2008). *Salmonellae* interplay with host cells. *Nat Rev Microbiol* 6, 53-66.
- Hell, S.W. (2009). Microscopy and its focal switch. *Nat Methods* 6, 24-32.
- Hensel, M. (2004). Evolution of pathogenicity islands of *Salmonella enterica*. *Int J Med Microbiol* 294, 95-102.
- Hensel, M., Klingauf, J., and Piehler, J. (2013). Imaging the invisible: resolving cellular microcompartments by superresolution microscopy techniques. *Biol Chem* 394, 1097-1113.
- Hizukuri, Y., Kojima, S., and Homma, M. (2010). Disulphide cross-linking between the stator and the bearing components in the bacterial flagellar motor. *J Biochem* 148, 309-318.

- Hochuli, E., Dobeli, H., and Schacher, A. (1987). New metal chelate adsorbent selective for proteins and peptides containing neighbouring histidine residues. *J Chromatogr* *411*, 177-184.
- Hoffmann, C., Gaietta, G., Bunemann, M., Adams, S.R., Oberdorff-Maass, S., Behr, B., Vildardaga, J.P., Tsien, R.Y., Ellisman, M.H., and Lohse, M.J. (2005). A FIAsh-based FRET approach to determine G protein-coupled receptor activation in living cells. *Nat Methods* *2*, 171-176.
- Horstmann, J.A., Lunelli, M., Cazzola, H., Heidemann, J., Kuhne, C., Steffen, P., Szefs, S., Rossi, C., Lokareddy, R.K., Wang, C., *et al.* (2020). Methylation of *Salmonella* Typhimurium flagella promotes bacterial adhesion and host cell invasion. *Nat Commun* *11*, 2013.
- Horstmann, J.A., Zschieschang, E., Truschel, T., de Diego, J., Lunelli, M., Rohde, M., May, T., Strowig, T., Stradal, T., Kolbe, M., *et al.* (2017). Flagellin phase-dependent swimming on epithelial cell surfaces contributes to productive *Salmonella* gut colonisation. *Cell Microbiol* *19*.
- Hosking, E.R., Vogt, C., Bakker, E.P., and Manson, M.D. (2006). The *Escherichia coli* MotAB proton channel unplugged. *J Mol Biol* *364*, 921-937.
- Huang, B., Babcock, H., and Zhuang, X. (2010). Breaking the diffraction barrier: super-resolution imaging of cells. *Cell* *143*, 1047-1058.
- Huang, B., Wang, W., Bates, M., and Zhuang, X. (2008). Three-dimensional super-resolution imaging by stochastic optical reconstruction microscopy. *Science* *319*, 810-813.
- Huch, M., Gehart, H., van Boxtel, R., Hamer, K., Blokzijl, F., Versteegen, M.M., Ellis, E., van Wenum, M., Fuchs, S.A., de Ligt, J., *et al.* (2015). Long-term culture of genome-stable bipotent stem cells from adult human liver. *Cell* *160*, 299-312.
- Iismaa, S.E., Kaidonis, X., Nicks, A.M., Bogush, N., Kikuchi, K., Naqvi, N., Harvey, R.P., Husain, A., and Graham, R.M. (2018). Comparative regenerative mechanisms across different mammalian tissues. *NPJ Regen Med* *3*, 6.
- Jackson, M.E., Pratt, J.M., Stoker, N.G., and Holland, I.B. (1985). An inner membrane protein N-terminal signal sequence is able to promote efficient localisation of an outer membrane protein in *Escherichia coli*. *EMBO J* *4*, 2377-2383.
- Jones, C.H., Dexter, P., Evans, A.K., Liu, C., Hultgren, S.J., and Hruby, D.E. (2002). *Escherichia coli* DegP protease cleaves between paired hydrophobic residues in a natural substrate: the PapA pilin. *J Bacteriol* *184*, 5762-5771.
- Kanonenberg, K., Schwarz, C.K., and Schmitt, L. (2013). Type I secretion systems - a story of appendices. *Res Microbiol* *164*, 596-604.
- Kawamoto, A., Morimoto, Y.V., Miyata, T., Minamino, T., Hughes, K.T., Kato, T., and Namba, K. (2013). Common and distinct structural features of *Salmonella* injectisome and flagellar basal body. *Sci Rep* *3*, 3369.
- Kelly-Wintenberg, K., South, S.L., and Montie, T.C. (1993). Tyrosine phosphate in a- and b-type flagellins of *Pseudomonas aeruginosa*. *J Bacteriol* *175*, 2458-2461.
- Keppler, A., Gendreizig, S., Gronemeyer, T., Pick, H., Vogel, H., and Johnsson, K. (2003). A general method for the covalent labeling of fusion proteins with small molecules *in vivo*. *Nat Biotechnol* *21*, 86-89.
- Keppler, A., Kindermann, M., Gendreizig, S., Pick, H., Vogel, H., and Johnsson, K. (2004). Labeling of fusion proteins of O6-alkylguanine-DNA alkyltransferase with small molecules *in vivo* and *in vitro*. *Methods* *32*, 437-444.
- Khan, S., Dapice, M., and Reese, T.S. (1988). Effects of mot gene expression on the structure of the flagellar motor. *J Mol Biol* *202*, 575-584.
- Khan, S., Ivey, D.M., and Krulwich, T.A. (1992). Membrane ultrastructure of alkaliphilic *Bacillus* species studied by rapid-freeze electron microscopy. *J Bacteriol* *174*, 5123-5126.
- Khan, S., Khan, I.H., and Reese, T.S. (1991). New structural features of the flagellar base in *Salmonella typhimurium* revealed by rapid-freeze electron microscopy. *J Bacteriol* *173*, 2888-2896.
- Kim, E.A., Price-Carter, M., Carlquist, W.C., and Blair, D.F. (2008a). Membrane segment organization in the stator complex of the flagellar motor: implications for proton flow and proton-induced conformational change. *Biochemistry* *47*, 11332-11339.
- Kim, T.J., Young, B.M., and Young, G.M. (2008b). Effect of flagellar mutations on *Yersinia enterocolitica* biofilm formation. *Appl Environ Microbiol* *74*, 5466-5474.

- Kirchweger, P., Weiler, S., Egerer-Sieber, C., Blasl, A.T., Hoffmann, S., Schmidt, C., Sander, N., Merker, D., Gerlach, R.G., Hensel, M., *et al.* (2019). Structural and functional characterization of SiiA, an auxiliary protein from the SPI4-encoded type 1 secretion system from *Salmonella enterica*. *Mol Microbiol* *112*, 1403-1422.
- Klein, T., Loschberger, A., Proppert, S., Wolter, S., van de Linde, S., and Sauer, M. (2011). Live-cell dSTORM with SNAP-tag fusion proteins. *Nat Methods* *8*, 7-9.
- Kocaoglu, O., and Carlson, E.E. (2016). Progress and prospects for small-molecule probes of bacterial imaging. *Nat Chem Biol* *12*, 472-478.
- Koirala, S., Mears, P., Sim, M., Golding, I., Chemla, Y.R., Aldridge, P.D., and Rao, C.V. (2014). A nutrient-tunable bistable switch controls motility in *Salmonella enterica* serovar Typhimurium. *mBio* *5*, e01611-01614.
- Kojima, S. (2015). Dynamism and regulation of the stator, the energy conversion complex of the bacterial flagellar motor. *Curr Opin Microbiol* *28*, 66-71.
- Kojima, S., and Blair, D.F. (2001). Conformational change in the stator of the bacterial flagellar motor. *Biochemistry* *40*, 13041-13050.
- Kojima, S., Takao, M., Almira, G., Kawahara, I., Sakuma, M., Homma, M., Kojima, C., and Imada, K. (2018). The Helix Rearrangement in the Periplasmic Domain of the Flagellar Stator B Subunit Activates Peptidoglycan Binding and Ion Influx. *Structure* *26*, 590-598 e595.
- Kolmer, J.A., and Liu, J.Q. (2000). Virulence and Molecular Polymorphism in International Collections of the Wheat Leaf Rust Fungus *Puccinia triticina*. *Phytopathology* *90*, 427-436.
- Kommnick, C.K., J.; Lepper, A.; Kurre, R. and Michael Hensel (2021). The orchestration of invasion – Functional interplay of effector proteins is essential for *Salmonella enterica* serovar Typhimurium to efficiently trigger invasion of highly polarized epithelial cells. unpublished.
- Koronakis, V., Koronakis, E., and Hughes, C. (1989). Isolation and analysis of the C-terminal signal directing export of *Escherichia coli* hemolysin protein across both bacterial membranes. *EMBO J* *8*, 595-605.
- Krieger, V., Liebl, D., Zhang, Y., Rajashekar, R., Chlanda, P., Giesker, K., Chikkaballi, D., and Hensel, M. (2014). Reorganization of the endosomal system in *Salmonella*-infected cells: the ultrastructure of *Salmonella*-induced tubular compartments. *PLoS Pathog* *10*, e1004374.
- Kuhlbrandt, W., and Davies, K.M. (2016). Rotary ATPases: A New Twist to an Ancient Machine. *Trends Biochem Sci* *41*, 106-116.
- Lai, Y.W., Ridone, P., Peralta, G., Tanaka, M.M., and Baker, M.A.B. (2020). Evolution of the Stator Elements of Rotary Prokaryote Motors. *J Bacteriol* *202*.
- Lancaster, M.A., and Knoblich, J.A. (2014). Organogenesis in a dish: modeling development and disease using organoid technologies. *Science* *345*, 1247125.
- Lang, J., Cheng, Y., Rolfe, A., Hammack, C., Vera, D., Kyle, K., Wang, J., Meissner, T.B., Ren, Y., Cowan, C., *et al.* (2018). An hPSC-Derived Tissue-Resident Macrophage Model Reveals Differential Responses of Macrophages to ZIKV and DENV Infection. *Stem Cell Reports* *11*, 348-362.
- Larsen, S.H., Adler, J., Gargus, J.J., and Hogg, R.W. (1974). Chemomechanical coupling without ATP: the source of energy for motility and chemotaxis in bacteria. *Proc Natl Acad Sci U S A* *71*, 1239-1243.
- Latasa, C., Echeverez, M., Garcia, B., Gil, C., Garcia-Ona, E., Burgui, S., Casares, N., Hervás-Stubbs, S., Lasarte, J.J., Lasa, I., *et al.* (2016). Evaluation of a *Salmonella* Strain Lacking the Secondary Messenger C-di-GMP and RpoS as a Live Oral Vaccine. *PLoS One* *11*, e0161216.
- Latasa, C., Roux, A., Toledo-Arana, A., Ghigo, J.M., Gamazo, C., Penades, J.R., and Lasa, I. (2005). BapA, a large secreted protein required for biofilm formation and host colonization of *Salmonella enterica* serovar Enteritidis. *Mol Microbiol* *58*, 1322-1339.
- Lecher, J., Schwarz, C.K., Stoldt, M., Smits, S.H., Willbold, D., and Schmitt, L. (2012). An RTX transporter tethers its unfolded substrate during secretion via a unique N-terminal domain. *Structure* *20*, 1778-1787.
- Lederberg, J.I., T. (1956). Phase variation in *Salmonella*. *Genetics* *41*, 743.
- Lee, L.K., Ginsburg, M.A., Crovace, C., Donohoe, M., and Stock, D. (2010). Structure of the torque ring of the flagellar motor and the molecular basis for rotational switching. *Nature* *466*, 996-1000.

- Lees, E.A., Forbester, J.L., Forrest, S., Kane, L., Goulding, D., and Dougan, G. (2019). Using Human Induced Pluripotent Stem Cell-derived Intestinal Organoids to Study and Modify Epithelial Cell Protection Against *Salmonella* and Other Pathogens. *J Vis Exp*.
- Lemon, K.P., Higgins, D.E., and Kolter, R. (2007). Flagellar motility is critical for *Listeria monocytogenes* biofilm formation. *J Bacteriol* 189, 4418-4424.
- Leslie, J.L., Huang, S., Opp, J.S., Nagy, M.S., Kobayashi, M., Young, V.B., and Spence, J.R. (2015). Persistence and toxin production by *Clostridium difficile* within human intestinal organoids result in disruption of epithelial paracellular barrier function. *Infect Immun* 83, 138-145.
- Li, X., Nadauld, L., Ootani, A., Corney, D.C., Pai, R.K., Gevaert, O., Cantrell, M.A., Rack, P.G., Neal, J.T., Chan, C.W., et al. (2014a). Oncogenic transformation of diverse gastrointestinal tissues in primary organoid culture. *Nat Med* 20, 769-777.
- Li, Y., Xu, C., and Ma, T. (2014b). In vitro organogenesis from pluripotent stem cells. *Organogenesis* 10, 159-163.
- Lloyd, S.A., and Blair, D.F. (1997). Charged residues of the rotor protein FliG essential for torque generation in the flagellar motor of *Escherichia coli*. *J Mol Biol* 266, 733-744.
- Los, G.V., and Wood, K. (2007). The HaloTag: a novel technology for cell imaging and protein analysis. *Methods Mol Biol* 356, 195-208.
- Ludwig, A., Garcia, F., Bauer, S., Jarchau, T., Benz, R., Hoppe, J., and Goebel, W. (1996). Analysis of the in vivo activation of hemolysin (HlyA) from *Escherichia coli*. *J Bacteriol* 178, 5422-5430.
- Mackman, N., Nicaud, J.M., Gray, L., and Holland, I.B. (1985). Genetical and functional organisation of the *Escherichia coli* haemolysin determinant 2001. *Mol Gen Genet* 201, 282-288.
- Macnab, R.M. (2004). Type III flagellar protein export and flagellar assembly. *Biochim Biophys Acta* 1694, 207-217.
- Main-Hester, K.L., Colpitts, K.M., Thomas, G.A., Fang, F.C., and Libby, S.J. (2008). Coordinate regulation of *Salmonella* pathogenicity island 1 (SPI1) and SPI4 in *Salmonella enterica* serovar Typhimurium. *Infect Immun* 76, 1024-1035.
- Malkusch, S., Endesfelder, U., Mondry, J., Gelleri, M., Verveer, P.J., and Heilemann, M. (2012). Coordinate-based colocalization analysis of single-molecule localization microscopy data. *Histochem Cell Biol* 137, 1-10.
- Mandadapu, K.K., Nirody, J.A., Berry, R.M., and Oster, G. (2015). Mechanics of torque generation in the bacterial flagellar motor. *Proc Natl Acad Sci U S A* 112, E4381-4389.
- Marcus, S.L., Brumell, J.H., Pfeifer, C.G., and Finlay, B.B. (2000). *Salmonella* pathogenicity islands: big virulence in small packages. *Microbes Infect* 2, 145-156.
- Mass, L., Holtmannspotter, M., and Zachgo, S. (2020). Dual-color 3D-dSTORM colocalization and quantification of ROXY1 and RNAPII variants throughout the transcription cycle in root meristem nuclei. *Plant J* 104, 1423-1436.
- Mertins, S., Allan, B.J., Townsend, H.G., Koster, W., and Potter, A.A. (2013). Role of motAB in adherence and internalization in polarized Caco-2 cells and in cecal colonization of *Campylobacter jejuni*. *Avian Dis* 57, 116-122.
- Metterlein, M.Y., L.; Buchfellner, A.; Ruf, B. (2018). Spot-Tag: a Nanobody-based Peptide-Tag System for Protein Detection, Purification and Imaging.
- Miller, S.S., S. (unpublished). Investigating the Role of the Bacterial Mechanosensitive Channel YnaI in *Salmonella* Pathogenesis.
- Minamino, T., and Imada, K. (2015). The bacterial flagellar motor and its structural diversity. *Trends Microbiol* 23, 267-274.
- Minamino, T., Imada, K., and Namba, K. (2008). Molecular motors of the bacterial flagella. *Curr Opin Struct Biol* 18, 693-701.
- Minamino, T., Kinoshita, M., and Namba, K. (2019). Directional Switching Mechanism of the Bacterial Flagellar Motor. *Comput Struct Biotechnol J* 17, 1075-1081.
- Minamino, T., Terahara, N., Kojima, S., and Namba, K. (2018). Autonomous control mechanism of stator assembly in the bacterial flagellar motor in response to changes in the environment. *Mol Microbiol* 109, 723-734.

- Minamino, T.M., Y.; Kawamoto, A.; Terashima, H.; Imada, K. (2018). *Salmonella* Flagellum. Mo, E., Peters, S.E., Willers, C., Maskell, D.J., and Charles, I.G. (2006). Single, double and triple mutants of *Salmonella enterica* serovar Typhimurium degP (htrA), degQ (hhoA) and degS (hhoB) have diverse phenotypes on exposure to elevated temperature and their growth in vivo is attenuated to different extents. *Microb Pathog* 41, 174-182.
- Morimoto, Y.V., and Minamino, T. (2014). Structure and function of the bi-directional bacterial flagellar motor. *Biomolecules* 4, 217-234.
- Muyldermans, S. (2013). Nanobodies: natural single-domain antibodies. *Annu Rev Biochem* 82, 775-797.
- Nakamura, S., and Minamino, T. (2019). Flagella-Driven Motility of Bacteria. *Biomolecules* 9.
- Navarro, M.V., Newell, P.D., Krasteva, P.V., Chatterjee, D., Madden, D.R., O'Toole, G.A., and Sondermann, H. (2011). Structural basis for c-di-GMP-mediated inside-out signaling controlling periplasmic proteolysis. *PLoS Biol* 9, e1000588.
- Newell, P.D., Boyd, C.D., Sondermann, H., and O'Toole, G.A. (2011). A c-di-GMP effector system controls cell adhesion by inside-out signaling and surface protein cleavage. *PLoS Biol* 9, e1000587.
- Nicaud, J.M., Mackman, N., Gray, L., and Holland, I.B. (1985). Characterisation of HlyC and mechanism of activation and secretion of haemolysin from *E. coli* 2001. *FEBS Lett* 187, 339-344.
- Nooh, M.M., and Bahouth, S.W. (2017). Visualization and quantification of GPCR trafficking in mammalian cells by confocal microscopy. *Methods Cell Biol* 142, 67-78.
- Ollis, A.A., Manning, M., Held, K.G., and Postle, K. (2009). Cytoplasmic membrane protonmotive force energizes periplasmic interactions between ExbD and TonB. *Mol Microbiol* 73, 466-481.
- Partridge, J.D., and Harshey, R.M. (2013). More than motility: *Salmonella* flagella contribute to overriding friction and facilitating colony hydration during swarming. *J Bacteriol* 195, 919-929.
- Paulick, A., Delalez, N.J., Brenzinger, S., Steel, B.C., Berry, R.M., Armitage, J.P., and Thormann, K.M. (2015). Dual stator dynamics in the *Shewanella oneidensis* MR-1 flagellar motor. *Mol Microbiol* 96, 993-1001.
- Perez-Mendoza, D., Coulthurst, S.J., Humphris, S., Campbell, E., Welch, M., Toth, I.K., and Salmond, G.P. (2011). A multi-repeat adhesin of the phytopathogen, *Pectobacterium atrosepticum*, is secreted by a Type I pathway and is subject to complex regulation involving a non-canonical diguanylate cyclase. *Mol Microbiol* 82, 719-733.
- Peters, B., Stein, J., Klingl, S., Sander, N., Sandmann, A., Taccardi, N., Sticht, H., Gerlach, R.G., Muller, Y.A., and Hensel, M. (2017). Structural and functional dissection reveals distinct roles of Ca²⁺-binding sites in the giant adhesin SiiE of *Salmonella enterica*. *PLoS Pathog* 13, e1006418.
- Peterson, L.W., and Artis, D. (2014). Intestinal epithelial cells: regulators of barrier function and immune homeostasis. *Nat Rev Immunol* 14, 141-153.
- Ponce de Leon-Rodriguez, M.D.C., Guyot, J.P., and Laurent-Babot, C. (2019). Intestinal in vitro cell culture models and their potential to study the effect of food components on intestinal inflammation. *Crit Rev Food Sci Nutr* 59, 3648-3666.
- Pott, J., and Hornef, M. (2012). Innate immune signalling at the intestinal epithelium in homeostasis and disease. *EMBO Rep* 13, 684-698.
- Rasmussen, T., and Rasmussen, A. (2018). Bacterial Mechanosensitive Channels. *Subcell Biochem* 87, 83-116.
- Reynaud, E.G., Krzic, U., Greger, K., and Stelzer, E.H. (2008). Light sheet-based fluorescence microscopy: more dimensions, more photons, and less photodamage. *HFSP J* 2, 266-275.
- Röder, J., Felgner, P., and Hensel, M. (2021a). Comprehensive Single Cell Analyses of the Nutritional Environment of Intracellular *Salmonella enterica*. *Front Cell Infect Microbiol* 11, 624650.
- Röder, J., Felgner, P., and Hensel, M. (2021b). Single-cell analyses reveal phosphate availability as critical factor for nutrition of *Salmonella enterica* within mammalian host cells. *Cell Microbiol* 23, e13374.

- Rowe, I., Anishkin, A., Kamaraju, K., Yoshimura, K., and Sukharev, S. (2014). The cytoplasmic cage domain of the mechanosensitive channel MscS is a sensor of macromolecular crowding. *J Gen Physiol* 143, 543-557.
- Rust, M.J., Bates, M., and Zhuang, X. (2006). Sub-diffraction-limit imaging by stochastic optical reconstruction microscopy (STORM). *Nat Methods* 3, 793-795.
- Rybtke, M., Berthelsen, J., Yang, L., Hoiby, N., Givskov, M., and Tolker-Nielsen, T. (2015). The LapG protein plays a role in *Pseudomonas aeruginosa* biofilm formation by controlling the presence of the CdrA adhesin on the cell surface. *Microbiologyopen* 4, 917-930.
- Sachs, N., Papaspyropoulos, A., Zomer-van Ommen, D.D., Heo, I., Bottinger, L., Klay, D., Weeber, F., Huelsz-Prince, G., Jakobachvili, N., Amatngalim, G.D., *et al.* (2019). Long-term expanding human airway organoids for disease modeling. *EMBO J* 38.
- Sahl, S.J., and Moerner, W.E. (2013). Super-resolution fluorescence imaging with single molecules. *Curr Opin Struct Biol* 23, 778-787.
- Sang, Y.R., J.; Ni, J.; Tao, J.; Lu, J.; Yao, J.-F. (2016). Protein Acetylation Is Involved in *Salmonella enterica* Serovar Typhimurium Virulence. *J Infect Dis* 213, 1836-1845.
- Sansonetti, P.J. (2004). War and peace at mucosal surfaces. *Nat Rev Immunol* 4, 953-964.
- Santiveri, M., Roa-Eguiara, A., Kuhne, C., Wadhwa, N., Hu, H., Berg, H.C., Erhardt, M., and Taylor, N.M.I. (2020). Structure and Function of Stator Units of the Bacterial Flagellar Motor. *Cell* 183, 244-257 e216.
- Satchell, K.J. (2011). Structure and function of MARTX toxins and other large repetitive RTX proteins. *Annu Rev Microbiol* 65, 71-90.
- Sauer, K., Camper, A.K., Ehrlich, G.D., Costerton, J.W., and Davies, D.G. (2002). *Pseudomonas aeruginosa* displays multiple phenotypes during development as a biofilm. *J Bacteriol* 184, 1140-1154.
- Schermelleh, L., Heintzmann, R., and Leonhardt, H. (2010). A guide to super-resolution fluorescence microscopy. *J Cell Biol* 190, 165-175.
- Schulte, M., Olschewski, K., and Hensel, M. (2021a). Fluorescent protein-based reporters reveal stress response of intracellular *Salmonella enterica* at level of single bacterial cells. *Cell Microbiol* 23, e13293.
- Schulte, M., Olschewski, K., and Hensel, M. (2021b). The protected physiological state of intracellular *Salmonella enterica* persists reduces host cell-imposed stress. *Commun Biol* 4, 520.
- Schumann, U., Edwards, M.D., Rasmussen, T., Bartlett, W., van West, P., and Booth, I.R. (2010). YbdG in *Escherichia coli* is a threshold-setting mechanosensitive channel with MscM activity. *Proc Natl Acad Sci U S A* 107, 12664-12669.
- Sepe, L.P., Hartl, K., Iftekhhar, A., Berger, H., Kumar, N., Goosmann, C., Chopra, S., Schmidt, S.C., Gurusurthy, R.K., Meyer, T.F., *et al.* (2020). Genotoxic Effect of *Salmonella* Paratyphi A Infection on Human Primary Gallbladder Cells. *mBio* 11.
- Shi, Y., Pellarin, R., Fridy, P.C., Fernandez-Martinez, J., Thompson, M.K., Li, Y., Wang, Q.J., Sali, A., Rout, M.P., and Chait, B.T. (2015). A strategy for dissecting the architectures of native macromolecular assemblies. *Nat Methods* 12, 1135-1138.
- Silverman, M., and Simon, M. (1974). Flagellar rotation and the mechanism of bacterial motility. *Nature* 249, 73-74.
- Smith, T.J., Font, M.E., Kelly, C.M., Sondermann, H., and O'Toole, G.A. (2018a). An N-Terminal Retention Module Anchors the Giant Adhesin LapA of *Pseudomonas fluorescens* at the Cell Surface: a Novel Subfamily of Type I Secretion Systems. *J Bacteriol* 200.
- Smith, T.J., Sondermann, H., and O'Toole, G.A. (2018b). Type 1 Does the Two-Step: Type 1 Secretion Substrates with a Functional Periplasmic Intermediate. *J Bacteriol* 200.
- Smits, A.H., and Vermeulen, M. (2016). Characterizing Protein-Protein Interactions Using Mass Spectrometry: Challenges and Opportunities. *Trends Biotechnol* 34, 825-834.
- Stader, J., Matsumura, P., Vacante, D., Dean, G.E., and Macnab, R.M. (1986). Nucleotide sequence of the *Escherichia coli* motB gene and site-limited incorporation of its product into the cytoplasmic membrane. *J Bacteriol* 166, 244-252.

- Stadler, C., Rexhepaj, E., Singan, V.R., Murphy, R.F., Pepperkok, R., Uhlen, M., Simpson, J.C., and Lundberg, E. (2013). Immunofluorescence and fluorescent-protein tagging show high correlation for protein localization in mammalian cells. *Nat Methods* 10, 315-323.
- Standish, A.J., Teh, M.Y., Tran, E.N.H., Doyle, M.T., Baker, P.J., and Morona, R. (2016). Unprecedented Abundance of Protein Tyrosine Phosphorylation Modulates *Shigella flexneri* Virulence. *J Mol Biol* 428, 4197-4208.
- Strauch, K.L., and Beckwith, J. (1988). An *Escherichia coli* mutation preventing degradation of abnormal periplasmic proteins. *Proc Natl Acad Sci U S A* 85, 1576-1580.
- Strauch, K.L., Johnson, K., and Beckwith, J. (1989). Characterization of degP, a gene required for proteolysis in the cell envelope and essential for growth of *Escherichia coli* at high temperature. *J Bacteriol* 171, 2689-2696.
- Suriyanarayanan, T., Periasamy, S., Lin, M.H., Ishihama, Y., and Swarup, S. (2016). Flagellin FliC Phosphorylation Affects Type 2 Protease Secretion and Biofilm Dispersal in *Pseudomonas aeruginosa* PAO1. *PLoS One* 11, e0164155.
- Syed, K.A., Beyhan, S., Correa, N., Queen, J., Liu, J., Peng, F., Satchell, K.J., Yildiz, F., and Klose, K.E. (2009). The *Vibrio cholerae* flagellar regulatory hierarchy controls expression of virulence factors. *J Bacteriol* 191, 6555-6570.
- Takashima, S., Gold, D., and Hartenstein, V. (2013). Stem cells and lineages of the intestine: a developmental and evolutionary perspective. *Dev Genes Evol* 223, 85-102.
- Thanabalu, T., Koronakis, E., Hughes, C., and Koronakis, V. (1998). Substrate-induced assembly of a contiguous channel for protein export from *E.coli*: reversible bridging of an inner-membrane translocase to an outer membrane exit pore. *EMBO J* 17, 6487-6496.
- Theunissen, S., De Smet, L., Dansercoer, A., Motte, B., Coenye, T., Van Beeumen, J.J., Devreese, B., Savvides, S.N., and Vergauwen, B. (2010). The 285 kDa Bap/RTX hybrid cell surface protein (SO4317) of *Shewanella oneidensis* MR-1 is a key mediator of biofilm formation. *Res Microbiol* 161, 144-152.
- Turner, J.R. (2009). Intestinal mucosal barrier function in health and disease. *Nat Rev Immunol* 9, 799-809.
- van de Linde, S., Sauer, M., and Heilemann, M. (2008). Subdiffraction-resolution fluorescence imaging of proteins in the mitochondrial inner membrane with photoswitchable fluorophores. *J Struct Biol* 164, 250-254.
- van der Flier, L.G., and Clevers, H. (2009). Stem cells, self-renewal, and differentiation in the intestinal epithelium. *Annu Rev Physiol* 71, 241-260.
- Virant, D., Traenkle, B., Maier, J., Kaiser, P.D., Bodenhofer, M., Schmees, C., Vojnovic, I., Pisak-Lukats, B., Endesfelder, U., and Rothbauer, U. (2018). A peptide tag-specific nanobody enables high-quality labeling for dSTORM imaging. *Nat Commun* 9, 930.
- Wagner, C., Barlag, B., Gerlach, R.G., Deiwick, J., and Hensel, M. (2014). The *Salmonella enterica* giant adhesin SiiE binds to polarized epithelial cells in a lectin-like manner. *Cell Microbiol* 16, 962-975.
- Wagner, C., Polke, M., Gerlach, R.G., Linke, D., Stierhof, Y.D., Schwarz, H., and Hensel, M. (2011). Functional dissection of SiiE, a giant non-fimbrial adhesin of *Salmonella enterica*. *Cell Microbiol* 13, 1286-1301.
- Waller, P.R., and Sauer, R.T. (1996). Characterization of degQ and degS, *Escherichia coli* genes encoding homologs of the DegP protease. *J Bacteriol* 178, 1146-1153.
- Wang, X., Tang, S., Wen, X., Hong, L., Hong, F., and Li, Y. (2018). Transmembrane TM3b of Mechanosensitive Channel MscS Interacts With Cytoplasmic Domain Cyto-Helix. *Front Physiol* 9, 1389.
- Waugh, D.S. (2005). Making the most of affinity tags. *Trends Biotechnol* 23, 316-320.
- Wille, T., Wagner, C., Mittelstadt, W., Blank, K., Sommer, E., Malengo, G., Dohler, D., Lange, A., Sourjik, V., Hensel, M., et al. (2014). SiiA and SiiB are novel type I secretion system subunits controlling SPI4-mediated adhesion of *Salmonella enterica*. *Cell Microbiol* 16, 161-178.
- Wilmes, S., Staufienbiel, M., Lisse, D., Richter, C.P., Beutel, O., Busch, K.B., Hess, S.T., and Piehler, J. (2012). Triple-color super-resolution imaging of live cells: resolving submicroscopic receptor organization in the plasma membrane. *Angew Chem Int Ed Engl* 51, 4868-4871.

- Wilson, M.L., and Macnab, R.M. (1988). Overproduction of the MotA protein of *Escherichia coli* and estimation of its wild-type level. *J Bacteriol* 170, 588-597.
- Wood, T.K., Gonzalez Barrios, A.F., Herzberg, M., and Lee, J. (2006). Motility influences biofilm architecture in *Escherichia coli*. *Appl Microbiol Biotechnol* 72, 361-367.
- Ye, L., Wang, J., Beyer, A.I., Teque, F., Cradick, T.J., Qi, Z., Chang, J.C., Bao, G., Muench, M.O., Yu, J., *et al.* (2014). Seamless modification of wild-type induced pluripotent stem cells to the natural CCR5Delta32 mutation confers resistance to HIV infection. *Proc Natl Acad Sci U S A* 111, 9591-9596.
- Yonekura, K., Maki-Yonekura, S., and Homma, M. (2011). Structure of the flagellar motor protein complex PomAB: implications for the torque-generating conformation. *J Bacteriol* 193, 3863-3870.
- Yousef-Coronado, F., Travieso, M.L., and Espinosa-Urgel, M. (2008). Different, overlapping mechanisms for colonization of abiotic and plant surfaces by *Pseudomonas putida*. *FEMS Microbiol Lett* 288, 118-124.
- Zhou, G., Yuan, J., and Gao, H. (2015). Regulation of biofilm formation by BpfA, BpfD, and BpfG in *Shewanella oneidensis*. *Front Microbiol* 6, 790.
- Zhou, J., and Blair, D.F. (1997). Residues of the cytoplasmic domain of MotA essential for torque generation in the bacterial flagellar motor. *J Mol Biol* 273, 428-439.
- Zhou, J., Fazzio, R.T., and Blair, D.F. (1995). Membrane topology of the MotA protein of *Escherichia coli*. *J Mol Biol* 251, 237-242.
- Zhou, J., Li, C., Zhao, G., Chu, H., Wang, D., Yan, H.H., Poon, V.K., Wen, L., Wong, B.H., Zhao, X., *et al.* (2017). Human intestinal tract serves as an alternative infection route for Middle East respiratory syndrome coronavirus. *Sci Adv* 3, eaao4966.
- Zhou, J., Lloyd, S.A., and Blair, D.F. (1998). Electrostatic interactions between rotor and stator in the bacterial flagellar motor. *Proc Natl Acad Sci U S A* 95, 6436-6441.
- Zhu, S., Takao, M., Li, N., Sakuma, M., Nishino, Y., Homma, M., Kojima, S., and Imada, K. (2014). Conformational change in the periplamic region of the flagellar stator coupled with the assembly around the rotor. *Proc Natl Acad Sci U S A* 111, 13523-13528.

VI. List of abbreviations

aa	amino acid
ABC	ATP-binding cassette
AHT	anhydrotetracycline
ATP	adenosine triphosphate
ATPase	adenosine triphosphatase
Blg	bacterial immunoglobulin domain
BTLCp	bacterial transglutaminase-like cysteine proteinase
Ca ²⁺	Calcium
CCW	counter clockwise
CDR	complementary determining regions
CFU	colony-forming units
c-di-GMP	Bis-(3'-5')-cyclic dimeric guanosine monophosphate
CLD	C39-like domain
CW	clockwise
IPTG	isopropyl β -D-1-thiogalactopyranoside
LB	Luria-Bertani
LPS	lipopolysaccharide
MCP	methyl-accepting chemotaxis protein
NbALFA	α -ALFA-tag nanobody
OAg	O-antigen
OM	outer membrane
ORF	open reading frame
PAP	periplasmic adaptor protein
PG	peptidoglycan
PGB	peptidoglycan-binding

PMF	proton motif force
PSF	point spread function
RTX	repeats-in-toxin
SCV	<i>Salmonella</i> -containing vacuole
SIF	<i>Salmonella</i> -induced filament
SPA	<i>Salmonella enterica</i> serovar Paratyphi
SPI	<i>Salmonella</i> pathogenicity island
SRM	super-resolution microscopy
STM	<i>Salmonella enterica</i> serovar Typhimurium
dSTORM	direct stochastic reconstruction microscopy
STY	<i>Salmonella enterica</i> serovar Typhi
T1SS	type 1 secretion system
T3SS	type 3 secretion system
TIRFM	total internal reflection microscopy
TM	transmembrane
WT	wild type

VII. Curriculum vitae

Persönliche Daten

Name: Nathalie Xenia Sander
Geburtsdatum: 19.01.1992

Studium

04/2018 – heute Promotionsstudium an der Universität Osnabrück
Promotionsprojekt mit dem Titel „Functional analysis and characterization of the type I secretion system and its substrate, the giant adhesin SiiE, of *Salmonella enterica*“ in der Abteilung Mikrobiologie unter der Betreuung von Prof. Dr. Michael Hensel

10/2015 – 03/2018 Masterstudiengang Biowissenschaften mit dem Schwerpunkt „Zell- und Molekularbiologie“ an der Universität Osnabrück
Abschluss Master of Science: Note 1,3
Masterarbeit: „The impact of endosomal remodeling on the intracellular lifestyle of *Salmonella enterica* – analysis of differentially regulated transporters“, Abteilung Mikrobiologie, Universität Osnabrück unter der Betreuung von Prof. Dr. Michael Hensel

10/2012 – 09/2015 Bachelorstudiengang Biowissenschaften an der Universität Osnabrück
Abschluss Bachelor of Science: Note 2,1
Bachelorarbeit: „Rolle der N-terminalen Domäne für die Retention des nicht-fimbrilliären Adhäsins SiiE in *Salmonella enterica*“, Abteilung Mikrobiologie, Universität Osnabrück unter der Betreuung von Prof. Dr. Michael Hensel

Auszeichnungen/Preise

2018 GBM Masterpreis, verliehen durch die Gesellschaft für Biochemie und Molekularbiologie

Schulabschluss

06/2011 Abitur Gymnasium Athenauem Stade

Teilnahme an Tagungen

10/2019 EMBO Workshop: Tools for Structural Biology of Membrane Proteins (Hamburg)

Poster "Role of the non-canonical membrane proteins SiiA and SiiB for the type I secretion system of *Salmonella enterica*"

10/2019 SFB944 Retreat (Bremen)

Vortrag "Role of the non-canonical membrane proteins SiiA and SiiB for the type I secretion system of *Salmonella enterica*"

09/2018 EMBO/EMBL Symposium: Organoids: Modelling Organ Development and Disease in 3D Culture (Heidelberg)

10/2018 Annual Minisymposium *Salmonella* (Dorfweil)

Vortrag and Poster „Molecular and cellular functions of the giant adhesin SiiE and the cognate type 1 secretion system of *Salmonella enterica*”

09/2018 SFB944 Retreat (Osnabrück)

Flash-Talk and Poster "Functional analysis and characterization of the type I secretion system and its substrate, the giant adhesin SiiE, of *Salmonella enterica*"

11/2017 Annual Minisymposium *Salmonella* (Freiburg)

Vortrag "The impact of SIF architecture on intracellular *Salmonella*"

VIII. List of publications

Structural and functional dissection reveals distinct roles of Ca²⁺-binding sites in the giant adhesin SiiE of *Salmonella enterica*.

Peters B, Stein J, Klingl S, Sander N, Sandmann A, Taccardi N, Sticht H, Gerlach RG, Muller YA, Hensel M.

PLoS Pathog. 2017 May 30; 13(5):e1006418. doi: 10.1371/journal.ppat.1006418. PMID: 28558023; PMCID: PMC5466336.

Proteomics of intracellular *Salmonella enterica* reveals roles of *Salmonella* pathogenicity island 2 in metabolism and antioxidant defense.

Noster J, Chao TC, Sander N, Schulte M, Reuter T, Hansmeier N, Hensel M.

PLoS Pathog. 2019 Apr 22;15(4):e1007741. doi: 10.1371/journal.ppat.1007741. PMID: 31009521; PMCID: PMC6497321.

Structural and functional characterization of SiiA, an auxiliary protein from the SPI4-encoded type 1 secretion system from *Salmonella enterica*.

Kirchweger P, Weiler S, Egerer-Sieber C, Blasl AT, Hoffmann S, Schmidt C, Sander N, Merker D, Gerlach RG, Hensel M, Muller YA.

Mol Microbiol. 2019 Nov;112(5):1403-1422. doi: 10.1111/mmi.14368. Epub 2019 Sep 17. PMID: 31419359.

IX. Danksagung

Es ist geschafft!

Fleiß und ein starker Wille lassen einen alles erreichen! Nachdem ich damals nach Meinung der Lehrer nicht einmal das Gymnasium schaffen sollte, habe ich nicht nur das und viel mehr geschafft, sondern stehe heute nun hier und reiche meine Doktorarbeit ein, ein unglaubliches Gefühl! Diesen Weg hätte ich dennoch ohne viele Menschen sicher nicht geschafft und deshalb möchte ich mich hiermit bei ihnen bedanken (in der Hoffnung niemanden zu vergessen).

Zunächst möchte ich mich bei Prof. Dr. Michael Hensel dafür bedanken, dass ich neben meiner Bachelor- und auch Masterarbeit, nun auch meine Doktorarbeit in seiner Abteilung anfertigen durfte. Vielen Dank für die Betreuung und Unterstützung, ebenso wie für die die Korrekturen meiner Arbeit, sowie die Ermöglichung von Konferenzbesuchen und lustigen Betriebsausflügen und Feiern mit der Arbeitsgruppe.

Mein zweiter Dank gilt Prof. Dr. Guntram Grassl für die Erstellung des Zweitgutachtens und für die tolle Zusammenarbeit, vor allem im Organoid-Projekt. Danke, dass ich mich immer bei der ganzen Arbeitsgruppe melden konnte und auch zum Erlernen der Techniken bei euch vorbeischauchen durfte. Mein weiterer Dank gilt Prof. Dr. Karlheinz Altendorf und Dr. Michael Holtmannspötter für die Bereitschaft Teil meiner Prüfungskommission zu sein. Ganz besonders möchte ich mich in diesem Zuge auch bei Michael für die vielen wütenden, wahnsinnigen, fluchenden und verzweifelten, aber immer sehr, sehr lustigen Stunden am TIRF und vor dem Auswerterechner bedanken. Mehr MEA!

Liebe Mibis, ganz herzlich möchte ich mich bei euch allen bedanken. Seit 2015 bin ich nun auch schon Teil der Arbeitsgruppe und ich möchte nicht einen der Momente mit euch allen missen müssen. Wir sind über die Jahre so eng zusammengewachsen, dass Probleme, Ängste und Freuden die anderen oft direkt persönlich mitnehmen und zusammen Lösungen gesucht und auch gefunden werden – und wenn wir dafür einen Sekt öffnen müssen! Ein ganz besonderer Dank gilt da natürlich auch Mullika (Monika und Ulla). Ihr habt mich wo es geht immer unterstützt und mitgefiebert, danke euch beiden. Danke euch allen für die schöne Zeit, mit vielen Lachern, aber auch ernsten Themen, schönen Frühstücksbuffets, Mittagessen und auch Abenden. Ich möchte mich hier auch sehr bei Jörg bedanken. Wir sind zwar auch oft aneinander gerasselt, sind aber inzwischen zu einem guten Team geworden, denke ich und können gut mit einander reden und auch lachen.

Danke auch an Dorothee, Laura, Vera, Tatjana, Jennifer, Felix, Marc, Carina, Pascal und Lena. Ich denke wir haben einen wilden Ritt zusammen durchgemacht! Eine Doktorarbeit verlangt einem einiges ab und ich bin froh, dass ich diese nervenaufreibende Zeit mit euch verbracht

habe – in guten wie in schlechten Zeiten. Euch habe ich alle mehr gesehen als irgendwen sonst, vor allem, dich Doro. Ich glaube wir waren manchmal dem Wahnsinn nah, als wir spät nachts noch im Labor standen, um das widerspenstige T1SS (nicht) aufzureinigen und Jannis uns mit Notfallrationen Essen versorgen musste. Ich denke dennoch gerne daran und an unsere schönen Abende und Konferenzen zurück. Felix, wir haben damals zusammen angefangen und uns immer auch unabhängig vom geteilten Projekt unterstützt und schließen nun auch beide gemeinsam ab, danke für die gemeinsame Zeit. Pascal und Lena, meine Gang auf der dunklen Seite, wo das Licht nicht scheint..oder an ist. Danke für all unsere schönen, lustigen und sehr lauten Momente, auch über das Labor hinaus.

Ein ganz besonderer Dank gilt natürlich Nani und Jenne. Ich bin sehr froh, dass wir uns gefunden haben und bereits so viele tolle Momente miteinander erlebt haben und auch noch erleben werden. Danke, dass ich mich immer auf euch verlassen kann und wir so viel Spaß zusammen haben. Jede Veranstaltung mit uns wird wahrhaftig zu einer – zu einer, an der niemand mehr etwas sagen kann, da unsere Frequenz und Lautstärke alles übertönt. Egal, wo wir sind und was wir tun, jeder Moment mit euch ist etwas Besonderes für mich. Das gilt natürlich auch für unsere wöchentlichen Treffen, Jenne, darauf freue ich jedes Mal aufs Neue.

Danke auch an die Jungs aus der Biophysik für unzählige witzige spontane Abende, hinter der Uni, im Heimlich oder sonst wo, es war ein Fest mit euch! Besonders möchte ich mich hierbei bei Max und Thomas bedanken, die über diese Momente hinaus immer ein offenes Ohr für mich hatten und für mich da waren.

Auch außerhalb der Uni gibt es natürlich besondere Menschen, die einen durch diese Zeit und darüber hinaus begleitet haben und auch noch werden. Zunächst einmal möchte ich Nena ganz herzlich danken. Danke dir für deine Unterstützung in jeglicher Form und in allen Bereichen. Von ernsten Gesprächen bis hin zu absurden Lösungsansätzen war wohl schon immer alles dabei. Danke, dass wir so gute Freunde sind! In dem Zuge möchte ich mich auch herzlich bei Flo, Jule, Dennis, Nina und Tom bedanken. Danke, dass ihr immer da seid!

Danke auch an mein Piloten-Team: Kai, Julian und Dave – wir sind schon hoch geflogen! Ein ganz besonderer Dank gilt hier aber Dave. Danke, dass du immer für mich da bist und mir bei allem zuhörst und mich unterstützt. Danke auch für unsere unzähligen Therapiesitzungen, in denen wir immer mindestens die Welt verändert und auch gerettet haben. Auch wenn ich deine Tipps manchmal als blödsinnig und unsinnig erachte, bin ich dennoch froh, dass du sie mir gibst und insgeheim nehme ich daraus ja auch sicherlich immer etwas mit. Ich bin froh, dass wir so tief miteinander verbunden sind.

Wem natürlich sehr viel Dank zu Teil wird, sind meine Eltern, Uta und Frank. Ich danke euch beiden sehr für die Unterstützung in den letzten Jahren, was sage ich, für die Unterstützung

schon mein ganzes Leben lang. Ihr habt mir bei allem immer freie Hand gelassen und mich immer unterstützt beim nach den Sternen greifen. Ohne euren Rückhalt hätte ich das alles niemals geschafft. Ihr habt mir immer gut zugesprochen und mir gesagt, dass ich das richtige tun werde. Zumindest dieses Kapitel habe ich nun abgeschlossen, mal sehen was ich mir nun einfallen lassen werde! Danke für alles.

Ganz zum Schluss möchte ich noch dem Menschen danken, mit dem ich in all dieser Zeit durch dick und dünn gegangen bin und ohne den ich weder die Zeit im Labor, noch die Schreibphase geschafft hätte – Jannis. Du hast mir den Rückhalt und die Stärke gegeben das alles durchzustehen und nicht aufzugeben. Danke für dein Verständnis und auch deine Ruhe Dinge anzugehen, das liegt mir manchmal ja nicht so. Ohne deine Ideen aus unseren Gesprächen wären manche Versuche vielleicht nicht durchgeführt nun. Danke für deine Unterstützung in allen Formen vom kochen bis hin zu nachts mit in der Uni sitzen. Trotz all der Anstrengungen und auch Schwierigkeiten zwischendurch, möchte ich nicht einen unserer gemeinsamen Momente missen müssen. Jedes unserer kleinen Rituale war wichtig, um alles so souverän zu meistern. Ich danke dir von Herzen für alles!

X. Erklärung über die Eigenständigkeit der erbrachten wissenschaftlichen Leistungen

Ich erkläre hiermit, dass ich die vorliegende Arbeit ohne unzulässige Hilfe Dritter und ohne Benutzung anderer als der angegebenen Hilfsmittel angefertigt habe. Die aus anderen Quellen direkt oder indirekt übernommenen Daten und Konzepte sind unter Angabe der Quelle gekennzeichnet.

Bei der Auswahl und Auswertung haben mir die unter III.5. ‚Contributions of Co-authors‘ aufgeführten Personen in der jeweils beschriebenen Weise unentgeltlich geholfen.

Weitere Personen waren an der inhaltlichen und materiellen Erstellung der vorliegenden Arbeit nicht beteiligt. Insbesondere habe ich hierfür nicht die entgeltliche Hilfe von Vermittlungs- bzw. Beratungsassistenten (Promotionsberater oder andere Personen) in Anspruch genommen. Niemand hat von mir unmittelbar oder mittelbar geldwerte Leistungen für Arbeiten erhalten, die im Zusammenhang mit dem Inhalt der vorgelegten Dissertation stehen.

Die Arbeit wurde bisher weder im In- noch im Ausland in gleicher oder ähnlicher Form einer anderen Prüfungsbehörde vorgelegt.

(Ort, Datum)

(Unterschrift)

XI. Supplements on DVD

PhD thesis as PDF file “Functional analysis and characterization of the type I secretion system and its substrate, the giant adhesin SiiE, of *Salmonella enterica*”

III.1. Conserved secretion mechanisms of the giant adhesin SiiE of *Salmonella enterica* and other two-step secreted adhesins. STM proteomic data cytosolic and secreted mini SiiE.

III.3. Functional interaction between SPI4-T1SS encoded proton channel SiiAB and the flagellum in *Salmonella enterica*. STM proteomic data WT and Δ siiAB.